Persulfate Activation by Biochar for Organic Contaminant Removal from Water

Dissertation

der Mathematisch-Naturwissenschaftlichen Fakultät

der Eberhard Karls Universität Tübingen

zur Erlangung des Grades eines

Doktors der Naturwissenschaften

(Dr. rer. nat.)

vorgelegt von

Yiling Zhuang

aus Fujian/China

Tübingen

2024

Gedruckt mit Genehmigung der Mathematisch-Naturwissenschaftlichen Fakultät der Eberhard Karls Universität Tübingen.

Tag der mündlichen Qualifikation:	30.04.2024
Dekan:	Prof. Dr. Thilo Stehle
1. Berichterstatter/-in:	Prof. Dr. Stefan B. Haderlein
2. Berichterstatter/-in:	Prof. Dr. Christian Zwiener

Acknowledgement

First of all, I would like to extend my warmest thanks to my supervisors, Stefan Haderlein and Stephanie Spahr. Without their exceptional guidance and support, this dissertation would not have reached completion. Stefan, I am profoundly grateful for your gracious agreement to continue supervising me even after my relocation to Berlin. Our regular online meetings provided invaluable feedback and sparked insightful discussions, which significantly propelling my work forward. Your generous praise and positive feedback during our meetings and manuscript reviews have always multipled my confidence. I also owe a special acknowledgment to Stephanie, who not only served as my supervisor but also became a cherished friend. I deeply appreciated her proactive meetings and engaging discussions over the past four years, her boundless creativity always infused our work with fresh ideas. Her unwavering availability, tirelessly responding to my emails and meticulously reviewed my manuscripts even during evenings and weekends, has been invaluable. Moreover, I have learned a lot with her humble and approachable demeanor which has fostered a more collaborative work environment and helped with my communication skills.

I offer special thanks to Holger Lutze. Despite our limited in-person interactions, our discussions *via* Zoom have been immensely beneficial, particularly in establishing and designing probe compound methodologies. His insightful questions in our meeting provided much food for thought and significantly contributed to the refinement of my research. Moreover, Holger's enthusiasm for research and agile thinking have always inspired me to strive for excellence. I am also grateful to Holger for agreeing to be a member of my defense committee.

My gratitude extends to Christian Zwiener for agreeing to be my second supervisor at outset of the dissertation and for serving as the dissertation reviewer and defense committee member. I also would like to express my gratitude to Christiane Zarfl for her invaluable contributions as a defense committee member and for engaging in profound discussions on my work.

Special thanks to Nikolas Hagemann for producing a series of excellent biochars under various pyrolysis conditions and from different feedstocks, which served as the fundamental and crucial materials for my experiments. Nikolas's expertise and constructive feedback during several meetings and manuscript revisions were invaluable and useful. I also would like to express my thankful to Jannis Grafmüller for his efficient assistance in conducting conductivity measurements on the biochars and especially grateful for his timely updates on experimental progress and generous sharing of information on Boehm titration.

I express my special appreciation to Andrea Paul and Friedrich Fink for their invaluable assistance with EPR and FTIR measurements and for engaging in thorough discussions on data interpretation, manuscript writing, and revisions, which significantly enhanced the quality of my dissertation. I am deeply grateful to Chen Sun from Zhejiang University for producing shrimp shell biochar, which brought new hope when other biochars failed to activate persulfate, thus opening new avenues for my research. Special thanks to Philipp Martin for his generous sharing of knowledge and expertise in GC IRMS in person or *via* emails, which greatly enhanced my understanding and proficiency in this area. I thank Johanna for her invaluable assistance in teaching me to use electrochemical instruments and resolving noise interference, which was crucial for obtaining accurate and reliable results regarding electron transfer.

Special thanks go to Christoph Reith, Karolin Gogler, and Jiangyang Li for their contributions to my research project, particularly for choosing it as the subject of their master thesis and internship research projects, and for their assistance with experiments and data analysis.

I am grateful to the technicians at the IGB CAB lab, especially Claudia Schmalsch, Paul Hawelitsch, Thomas Rossoll, Marvin Sens, Christiane Herzog, and Tobias Goldhammer, for their invaluable assistance in conducting laboratory work and sample measurements. A heartfelt thank you to Claudia for helping me familiarize myself with the laboratory when I first arrived at IGB, her support allowed me to quickly adapt to the new environment, and thank you for her tirelessly addressed and answered my

questions over the following two and a half years. Thank you for Paul's patient assistance in learning and operating GC IRMS. Although the results of IRMS were not presented in my dissertation, the knowledge gained was invaluable and maybe will be one day applied to my future research endeavors.

I express my gratitude to the technical team in Tübingen, including Monika Hertel, Sara Cafisso, Stephanie Nowak, and Renate Seelig, for their invaluable assistance during my time in the Tübingen laboratory. Thank you for creating a cooperative and relaxed atmosphere that made my time in Tübingen enjoyable and memorable.

I am deeply grateful to Guoxiang Li for his help upon my arrival in Germany, including picking me up from the train station and helping me quickly adapt to German life, demonstrating unwavering support throughout my PhD journey.

I thank the IGB Lunch group, including but not limited to Yuyuan Liu, Vanderville Villegas, Kyla Sehner, Erika Martinez Ruiz, Athena Karapli-Petritsopoulou, and Emily Booms, for their invaluable camaraderie and memorable moments during our lunch breaks. I will always cherish the laughter and discussions shared with this group, as well as the unique memories, including our elevator bets, which added much joy and fun to my life at IGB. Special thanks to my friend Yuyuan Liu for her heartfelt conversations, sharing both joys and sorrows in our work and life, and always thinking of me when cooking delicious food, which was especially precious considering the lack of a cafeteria at IGB.

Lastly, I want to express my deepest gratitude to my boyfriend Yilin Wei and his family for their unwavering support and understanding throughout the challenges of pursuing a PhD. Yilin, thank you for being my closest friend and confidant, sharing in all the ups and downs of this journey. What unforgettable and precious memories that we have successfully navigated a long-distance relationship spanning four years, and I am excited for the adventures that lie ahead. Finally, I want to express my deepest gratitude to my family—my father, mother, sister, and brother—for their unwavering support, understanding, and encouragement. You have always been my source of courage and confidence, and I am endlessly grateful for your love and support.

Table of Contents

Summary

Persulfate-based oxidation processes using e.g., peroxydisulfate ($S_2O_8^{2-}$) have become increasingly popular for water treatment to remove organic contaminants. Peroxydisulfate can be effectively activated by biochar in the presence and absence of Fe(III) to form reactive species that react with organic contaminants. However, systematic studies on the performance of different biochars and formation of reactive species in different water matrices are lacking. The goal of this dissertation was to (i) assess the treatment efficiency of biochar and persulfate with and without dissolved iron for the removal of organic contaminants, (ii) investigate the effect of water matrix components on reactive species formation and treatment performance, (iii) gain insights into the role of biochar pyrolysis conditions on persulfate activation and contaminant removal, and (iv) explore the combined use of biochar and persulfate for the treatment of urban stormwater runoff.

In laboratory batch experiments, a biochar produced from beech wood at 450°C was successfully employed to activate peroxydisulfate in the presence of Fe(III) at pH 2.5 to degrade an organic model compound, the insect repellent *N,N*-diethyl-*m*-toluamide (DEET) in pure water, synthetic water, and a mining-impacted surface water. By using carefully selected scavengers and probe compounds on the basis of competition kinetics calculations, the major reactive species in the biochar/Fe(III)/peroxydisulfate system were identified as sulfate radicals ($SO_4^{\bullet-}$) in pure water. In the presence of chloride at low (0.1 mM) and higher (1 mM) concentrations, the reactive species shifted from $SO_4^{\bullet-}$ to hydroxyl radicals and reactive chlorine species, respectively. These results show that the water matrix has a strong impact on the formation of reactive species, which is important to tailor and assess the application of this oxidation process to specific requirements at full scale.

Comparing four biochars produced from beech wood at different pyrolysis temperatures of 450, 600, 750°C, biochar produced at 450°C removed DEET most efficiently with Fe(III) and persulfate at pH 2.5. This biochar contained high amounts

of surface oxygen functional groups and persistent free radicals as redox-active moieties that likely accelerated Fe(III) reduction and persulfate activation. To modulate the redox properties, four biochars were produced from softwood sawdust to which 0 – 43 weight percent (wt%) of ash was amended during pyrolysis at 500°C. The biochar with 16 wt% ash amendment resulted in the best DEET removal in the presence of Fe(III) and persulfate. Ash-amended biochars contained surface oxygen function groups, persistent free radicals and, in addition, crystalline iron minerals, which promoted Fe(III) reduction and persulfate activation. These results inform future production of engineered biochars with fine-tuned redox properties that enable optimized performance for specific applications in water treatment.

One biochar produced from shrimp shells at 750°C was found to directly activate peroxydisulfate at circumneutral pH forming non-radical reactive species, most likely singlet oxygen ($^1O_2$). In laboratory batch experiments, this biochar/peroxydisulfate system was investigated for its potential to remove persistent and mobile organic contaminants from urban stormwater, which can otherwise not be well removed in conventional stormwater treatment systems. Out of the 11 organic contaminants tested, one was removed through adsorption onto biochar (diuron) and four were removed through oxidation (1,3-diphenylguanidine, 2-hydroxybenzothiazole, 1*H*-benzotriazole, 5-methyl-benzotriazole). As $^1O_2$ reacts selectively with organic compounds *via* an electrophilic substitution reaction, the oxidation process performed well in different water matrices and was only slightly impacted by dissolved organic carbon and high chloride concentrations as often found in stormwater runoff. This work provides an important first step towards applying persulfate-based oxidation processes for stormwater purification.

Keywords: water treatment, persulfate-based oxidation processes, biochar, organic contaminants, reactive species, redox-active properties, stormwater treatment

Zusammenfassung

Oxidationsverfahren auf Persulfatbasis, bei denen zum Beispiel Peroxodisulfat ($S_2O_8^{2-}$) eingesetzt wird, werden bei der Wasseraufbereitung zur Entfernung organischer Verunreinigungen immer beliebter. Peroxodisulfat kann durch Biokohle in Gegenwart und Abwesenheit von Fe(III) effektiv aktiviert werden, um reaktive Spezies zu bilden, die mit organischen Verunreinigungen reagieren. Es fehlen jedoch systematische Studien über die Leistungsfähigkeit verschiedener Biokohlen und die Bildung reaktiver Spezies in unterschiedlichen Wassermatrizes. Ziel dieser Dissertation war es, (i) die Behandlungseffizienz von Biokohle und Persulfat mit und ohne gelöstem Eisen zur Entfernung organischer Verunreinigungen zu bewerten, (ii) die Auswirkungen von Komponenten der Wassermatrix auf die Bildung reaktiver Spezies und die Behandlungsleistung zu untersuchen, (iii) Einblicke in die Rolle der Biokohle-Pyrolysebedingungen auf die Persulfataktivierung und die Entfernung von Verunreinigungen zu gewinnen und (iv) die kombinierte Verwendung von Biokohle und Persulfat für die Aufreinigung von städtischem Niederschlagsabfluss zu untersuchen.

In Batch-Laborexperimenten wurde eine aus Buchenholz bei 450°C hergestellte Biokohle erfolgreich zur Aktivierung von Peroxodisulfat in Gegenwart von Fe(III) bei pH 2,5 eingesetzt, um eine organische Modellverbindung, das Insektenabwehrmittel *N,N*-Diethyl-*m*-toluamid (DEET), in reinem Wasser, synthetischem Wasser und einem durch Bergbau beeinflussten Oberflächenwasser abzubauen. Durch den Einsatz sorgfältig ausgewählter Scavenger und Sondenverbindungen auf der Grundlage von Berechnungen der Kompetitionskinetik, wurden die wichtigsten reaktiven Spezies im Biokohle/Fe(III)/Peroxodisulfat-System als Sulfatradikale ($SO_4^{\bullet-}$) in reinem Wasser identifiziert. Bei Anwesenheit von Chlorid in niedrigen (0,1 mM) und höheren (1 mM) Konzentrationen veränderten sich die reaktiven Spezies von $SO_4^{\bullet-}$ zu Hydroxylradikalen bzw. reaktiven Chlorspezies. Diese Ergebnisse zeigen, dass die Wassermatrix einen starken Einfluss auf die Bildung reaktiver Spezies hat, was wichtig ist, um die Anwendung dieses Oxidationsprozesses auf spezifische Anforderungen im

großtechnischen Maßstab anzupassen und zu bewerten.

Ein Vergleich von vier Biokohlen, die aus Buchenholz bei unterschiedlichen Pyrolysetemperaturen (450, 600, 750°C) hergestellt wurden, ergab, dass die bei 450°C hergestellte Biokohle DEET am effizientesten mit Fe(III) und Persulfat bei pH 2,5 entfernte. Diese Biokohle enthielt einen hohen Gehalt an funktionellen Sauerstoffgruppen auf der Oberfläche und persistenten freien Radikalen als redox-aktive Bestandteile, die wahrscheinlich die Fe(III)-Reduktion und Persulfat-Aktivierung beschleunigten. Um die Redoxeigenschaften zu modifizieren, wurden vier Biokohlen aus Weichholzsägemehl hergestellt, dem während der Pyrolyse bei 500 °C Asche in Mengen von 0 bis 43 Gewichtsprozent (Gew.-%) zugesetzt wurde. Die Biokohle mit 16 Gew.-% Aschezusatz führte zur besten DEET-Entfernung in Gegenwart von Fe(III) und Persulfat. Die mit Asche versetzten Biokohlen enthielten funktionale Sauerstoffgruppen an der Oberfläche, persistente freie Radikale und zusätzlich kristalline Eisenminerale, die die Reduktion von Fe(III) und die Aktivierung von Persulfat begünstigten. Diese Ergebnisse liefern wichtige Erkenntnisse für die künftige Herstellung von Biokohlen mit angepassten Redox-Eigenschaften, die eine optimierte Leistung für bestimmte Anwendungen in der Wasseraufbereitung ermöglichen.

Eine Biokohle, die bei 750 °C aus Krabbenschalen hergestellt wurde, aktivierte Peroxodisulfat direkt bei neutralem pH-Wert und bildete dabei nichtradikalische reaktive Spezies, höchstwahrscheinlich Singulett-Sauerstoff ($^1O_2$). In Batch-Laborexperimenten wurde dieses Biokohle/Peroxodisulfat-System auf sein Potenzial hin untersucht, persistente und mobile organische Verunreinigungen aus städtischem Regenwasser zu entfernen, die in herkömmlichen Regenwasserbehandlungs-systemen nicht gut entfernt werden können. Von den 11 getesteten organischen Schadstoffen wurde einer durch Adsorption an Biokohle (Diuron) und vier durch Oxidation (1,3-Diphenylguanidin, 2-Hydroxybenzothiazol, 1H-Benzotriazol, 5-Methylbenzotriazol) entfernt. Da $^1O_2$ selektiv mit organischen Verbindungen über eine elektrophile Substitutionsreaktion reagiert, zeigte der Oxidationsprozess in verschiedenen Wassermatrizes gute Ergebnisse und wurde nur geringfügig durch gelösten organischen Kohlenstoff und hohe Chloridkonzentrationen beeinträchtigt,

wie sie häufig in Regenabflüssen vorkommen. Diese Arbeit ist ein wichtiger erster Schritt auf dem Weg zur Anwendung persulfatbasierter Oxidationsverfahren für die Aufreinigung von Niederschlagsabflüssen.

Stichworte: Wasseraufbereitung, persulfatbasierte Oxidationsprozesse, Biokohle, organische Schadstoffe, reaktive Spezies, redoxaktive Eigenschaften, Regenwasserbehandlung

Chapter 1

Introduction

1.1 Occurrence, risks, and removal of synthetic organic contaminants in the water cycle

Providing safe and clean water for human and environmental health is a key challenge of international concern[1]. With increasing urbanization, industrialization, and population growth, pollution of water resources with synthetic organic chemicals such as pesticides, pharmaceuticals, personal care products, flame retardants, and other industrial compounds is increasing[2,3]. More than 350,000 chemicals and chemical mixtures have been registered for production and use in the global market, with the number of newly introduced chemicals continually rising[4]. Many of these organic chemicals can enter the aquatic environment through insufficiently treated municipal and industrial wastewater treatment plant (WWTP) effluents[5–8] or through untreated urban stormwater runoff [9–11], and can have adverse effects on aquatic organisms and human health even at trace levels[12–14]. In order to protect aquatic ecosystems and drinking water resources from contamination, it is crucial to remove organic chemicals from wastewater and stormwater prior to discharge into rivers or infiltration into groundwater[15]. The development and implementation of efficient and reliable water treatment technologies to clean-up impaired freshwater resources is an important element to ensure a sustainable management of water resources, particularly in urban areas[16,17].

Currently, WWTP effluents and stormwater runoff are discharged into surface waters or groundwater aquifers, which are important drinking water resources. However, conventional WWTPs cannot fully remove trace organic contaminants, because many of them are polar or ionizable, hardly sorb, and are recalcitrant to biodegradation[5,18]. To achieve an efficient removal of trace organic contaminants from water, additional treatment steps are often necessary. While advanced water treatment technologies using e.g., membranes[19,20] or electrochemical technologies[21] can efficiently purify wastewater and greywater and even allow for direct potable reuse, these technologies are energy intensive and not yet widely applied[19–21]. Activated

carbon and ozonation are more economically feasible advanced water treatment technologies, which are currently being implemented to upgrade certain WWTPs, e.g., in Switzerland or parts of Germany to enhance the removal of trace organic contaminants from WWTP effluents[22,23].

In addition to activated carbon and ozonation, intensive research efforts have been directed to the development and application of alternative water treatment processes using e.g. more sustainable adsorbents such as biochar[24–26] and advanced oxidation processes (AOPs) using chemical oxidants such as hydrogen peroxide (H_2O_2) or persulfate. In AOPs, highly reactive species are formed from chemical oxidants including hydroxyl radicals ($^{\bullet}OH$)[27–29] or sulfate radicals ($SO_4^{\bullet-}$), which can react quickly with many organic chemicals in water[30,31]. Persulfate-based oxidation processes have gained growing attention as they have advantages such as a high oxidant stability during transport and storage and good treatment performance for many organic contaminants[32,33]. To date, peroxydisulfate ($S_2O_8^{2-}$, PDS) and peroxymonosulfate (HSO_5^-, PMS) (collectively referred to as persulfate) have been frequently used in both laboratory experiments and field studies, particularly for in situ chemical oxidation to remediate contaminated sites[30,31].

However, persulfate needs to be activated to form reactive species for organic contaminant removal[30,31]. Currently existing persulfate activation methods include thermal or radiation activation, which require high energy input and can hardly be used in decentralized water treatment systems[34,35]. Persulfate can also be activated by transition metal ions such as Fe(II)[36–38]. This Fenton-like process has been intensively studied but has several limitations because dissolved Fe(II) is rapidly depleted during persulfate activation and the formed Fe(III) is only slowly reduced back to Fe(II) leading to the accumulation of iron-containing sludge as hazardous waste also at low pH values. More research is needed to investigate alternative and economical methods that allow for an efficient and reliable activation for persulfate with applications in either centralized water treatment using e.g., water treatment reactors or decentralized water treatment in nature-based systems.

1.2 Biochar for water treatment

Biochar is a carbon-rich solid produced by the heating of biomass under oxygen-limited conditions[39,40]. Biochar can be produced from a variety of biomass feedstocks such as energy crops, agricultural and forestry wastes, compost (green waste), and sewage sludge[41–43]. Due to its large surface area, complex porosity, and variable surface composition, biochar is attracting interest as a promising multifunctional material for different environmental applications[39,40]. In addition to its beneficial use in agronomic and engineering applications[44,45], biochar has been shown to bear great potential as cost-effective and sustainable adsorbent to remove contaminants from wastewater[46–48] and stormwater[49–51]. Biochar might, thus, serve as an alternative adsorbent to activated carbon for water treatment[52–54].

Biochar contains redox-active components such as quinone-hydroquinone moieties and/or condensed aromatic structures[40,55,56] that can reversibly accept and donate electrons[57,58]. Therefore, biochar functions similarly to natural organic matter in many (bio)geochemically and environmentally relevant redox reactions[59,60], such as denitrification[61], iron mineral reduction[62,63], and organic contaminant transformation[64–66]. Biochar also contains persistent free radicals (PFRs), i.e. moieties with unpaired electrons, which form during the pyrolysis process[67]. PFRs potentially play a crucial role in the degradation of contaminants, such as sulfamethoxazole[67,68]. Recent studies have demonstrated that PFRs can activate chemical oxidants such as persulfate leading to the formation of highly reactive oxygen species, such as $SO_4^{\bullet-}$ [69,70]. The redox properties of biochar may thus greatly broaden the application of biochar for pollution control. Current knowledge suggests that the feedstock materials and pyrolysis conditions greatly impact the biochar properties[71–74]. For instance, the pyrolysis temperature has been shown to impact the biochar redox properties, which govern e.g., the biochar performance for Cr(VI) reduction[75] and methane production in anaerobic digestion of waste activated sludge[76]. However, little is known about the effects of biochar properties on persulfate activation in water treatment.

1.3 Persulfate-based oxidation processes for contaminant removal from water

Persulfate has gained increasing attention as oxidant to degrade recalcitrant organic compounds in water[30,31]. In persulfate-based oxidation processes, $SO_4^{\bullet-}$ and other reactive oxygen species are formed, which can react with organic contaminants[30,77,78]. $SO_4^{\bullet-}$ have a high redox potential (2.5 – 3.1 V) and are more selective compared to $^{\bullet}OH$, which are formed in $^{\bullet}OH$-based AOPs such as the Fenton process (Fe/H_2O_2), ozone/H_2O_2 or UV/H_2O_2[79–81]. To release $SO_4^{\bullet-}$, the peroxide bond in the persulfate molecule needs to be cleaved[77,82], which can be achieved by UV-radiation[83,84], heat[34,85], metal ions[86,87], and carbon materials, such as biochar[88,89]. During persulfate activation, persulfate can produce radical species, mainly $SO_4^{\bullet-}$ and $^{\bullet}OH$, as well as reactive non-radical species[90–92].

Figure 1.1 shows possible oxidative reaction pathways that can be induced upon persulfate activation by biochar in the presence or absence of metal ions[30,31]. In the past, it was generally assumed that radical reactions dominate in persulfate-based oxidation systems and in the degradation of organic contaminants (pathway (i) in Figure 1.1)[93–95]. Recent studies have shown that persulfate can also oxidize organic compounds *via* non-radical mechanisms without the involvement of radical species[92,96,97]. Singlet oxygen ($^1O_2$) has been reported to form during persulfate activation with carbonaceous materials such as biochar, where ketone groups react with persulfate to form $^1O_2$ (pathway (ii))[98,99]. $^1O_2$ can then react with organic contaminants, which is an even more selective way than reactions with $SO_4^{\bullet-}$ as $^1O_2$ can only react with electron-rich moieties[98,100,101]. When metal ions, such as Fe(III), are present in their reduced form, high-valent metal species (e.g. Fe(IV), Fe(V)) have been proposed to form as reactive species in persulfate-based oxidation processes (pathway (iii))[102–104]. Another non-radical oxidative reaction pathway is mediated electron transfer from organic compounds (as electron donor) to persulfate (as electron acceptor) involving conductive catalysts, such as biochar as electron transfer mediator (pathway (iv))[105,106].

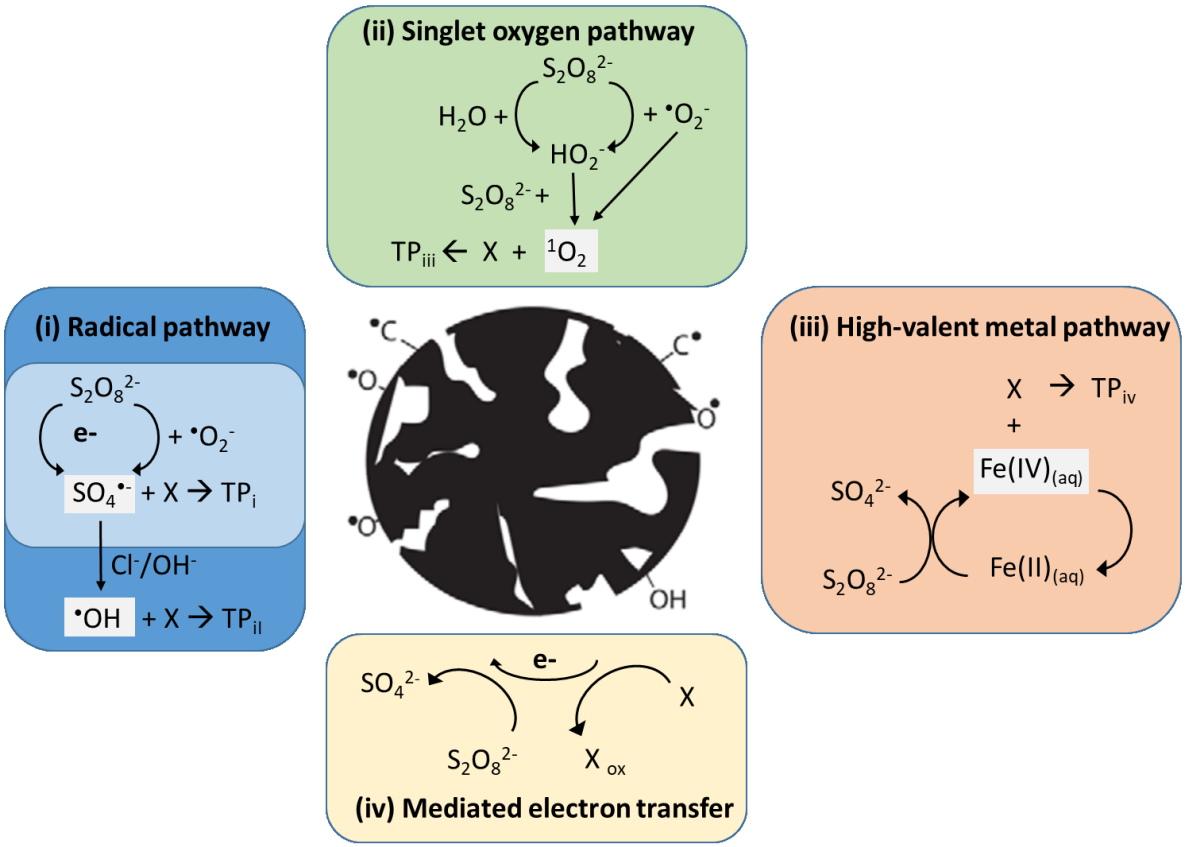

Figure 1.1. Possible oxidative reaction pathways induced by persulfate activation by biochar (X: organic contaminants; TP: transformation products)[30,31].

1.4 Combination of biochar and persulfate for organic contaminant removal from water

1.4.1 Persulfate activation by biochar in the presence of iron at acidic conditions

Persulfate-based Fenton-like processes that form highly reactive species for oxidative water treatment have attracted much attention, especially for the treatment of industrial wastewaters containing a mixture of pollutants in a wide range of concentrations[107–109]. However, the oxidation efficiency of the conventional Fe(II)/persulfate system is limited by the sluggish Fe(III)/Fe(II) cycling and Fe(III) precipitation also at low pH values[8–11]. To address this problem, previous studies have demonstrated that the Fe(III)/Fe(II) cycling can be enhanced by the addition of redox-active biochars in the

presence of Fe(III) at acidic condition[113–116]. The proposed mechanism was that biochar induces Fe(III) reduction to Fe(II), which can activate persulfate to reactive species that react with organic contaminants[113–116]. However, different studies reported conflicting findings concerning the formation of major reactive species in the biochar/Fe(III)/persulfate system[113–116]. Moreover, the role of biochar properties for the Fe(III) reduction and persulfate activation remains unclear.

Reactive species such as $SO_4^{\bullet-}$ or $^{\bullet}OH$ have very short lifetimes in the range of microsecond (µs)[117], which complicates their direct detection and quantification. Although direct methods such as electron paramagnetic resonance (EPR) spin trapping[118] or laser flash photolysis and pulse radiolysis hyphenated with fast UV-vis spectroscopy[119,120] are available for the detection and characterization of radicals, expensive specialist non-portable instrumentation and considerable expertise are needed with limited availability to most researchers[121]. The use of probe compounds can serve as an alternative indirect method for the identification of major reactive species in advanced oxidation processes[90]. Probe compounds are chemicals that should react rapidly and selectively with a particular reactive species of interest[90,121–123]. Probe compounds should ideally have known reaction rate constants and known reaction mechanisms for the reaction with the reactive species at study, and should not interact with other components in the system under investigation[90,121–123]. The use of probe compounds offers many benefits as they are readily available and easy to quantify with frequently available instrumentation such as high-performance liquid chromatography (HPLC). The accurate identification of the major reactive species is crucial for the development and assessment of persulfate-based oxidation processes to identify suitable applications in terms of target contaminants as well as water matrix[121]. However, inappropriate usage of probe compounds can result in misleading mechanistic interpretations, such as overlooking or overestimating the contribution of certain reactive species.

In the biochar/Fe(III)/persulfate system, the performance of biochar for Fe(III) reduction and persulfate activation to reactive species is highly depend on the biochar

properties, especially the redox properties[113,114]. The biochar pyrolysis conditions, particularly the pyrolysis temperature, can significantly impact the biochar redox properties[113,114]. Surface functional groups, such as quinone functional groups, have been shown to be the major redox-active moieties in biochars produced at low pyrolysis temperature <600°C[68,69,124]. At pyrolysis temperatures above 600°C, conjugated aromatic structures, like conjugated π-electron systems, are formed and proposed to be redox-active[58,125]. However, little is known about the role of redox-active moieties of biochars for persulfate activation and organic contaminant transformation in the biochar/Fe(III)/persulfate system. It is of great interest to optimize the redox-active properties of biochar in order to improve the performance of biochar. Wood ash, a by-product of biomass power plants with high mineral content and pH buffering capacity[126,127], has recently been explored as amendment during the biochar pyrolysis procedure[127–129]. The produced ash-amended biochars possessed enhanced redox-active properties with higher electron exchange capacity than biochar without ash amendment[129]. Ash-amended biochars, therefore, bear potential for application in the biochar/Fe(III)/persulfate system but have not yet been tested for organic contaminant removal in this oxidation process.

1.4.2 Persulfate activation by biochar at circumneutral pH

Certain biochars have been shown to activate persulfate also in the absence of transition metals, which offers the possibility to treat water with only biochar and persulfate at circumneutral pH[130,131]. Biochar-mediated persulfate-based oxidation processes have been successfully used to abate organic contaminants in wastewater[132,133], surface water[134], and groundwater[131,134]. So far, no attempts have been made to employ the biochar/persulfate system for the treatment of stormwater, which often carries numerous trace organic contaminants such as herbicides, plasticizers, corrosion inhibitors, and tire wear chemicals[9,10,135]. Many organic contaminants in urban stormwater are persistent and mobile and thus difficult to remove by conventional stormwater treatment, which is based on sedimentation (e.g.,

in stormwater ponds), sorption (e.g., in biofilters), or biodegradation (e.g., in constructed wetlands)[31,136–139]. Recently, there have been growing efforts to remove trace organic contaminants from urban stormwater through the amendment of biofilters with biochar[49–51,140]. However, it remains a major challenge to remove highly mobile trace organic contaminants from stormwater due to their low sorption tendency[9,10]. The synergistic combination of biochar and persulfate holds promise for stormwater purification because (i) trace organic compounds may sorb onto the carbonaceous material and (ii) highly reactive species formed upon persulfate activation through biochar may react with trace organic compounds.

1.5 Objectives and approach

The objective of this dissertation was to investigate persulfate activation by biochar for organic contaminant removal from water (i) in the presence of dissolved iron under acidic conditions and (ii) in metal-free systems at circumneutral pH. To this end, laboratory batch experiments were conducted to study the transformation of selected organic compounds in different water matrices, including pure water, synthetic water, and real water. The specific goals of this work were:

1. To investigate the major reactive species formed during the activation of persulfate by biochar and Fe(III) to remove organic contaminants in different water matrices, using carefully selected probe compounds and scavengers as well as rigorous competition kinetics calculations.

2. To gain insights into the role of biochar pyrolysis conditions and ash amendments to the feedstock on the reduction of Fe(III), activation of persulfate, and organic contaminant removal in the biochar/Fe(III)/persulfate system.

3. To assess the applicability of biochar and persulfate for the removal of different organic contaminants from urban stormwater with focus on reactive species formation and the impact of water matrix constituents on treatment performance.

Chapter 2 addresses the question of whether non-radical or radical species are formed in the biochar/Fe(III)/persulfate system and investigates the effects of water matrix components on the formation of reactive species by using different scavengers and probe compounds based on competition kinetics calculations. A biochar produced from beech wood at 450°C was successfully employed in laboratory batch experiments to activate persulfate in the presence of Fe(III) at pH 2.5 to degrade an organic model compound, the insect repellent *N,N*-diethyl-*m*-toluamide (DEET) in pure water, a synthetic water, and a surface water.

Chapter 3 focuses on the effects of biochar pyrolysis conditions and ash amendments to the feedstock on Fe(III) reduction and persulfate activation for DEET removal in the biochar/Fe(III)/persulfate system. Eight biochars were employed in laboratory batch experiments, four of which were produced from beech wood at different pyrolysis temperatures and four from softwood sawdust with different ash amendments during pyrolysis. The biochars were compared for their efficiency to remove DEET from water in the presence of persulfate and Fe(III) at pH 2.5. The performance of the biochars was discussed in terms of biochar characteristics, particularly the redox-active properties.

Chapter 4 investigates the treatment efficiency of biochar and persulfate for the removal of a range of organic contaminants from stormwater and the effect of water matrix components on the treatment performance. Laboratory batch experiments were conducted using a shrimp shell biochar pyrolyzed at 750°C to activate persulfate for the removal of 11 selected organic compounds from pure water, a synthetic water matrix, and street runoff. Using a set of probe compounds and scavengers, the major reactive species were examined and the reactivity of different organic contaminants was evaluated based on quantitative structure–activity relationships.

Chapter 5 is a general conclusion section, where open questions and directions for future research are discussed.

Chapter 2

Effect of the water matrix on formation of reactive species during persulfate activation by biochar and iron

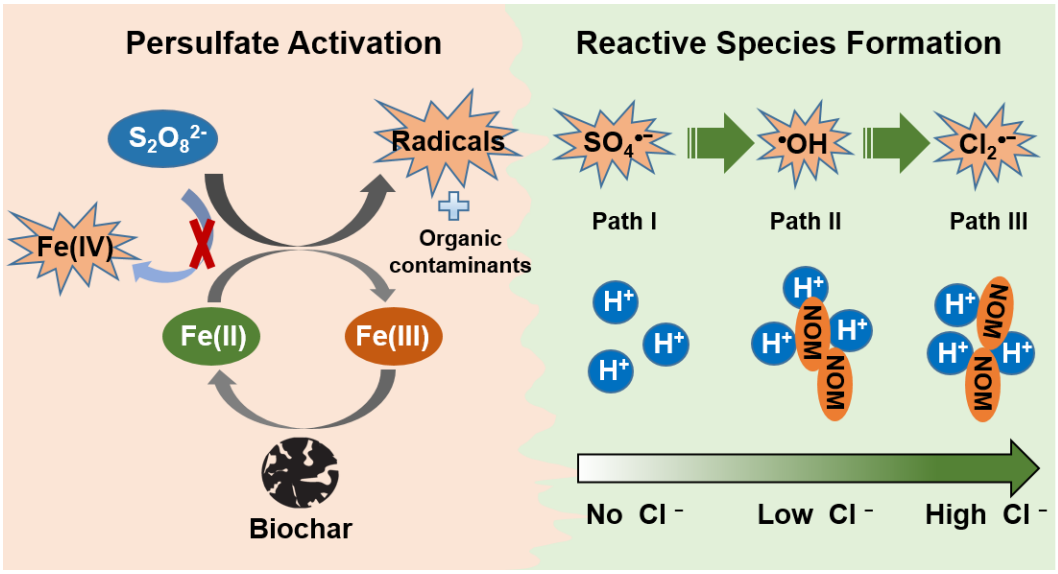

Yiling Zhuang, Stephanie Spahr, Holger V. Lutze, Christoph J. Reith, Nikolas Hagemann, Andrea Paul, Stefan B. Haderlein. Submitted to *Water Research*.

Y. Zhuang: designed and conducted the experiments, analyzed data, produced all figures, wrote and revised the manuscript; S. Spahr: supervised the project, contributed to the experimental design and discussion of the results, revised the manuscript; H. V. Lutze: contributed to the experimental design and discussion of results, revised the manuscript; C. J. Reith: contributed to the development of batch experiments and helped to conduct batch experiments during master thesis, performed electrochemical measurements and the corresponding data analysis, and revised the manuscript; N. Hagemann: provided the biochar sample, conducted the biochar electrical conductivity measurements, revised the manuscript; A. Paul: performed continuous X-band electron spin resonance (ESR) spectra measurements and the corresponding data analysis, revised the manuscript; S. B. Haderlein: supervised the project, contributed to the experimental design and discussion of the results, revised the manuscript.

Abstract

Fenton-like processes using persulfate for oxidative water treatment and contaminant removal can be enhanced by the addition of redox-active biochar, which accelerates the reduction of Fe(III) to Fe(II) and increases the yield of reactive species that react with organic contaminants. However, available data on the formation of non-radical or radical species in the biochar/Fe(III)/persulfate system are inconsistent, which limits the evaluation of treatment efficiency and applicability in different water matrices. Based on competition kinetics calculations, we employed different scavengers and probe compounds to systematically evaluate the effect of water matrix components, particularly chloride, on the formation of major reactive species in the biochar/Fe(III)/persulfate system for the removal of *N,N*-diethyl-*m*-toluamide (DEET) as a model compound. We show that the transformation of methyl phenyl sulfoxide (PMSO) to methyl phenyl sulfone ($PMSO_2$) cannot serve as a reliable indicator for Fe(IV), as previously suggested, because sulfate radicals also induce $PMSO_2$ formation. In pure water, sulfate radicals were indeed the major reactive species in the biochar/Fe(III)/persulfate system. Low chloride concentrations (0.1 mM) shifted the major reactive species to hydroxyl radicals. Higher chloride concentrations (1 mM), as present in a mining-impacted acidic surface water, resulted in the formation of another reactive species, possibly $Cl_2^{\bullet-}$, and more efficient DEET degradation than in pure water. To tailor the application of this oxidation process, the water matrix must be considered as a decisive factor for reactive species formation and contaminant removal.

2.1 Introduction

Persulfate-based oxidation processes using peroxydisulfate ($S_2O_8^{2-}$, PDS) or peroxymonosulfate (PMS) for pollutant abatement have gained increasing interest in water treatment and environmental remediation[30,141,142]. PDS has advantages such as high stability during transport and storage, and the formation of highly reactive sulfate radicals ($SO_4^{\bullet-}$)[77,78], which can react to hydroxyl radicals (•OH) in presence of chloride or at high pH[143,144]. PDS can be activated by reduced transition metals such as Fe(II), which has been extensively studied as Fenton-like process[110,111,145]. However, the rapid depletion of dissolved Fe(II) during PDS activation, together with a low reduction rate of Fe(III) to Fe(II), and the accumulation of iron-containing sludge, severely limit the applicability of this Fenton-like process[110–112,145]. Previous studies have successfully applied redox-active biochars to catalytically activate PDS in the presence of Fe(III) under acidic conditions[113–116,146]. Biochar accelerated the reduction of Fe(III) to Fe(II), which activated PDS to reactive species for the removal of organic contaminants[113–116,146].

However, there are contrasting findings on the major reactive species formed in the biochar/Fe(III)/PDS system[113–116]. While some studies found evidence for radical-based processes, involving mainly $SO_4^{\bullet-}$[115,116], others reported indications of non-radical processes, particularly involving Fe(IV)[113,114]. Knowledge about the main reactive species is crucial already at an early stage of the development of a new oxidation process, such as the biochar/Fe(III)/PDS system, to identify suitable applications in terms of target contaminants as well as potential water matrix effects on treatment performance[121]. Identifying the major reactive species in oxidation processes is, however, challenging. Specialized instrumentation for direct measurements of short-lived reactive species is not readily available to most researchers[147–149]. Alternatively, probe compounds play a crucial role as specific indicators for reactive species[121,147,148,150], but must be selected and used with great care to avoid misinterpretation of the results. For instance, studies postulating the presence of Fe(IV) in the biochar/Fe(III)/PDS system are predominantly based on the

observed transformation of methyl phenyl sulfoxide (PMSO) to methyl phenyl sulfone ($PMSO_2$)[113,114]. There is, however, increasing concern about the use of PMSO as a specific probe compound for Fe(IV)[122,123,151], because the transformation of sulfoxide to sulfone is not specific to high-valent metal species[123] and there can be other pathways that promote $PMSO_2$ formation[122,123,151]. In persulfate-based processes, the role of $SO_4^{\bullet-}$ in $PMSO_2$ formation is still unclear.

Furthermore, little is known about the effects of water matrix components such as dissolved organic carbon (DOC) and major ions such as chloride (Cl^-) on the formation of reactive species in the biochar/Fe(III)/PDS system and how they affect contaminant removal in real waters. In principle, $SO_4^{\bullet-}$ react more substrate-specific than $^{\bullet}OH$, leading to a lower scavenging rate in real water matrices[30,121]. However, major water matrix components, especially Cl^-, can shift $SO_4^{\bullet-}$-based processes to $^{\bullet}OH$ or reactive chlorine species, depending on the Cl^- concentration and the presence of DOC and bicarbonate[143,144,152]. Such effects of DOC and Cl^- on the formation of reactive species have previously been demonstrated in homogeneous PDS systems in which PDS was activated by UV[143,153], heat[152,154], or alkaline conditions[152]. In the heterogeneous biochar/ Fe(III)/PDS system, the effect of DOC and Cl^- has so far only been studied on the removal of pollutants[113]. Systematic experimental evidence for the impact of water matrix components on reactive species formation is still lacking.

The objectives of this study were therefore (i) to identify the major reactive species in the biochar/Fe(III)/PDS system and (ii) to investigate the effects of water matrix components on reactive species formation and organic contaminant removal. To this end, we established a biochar/Fe(III)/PDS system that degraded an organic model compound, the insect repellent *N,N*-diethyl-*m*-toluamide (DEET) at pH 2.5. DEET, which is frequently detected in the aquatic environment, cannot be effectively removed by conventional water treatment[155,156] and was selected as representative of other similar alkyl aromatic compounds[157]. To determine the major reactive species formed in the biochar/Fe(III)/PDS system in the absence and presence of DOC and Cl^-, we employed a combination of scavengers and probe compounds. Furthermore, we showed the applicability of this heterogeneous oxidation process to a real water matrix.

2.2 Materials and Methods

A list of all chemicals including supplier and purity is provided in section S2.1 in the Supporting Information.

2.2.1 Biochar preparation

Biochar was produced in a PYREKA (Pyreg GmbH, Dörth, Germany) continuously operating screw reactor, which is described elsewhere[53]. Beech wood was used as feedstock and pyrolyzed at 450°C under N_2 atmosphere with a flow rate of 2 L min^{-1} and a residence time of 10 min. The biochar sample was ground to a particle size of < 200 µm using a ball mill (Figure S2.1) and stored in a desiccator until further use. For details on the biochar characterization see Section S2.2.

2.2.2 DEET degradation with biochar, Fe(III) and PDS in pure water

Batch experiments were performed at room temperature in 40 mL amber glass vials on an overhead shaker. 30 mg of biochar was added to 30 mL deionized water to prepare a suspension of 1 g biochar L^{-1}. The initial pH of the suspension was adjusted to 2.5 with 0.25 M H_2SO_4. DEET was added to the suspension from an aqueous 10 mM stock solution to reach a nominal concentration of 50 µM. After 30 min contact time, sorption of DEET on the biochar reached an apparent equilibrium (Figure S2.2) and the measured aqueous DEET concentration was taken as initial value. Subsequently, 60 µL of Fe(III) was added from a 0.05 M aqueous Fe(III) sulfate stock solution to reach an initial concentration of 0.2 mM, followed by excess PDS addition (240 µL) from a 1 M aqueous stock solution to obtain an initial, nominal PDS concentration of 8 mM. At predefined time points, 1 mL sample was withdrawn and mixed with 100 µL of pure methanol (2 M in the sample, ≈ 9% v/v) and 5.5 µL NaOH (10 mM in the sample, ≈ 1% v/v, pH > 11) to quench the reaction and precipitate iron. Samples were filtered through 0.22 µm PES syringe filters (BGB Analytik, Germany; 88.5 ± 0.7% DEET recovery) into 1.5 mL amber glass vials and stored in the dark at

4°C until DEET analysis. The pH was measured at the end of the experiment and remained constant at 2.5 ± 0.1. Control experiments were set up identically to assess the stability of DEET, sorption of DEET onto biochar, and reaction of DEET with (i) PDS, (ii) Fe(III), (iii) PDS and Fe(III), (iv) biochar and PDS, and (v) biochar and Fe(III). The experimental procedure is illustrated in Figure S2.3. To demonstrate the role of biochar for enhanced DEET transformation, we added three consecutive spikes of DEET (nominal concentration of 50 µM, each spike one hour apart) to the same 1 g biochar L^{-1} suspension containing 50 µM Fe(III) and 8 mM PDS. Samples were withdrawn at predefined time points for DEET analysis.

2.2.3 Effects of the water matrix on DEET removal and reactive species

Surface water impacted by past lignite mining activities was sampled in the Greifenhainer Fließ, a tributary of the Spree River (51°45'28.8"N 14°08'54.0"E, Brandenburg, Germany) in December 2021. The water sample was analyzed for pH, electrical conductivity, O_2 concentration, total and dissolved organic carbon, major ions such as Cl^- and SO_4^{2-}, as well as metals including iron species (see Section S2.16 and Table S2.3). DEET degradation experiments in acidic surface water followed the same procedure as described above, except that the pH of the 1 g biochar L^{-1} suspension was not adjusted, and no additional iron was added due to the low pH of 3.6 and high iron content (0.05 mM Fe(III)) of the surface water. Experiments in a synthetic water matrix containing 4.3 mg L^{-1} DOC (from Suwannee River humic acid) and 0.05 mM Fe(III) (from iron(III) sulfate) in the presence of 0.1 mM or 1 mM chloride also followed the procedure explained above.

2.2.4 Identification of reactive species using scavengers and probe compounds

Following the method suggested by Pestovsky et al.(2006)[158], 200 µM PMSO was added to a 1 g biochar L^{-1} suspension containing 0.2 mM Fe(III) and 8 mM PDS at pH

2.5. Batch experiments followed the procedure described above for DEET degradation. At predetermined time intervals, samples (1 mL) were withdrawn, quenched immediately with 100 µL of aqueous DMSO (2 M in samples, ≈ 9% v/v), and analyzed for PMSO and $PMSO_2$. Control experiments were conducted with 200 µM PMSO and only PS, only biochar, only Fe(III), and combinations thereof. To investigate whether $PMSO_2$ is formed during reaction of PMSO with $SO_4^{\bullet-}$, PDS was thermally activated at 60°C in the presence 200 µM PMSO and 20 mM *tert*-butanol (TBA), which was added to suppress formation of •OH (93% scavenged) from the reaction of $SO_4^{\bullet-}$ with small amounts of Cl^-[143]. To study the reaction of PMSO with reactive chlorine species, PDS was thermally activated at 60°C in the presence of 50 µM PMSO and 1 mM chloride. PMSO reacted with 95% of the $SO_4^{\bullet-}$ to form reactive chlorine species. Experimental details and competition kinetics calculations are shown in Section S2.11 and S2.12.

To investigate radical species in the biochar/Fe(III)/PDS system, we added different scavengers to a 1 g biochar L^{-1} suspension containing 50 µM DEET, 0.2 mM Fe(III), and 8 mM PDS. Methanol (300 mM final concentration) was added to completely scavenge > 99% of both $SO_4^{\bullet-}$ (k ($SO_4^{\bullet-}$) = 1.1 × 10^7 M^{-1} s^{-1} [159]) and •OH (k (•OH) = 9.7 × 10^8 M^{-1} s^{-1} [119]). TBA (10 mM final concentration) was employed to scavenge 96% of •OH (k (•OH)= 6.0 × 10^8 M^{-1} s^{-1} [119]) but only 14% of $SO_4^{\bullet-}$ (k ($SO_4^{\bullet-}$) = 8.0 × 10^5 M^{-1} s^{-1} [159]). Additionally, DEET degradation experiments were conducted in the presence of different TBA concentrations (10 – 1000 mM), all resulting in > 95% scavenging of •OH and 14% - 94% scavenging of $SO_4^{\bullet-}$. Calculations of the fractions that react with an oxidant are based on the principles of competition kinetics[160] and are described in Section S2.12. For competition kinetics experiments, 4-nitrobenzoic acid (*p*NBA) and 4-chlorobenzoic acid (*p*CBA) were added as probe compounds to a 1 g biochar L^{-1} suspension containing 0.2 mM Fe(III) and 8 mM PDS. Both *p*CBA and *p*NBA favor the reaction with radicals rather than Fe(IV)[161]. *p*NBA readily reacts with •OH (2.6 × 10^9 M^{-1} s^{-1} [119]) but has a low reactivity towards $SO_4^{\bullet-}$ (≤ 10^6 M^{-1} s^{-1} [120]). *p*CBA reacts quickly with both $SO_4^{\bullet-}$ (3.6 × 10^8 M^{-1} s^{-1} [120]) and •OH (5 × 10^9 M^{-1} s^{-1} [119]). The competition kinetics approach can indicate the

major reactive species present. For instance, hardly any degradation of *p*NBA together with the degradation of a high fraction of *p*CBA would be indicative of a $SO_4^{\bullet-}$-based process[143]. The ratio of the first order degradation kinetics was obtained as the slope in a plot of $\ln(c/c_0)$ (*p*CBA) vs. $\ln(c/c_0)$ (*p*NBA)[143,160]. A $SO_4^{\bullet-}$-based oxidation process is characterized by a very small slope, while an $^{\bullet}OH$-based oxidation process leads to a theoretical slope of *k* ($^{\bullet}OH$ + *p*NBA)/*k* ($^{\bullet}OH$ + *p*CBA) of 0.52[119] (for further details on this methodology see Lutze et al.[143]). Both probe compounds were added in low concentrations (4 µM for experiments in pure water and 5 µM for experiments in real water matrix) to ensure less than 10% scavenging of $^{\bullet}OH$ and $SO_4^{\bullet-}$ by the probe compounds. A sorption control containing only *p*CBA, *p*NBA, and biochar was conducted to correct the transformation rates of *p*CBA and *p*NBA for sorption (Section S2.13, Figure S2.15). A control containing only *p*CBA, *p*NBA, and PDS showed no transformation of the probe compounds in the reaction time (Figure S2.16).

2.2.5 Analytical methods

High performance liquid chromatography (HPLC) analyses

The concentrations of DEET, PMSO, $PMSO_2$, *p*CBA, and *p*NBA were quantified by HPLC (1200 Series, Agilent) with UV-vis detection at 210 nm for DEET, 230 nm for PMSO, 215 nm for $PMSO_2$, 234 nm for *p*CBA, and 262 nm for *p*NBA. Aqueous samples were analyzed using an Agilent ZORBAX Eclipse XDB-C18 column (4.6 mm x 150 mm, 5 µm) and a ZORBAX Eclipse XDB-C18 guard cartridge. For DEET analysis, 10 µL of sample was injected and the eluent mixture consisted of 60% methanol and 40% water (pH 3, 1 mM H_2SO_4) at a flow rate of 0.5 mL min^{-1}. Concentrations were quantified by external calibration from 2 to 100 µM. For PMSO and $PMSO_2$ analysis, 20 µL of sample was injected and the mobile phase consisted of 75% water with 1% formic acid and 25% acetonitrile with a flow rate of 0.5 mL min^{-1}. PMSO and $PMSO_2$ concentrations were quantified by external calibration from 1 to 250 µM and 0.5 to 125 µM, respectively. Analysis of *p*CBA and *p*NBA was carried out by injecting 50 µL of sample with an eluent mixture of 70% methanol and 30% water (pH 3, 1 mM H_2SO_4)

at a flow rate of 0.5 mL min^{-1}. Concentrations were quantified by external calibration from 0.025 to 5 µM.

Data evaluation

Pseudo-first order rate constants (k_{obs}) and half-life times ($t_{1/2}$) were calculated according to eq. (1) and eq. (2), respectively:

$$\ln\frac{c_t}{c_0} = -k_{obs} \cdot t \quad (1)$$

$$t_{1/2} = \frac{\ln 2}{k_{obs}} \quad (2)$$

where c_t is the concentration of the analyte at time t and c_0 is the initial analyte concentration in the biochar suspension after 30 min sorption equilibrium.

The fraction of a reactive species, f, reacting with a certain compound in competition with other substrates can be calculated with the corresponding known concentrations and reaction rate constants[143,154]. The fraction corresponds to the concentration ($c_{compound}$) times the reaction rate constant ($k_{compound}$) of the compound at study, divided by the sum of the concentrations (c_1, c_2 to c_n) times the reaction rate constants (k_1, k_2 *to* k_n) of all substrates that can react with the reactive species according to eq. (3):

$$f = \frac{c_{compound} \cdot k_{compound}}{c_{compound} \cdot k_{compound} + c_1 \cdot k_1 + c_2 \cdot k_2 + \cdots + c_n \cdot k_n} \quad (3)$$

2.3 Results and discussion

2.3.1 DEET degradation by PDS activation with biochar and Fe(III)

As shown in Figure 2.1a, DEET was efficiently degraded in the presence of biochar, Fe(III), and PDS resulting in 88 ± 3% DEET removal within two hours. DEET degradation followed pseudo-first order kinetics with a k_{obs} of (2.9 ± 0.1) × 10^{-4} s^{-1} (Figure S2.4) and a half-life time of 39 ± 4 min. In control batches with PDS only, biochar only, Fe(III) only, and combinations thereof, DEET removal was much less efficient (<5.5 – 29%, Figure 2.1a). Our results agree with previous studies also

reporting enhanced contaminant removal in the presence of biochar, Fe(III), and PDS using sulfamethoxazole or bisphenol A as model compounds[113–116]. The accelerated DEET degradation in the biochar/Fe(III)/PDS system indicates biochar-mediated Fe(III) reduction leading to continuous PDS activation upon reaction with Fe(II) as reported previously[113–116].

We compared the degradation of DEET in the heterogeneous biochar/Fe(III)/PDS system with DEET degradation in a homogeneous Fe(II)/PDS reference system, both containing 8 mM PDS but different concentrations of Fe(III) and Fe(II), respectively (Figure 2.1b). In the Fe(II)/PDS system, DEET removal within two hours reaction time increased with increasing Fe(II) to PDS ratios from 1:160 to 1:16, corresponding to Fe(II) concentrations of 0.05 mM to 0.5 mM, respectively. To achieve 87% DEET degradation in the homogeneous reference system, 0.5 mM Fe(II) had to be applied with 8 mM PDS (Fe(II) to PDS ratio of 1:16). In the biochar/Fe(III)/PDS system, in contrast, 86% DEET degradation was already obtained by adding 0.1 mM Fe(III), corresponding to an Fe(III) to PDS ratio of 1:80 (Figure 2.1b). While dissolved Fe(II) can activate PDS in the homogeneous Fe(II)/PDS system, high input of Fe(II) is required due to rapid Fe(II) depletion and formation of Fe(III), which is only slowly reduced to Fe(II) by PDS (6.6×10^{-2} M^{-1} s^{-1})[111,112,162].

Efficient DEET degradation in biochar suspensions with sub-stoichiometric Fe(III) to PDS addition indicates biochar-mediated enhanced Fe(III) reduction to Fe(II), which reacts with PDS. The Fe(III) formed can in turn be reduced back to Fe(II) by biochar. In fact, the biochar used here successfully reduced Fe(III) to Fe(II) (Figure S2.5) due to its redox-active properties. The biochar possessed a high electron donating capacity (EDC, 413 ± 22 µmol e^- (g biochar)$^{-1}$, Table S2.1), which is in the same order of magnitude as other biochars[58]. The biochar also contained a high concentration of persistent free radicals (PFR, $(3.50 \pm 0.40) \times 10^{19}$ spins (g biochar)$^{-1}$, Table S1), i.e. moieties with unpaired electrons that can contribute to the EDC[68,163] and were suggested to directly activate PDS[68,69,124].

The addition of biochar to the Fe(II)/PDS system markedly increased the DEET degradation rate, indicating the role of biochar for Fe(III)/Fe(II) cycling (Figure S2.6).

Further evidence for accelerated iron cycling was obtained from adding three consecutive spikes of DEET (50 µM each, 60 min apart) to the same 1 g L^{-1} biochar suspension containing 50 µM Fe(III) and 8 mM PDS (Figure S2.7). After three hours, 61% of the added 150 µM DEET was removed, exceeding the present Fe(III) concentration by a factor of 1.8. In another experiment, the degraded DEET (739 µM) exceeded the Fe(III) present (200 µM) by a factor of 3.7 (Figure S2.8). The here used biochar thus enhanced Fe(III) reduction and facilitated PDS activation, as suggested by other studies[113–116], leading to the generation of reactive species and DEET degradation.

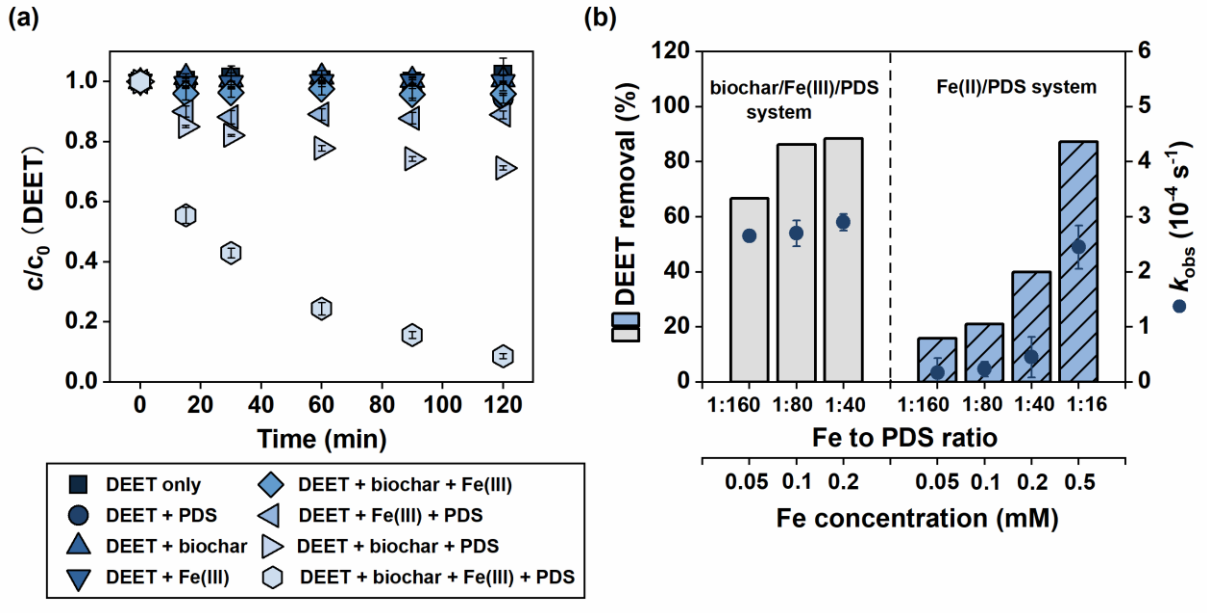

Figure 2.1. (a) DEET removal in the biochar/Fe(III)/PDS system and corresponding control experiments with DEET only, DEET and PDS, DEET and biochar, DEET and Fe(III), and combinations thereof. [Biochar] = 1 g L^{-1}, [Fe(III)] = 0.2 mM, [PDS] = 8 mM, $[DEET]_0 = c_0$ ~ 40 µM after sorption equilibrium, c = measured DEET concentration over time, pH 2.5. (b) DEET removal in the biochar/Fe(III)/PDS system (grey, solid bars) and the Fe(II)/PDS reference system (blue, patterned bars) at different molar Fe to PDS ratios and corresponding pseudo-first order rate constants (k_{obs}). [Fe(III)] = 0.05 - 0.2 mM for biochar/Fe(III)/PDS system, [Fe(II)] = 0.05 - 0.5 mM for Fe(II)/PDS system, [PDS] = 8 mM, $[DEET]_0$ ~ 40 µM, pH 2.5, reaction time = 2 h. Error bars indicate the standard deviation of triplicate experiments.

2.3.2 Identification of reactive species in the biochar/Fe(III)/PDS system

Fe(IV) species

PMSO has been postulated as a specific probe compound to determine the presence of Fe(IV), as it reacts with the latter via a 2-electron transfer step to form a characteristic sulfone product, $PMSO_2$[158]. Figure 2.2a shows PMSO transformation to $PMSO_2$ in the biochar/Fe(III)/PDS system. Within two hours, PMSO was completely oxidized following pseudo-first order kinetics with a reaction rate constant of (3.2 ± 0.2) × 10^{-4} s^{-1} (Figure S2.9). The yield of $PMSO_2$ (i.e., mole of $PMSO_2$ formed per mole of PMSO transformed) was 62%. Tang et al. (2023) and Liang et al. (2021) reported a similar conversion of PMSO to $PMSO_2$ (yields between 40 and 63%) in the presence of low pyrolysis temperature biochars (< 500°C), Fe(III), and PDS[113,114]. Both studies concluded that Fe(IV) was present[13,114]. However, there is increasing concern about the selectivity of PMSO as a specific probe compound for Fe(IV)[122,123,151]. Lei et al (2023) reported that PMS itself can transform PMSO to $PMSO_2$[122]. Chen et al (2023) revealed that oxidation products of PMSO, formed via the reaction with •OH, can enhance $PMSO_2$ formation in the homogeneous Fenton reaction due to complexation of the PMSO oxidation products with Fe(III)[123].

Originally, PMSO was used to distinguish •OH and Fe(IV)[158,164]. The PMSO transformation products indicative for the presence of •OH were defined as methanesulfinic acid and formaldehyde, whereas the reaction of PMSO with Fe(IV) formed $PMSO_2$[158,164]. Whether PMSO can be used in a similar way to distinguish between $SO_4^{\bullet-}$ and Fe(IV) has not been well investigated. In a clean $SO_4^{\bullet-}$-based reaction system, in which PDS was activated by heat and •OH formation was suppressed by addition of TBA, PMSO was also transformed to $PMSO_2$ with 21% yield (Figures 2.2b and S2.10). No self-decomposition of PMSO was observed through heat (Figure S2.11) and PDS alone did not convert PMSO to $PMSO_2$ (Figure S2.12). Thus, in $SO_4^{\bullet-}$-based oxidation systems, PMSO cannot serve as a unique indicator for Fe(IV).

Yao et al (2022) found similar results for thermal activation of PMS at 60°C, which resulted in a $PMSO_2$ yield of 100%[151]. This much higher $PMSO_2$ yield might be due to the ability of PMS itself to transform sulfoxide to sulfone with considerable rate constants[122]. Contrary results were reported by Wang et al (2018), who found that $SO_4^{\bullet-}$ oxidized PMSO to biphenyl compounds rather than $PMSO_2$ during PDS activation by UV[102]. However, the addition of HCl for pH adjustment likely shifted the reactive species formed from $SO_4^{\bullet-}$ to HO• or reactive chlorine species[143,165–167] both of which do not transform PMSO into $PMSO_2$ as show in Figure S2.13 and other studies[158,164,168]. Consequently, studies employing PMSO and $PMSO_2$ to distinguish Fe(IV) from $SO_4^{\bullet-}$ need to be carefully reassessed.

The higher $PMSO_2$ formation in the biochar/Fe(III)/PDS system (Figure 2.2a) compared to the heat/PDS system (Figure 2.2b) is likely due to the continuous reduction of Fe(III) to Fe(II), leading to PDS activation and formation of $SO_4^{\bullet-}$. Although we cannot strictly rule out the formation of Fe(IV), our results suggest that $SO_4^{\bullet-}$ are the predominant reactive species in the biochar/Fe(III)/PDS system.

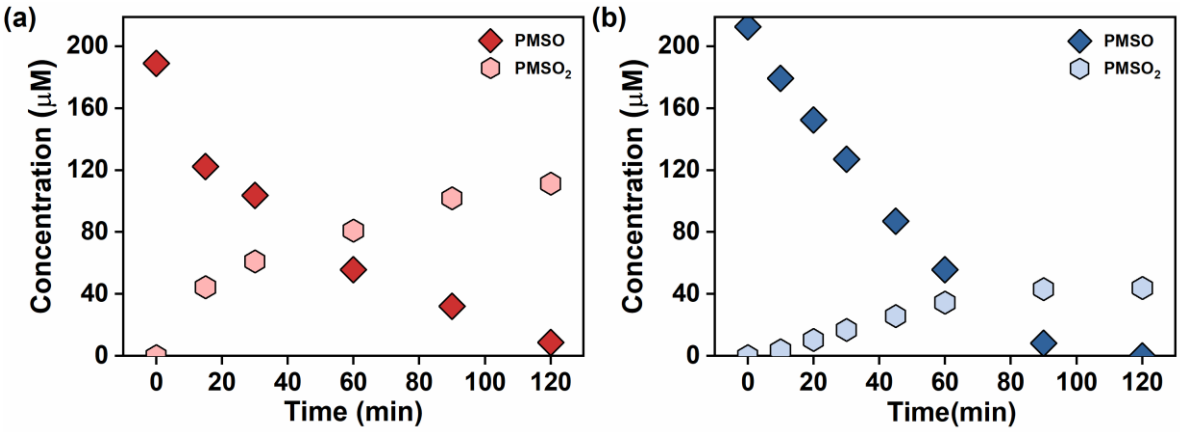

Figure 2.2. (a) PMSO transformation and $PMSO_2$ formation in the biochar/Fe(III)/PDS system. [Fe(III)] = 0.2 mM, [Biochar] = 1 g L^{-1}, [PDS] = 8 mM, $[PMSO]_{0,\ after\ 30min\ sorption}$ = 189 μM, pH 2.5. (b) PMSO transformation and $PMSO_2$ formation in the heat/PDS control system. [PDS] = 8 mM, [PMSO] = 200 μM, [TBA] = 20 mM, pH 2.5, 60°C in a water bath.

Radical species

To further elucidate which reactive species were present in the biochar/Fe(III)/PDS system, we investigated DEET removal in the presence of two scavengers, namely methanol and TBA. Note that competition kinetics calculations, as discussed in Section S2.12, are pivotal for a valid design and interpretation of scavenger experiments based on the fraction of reactive species scavenged. TBA, which solely scavenged $^{\bullet}OH$ at the applied dosages (96% scavenging of $^{\bullet}OH$ and 14% scavenging of $SO_4^{\bullet-}$), had no effect on DEET degradation. Methanol, which scavenged > 99% of both $SO_4^{\bullet-}$ and $^{\bullet}OH$, completely stopped the reaction (Figure 2.3a). These observations indicate that $SO_4^{\bullet-}$ are the dominant reactive species in the biochar/Fe(III)/PDS system. The involvement of $SO_4^{\bullet-}$ was further verified by performing DEET degradation experiments in the presence of varying TBA concentrations from 10 mM to 1 M, resulting in an increased fraction of $SO_4^{\bullet-}$ scavenged from 14% to 94% (for detailed calculations see Section S2.12). With increasing TBA concentration, DEET degradation was increasingly inhibited (Figure S2.14), suggesting a $SO_4^{\bullet-}$-based oxidation process. In a purely $^{\bullet}OH$-based process, the scavenging effect would already be observed at TBA doses well below 10 mM.

To validate the formation of $SO_4^{\bullet-}$ as major reactive species in the biochar/Fe(III)/PDS system, we employed *p*CBA and *p*NBA as probe compounds and conducted competition kinetics experiments. From the sorption-corrected competition kinetics plot in Figure 2.3b, a nearly horizontal line was obtained, because hardly any *p*NBA was degraded, while *p*CBA was degraded to a large extent. These results clearly indicate that $SO_4^{\bullet-}$ are the major reactive species in the biochar/Fe(III)/PDS system, in agreement with the scavenger experiments. The steady-state concentration of sulfate radicals $[SO_4^{\bullet-}]_{ss}$ was determined to be 2.69×10^{-11} M using *p*CBA as probe compound (Section S2.15 and Figure S2.17). It is noteworthy that *p*NBA and *p*CBA will hardly be reactive towards Fe(IV)[161].

Previous studies on the biochar/Fe(III)/PDS system collectively reported PDS activation by accelerated Fe(III) reduction to Fe(II) but did not provide a coherent

picture concerning the reactive species involved[113–116]. Liang et al.[113] and Tang et al.[114] reported an Fe(IV)-based non-radical pathway for the degradation of sulfamethoxazole and phenanthrene, respectively. Wang et al.[115] and Zeng et al.[116] proposed radical pathways, involving $SO_4^{\bullet-}$ and $O_2^{\bullet-}$, respectively, for target compound transformation. This could be due to different biochars giving rise to different reactive species, or to inconclusive interpretation of results from scavenger or probe compound experiments. Concentrations of scavengers and probe compounds used to diagnose reactive species should be carefully chosen by competition kinetics calculations taking into account all water matrix components with their known reaction rate constants[121,169] as shown exemplarily in Section S2.12. Caution should be advised if scavengers or probe compounds do not react selectively or form secondary reactive species or unidentified products. Moreover, the addition of chemicals (e.g. for pH adjustment) has to be carefully evaluated to avoid changes in the reaction kinetics or shifts in reactive species.

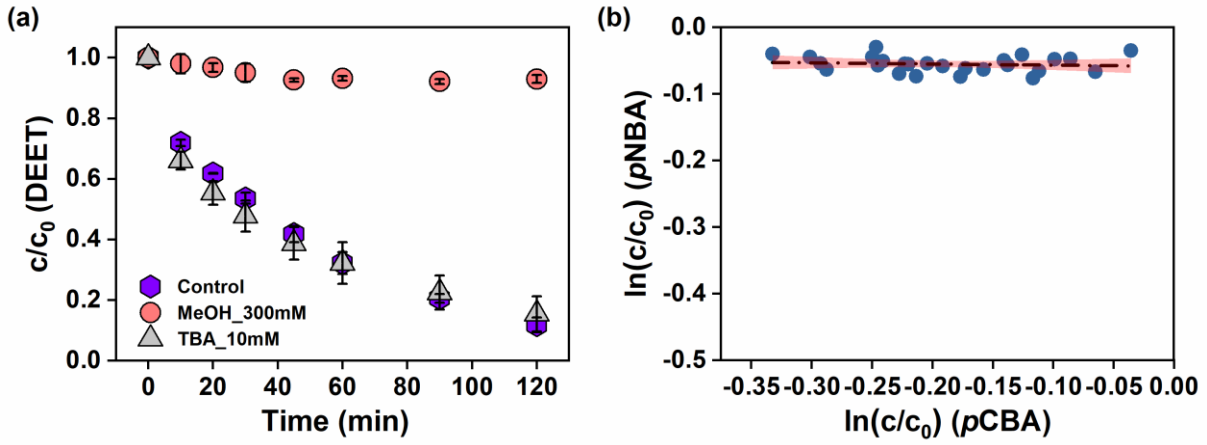

Figure 2.3. (a) DEET degradation over time in the biochar/Fe(III)/PDS system in the absence (control) and presence of 300 mM methanol and 10 mM *tert*-butanol (TBA). [Biochar] = 1 g L^{-1}, [Fe(III)] = 0.2 mM, [PDS] = 8 mM, $[DEET]_0 = c_0 \sim 40$ µM, pH 2.5; (b) Sorption-corrected competition plot $\ln(c/c_0)$ of *p*CBA vs. *p*NBA in the biochar/Fe(III)/PDS system (slope -0.017 ± 0.031; intercept -0.058 ± 0.006). [Biochar] = 1 g L^{-1}, [Fe(III)] = 0.2 mM, [PDS] = 8 mM, $[pCBA]_{0,\text{after 30min sorption}}$ = 1.5 µM; $[pNBA]_{0,\text{ after 30min sorption}}$ = 1.7 µM, pH 2.5. Red areas show the 95% confidence intervals of the linear fit.

2.3.3 Effects of the water matrix on reactive species formation and DEET degradation

A biochar concentration of 1 g L^{-1} together with 8 mM PDS was applied to degrade 50 µM DEET in lignite mining-impacted surface water with a low pH of 3.6 and a Fe(III) concentration of 0.05 mM. DEET was almost completely degraded after two hours (Figure S2.18a). DEET disappearance in the acidic surface water followed pseudo-first order kinetics (Figure S2.18b) with a k_{obs} of (4.2 ± 0.1) × 10^{-4} s^{-1}. This value is approximately 1.5-times greater than the degradation rate constant obtained from experiments in ultrapure water containing 0.2 mM Fe(III) at pH 2.5 (Figure S2.4). The water matrix thus did not inhibit DEET transformation, but rather enhanced the removal of DEET, possibly due to the formation of reactive species other than sulfate radicals.

To investigate the major reactive species formed in this surface water matrix, *p*NBA and *p*CBA were employed in analogy to the competition degradation experiment shown in Figure 2.3b. The competition plot of $\ln(c/c_0)$ (*p*CBA) vs. $\ln(c/c_0)$ (*p*NBA) shown in Figure 2.4a yielded a slope of 0.8 ± 0.01. This slope is neither indicative for a $SO_4^{\bullet-}$-based process (leading to hardly any correlation), nor for an $^{\bullet}OH$-based process (leading to a slope of 0.52)[143]. Water matrix constituents likely converted the $SO_4^{\bullet-}$-based process to an oxidation process governed by reactive species other than $SO_4^{\bullet-}$ or $^{\bullet}OH$. Table S2.3 shows that the mining-impacted surface water contained approximately 1 mM of Cl^- (31 mg L^{-1}). Cl^- reacts rapidly with $SO_4^{\bullet-}$ (k = 2.88 × 10^8 M^{-1} s^{-1}) to form chlorine atoms ($Cl^{\bullet}$), which can further react to other reactive species such as dichlorine radical anions ($Cl_2^{\bullet-}$)[143,167].

To test the impact of Cl^- on the formation of reactive species in the biochar/Fe(III)/PDS system, we conducted competition kinetics experiments with *p*NBA and *p*CBA in a synthetic water matrix simulating the surface water characteristics (pH 3.6, 0.05 mM Fe(III), 4.3 mg L^{-1} DOC as Suwannee River humic acid) in the presence of 1 mM Cl^-. The competition plot in the synthetic water matrix (Figure 2.4b) showed the same slope as obtained from the real mining-impacted surface water (Figure 2.4a). This observation suggests that Cl^- caused the shift from

$SO_4^{\bullet-}$ to potentially chlorine radical species.

Cl^- can react with $SO_4^{\bullet-}$ to form $Cl^\bullet$ (reaction (1) in Table 2.1), which in turn can react with H_2O to form $HOCl^{\bullet-}$ and eventually $^\bullet OH$ (see Lutze et al.[143] for all reactions involved in the oxidation of Cl^-). In fact, an additional experiment with *p*NBA and *p*CBA in the same synthetic water matrix but low Cl^- concentration of 0.1 mM suggested an $^\bullet OH$-based oxidation process (Figure S2.19). At a low Cl^- concentration of 0.1 mM, the contribution of Cl^- to the overall $SO_4^{\bullet-}$ scavenging was calculated to be 44%, and the remaining 56% is contributed by DOC (Section S2.18).

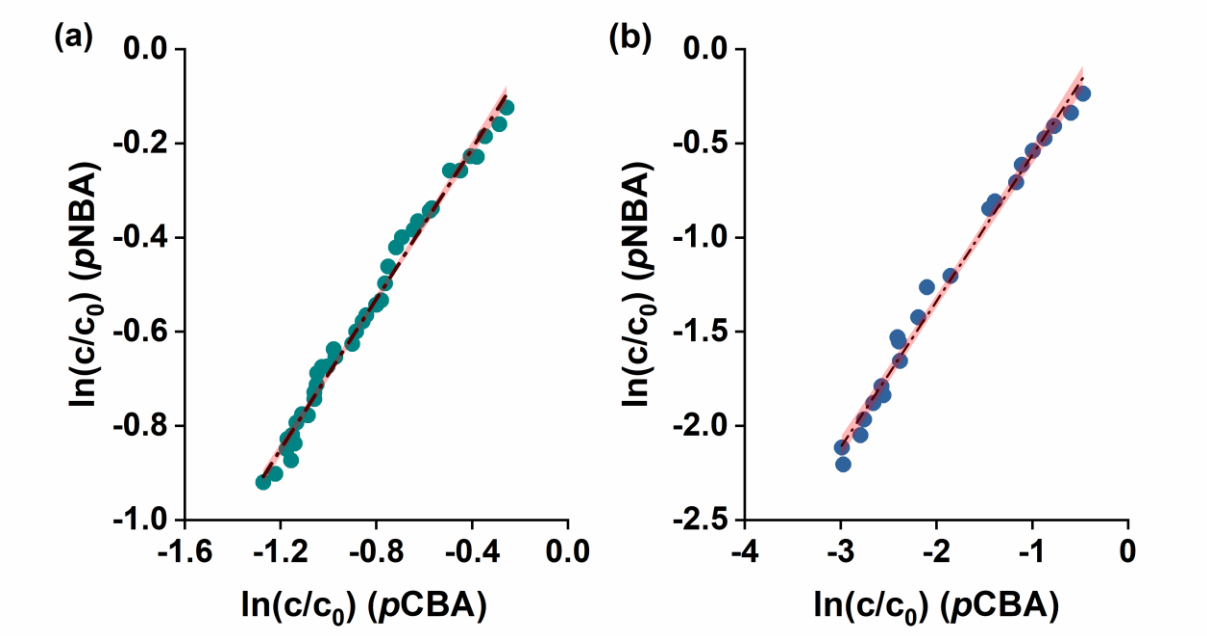

Figure 2.4. (a) Sorption-corrected competition plot $\ln(c/c_0)$ of *p*CBA vs. *p*NBA in mining-impacted surface water (pH 3.6) containing 0.05 mM Fe(III), 1mM Cl^-, and other constituents (Table S3) (slope 0.8 ± 0.01; intercept 0.11 ± 0.01). [Biochar] = 1g L^{-1}, [PDS] = 8 mM, $[pCBA]_{0,\text{ after 30min sorption}}$ = 1.64 µM; $[pNBA]_{0,\text{ after 30min sorption}}$ = 2.31 µM. The reaction was initiated by adding PDS after 30 min sorption. (b) Sorption-corrected competition plot $\ln(c/c_0)$ of *p*CBA vs. *p*NBA in synthetic water containing 4.3 mg/L DOC (Suwannee River humic acid) and 1 mM Cl^- (slope 0.8 ± 0.02; intercept 0.2 ± 0.03). [Biochar] = 1 g L^{-1}, Fe(III) = 0.05 mM, [PDS] = 8 mM, $[pCBA]_{0,\text{ after 30min sorption}}$ = 1.97 µM; $[pNBA]_{0,\text{ after 30min sorption}}$ = 2.55 µM, pH 3.6 (adjusted with H_2SO_4). Red areas show the 95% confidence intervals of the linear fit.

At a higher Cl^- concentration of 1 mM and low pH as present in the surface water, a significant amount of $Cl^\bullet$ may react with Cl^- to form $Cl_2^{\bullet-}$ according to reaction (4) in Table 2.1. The scavenging of $SO_4^{\bullet-}$ and $^\bullet OH$ was mainly driven by Cl^- (≈ 90%, reactions (1), (2), (3) in Table 2.1, for calculations see Section S2.18) to form $Cl^\bullet$. With excess Cl^-, the scavenging of $Cl^\bullet$ by Cl^- competes with the reaction forming $^\bullet OH$ (see Lutze et al.[143]), resulting in the formation of $Cl_2^{\bullet-}$ (reaction (4)). At low pH values (< 4), the formation of $Cl_2^{\bullet-}$ is favored compared to neutral conditions[143,165,166]. The rate constant of $Cl_2^{\bullet-}$ formation (reaction (4)) depends on both the concentration of Cl^- and H^+ and can be calculated using the rate constants of reactions (2) and (3)[170], which can predict the major reactive species of radical-based oxidation processes at different conditions. While it was beyond the scope of this study to identify the reactive chlorine species, also Fang et al. suggested $Cl_2^{\bullet-}$ as predominant reactive species in a PDS-based oxidation process in the presence of high Cl^- concentrations (up to 100 mM)[144]. Although $Cl_2^{\bullet-}$ is less reactive than $SO_4^{\bullet-}$, it reacts preferentially with compounds having electron-rich moieties such as tertiary amine moieties, as present in DEET[171].

Table 2.1 Reactions involved in the oxidation of Cl^- with corresponding second order reaction rate constants and references.

No.	Reaction	Second order reaction rate constant (k / M^{-1} s^{-1})	Ref.
(1)	$SO_4^{\bullet-} + Cl^- \rightarrow Cl^\bullet + SO_4^{2-}$	2.7×10^8	167
(2)	$^\bullet OH + Cl^- \rightarrow HOCl^{\bullet-}$	4.3×10^9	170
(3)	$HOCl^{\bullet-} + H^+ \rightarrow Cl^\bullet + H_2O$	2.1×10^{10}	170
(4)	$Cl^\bullet + Cl^- \rightarrow Cl_2^{\bullet-}$	8×10^9	172

2.4 Implications for water treatment

Knowledge of the major reactive species is critical for assessing the applicability and efficiency of any oxidation process used for water treatment. To analyze the types of reactive species and their exposure in the water matrix, probe compounds are widely employed[173–175]. However, inappropriate selection or use of probe compounds can compromise mechanistic insights and lead to overlooking reactive species or overestimating their contribution. In particular, studies on the use of PMSO as a specific indicator for the presence of Fe(IV) in persulfate-based oxidation systems need careful reassessment, as our study provides evidence that $PMSO_2$ is also formed via the reaction of PMSO with $SO_4^{\bullet-}$.

Based on a careful selection of probe compounds and scavengers and rigorous competition kinetics calculations, our study shows for the first time that water matrix components, especially chloride, shift the formation of reactive species in the heterogeneous biochar/Fe(III)/PDS system in both a synthetic and an actual water matrix. While $SO_4^{\bullet-}$ were the major reactive species at acidic conditions in ultra-pure water, low chloride concentrations (0.1 mM) resulted in an $^{\bullet}OH$-based process, and high chloride concentrations (1 mM) formed other reactive species, possibly $Cl_2^{\bullet-}$. In order to tailor this oxidation process to specific applications at full-scale, the effects of the water matrix on the formation of reactive species must be known. We demonstrate that the biochar/Fe(III)/PDS system can be successfully applied in a real water matrix to degrade the model compound DEET. However, the reactive species formed might be very different depending on the pH and composition of the treated water. Future studies should combine the evaluation of the degradation efficiency of the actual target pollutants with studies of the major reactive species, which may also help to assess the unintentional formation of by-products or transformation products.

Acknowledgement

This work was funded by the China Scholarship Council (CSC, File No. 201904910454). We thank Claudia Schmalsch, Monika Hertel, Johanna Schlögl, and Guo-xiang Li for support in the laboratory, Tobias Goldhammer and Thomas Rossoll for providing and analyzing the surface water sample, and Viola Bartsch and Jannis Grafmüller of Ithaka for conductivity measurements.

Supporting Information to

Chapter 2

S2.1 Chemicals

All chemicals in this study were used as received. Sodium persulfate (PDS, $Na_2S_2O_8$, ≥ 99% for analysis EMSURE®), methanol (MeOH, HPLC grade ≥ 99.9%), 2,2'-azino-bis(3-ethylbenzothiazoline-6-sulfonic acid) diammonium salt (ABTS, ≥ 98.0%), formic acid (eluent additive for LC/MS, Fluka®), *tert*-butanol (TBA, ≥ 99.0%), 4-nitrobenzoic acid (*p*NBA, ≥ 98.0% for HPLC), and 4-chlorobenzoic acid (*p*CBA, 99% for HPLC) were purchased from Sigma-Aldrich. Sulfuric acid (H_2SO_4, 95-97 % for analysis EMSURE®), sodium hydroxide solution (NaOH, 1 M, TitriPUR®), potassium chloride (KCl, for analysis EMSURE®), monopotassium phosphate (KH_2PO_4, for analysis EMSURE®), sodium chloride (NaCl, for analysis EMSURE®), and iron(II) sulfate heptahydrate ($FeSO_4 \cdot 7\ H_2O$, 99.5-102.0% for analysis EMSURE®) were purchased from Merck. 3-(2-pyridyl)-5,6-diphenyl-1,2,4-triazine-p,p'-disulfonic acid, disodium salt hydrate (ferrozine, 97+%, ACROS Organics™), ammonium acetate (98+%, ACROS Organics™), methyl phenyl sulfoxide (PMSO, 98+%), and dimethyl sulfoxide (DMSO, >99.5%) were purchased from Fisher Scientific. Iron(III) sulfate hydrate ($Fe_2(SO4)_3 \cdot H_2O$, 21-23% Fe basis puriss. p.a.) was purchased from Fluka. *N,N*-diethyl-*m*-toluamide (DEET, ≥ 98%) was purchased from Tokyo Chemical Industry (TCI). Methyl phenyl sulfone ($PMSO_2$, 98%) was purchased from Fluorochem. Acetonitrile (≥ 99.9% for HPLC, Chemsolute™) was purchased from Th. Geyer. Mn^{2+} in ZnS (100% manganese isotope ^{55}Mn with the nuclear spin of I = 5/2) was from Magnettech GmbH, Berlin. Suwannee River humic acid and Suwannee River standard fulvic acid were from the International Humic Substances Society (IHSS), St. Paul, MN, USA. *N,N*-bis(3-sulfonatopropyl)-4-4'-bipyridinium (zwitterionic viologen, ZiV) was synthesized in the lab and characterized by Fourier-transform infrared spectroscopy (FTIR), for details see [176]. Aqueous solutions were prepared with deionized water (18.1 MΩ x cm, Arium® Pro Water Purification System).

S2.2 Biochar characterization

S2.2.1 Size distribution

The biochar size distribution was determined by a Mastersizer 2000 (Malvern Inc., UK) coupled with a sample dispersion unit (Hydro 2000S, Malvern Inc., UK) using the wet sample mode. A 10 g biochar L^{-1} suspension was prepared and kept on the table shaker overnight to obtain a fully dispersed suspension before measurement. The sample was continuously stirred until measurement. A 15% obscuration bar was applied to ensure identical sample amounts between biochar samples added. Data quality was optimized by adjusting the stir speed to a residual of weight below 1%. Results show in Figure S2.1.

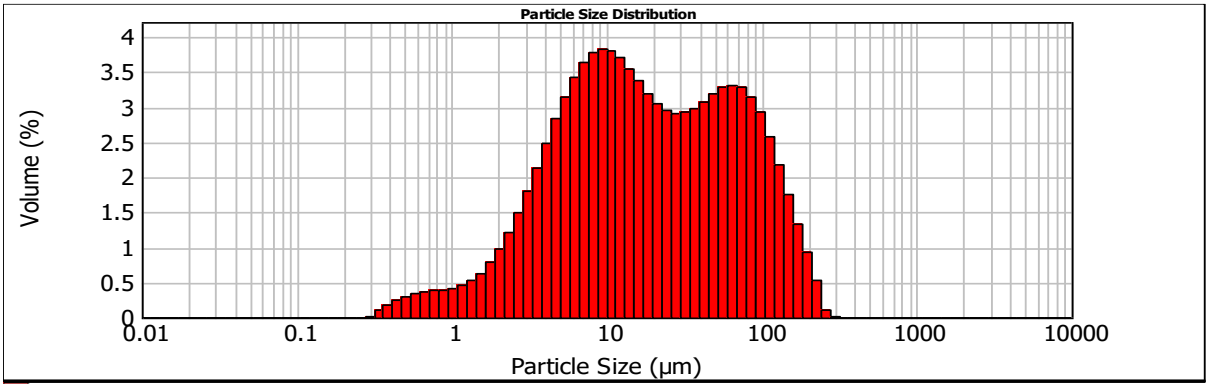

Figure S2.1. Biochar particle size distribution.

S2.2.2 Electron exchange capacity (EEC)

The electron exchange capacity (EEC), which is the sum of the electron accepting capacity (EAC) and electron donating capacity (EDC), was determined by mediated electrochemical reduction (MER) and mediated electrochemical oxidation (MEO) modified from the method reported by Klüpfel et al., 2014[58]. All analyses were conducted under anoxic conditions in a glovebox. A 10 g biochar L^{-1} suspension was prepared and stirred for at least 24 h before analysis. For the electrochemical setup, the working electrodes as well as the reaction vessels were eight glassy carbon cells (each 9 mL, Sigradur G, HTW, Germany) with copper wires attached (four for MER and four for MEO). The counter electrodes were coiled platinum wires (0.5 mm, 99.9%, Sigma-Aldrich Co., USA) connected to platinum gauzes (52 mesh, 99.9%, Sigma Aldrich Co., USA) in glass tubes with porous glass frits filled with phosphate buffer (0.1 M KCl, 0.1 M KH_2PO_4, pH 7). The reference electrodes were Ag/AgCl electrodes (Bioanalytical Systems Inc., USA) but redox potentials are reported with reference to the standard hydrogen electrode. To start the measurement, 7 mL phosphate buffer solution was added into the continuously stirred reaction vessels, and redox potentials (E_h = -0.38 V for MER and +0.61 V for MEO) were applied using an eight-channel potentiostat CHI1000 (CH Instruments, USA). Subsequently, 100 µL of a 10 mM mediator stock solution, either zwitterionic viologen (ZiV) for reduction or 2,2'-azino-bis(3-ethylbenzothiazoline-6-sulfonic acid) (ABTS) for oxidation, was spiked to be completely oxidized or reduced. Then, different amounts of biochar samples were added consecutively into the vessels and caused sharp and clear current peaks. For the data analysis, the current peaks were integrated by Matlab R2020Ra over an analysis time of 4000 s. The electron accepting capacity (EAC) and electron donating capacity (EDC) were calculated in µmol e^- $(g\ biochar)^{-1}$ according to Klüpfel et al., 2014[58]. Furthermore, the obtained EAC and EDC values were normalized to the carbon mass of the biochar in µmol e^- $(g\ carbon)^{-1}$ according to the carbon content in Table S2.1.

S2.2.3 Electrical conductivity (EC)

The electrical conductivity was determined using a “Black Gauß” (Eurofins Umwelt Ost GmbH, Freiberg, Germany), measurement and calculations are described in detail elsewhere[177].

S2.2.4 Persistent free radicals (PFRs)

Continuous X-band electron spin resonance (ESR) spectra were recorded with an ESR spectrometer (MiniScope MS 300, Magnettech GmbH, Berlin, Germany) for the determination of persistent free radicals. For the estimation of spin concentrations, the spectra of biochar were accumulated 3-fold over 90 s at a microwave power of 0.1 mW (sweep width 15 mT). Suwanne River standard fulvic acid (1S101F) was used as a reference for the calculation of spin concentrations with a free radical content of 0.54×10^{17} spins g^{-1} (IHSS). The g-values were determined in separate scans by measuring a certified internal manganese standard (Mn^{2+} in ZnS) simultaneously with the samples.

S2.2.5 Specific surface area

The specific surface area of the biochar was determined using 5-point Brunauer–Emmett–Teller (BET) measurements (TU Freiberg, Germany). The samples were prepared in a gas adsorption sample preparation device Smart VacPrep (Micromeritics, Germany) and measured in a surface area system ASAP 2460 (Micromeritics, Germany).

S2.2.6 Elemental composition

The elemental composition as well as the ash and water contents of the biochar were analyzed by Eurofins Ost GmbH (Freiberg, Germany) according to the European Biochar Certificate (EBC, 2023) (www.european-biochar.org).

S2.2.7 Average carbon oxidation state (C_{ox}), double bond equivalent (DBE) and aromaticity index (AI)

The average carbon oxidation state (C_{ox}), double bond equivalent (DBE), and aromaticity index (AI) of the biochar were calculated from the elemental composition (Table S2.1), where C_{ox} was derived from equations reported by Masiello et al., 2008[178], and DBE and AI were obtained from the molecular formulas according to Koch and Dittmar, 2006[179]. The average carbon oxidation state C_{ox} was calculated using Equation S2.1.

$$C_{ox} = \frac{2[O] - [H] - k[N] - m[S]}{[C]} \quad \text{(S2.1)}$$

where [O], [H], [N], [S] and [C] is the content of the element O, H, N, S and C, respectively, and k and m are factors that describe the oxidation state of N and S, respectively. k can vary between -3 (for ammonia) and +5 (for nitrate) and m between -2 (for sulfide) and +6 (for sulfate)[178]. Because of the small sulfur content (Table S2.1), the contribution of sulfur is negligible and m = 0 was used for the calculations. Varying k between the extreme values of -3 and +5 for fully reduced and oxidized N did not change the overall trend of the biochar, and the values reported in Table S2.1 were calculated from k = +5 [58].

The double bond equivalent normalized to the total number of carbons DBE/C was calculated following Equation S2.2. As DBE/C = 0.67 for benzene, a threshold of DBE/C ≥ 0.67 can be set for the presence of condensed aromatic ring structures[179].

$$DBE/C = \frac{1 + 0.5\,(2C - H + N)}{C} \quad \text{(S2.2)}$$

The aromaticity index (AI) was calculated following Equation S2.3 and takes into account heteroatoms that contribute to aromatic structures. A threshold of AI ≥ 0.67 was set for the presence of condensed aromatic ring structures[179].

$$AI = \frac{DBE_{AI}}{C_{AI}} = \frac{1 + O - C - S - 0.5\,(H + N)}{C - O - S - N} \quad \text{(S2.3)}$$

where DBE_{AI} is the minimum number of C-C double bonds plus rings in a common molecular structure containing heteroatoms [179] and C_{AI} is the number of C atoms reduced by the number of potential double bonds contributed by heteroatoms[179]

Table S2.1. BET surface area, persistent free radical (PFR) concentration, electrical conductivity (EC), electron accepting and donating capacity (EAC, EDC), elemental composition, as well as water and ash content of the biochar. Values in % are given on a dry basis in mmol element (g char)$^{-1}$.

Characteristic	Value	Characteristic	Value
BET surface area (m^2 g^{-1})	120 ± 7	C (%)	65.4
PFRs (10^{19} spins g^{-1})	3.50 ± 0.40	H (%)	27.9
g-value	2.0028	O (%)	6.2
EC[a] (mS cm^{-1})	(7.6 ± 0.3) × 10^{-5}	N (%)	0.40
EAC (µmol e^- (g biochar)$^{-1}$)	359 ± 23	S (%)	0.02
EAC (µmol e^- (g carbon)$^{-1}$)	549 ± 35	H/C (mol H (mol C)$^{-1}$)	0.43
EDC (µmol e^- (g biochar)$^{-1}$)	413 ± 22	O/C (mol O (mol C)$^{-1}$)	0.095
EDC (µmol e^- (g carbon)$^{-1}$)	632 ± 33	DBE/C[b] (mol DBE (mol C)$^{-1}$)	0.80
EEC (µmol e^- (g biochar)$^{-1}$)	772 ± 45	AI[c] (mol DBE_{AI} (mol C_{AI})$^{-1}$)	0.78
EEC (µmol e^- (g carbon)$^{-1}$)	1181 ± 56	C_{ox}[d]	-0.27

[a] Electrical conductivity measured at a pressure of 5 tons

[b] Double-bond equivalent normalized by total number of carbons

[c] Aromaticity index

[d] Average carbon oxidation state

S2.3 Sorption of DEET on biochar

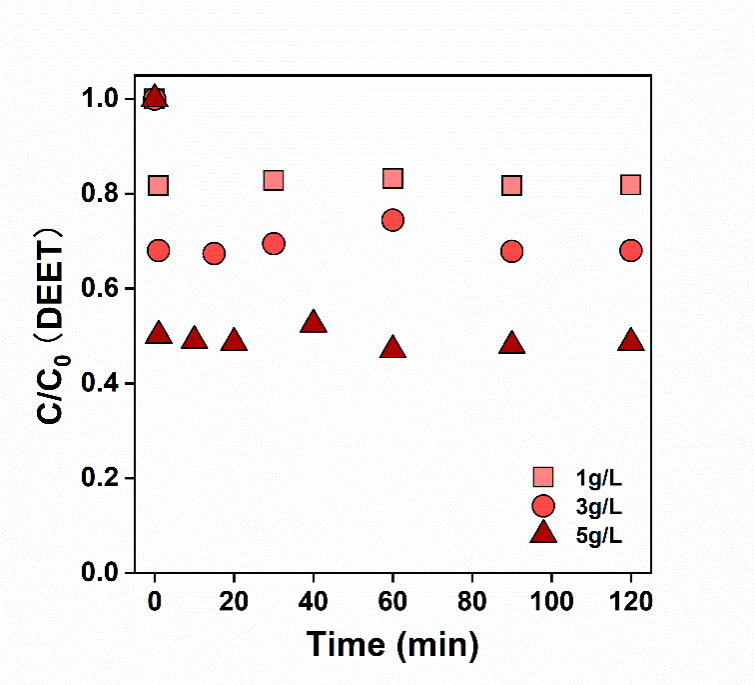

Figure S2.2. Adsorption of DEET onto biochar with different biochar dosages (1 g L^{-1}, 3 g L^{-1}, 5 g L^{-1}). c_0 = 50 µM, pH 6 - 8 (no pH adjustment) in deionized water.

S2.4 Experimental procedure of the batch experiments

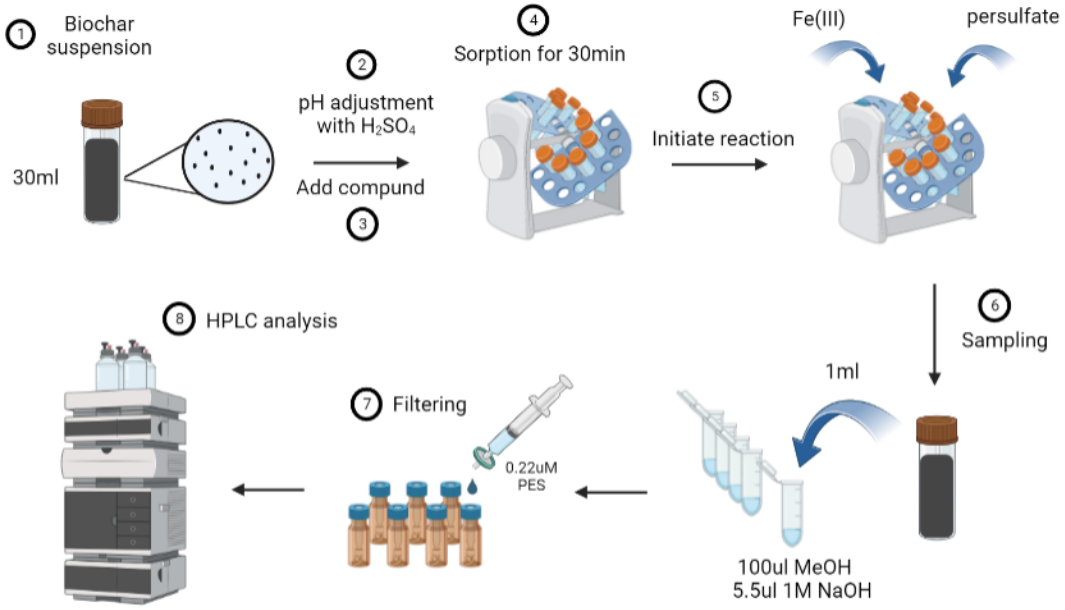

Figure S2.3. Experimental procedure of the batch experiments in presence of biochar, Fe(III), and persulfate. Figure generated with BioRender (https://biorender.com/).

S2.5 DEET removal and degradation kinetics in pure water in the biochar/Fe(III)/PDS system

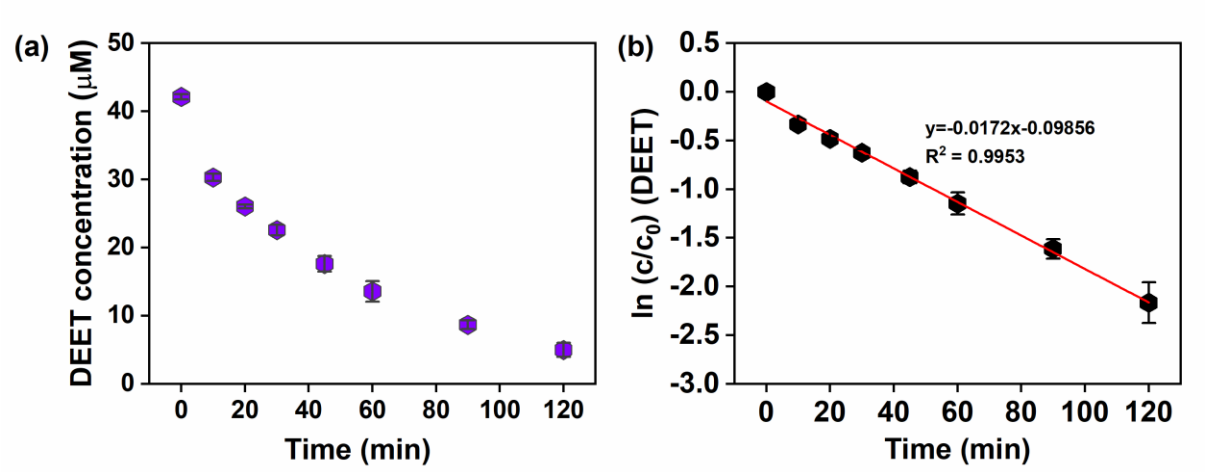

Figure S2.4. (a) DEET removal in biochar/Fe(III)/PDS system. (b) DEET degradation in biochar/Fe(III)/PDS system followed pseudo-first order reaction kinetics with k_{obs} = (2.9 ± 0.1) × 10^{-4} s^{-1}. [Biochar] = 1 g L^{-1}, [Fe(III)] = 0.2 mM, [PDS] = 8 mM, $[DEET]_0 = c_0$ ~ 40 μM, pH 2.5 in deionized water. Error bars represent standard deviations of triplicate experiments.

S2.6 Fe(II) formation from Fe(III) in a biochar suspension

To assess the Fe(II) formation potential of the biochar, a 1 g biochar L^{-1} suspension was spiked with 0.2 mM Fe(III). The dissolved Fe(II) concentration was measured over the time course of two hours using a modified Ferrozine assay Stookey et al., 1970[180] as described by Amstaetter et al., 2012[181]. Briefly, aliquots of aqueous samples were filtered and spiked immediately into 1 M HCl in disposable cuvettes (1.5 mL, BrandTech) to protect Fe(II) from oxidation. Then, the Ferrozine reagent was added to form a purple colored Fe^{2+} complex, which was quantified spectrophotometrically at 562 nm after incubation in the dark for 5 min.

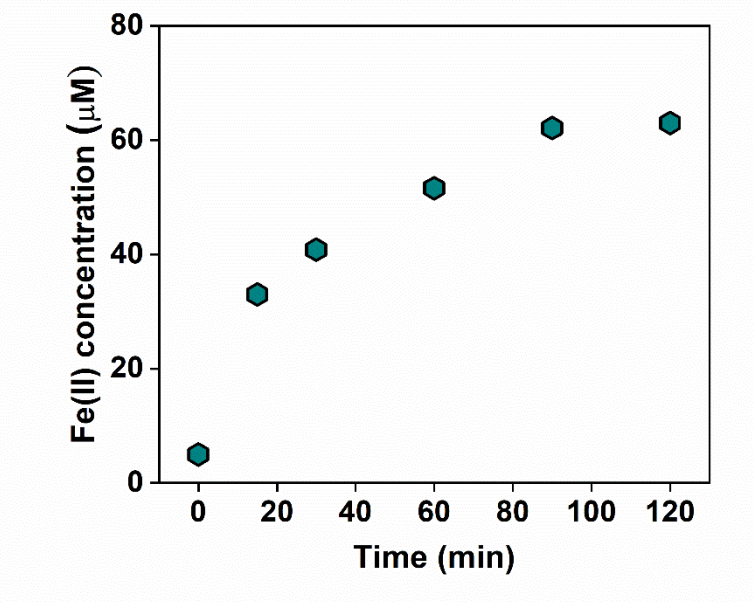

Figure S2.5. Fe(II) formation in biochar suspension spiked with Fe(III). [Biochar] = 1 g L^{-1}, [Fe(III)] = 0.2 mM, pH 2.5 in deionized water.

S2.7 Effect of biochar on DEET degradation in the Fe(II)/PDS system

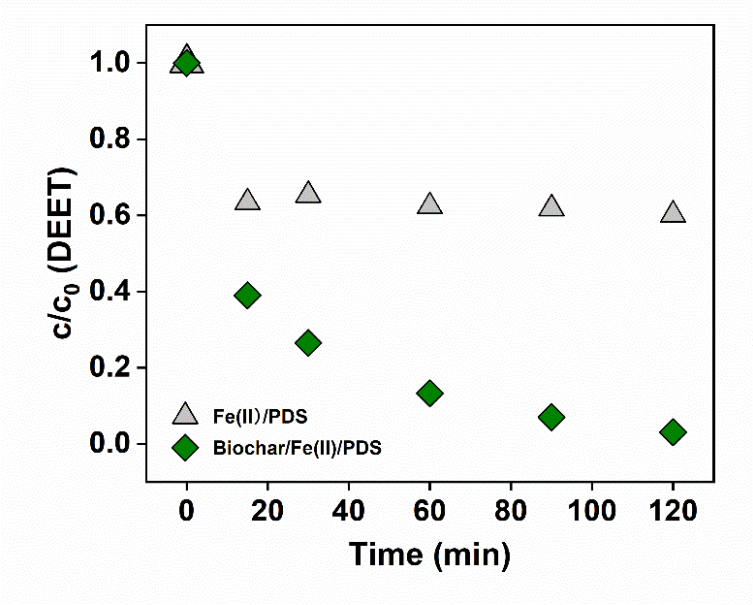

Figure S2.6. DEET removal in the Fe(II)/PDS system in the absence of biochar and in the presence of biochar. [Biochar] = 1 g L^{-1}, [Fe(II)] = 80 µM, [PDS] = 8 mM, $[DEET]_0 = c_0 \sim 40$µM, c = measured DEET concentration over time, pH 2.5 in deionized water.

S2.8 Removal and degradation kinetics of three consecutive spikes of DEET in pure water in the biochar/Fe(III)/PDS system

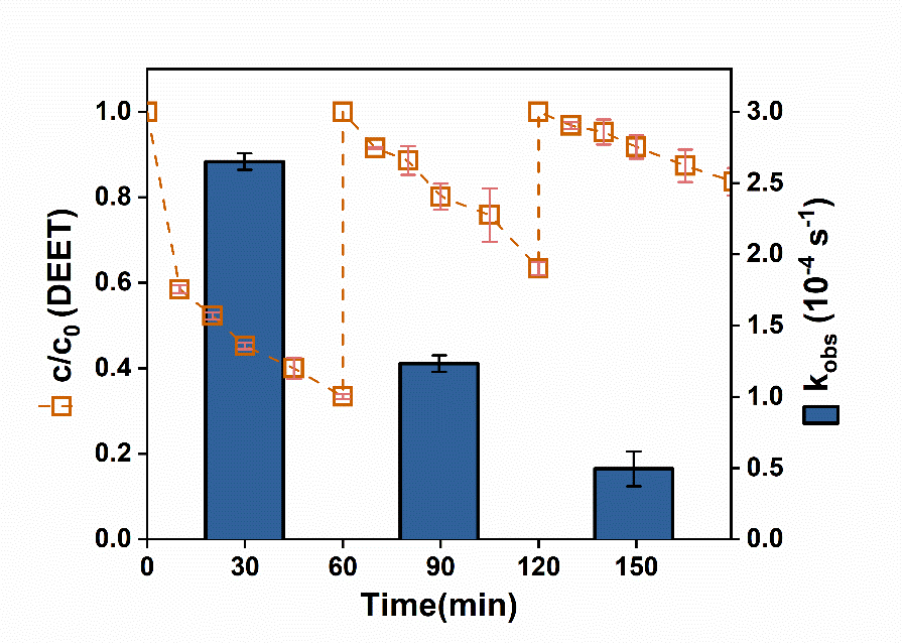

Figure S2.7. Removal of three consecutive spikes of DEET in the biochar/Fe(III)/PDS system and corresponding pseudo-first order rate constants (k_{obs}). [Biochar] = 1 g L^{-1}, [Fe(III)] = 50 μM, [PDS] = 8 mM, [DEET] = 50 μM nominal for each spike, pH 2.5 in deionized water. c_0 is the measured DEET concentration after each spike and c is the measured DEET concentration over time. Error bars indicate the standard deviation of triplicate experiments.

S2.9 DEET degradation in pure water in the biochar /Fe(III)/PDS system over time

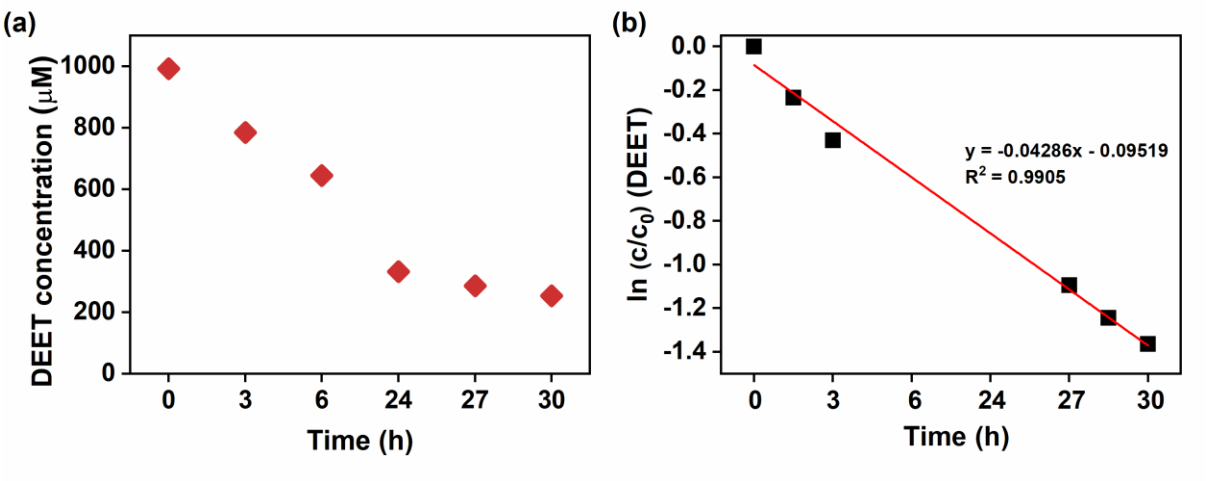

Figure S2.8. (a) DEET degradation over time in the biochar/Fe(III)/PDS system**.** (b) Determination of the pseudo-first order rate constant (k_{obs} = (7.1 ± 0.4) × 10^{-4} s^{-1}) for DEET degradation in the biochar/Fe(III)/PDS system. [Biochar] = 1 g L^{-1}, [Fe(III)] = 0.2 mM, [PDS] = 8 mM, $[DEET]_0$ = 1 mM, pH 2.5 in deionized water.

S2.10 Degradation kinetics of PMSO in the biochar /Fe(III)/PDS system

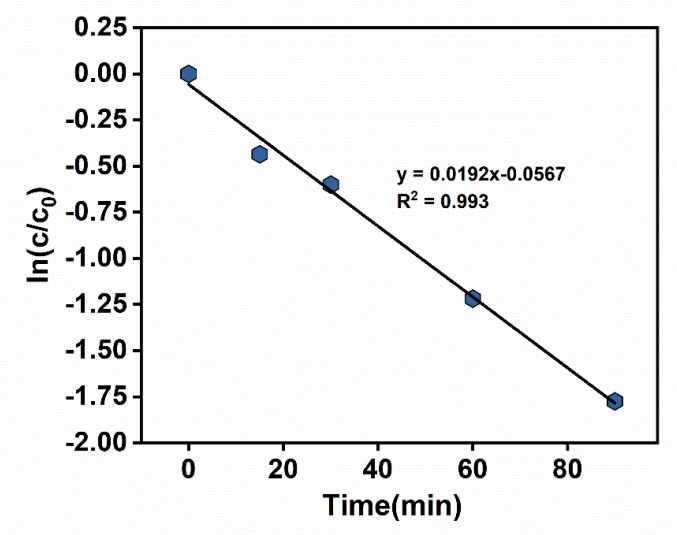

Figure S2.9. PMSO degradation in the biochar/Fe(III)/PDS system followed pseudo-first order reaction kinetics (k_{obs} =(3.2 ± 0.2) × 10^{-4} s^{-1}). [Biochar] = 1 g L^{-1}, [Fe(III)] = 0.2 mM, [PS] = 8 mM, [PMSO] = 200 μM, pH 2.5 in deionized water.

S2.11 PMSO transformation via $SO_4^{\bullet-}$ or reactive chlorine species

S2.11.1 Reaction of PMSO with $SO_4^{\bullet-}$

To investigate the reaction of PMSO with $SO_4^{\bullet-}$, PDS was thermally activated at 60°C in a water bath. Batch experiments were performed in 100 mL Schott bottles containing 50 mL deionized water with 200 µM PMSO. In order to ensure $SO_4^{\bullet-}$ is the sole reactive species in the system, 20 mM TBA was added to suppress the formation of $^{\bullet}OH$ from the reaction of $SO_4^{\bullet-}$ with Cl^- [143] (93% of $^{\bullet}OH$ scavenged, see section S12). Small concentrations of Cl^- may be introduced by the use of incompletely deionization water, impure chemicals, or from pH measurements. After heating up the reaction solution, 8 mM PDS was added to initiate the reaction. At predefined time points, 1 mL sample was withdrawn and immediately added into iced DMSO (2 M in the sample, ≈ 9% v/v) and chilled on an ice bath to quench the reaction. The pH was maintained at 2.5 ± 0.1 by addition of sulfuric acid or sodium hydroxide. A corresponding control containing only PMSO was conducted simultaneously to study the stability of PMSO at 60°C.

Degradation kinetics of PMSO in the heat/PDS system

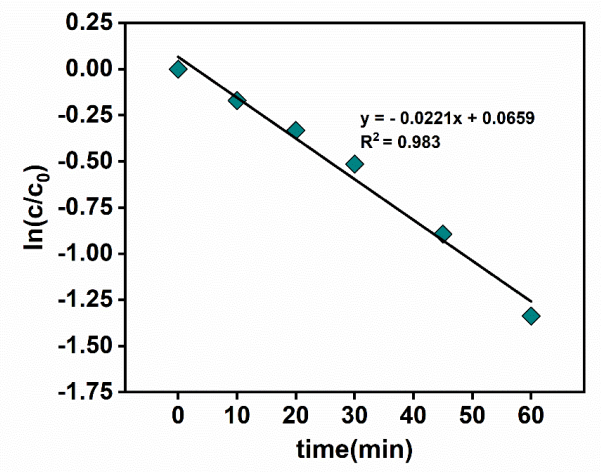

Figure S2.10. PMSO degradation in the heat/PDS control system without Cl^- addition followed pseudo-first order reaction kinetics (k_{obs} = (3.7 ± 0.2) × 10^{-4} s^{-1}). [PDS] = 8 mM, [PMSO] = 200 µM, [TBA] = 20 mM, pH 2.5 in deionized water, 60°C in a water bath.

Stability of PMSO in water at 60°C

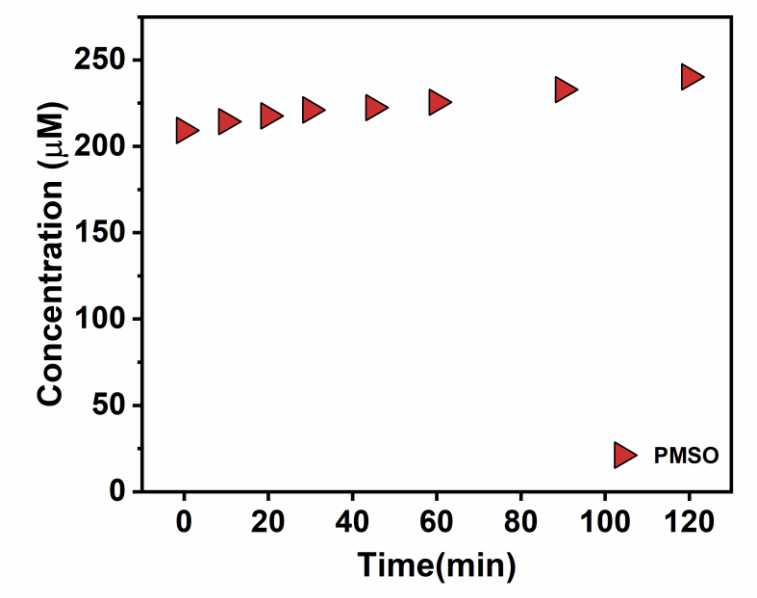

Figure S2.11. Concentration of PMSO in water at 60°C over time. [PMSO] = 200 μM, pH 2.5 in deionized water, 60°C in a water bath.

PMSO transformation and $PMSO_2$ formation in control systems

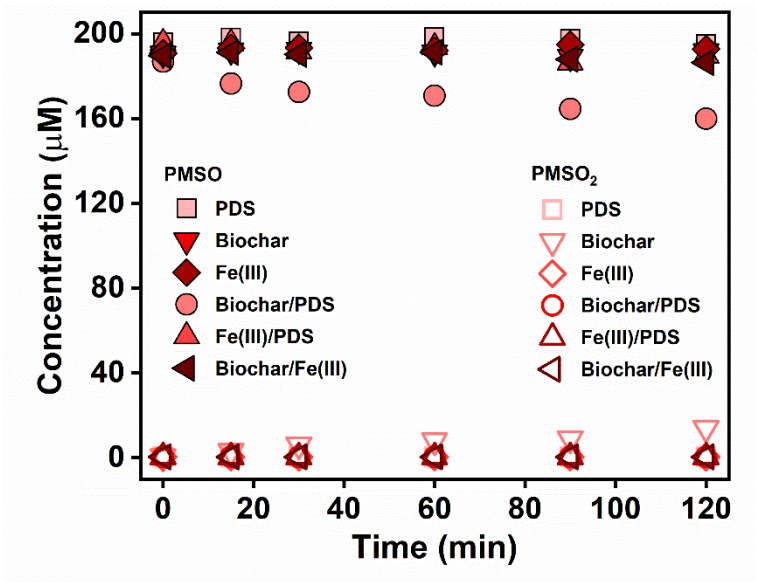

Figure S2.12. PMSO transformation and $PMSO_2$ formation in different control systems with only PDS, only biochar, only Fe(III), and combinations thereof. [Biochar] = 1 g L^{-1}, [Fe(III)] = 0.2 mM, [PDS] = 8 mM, [PMSO] = 200 μM, pH 2.5 in deionized water.

S2.11.1 Reaction of PMSO with reactive chlorine species

To investigate $PMSO_2$ formation from PMSO upon reaction with reactive chlorine species, 1 mM Cl^- from a 1 M NaCl aqueous stock solution was added into 50 μM PMSO solution. 95% of the $SO_4^{\bullet-}$ reacted with Cl^- to form reactive chlorine species (for calculation see Section S2.12). The sampling procedure and pH adjustment were identical as described above.

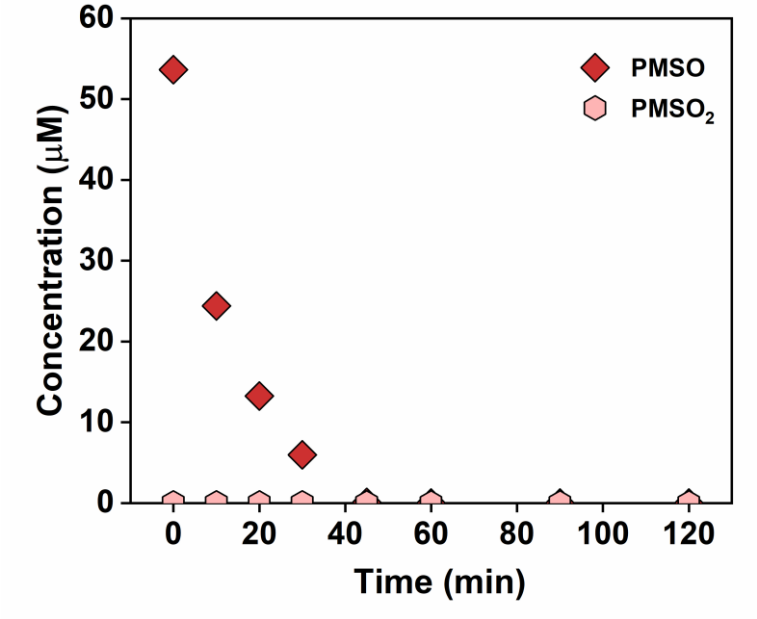

Figure S2.13. PMSO transformation and $PMSO_2$ formation in the heat/PDS system in presence of 1 mM Cl^-. [PDS] = 8 mM, [PMSO] = 50 μM, [Cl^-] = 1 mM, pH 2.5 in deionized water, 60°C in a water bath.

S2.12 Calculations of fractions reacting with an oxidant or reactive species

The fraction of a reactive species reacting with a certain compound in competition with other substrates that can also react with the reactive species of interest can be calculated with their corresponding known concentrations and reaction rate constants. The following example gives the fraction of reactive species reacting with a scavenger competing with DEET.

$$f\,(\text{scavenger}) = \frac{[\text{scavenger}]\ \times k_1}{[\text{scavenger}]\ \times\ k_1 + [\text{DEET}] \times k_2} \qquad \text{(S2.4)}$$

where [scavenger] is the concentration of the scavenger, [DEET] is the concentration of DEET, k_1 is the second order reaction rate constant of the reaction of the reactive species with the scavenger, and k_2 is the second order reaction rate constant of the reaction of the reactive species with DEET.

(a) PMSO as probe compound in the heat/PDS system

Reaction rate constants:

PMSO: k (•OH) = 3.61 × 10^9 M^{-1} s^{-1}; k ($SO_4^{\bullet-}$) = 3.17 × 10^8 M^{-1} s^{-1}

TBA: k (•OH) = 6.0 × 10^8 M^{-1} s^{-1}; k ($SO_4^{\bullet-}$) = 8.0 × 10^5 M^{-1} s^{-1}

Cl^-: k (•OH) = 4.3 × 10^9 M^{-1} s^{-1}; k ($SO_4^{\bullet-}$) = 2.8 × 10^8 M^{-1} s^{-1}

Experiment 1: PMSO transformation to $PMSO_2$ via $SO_4^{\bullet-}$ in presence of 20 mM TBA

Concentrations: [PDS] = 8 mM, [PMSO] = 200 µM, [TBA] = 20 mM, [Cl^-] = 45 µM (assumed based on IC measurement of Cl^-)

The fraction of •OH reacting with TBA in the presence of PMSO and Cl^-:

$$f\,(\text{TBA}) = \frac{[\text{TBA}]\ \times k_{\text{OH}^\bullet,\ \text{TBA}}}{[\text{TBA}]\ \times k_{\text{OH}^\bullet,\ \text{TBA}} + [\text{PMSO}] \times k_{\text{OH}^\bullet,\ \text{PMSO}} + [\text{Cl}^-] \times k_{\text{OH}^\bullet,\ \text{Cl}^-}} = 93\%$$

The fraction of $SO_4^{\bullet -}$ reacting with TBA in the presence of PMSO and Cl^-:

$$f(\mathrm{TBA}) = \frac{[\mathrm{TBA}] \times k_{SO_4^{\bullet -},\ \mathrm{TBA}}}{[\mathrm{TBA}] \times k_{SO_4^{\bullet -},\ \mathrm{TBA}} + [\mathrm{PMSO}] \times k_{SO_4^{\bullet -},\ \mathrm{PMSO}} + [Cl^-] \times k_{SO_4^{\bullet -},\ Cl^-}} = 17\%$$

Experiment 2: PMSO transformation to $PMSO_2$ via reactive chlorine species

Concentrations:

[PDS] = 8 mM, [PMSO] = 50 μM, $[Cl^-]$ = 1mM

The fraction of $SO_4^{\bullet -}$ reacting with Cl^- in the presence of PMSO:

$$f(Cl^-) = \frac{[Cl^-] \times k_{SO_4^{\bullet -},\ Cl^-}}{[Cl^-] \times k_{SO_4^{\bullet -},\ Cl^-} + [\mathrm{PMSO}] \times k_{SO_4^{\bullet -},\ \mathrm{PMSO}}} = 95\%$$

(b) Scavenger experiments in the biochar/Fe(III)/PDS system:

Reaction rate constants:

MeOH: k ($^{\bullet}OH$) = 9.7×10^8 M^{-1} s^{-1}; k ($SO_4^{\bullet -}$) = 1.1×10^7 M^{-1} s^{-1}

TBA: k ($^{\bullet}OH$) = 6.0×10^8 M^{-1} s^{-1}; k ($SO_4^{\bullet -}$) = 8.0×10^5 M^{-1} s^{-1}

DEET: k ($^{\bullet}OH$) = 5.0×10^9 M^{-1} s^{-1} [182]; k ($SO_4^{\bullet -}$) = 1.9×10^9 M^{-1} s^{-1} [183]

Experiment 1: 1g L^{-1} biochar, 0.2 mM Fe(III), 8 mM PDS, 50 μM DEET, 300 mM MeOH

The fraction of $^{\bullet}OH$ reacting with MeOH:

$$f(\mathrm{MeOH}) = \frac{[\mathrm{MeOH}] \times k_{\bullet \mathrm{OH},\ \mathrm{MeOH}}}{[\mathrm{MeOH}] \times k_{\bullet \mathrm{OH},\ \mathrm{MeOH}} + [\mathrm{DEET}] \times k_{\bullet \mathrm{OH,DEET}}} = 100\%$$

The fraction of $SO_4^{\bullet -}$ reacting with MeOH:

$$f(\mathrm{MeOH}) = \frac{[\mathrm{MeOH}] \times k_{SO_4^{\bullet -},\ \mathrm{MeOH}}}{[\mathrm{MeOH}] \times k_{SO_4^{\bullet -},\ \mathrm{MeOH}} + [\mathrm{DEET}] \times k_{SO_4^{\bullet -},\ \mathrm{DEET}}} = 99\%$$

Experiment 2: 1g L^{-1} biochar, 0.2 mM Fe(III), 8 mM PDS, 50 μM DEET, 10 mM TBA

The fraction of $^{\bullet}OH$ reacting with TBA:

$$f(\mathrm{TBA}) = \frac{[\mathrm{TBA}] \times k_{\bullet \mathrm{OH},\ \mathrm{TBA}}}{[\mathrm{TBA}] \times k_{\bullet \mathrm{OH},\ \mathrm{TBA}} + [\mathrm{DEET}] \times k_{\bullet \mathrm{OH,DEET}}} = 96\%$$

The fraction of $SO_4^{\bullet -}$ reacting with TBA:

$$f\,(\mathrm{TBA}) = \frac{[\mathrm{TBA}] \times k_{SO_4^{\bullet -},\ \mathrm{TBA}}}{[\mathrm{TBA}] \times k_{SO_4^{\bullet -},\ \mathrm{TBA}} + [\mathrm{DEET}] \times k_{SO_4^{\bullet -},\ \mathrm{TBA}}} = 14\%$$

Experiment 3: 1g L^{-1} biochar, 0.2 mM Fe(III), 8 mM PDS, 50 µM DEET, 10 – 1000 mM TBA

Table S2.2. Fractions of $SO_4^{\bullet -}$ and $^{\bullet}OH$ reacting with TBA for different TBA concentrations present.

TBA concentration (mM)	Fraction (%) $^{\bullet}OH$	Fraction (%) $SO_4^{\bullet -}$
10	96	14
50	99	44
100	100	62
200	100	76
300	100	83
500	100	89
1000	100	94

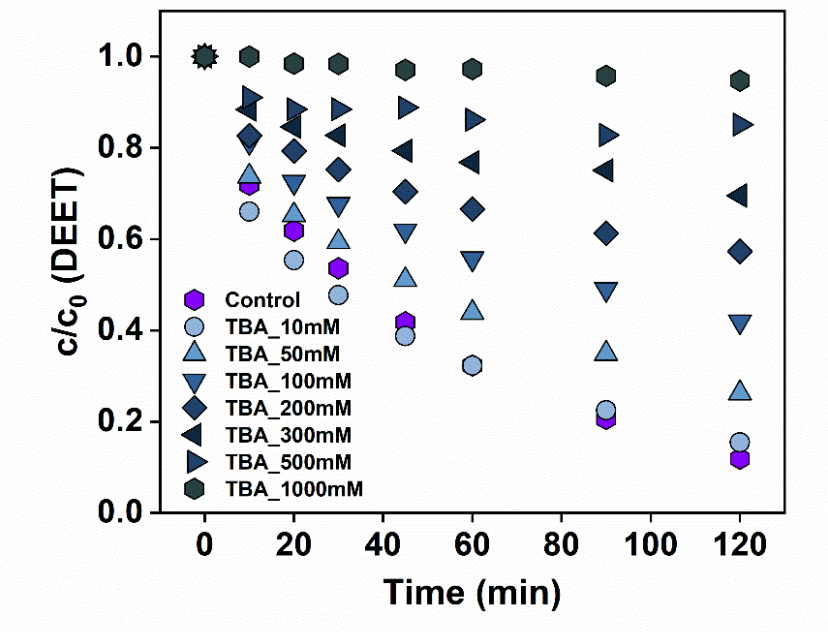

Figure S2.14. DEET degradation in the biochar/Fe(III)/PDS system in the absence (control) and presence of different concentrations of *tert*-butanol (TBA). [Biochar] = 1 g L^{-1}, [Fe(III)] = 0.2 mM, [PDS] = 8 mM, $[DEET]_0 = c_0$ ~ 40 µM, [TBA] = 10 - 1000 mM, pH 2.5 in deionized water.

S2.13 Sorption-corrected transformation rates of *p*CBA and *p*NBA

Competition kinetics experiments with *p*CBA and *p*NBA were accompanied by sorption controls with only *p*CBA, *p*NBA, and biochar. Sampling started after 30 minutes. The transformation rates of *p*CBA and *p*NBA were corrected by sorption. The function of sorption c/c_0 vs. time followed a linear equation. Subtracting the sorption rate from the degradation rate yielded the reactive transformation of *p*CBA and *p*NBA.

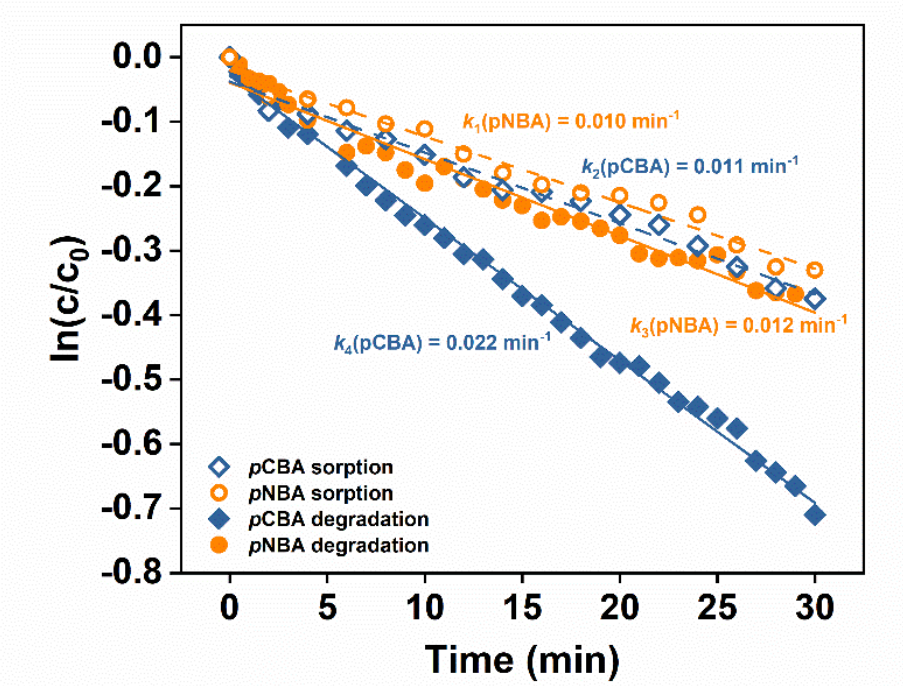

Figure S2.15. Sorption and degradation kinetics of *p*CBA and *p*NBA in the biochar/Fe(III)/PDS system. [Biochar] = 1 g L^{-1}, Fe(III) = 0.2mM, [PDS] = 8 mM, $[pCBA]_{spiked}$ = $[pNBA]_{spiked}$ = 4 μM, $[pCBA]_{0,\ after\ 30min\ sorption}$ = 1.5 μM, $[pNBA]_{0,\ after\ 30min\ sorption}$ = 1.7 μM, c is the measured *p*CBA and *p*NBA concentration over time, pH 2.5 in deionized water.

S2.14 Stability of *p*CBA and *p*NBA in the presence of persulfate

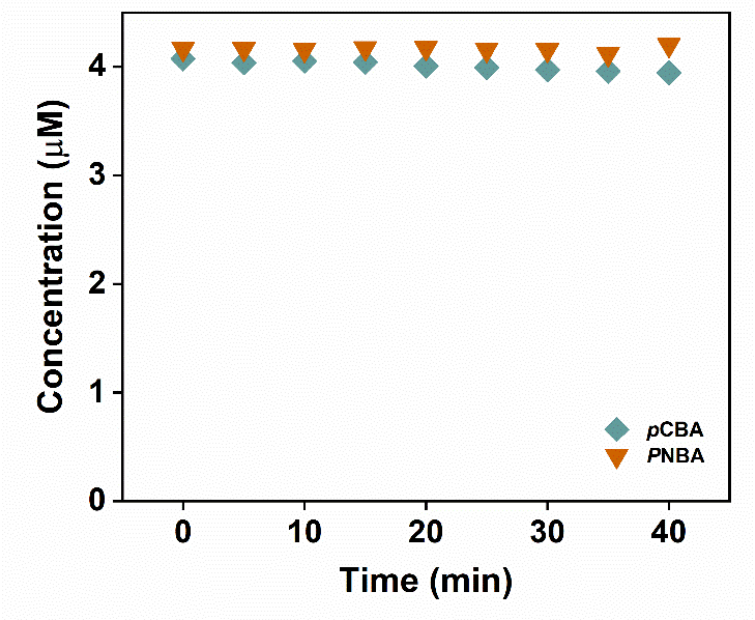

Figure S2.16. Stability of *p*CBA and *p*NBA in the presence of PDS over time. [PDS] = 8 mM, $[pCBA]_0 = [pNBA]_0$ = 4 μM, pH 2.5 in deionized water.

S2.15 Determination of steady-state concentration of sulfate radicals in the biochar/Fe(III)/PDS system

The steady-state concentration of sulfate radicals, $[SO_4^{\bullet-}]_{ss}$ was calculated using Equations S2.5 – S2.7. The pseudo-first order rate constant k_{obs} for *p*CBA degradation was determined using Figure S2.17.

$$\ln\frac{[p\mathrm{CBA}]}{[p\mathrm{CBA}]_0} = -k_{SO_4^{\bullet-},\ p\mathrm{CBA}}[SO_4^{\bullet-}]_{ss}t \quad \text{(S2.5)}$$

$$\ln\frac{[p\mathrm{CBA}]}{[p\mathrm{CBA}]_0} = -k_{obs}t \quad \text{(S2.6)}$$

$$[SO_4^{\bullet-}]_{ss} = \frac{k_{obs}}{k_{SO_4^{\bullet-},\ p\mathrm{CBA}}} \quad \text{(S2.7)}$$

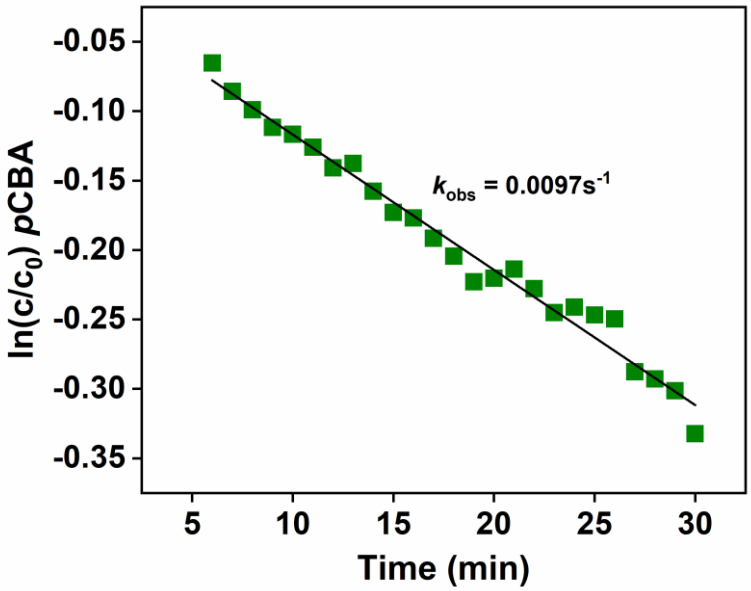

Figure S2.17. Determination of the pseudo-first order rate constant k_{obs} for *p*CBA degradation. [Biochar] = 1g L^{-1}, [Fe(III)] = 0.2mM, [PDS] = 8mM, $[p\mathrm{CBA}]_{0,\text{after 30min sorption}} = c_0$ = 1.5 µM, c is the measured *p*CBA concentration over time, pH 2.5 in deionized water. After 30min sorption of *p*CBA onto biochar, the reaction was initiated by adding Fe(III) and PDS. $\ln(c/c_0)$ values were calculated from the sorption corrected data.

S2.16 Characterization of the mining-impacted surface water

Electrical conductivity, pH, and dissolved O_2 concentration were measured using a multi-parameter probe (Multi 3430, WTW, Germany). The total organic carbon (TOC), dissolved organic carbon (DOC), dissolved inorganic carbon (DIC), total nitrogen (TN), and total dissolved nitrogen (TDN) were analyzed by a TOC analyzer (TOC/TN, Shimadzu, Japan). The total phosphorus (TP) and soluble reactive phosphorus (SRP) were determined by a modified ammonium molybdate spectrophotometric method [184]. The concentration of major ions (Cl^-, SO_4^{2-}, NH_4^+, NO_2^-, NO_3^-) was determined by ion chromatography (930 Compact IC Flex, Metrohm, Germany). The detection of iron species with different valence states, including total Fe (Fe_{tot}), Fe(II), and Fe(III) was performed by a UV-vis spectrophotometer (Varian Cary 1E, USA) using 1.10-phenanthroline spectrometric method[185]. Briefly, 1 ml sample was immediately spiked into 500 µL acetate buffer to protect Fe(II) from oxidizing to Fe(III) in disposable cuvettes (1.5 mL, BrandTech. GmbH). Then, 500 µL 1,10-phenanthroline was added to form an orange-red complex. The complex was quantified spectrophotometrically at 510 nm after incubation for 20 min in the dark. Fe_{tot} was measured using the same procedure as Fe(II), but ascorbic acid was added in addition to reduce Fe(III) to Fe(II). Subsequently, the Fe(III) concentration was calculated as the difference between Fe_{tot} and Fe(II). Other metals list in Table S2.3 were determined by inductively coupled plasma optical emission spectroscopy (iCAP 7000 series, Thermo Fisher Scientific Inc. USA).

Table S2.3. Characteristics and composition of the mining-impacted surface water.

Parameter	Value	Parameter	Value
pH	3.6	Cl^- (mg L^{-1})	31[b]
Electrical conductivity (µS cm^{-1})	1299	SO_4^{2-} (mg L^{-1})	603
O_2 (mg L^{-1})	10.77	Al (mg L^{-1})	0.08
TOC (mg L^{-1})	4.2	B (mg L^{-1})	0.04
DOC (mg L^{-1})	4.2	Ca (mg L^{-1})	174.1
DIC (mg L^{-1})	2.8	Cu (mg L^{-1})	0.161
TN (mg L^{-1})	1.1	Fe (mg L^{-1})	8.06
TDN (mg L^{-1})	0.9	K (mg L^{-1})	7.77
TP (mg L^{-1})	0.04	Mg (mg L^{-1})	26.78
SRP (mg L^{-1})	0.009	Mn (mg L^{-1})	0.41
Fe_{tot} (mg L^{-1})	8.75	Na (mg L^{-1})	20.4
Fe(II) (mg L^{-1})	5.05	P (mg L^{-1})	<0.01
Fe(III) (mg L^{-1})	2.86[a]	S (mg L^{-1})	187.9
NH_4^+ - N (mg L^{-1})	0.47	Si (mg L^{-1})	6.68
NO_2^- - N (mg L^{-1})	<0.005	Zn (mg L^{-1})	0.21
NO_3^- - N (mg L^{-1})	0.27	-	-

[a] Fe(III) concentration is approx. 0.05 mM

[b] Cl^- concentration is approx. 1 mM

S2.17 DEET degradation in mining-impacted surface water by biochar and PDS

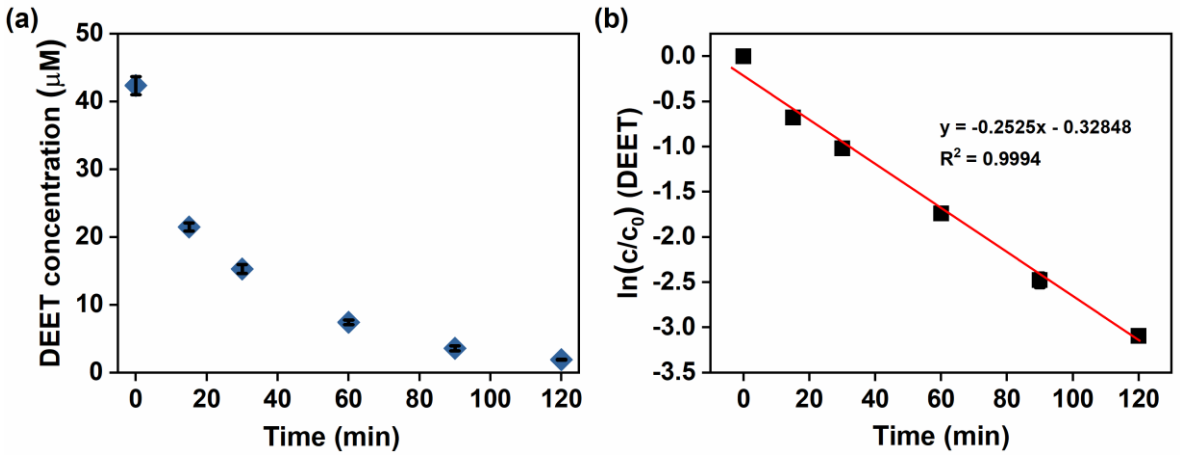

Figure S2.18. DEET degradation over time after application biochar and PDS to mining-impacted surface water (pH 3.6, Table S3) containing 0.05 mM Fe(III). (b) Determination of the pseudo-first order rate constant (k_{obs} = (4.2 ± 0.05) × 10^{-4} s^{-1}) for DEET degradation in mining-impacted surface water with biochar and PDS. [Biochar] = 1 g L^{-1}, [PDS] = 8 mM, $[DEET]_0 = c_0$ ~ 40 µM.

S2.18 Competition kinetics calculations and competition plot ln(c/c$_0$) of *p*CBA vs. *p*NBA in a synthetic water matrix in the presence of 0.1 mM Cl^-

The prepared synthetic water matrix (4.3 mg L^{-1} DOC as Suwannee River humic acid and 0.05 mM Fe(III) as iron(III) sulfate) contained 0.1 mM Cl^- (measured by ion chromatography). To simulate the mining-impacted surface water, 1 mM Cl^- was added to the synthetic water matrix. The fractions of reactive species (either $SO_4^{\bullet-}$ or $^\bullet OH$) reacting with certain reactants in competition with other present solutes are calculated according to Equation S2.4 using the concentrations and reaction rate constants in Table S2.4.

Table S2.4. Concentrations and reaction rate constants of the reactants used for competition kinetics calculations.

Reactants	Concentration	Rate constant ($SO_4^{\bullet-}$)	Rate constant ($^\bullet OH$)
Cl^-	0.1 mM or 1 mM	2.80×10^8	4.30×10^9
DOC	4.2 mg L^{-1}	6.80×10^3	1.40×10^4
PDS	8 mM	6.10×10^5	1.00×10^6
*p*CBA	2.08 μM	3.60×10^8	5.00×10^9
*p*NBA	2.91 μM	1.00×10^6	2.60×10^9

Table S2.5. Calculated fractions of $^\bullet OH$ and $SO_4^{\bullet-}$ reacting with Cl^-, DOC, *p*CBA, or *p*NBA.

Reactants	0.1 mM Cl^-	1 mM Cl^-
	Fraction (%)	Fraction (%)
Cl^- + $SO_4^{\bullet-}$	44	89
DOC + $SO_4^{\bullet-}$	47	9
*p*CBA + $^\bullet OH$	2	0
*p*CBA + $SO_4^{\bullet-}$	1	0
*p*NBA + $^\bullet OH$	2	0
*p*NBA + $SO_4^{\bullet-}$	0	0

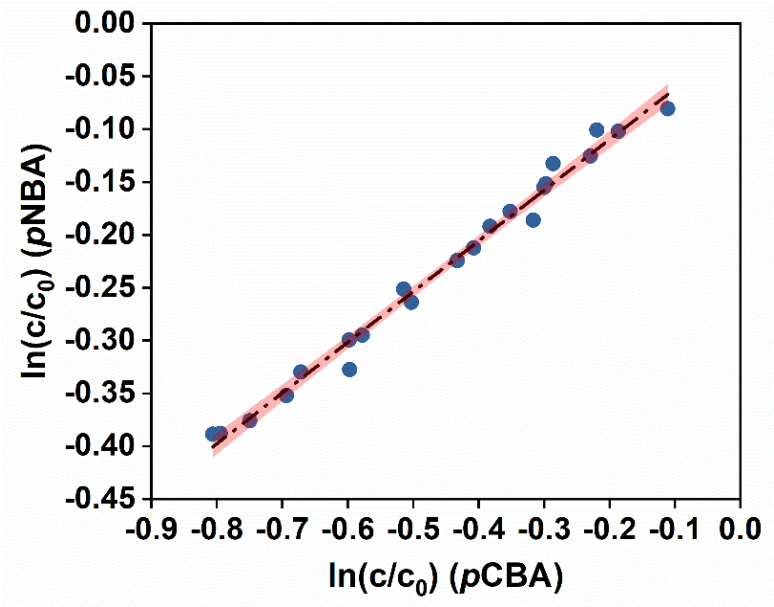

Figure S2.19. Sorption-corrected competition plot ln(c/c_0) of *p*CBA vs. *p*NBA in synthetic water containing 0.1 mM Cl^- (slope 0.480 ± 0.012; intercept 0.214 ± 0.039). [Biochar] = 1 g L^{-1}, Fe(III) = 0.05 mM, [PDS] = 8 mM, [DOC] = 4.3 mg L^{-1} (Suwannee River humic acid), $[pCBA]_{0,\ after\ 30min\ sorption}$ = 2.08 µM; $[pNBA]_{0,\ after\ 30min\ sorption}$ = 2.91 µM, pH 3.6 (adjusted with H_2SO_4). Red bands indicate the 95% confidence intervals of the linear fit. The slope is indicative of an •OH-based process (theoretical slope of 0.52).

Chapter 3

Activation of persulfate by biochar and iron: role of biochar pyrolysis condition and ash amendments

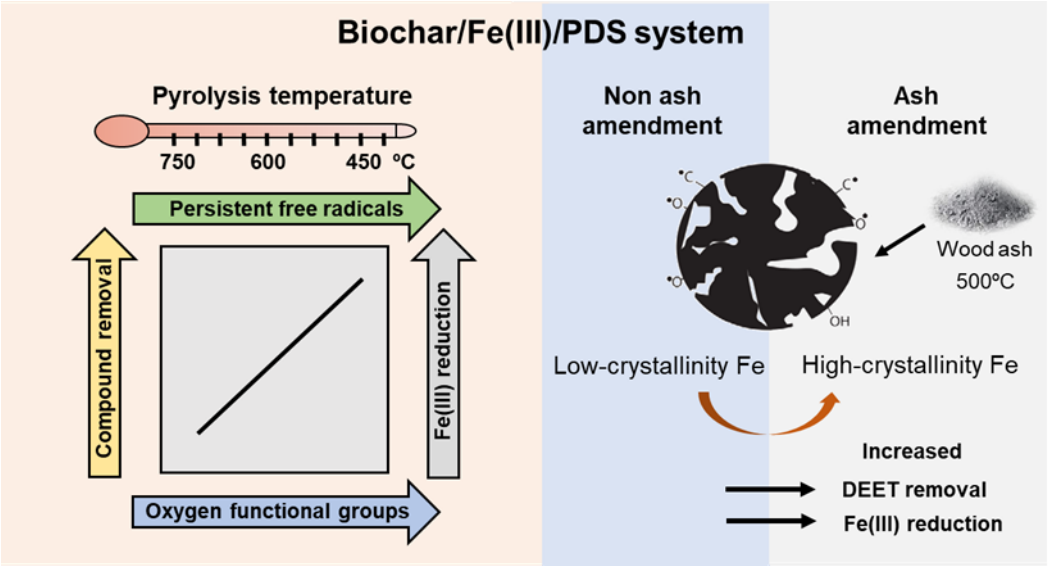

Yiling Zhuang, Stefan B. Haderlein, Nikolas Hagemann, Jannis Grafmüller, Karolin Gogler, Andrea Paul, Friedrich Fink, Stephanie Spahr. In preparation for publication.

Y. Zhuang: designed and performed the experiments, analyzed data, produced all figures, wrote and revised the manuscript; S. B. Haderlein: supervised the project, contributed to the experimental design and discussion of the results, revised the manuscript; N. Hagemann: provided the biochar samples, contributed to the discussion of the results; J. Grafmüller: conducted the biochar electrical conductivity measurements and the corresponding data analysis; A. Paul: performed continuous X-band electron spin resonance (ESR) spectra measurements and the corresponding data analysis; F. Fink: performed Fourier-transform infrared spectroscopy (FTIR) spectroscopy and the corresponding data analysis, wrote the experimental section on FTIR spectroscopy; K. Gogler: contributed to the development of batch experiments and helped to conduct batch experiments during master thesis; S. Spahr: supervised the project, contributed to the experimental design and discussion of the results, revised the manuscript.

Abstract

Redox-active biochars can enhance contaminant removal in persulfate-based Fenton-like water treatment by facilitating Fe(III) reduction to Fe(II). Depending on the feedstock and pyrolysis conditions, however, the biochar properties can vary greatly, so that it remains unclear which biochars are best suited for Fe(III) reduction and persulfate activation. We investigated eight biochars for their extent to which they can activate persulfate with Fe(III) to remove *N,N*-diethyl-*m*-toluamide (DEET) from water. Four of the biochars were produced from beech wood at different pyrolysis temperatures of 450, 600, 750°C and four biochars were produced from softwood sawdust to which 0 – 43 weight percent (wt%) ash was amended during pyrolysis at 500°C. Beech wood biochar produced at 450°C removed DEET most efficiently with a half-life time of 39 ± 4 min, likely due to the high concentration of surface oxygen functional groups and persistent free radicals that accelerated Fe(III) reduction and formation of reactive species. For the ash-amended biochars, biochar with 16 wt% ash amendment showed the best DEET removal with a half-life time of 27 ± 0.6 min, which is 10-times faster compared to a non-ash-amended biochar. Ash amendment led to the formation of crystalline iron minerals in biochars, which likely promoted Fe(III) reduction and persulfate activation. Our results can support the future production of engineered biochars with fine-tuned redox-active properties that enable customized performance tailored to specific applications in water treatment.

3.1 Introduction

Fenton-like processes using peroxydisulfate ($S_2O_8^{2-}$, PDS) for oxidative water treatment and contaminant removal have gained much attention for environmental applications[30,141,142]. However, the oxidation efficiency of the Fe(II)/PDS system is limited by the sluggish Fe(III)/Fe(II) cycling and Fe(III) precipitation[8–11]. The PDS-based Fenton-like system can be enhanced by the addition of redox-active biochars[115,132,186]. Biochars can enhance the reduction of Fe(III) to Fe(II), which activates PDS to reactive species for the removal of organic contaminants[113–116,146]. However, the performance of different biochars for Fe(III) reduction and PDS activation can highly depend on its redox-active properties, especially the electron donating capacity (EDC). The redox-active properties of biochar derive from the presence of redox-active moieties, including certain functional groups, persistent free radicals (PFRs), redox-active forms of metals like iron and manganese oxides, and conjugated aromatic structures[187–189]. The redox-active properties of biochars are highly variable depending on the precursor materials and pyrolysis conditions used[40,190].

The pyrolysis temperature of biochar plays a crucial role for the formation of redox-active moieties. Surface functional groups, such as quinone functional groups, have been shown to be the major moieties contributing to EDC at low charring pyrolysis temperature <600°C[68,69,124]. At pyrolysis temperatures above 600°C, conjugated aromatic structures, like conjugated π-electron systems, with bulk electrical conductivity are formed and proposed to also have a contribution to EDC[58,125]. The electrochemical properties associated with biochar surface functional groups can promote electron transfer through charging-discharging cycles where biochar acts as a “battery”[106]. In contrast, biochars with high bulk electrical conductivity may function as an “electrical conduit” that can undergo direct electron transfer through carbon matrices[106]. The nature of redox-active moieties in biochars can thus affect the mechanism and efficiency of Fe(III) reduction and PDS activation in the biochar/Fe(III)/PDS system.

So far, the impact of pyrolysis temperature on the biochar performance and reactive species formation in the biochar/Fe(III)/PDS system has been investigated[113,114]. Liang et al. 2021 suggested a fast Fe(III)/Fe(II) circulation and an Fe(IV) dominated pathway when employing biochar produced at 400°C[113]. In contrast, high-temperature biochars produced at 700 °C could not maintain the Fe(III)/Fe(II) cycling, and the contaminant degradation was governed by a mediated electron transfer from organics to persulfate by biochar[113]. Tang et al. 2023 reported the formation of radical species in the biochar/Fe(III)/PDS system, where the yield of radical species increased and then decreased, while the non-radical contribution of Fe(IV) increased with decreasing pyrolysis temperature from 700°C to 350°C[114]. However, little is known about the role of biochar pyrolysis conditions and the resulting redox-active moieties for the performance of biochars in PDS activation and organic contaminant transformation in the biochar/Fe(III)/PDS system.

To manipulate the redox-active properties of biochars, wood ash, a by-product of biomass power plants with high mineral conetent and pH buffering capacity[126,127], has been used as an amendment during biochar pyrolysis[127–129]. Ash-amended biochars have shown an improved performance for the removal of inorganic contaminants such as heavy metals from water[127], and for agricultural crop production[128,129]. Ash-amended biochars have also been reported to possess enhanced redox properties with both higher electron donating and electron accepting capacity[129], which bears potential for application in the biochar/Fe(III)/PDS system. However, to the best of our knowledge, ash-amended biochars have not yet been tested for organic contaminant removal in Fenton-like PDS-based oxidation processes.

The main objectives of this work were (i) to investigate the effects of the pyrolysis conditions, specifically the pyrolysis temperature and ash amendments, on organic contaminant removal in the biochar/Fe(III)/PDS system and (ii) to gain insights into the role of redox-active moieties for Fe(III) reduction and PDS activation. To this end, we performed laboratory batch experiments with biochars produced under different pyrolysis conditions and studied the degradation kinetics of the insect repellent *N,N*-diethyl-*m*-toluamide (DEET) as our model compound upon activation of PDS in the

presence of Fe(III) at pH 2.5. We evaluated the performance of the different biochars for DEET removal in the biochar/Fe(III)/PDS system with respect to the biochar characteristics, particularly the redox properties and redox-active moieties.

3.2 Materials and methods

A list of all chemicals including suppliers and purities is provided in Section S3.1 of the Supporting Information.

3.2.1 Biochar preparation

The pyrolysis of the biochars was performed in a PYREKA (Pyreg GmbH, Dörth, Germany) continuously operating screw reactor, which is described in Hagemann et al[53]. If not mentioned otherwise, the reactor was purged with N_2 with a flow rate of 2 L min^{-1} and a residence time of 10 min. Four biochars were produced from beech wood as feedstock at three different temperatures (450°C, 600°C, and 750°C). One biochar was produced at 450°C with a higher N_2 flow rate of 10 L min^{-1}. In the following, the four beech wood biochars are referred to as BC450, BC450HF ("high flow"), BC600, and BC750. To study the impact of ash amendments, four biochars were produced at 500°C from softwood sawdust to which wood ash (bottom ash, dry matter basis) was added. Different amounts of 0, 8.9, 16.4, and 42.6 weight percent (wt %) of ash were amended in the pyrolysis process as described in Grafmüller et al[129], resulting in biochars with an actual ash content of 2.3%, 24.4%, 41.1%, and 69.0%, respectively. The four softwood sawdust biochars are referred to as BC-ash0 ("biochar-0 wt% ash additive"), BC-ash9, BC-ash16, and BC-ash43. All biochars were ground using an impact mill (Kinematica AG, Lucerne, Switzerland) to a particle size of < 200 µm (Figure S3.1) and kept in a desiccator until further use.

3.2.2 Batch experiments with biochar, PDS and Fe(III)

Batch experiments were conducted in 40 mL amber glass vials at room temperature on an overhead shaker. 1 g L^{-1} biochar suspension was prepared with 30 mg biochar in 30 mL deionized water and the initial pH was adjusted to 2.5 with 0.25 M H_2SO_4. DEET was added to the biochar suspension from an aqueous 10 mM stock solution to achieve a nominal initial concentration of 50 µM DEET. For experiments with BC750, a nominal initial concentration of 100 µM was used due to the high adsorption capacity of BC750. After 30 min contact time, an apparent sorption equilibrium was reached (Figure S3.6). Subsequently, the reaction was initiated by adding 60 µL of Fe(III) from a 0.05 M aqueous Fe(III) stock solution to reach an initial concentration of 0.2 mM Fe(III), followed by adding 240 µL of PDS from a 1 M aqueous stock solution to obtain an initial nominal PDS concentration of 8 mM. At pre-defined time intervals, 1 mL aliquots were sampled and immediately added into a mixture of 100 µL methanol (2 M in the sample, ≈ 9% v/v) and 5.5 µL NaOH (10 mM in the sample, ≈1% v/v, pH > 11) to quench the reaction and precipitate iron. Samples were filtered through 0.22 µm syringe filters (PES, BGB Analytik, Germany; 88.5 ± 0.7% DEET recovery) and collected into sample vials for DEET analysis. The pH was monitored and controlled at 2.5 ± 0.1 by adding small amounts H_2SO_4 or NaOH during the reaction. Control experiments including biochar only (as sorption control), Fe(III) only, PDS only, and combinations thereof in presence of DEET were investigated identically with the procedure described above.

3.2.3 Fe(II) formation experiment

To assess the Fe(II) formation potential of the biochars, 1g biochar L^{-1} suspensions were spiked with 0.2 mM Fe(III), and the dissolved Fe(II) concentration was measured over the course of two hours using a modified Ferrozine assay adopted from Stookey et al.[180] as described by Amstaetter et al.[181]. Briefly, aliquots of aqueous samples were filtered and spiked immediately into 1 M HCl in disposable cuvettes (1.5 mL, BrandTech) to protect Fe(II) from oxidation. Then, the Ferrozine reagent was added

to form a purple colored Fe^{2+} complex, which was quantified spectrophotometrically at 562 nm after incubation in the dark for 5 min.

3.2.4 Biochar charaterization

Electron exchange capacity (EEC)

The electron exchange capacity (EEC) was determined using a mediated electrochemical reduction (MER) and mediated electrochemical oxidation (MEO) method adopted from Klüpfel et al[58]. All analyses were conducted in a glovebox under anoxic conditions. The biochars were placed under vacuum in the antechamber overnight to remove adsorbed O_2 and then transferred into the glovebox to prepare a 10 g L^{-1} biochar suspension in anoxic deionized water. The biochar suspensions were stirred at least 24 hours to ensure complete dispersion before analysis. For the electrochemical setup and measurement details see Section S3.2. The electron accepting capacity (EAC) and electron donating capacity (EDC) were calculated in µmol e^- (g biochar)$^{-1}$ according to Klüpfel et al., 2014[58]. Furthermore, the obtained EAC and EDC values were normalized to the carbon mass of the biochar in µmol e^- (g carbon)$^{-1}$ according to the carbon content (Table S3.2 and S3.3).

Electrical conductivity

The electrical conductivity was determined using a “Black Gauß” (Eurofins Umwelt Ost GmbH, Freiberg, Germany), and measurements and calculations are described in detail elsewhere[177].

Persistent free radicals

The persistent free radicals (PFRs) were determined by continuous wave X-band electron spin resonance (ESR) spectroscopy (MiniScope MS 300, Magnettech GmbH, Berlin, Germany). The spectra were accumulated 3-fold over 90 s at a microwave power of 0.1 mW (sweep width 15 mT) and Suwanne River standard fulvic acid (1S101F, IHSS) was used as a reference with a free radical content of 0.54 x 10^{17}

spins g^{-1} for the calculation of spin concentrations. The g-values were determined in separate scans by measuring a certified internal manganese standard (Mn^{2+} in ZnS) simultaneously with the samples.

Size distribution, elemental composition, and surface area

The biochar size distribution was determined by a Mastersizer 2000 (Malvern Inc., UK). The elemental composition as well as the ash and water contents of the beech wood biochars were analyzed at Eurofins (Freiberg, Germany) according to the European Biochar Certificate (www.european-biochar.org). For the ash-amended biochars see Grafmüller et al[129]. The specific surface area of the beech wood biochars was determined using Brunauer–Emmett–Teller (BET) measurements, see Section S3.2 and for the determination of ash-amended biochars see Grafmüller et al[129].

Surface functional groups and metal content

The functional groups on the biochar surface were characterized by attenuated total reflectance Fourier transform infrared (ATR-FTIR) spectroscopy. The spectra were recorded using a Nicolet 670 FT-IR spectrometer (Thermo Fisher Scientific GmbH) equipped with an EverGlo source, a KBr beam splitter, and a deuterated L-alanine-doped triglycene sulphate (DLaTGS) detector. In situ X-ray diffraction analysis (XRD) measurements were performed for the investigation of biochar surface structure properties on a Bruker D2 PHASER X-ray diffractometer. The metal content of the biochars was determined by inductively coupled plasma-optical emission spectroscopy (ICP-OES, ICP iCAP7000series, Thermo Fisher Scientific Inc.) after microwave acid digestion. For detailed information of the biochar characterization see Section S3.2.

3.2.5 DEET quantification

The concentration of DEET in aqueous solutions was quantified by high-performance liquid chromatography equipped with a diode array detector (HPLC UV-vis, 1200 Series, Agilent, USA). The wavelength was set to 210 nm. 10 µL of sample was injected and analyzed with a C18 column (150 mm × 4.6 mm, 5 µm, ZORBAX Eclipse XDB-C18, Agilent). The eluent mixture consisted of 60% methanol and 40% water (pH 3, 1 mM H_2SO_4) at a flow rate of 0.5 mL min^{-1}. DEET concentrations were quantified by external calibration from 2 to 200 µM.

3.2.6 Data analysis

Pseudo-first order rate constants (k_{obs}) and half-life times ($t_{1/2}$) were calculated according to eq. (1) and eq. (2), respectively:

$$\ln\frac{c_t}{c_0} = -k_{obs} \cdot t \quad (1)$$

$$t_{1/2} = \frac{\ln 2}{k_{obs}} \quad (2)$$

where c_t is the concentration of DEET at time t and c_0 is the measured initial DEET concentration in the biochar suspension after 30 min sorption equilibrium.

3.3 Results and discussion

3.3.1 Impact of biochar pyrolysis temperature on DEET removal in the presence of PDS and Fe(III)

Performance of beech wood biochars

As shown in Figure 3.1a, DEET was removed most efficiently with the two low-temperature biochars BC450 and BC450HF in the biochar/Fe(III)/PDS system. BC450 resulted in 88 ± 3% DEET removal within two hours following pseudo-first order kinetics with a k_{obs} of (2.9 ± 0.1) × 10^{-4} s^{-1} (Figure S3.8) and a $t_{1/2}$ of 39 ± 4 min. The k_{obs} for DEET degradation in the BC450HF/Fe(III)/PDS system was (2.2 ± 0.1) × 10^{-4} s^{-1} and only slightly lower than the one obtained in the BC450/Fe(III)/PDS system (Figure S3.8). The N_2 flow rate during feedstock pyrolysis thus had a minor effect on the performance of the biochars, which is reflected in similar biochar properties (Table S3.2).

In contrast, the pyrolysis temperature had a significant effect on the biochar properties and DEET degradation. When BC600 was employed together with Fe(III) and PDS, the $t_{1/2}$ of DEET was 227 ± 9 min with a k_{obs} of (0.4 ± 0.1) × 10^{-4} s^{-1} (Figure S3.6). The latter is 7.3 times lower than the k_{obs} in the BC450/Fe(III)/PDS system. Experiments with BC750 did not lead to DEET removal (Figure 3.1a). On the contrary, we observed a sharp increase in aqueous DEET concentration after PDS addition, indicating desorption of DEET from BC750 rather than transformation. Decreasing DEET degradation rate constants with increasing pyrolysis temperatures suggest distinctly different biochar properties affecting PDS activation or formation of reactive species. In control batches with PDS only, biochar only, Fe(III) only, and combinations thereof, DEET removal was much less efficient (< 5.5 – 29%, Figure S3.7). The accelerated DEET degradation in the biochar/Fe(III)/PDS system indicates biochar-mediated Fe(III) reduction leading to continuous PDS activation upon reaction with Fe(II) as shown in our previous study (Chapter 2) and reported elsewhere[113–116].

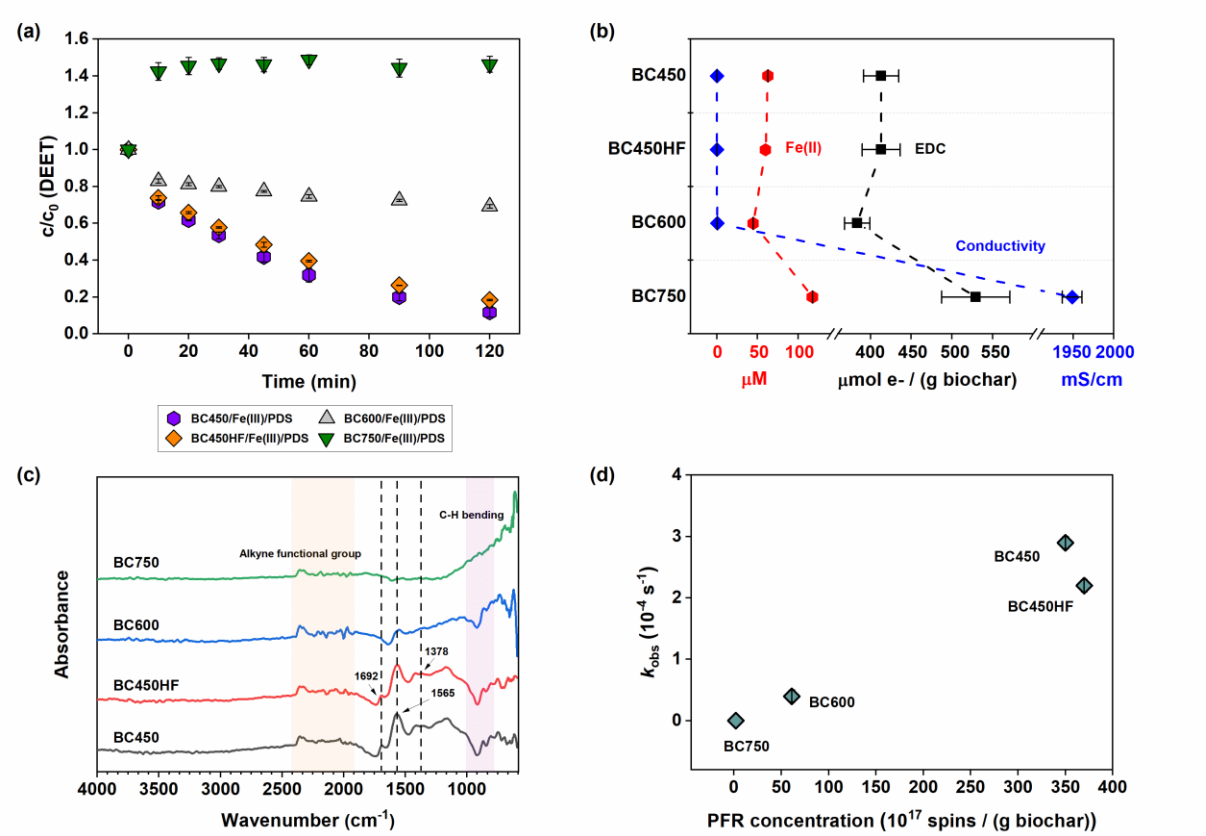

Figure 3.1. (a) DEET removal in the biochar/Fe(III)/PDS system with beech wood biochars pyrolyzed at different conditions (BC450, BC450HF, BC600, and BC750). [Biochar] = 1 g L^{-1}, [Fe(III)] = 0.2 mM, [PDS] = 8 mM, $[DEET]_0$ = c_0 ~ 40 µM after sorption equilibrium, c = measured DEET concentration over time, pH 2.5. (b) Electron donating capacity (EDC, E_h (MEO) = 0.61 V, black) and electrical conductivity (EC, pressure 5 tons, blue) of BC450, BC450HF, BC600, and BC750, and corresponding Fe(II) formation (red) in biochar suspensions spiked with Fe(III). [Biochar] = 1 g L^{-1}, [Fe(III)] = 0.2 mM, pH 2.5. (c) ATR-FTIR spectra of BC450, BC450HF, BC600, and BC750. (d) Persistent free radical (PFR) concentrations and DEET removal rate constants (k_{obs}) of BC450, BC450HF, BC600, and BC750. Error bars indicate the standard deviation of triplicate experiments.

Fe(III) reduction

In batch experiments containing suspensions of the individual biochars and 0.2 mM Fe(III), we monitored Fe(II) formation for two hours (Figures 3.1b and S3.9). All biochars successfully reduced Fe(III) to Fe(II) in aqueous solution, with BC750 leading to the highest Fe(II) formation (120 µM), followed by BC450 and BC450HF (60 µM), and BC600 (40 µM).

Redox-active properties of biochars

BC750 exhibited the highest EDC value (529 ± 42 µmol e^- (g biochar)$^{-1}$), followed by BC450 and BC450HF (413 ± 22 µmol e^- (g biochar)$^{-1}$ and 413 ± 23 µmol e^- (g biochar)$^{-1}$), and BC600 (384 ± 16 µmol e^- (g biochar)$^{-1}$) (Table S3.2). This observed effect of pyrolysis temperature on biochar EDC values is consistent with other studies[58,188].

The EDC of biochars can originate from various redox-active moieties including both organic and inorganic constituents[58]. FTIR analyses of the biochars showed peaks of C=O conjugated ketones at 1692 cm^{-1}, -COOH at 1565 cm^{-1} and phenolic-OH at 1378 cm^{-1} in each BC450, BC450HF, and BC600 (Figure 3.1c). The peak intensities of those oxygen-containing functional groups, which may be involved in electron transfer reactions, decreased with increasing pyrolysis temperature. No redox-active functional groups were observed at a pyrolysis temperature of 750°C.

Persistent free radicals (PFRs), i.e. moieties with unpaired electrons, can also contribute to the EDC of biochars[68,163]. The g-values of all biochars were < 2.0030 indicating the presence of carbon-centered PFRs[191], which can form during pyrolysis from hemicellulose, cellulose, and lignin as organic radical precursors[163]. The PFR concentrations decreased with increasing pyrolysis temperatures (Table S3.2), in agreement with previous studies showing PFR elimination on biochar surfaces at high pyrolysis temperatures (> 700°C)[68,116,192]. BC450 and BC450HF displayed the highest PFR concentrations in the range of (3.5 ± 0.4) × 10^{19} spin (g biochar)$^{-1}$, which is two orders of magnitude higher than that of BC750 (1.9 ± 0.1) × 10^{17} spin (g biochar)$^{-1}$) (Table S3.2).

Inorganic redox-active metal species, mainly Fe and Mn, may also contribute to the EDC of biochars. Both the Fe and Mn concentration increased with increasing pyrolysis temperature (Table S3.1). BC750 contained the highest Fe and Mn contents of 10.6 µmol (g biochar)$^{-1}$and 9.6 µmol (g biochar)$^{-1}$, respectively. However, when calculating the molar ratios of Fe and Mn content to the EDC, all the biochars showed similar ratios. For all biochars, the Fe and Mn contents could each only explain between 1.3 – 2.0% of the measured EDCs (Table S3.1). Neither Fe nor Mn minerals were found in XRD spectra, which further indicates that no redox-active minerals were formed in beech wood biochars (Figure S3.4).

The EC of the biochars increased with increasing pyrolysis temperature (Figure 3.1b, Figure S3.5 and Table S3.2). BC450 showed the lowest EC of (7.6 ± 0.3) × 10^{-5} mS cm^{-1}, while BC750 exhibited an 8 orders of magnitude higher EC of 1949 ± 12 mS cm^{-1}. Such differences in EC are generally derived from formation of graphene-like structures at high pyrolysis temperatures with conjugated π-electron systems that facilitate direct electron transfer through the carbon matrix[106,193]. These results are consistent with the lowest H/C and O/C ratios of BC750 suggesting a high degree of aromatic condensation (Table S3.2).

Altogether, our results indicate that for biochars produced at lower pyrolysis temperature (< 600°C), oxygen-containing functional groups and PFRs were the main moieties contributing to the EDC. In contrast, for biochars produced at high pyrolysis temperature (750°C), the EDC was attributed to conductive graphene-like structures.

Impact of redox-active properties of biochars on Fe(III) reduction and DEET degradation

The pyrolysis of beech wood at different temperatures led to biochars with distinctive electrochemical properties that impacted the reduction of Fe(III) and DEET degradation in the biochar/Fe(III)/PDS system. Fe(III) reduction increased with increasing EDC values of the biochars (Figure 3.1b). However, while all biochars possessed an EDC and were able to reduce Fe(III), DEET was only degraded in the presence of low pyrolysis temperature biochars (< 600°C) in the biochar/Fe(III)/PDS

system. These results indicate that oxygen-containing functional groups and PFRs in the BC450, BC450HF, and BC600 might play a key role for DEET degradation in the biochar/Fe(III)/PDS system. In fact, a positive correlation was obtained for PFR concentration of the biochars and DEET removal (Figure 3.1d). BC750, in contrast, contained conductive graphene-like structures that likely contributed to high EDCs and Fe(III) reduction, but did not support and rather inhibit DEET degradation in the biochar/Fe(III)/PDS system.

The addition of low temperature pyrolyzed biochar in the biochar/Fe(III)/PDS system appeared to initiate an efficient Fe(III)/Fe(II) cycling induced by the high amount of oxygen-containing functional groups and PFRs that may form reactive species leading to DEET transformation (Chapter 2). In contrast, the high-temperature biochar with its high EC attributed to high content of conjugated aromatic structures, may have favored a mediated electron transfer pathway[106], in which electron transfer from organics (electron donor) to persulfate (electron acceptor) mediated by biochar. This pathway may be specific for certain target reactants and thus less effective for DEET degradation. Our results were consistent with the findings of Liang et al. 2021 who reported fast Fe(III)/Fe(II) circulation due to transformation between semiquinone radicals and quinones in biochars produced at 400°C[113]. In case of high-temperature biochars with high content of conjugated aromatic structures, contaminant degradation by electron transfer pathway has been suggested[113,194,195].

3.3.2 Impact of feedstock and ash amendments in biochar pyrolysis for DEET degradation in the presence of PDS and Fe(III)

Beech wood biochar versus softwood sawdust

A different type of biochar was produced from softwood sawdust at 500°C (BC-ash0). This biochar had an EDC of 42 ± 6 μmol e^- (g biochar)$^{-1}$, which is almost 10 times lower than the beech wood biochar produced at 450°C (BC450). The k_{obs} for DEET degradation in the BC-ash0/Fe(III)/PDS system was (0.4 ± 0.1) × 10^{-4} s^{-1} (Figure 3.2a and Figure S3.10) and thus 7.25 times lower than in the BC450/Fe(III)/PDS system (k_{obs} = (2.9 ± 0.1) × 10^{-4} s^{-1}) (Figure 3.1a). The BC-ash0 contained oxygen-containing functional groups (C=O and -COOH, see Figure S3.3), and a relative high concentration of PFRs ((2.72 ± 0.05) × 10^{18} spin (g biochar)$^{-1}$). However, the concentration of PFRs of BC-ash0 was one order of magnitude lower than that of BC450 ((3.5 ± 0.4) × 10^{19} spin (g biochar)$^{-1}$), which might explain the lower EDC and DEET degradation of BC-ash0 compared to BC450. These findings indicate that feedstock might play a role for the formation of redox-active properties of biochar. To enhance the redox properties and performance of biochars, the feedstock pyrolysis process might be modified e.g., through the amendment of ash, which has been shown to lead to biochars with high EDC values[129].

EDC and performance of ash-amended softwood sawdust biochars

To investigate the effects of ash amendments on the redox properties and performance of the biochars in the biochar/Fe(III)/PDS system, different amounts of ash (9, 16, 43 wt%) were added to softwood sawdust during pyrolysis. All ash-amended biochars possessed significantly higher EDCs compared to the non-ash amended control biochar BC-ash0 (Figure 3.2b). Ash amendments of 9 wt%, 16 wt%, and 43 wt% led to an 8-, 14-, and 5-fold increase in biochar EDC compared to BC-ash0, respectively (Table S3.3). BC-ash16 possessed the highest EDC of 590 ± 12 μmol e^- (g biochar)$^{-1}$ (Figure 3.2b and Table S3.3). Notably, the EDC did not increase

linearly with ash amendment indicating that there is an optimum ash addition. Yet, the here tested ash amendments all resulted in biochars with enhanced redox-active properties. The raw ash itself has a low EDC value of 53 μmol e^- (g ash)$^{-1}$)[129], indicating that the ash itself may not have caused the increase in EDC values of the ash-amended biochars. Additional redox-active moieties may have been formed in the biochars during pyrolysis in the presence of ash.

In biochar suspensions spiked with 0.2 mM of Fe(III), all ash-amended biochars produced more Fe(II) than the biochar without ash amendment (Figure 3.2b). BC-ash16 produced most Fe(II) (68 μM), followed by BC-ash43 (53 μM) and BC-ash9 (42 μM). BC-ash0 formed only little Fe(II) (8 μM). The Fe(II) formation was consistent with the EDC values.

Due to the high EDC values and the Fe(III) reduction potential, ash-amended biochars might show good performance for pollutant removal in the biochar/Fe(III)/PDS system. In fact, all ash-amended biochars outperformed the non-ash amended control biochar in terms of DEET removal in the presence of Fe(III) and PDS (Figure 3.2a). The DEET degradation rate constants k_{obs} of BC-ash9, BC-ash16 and BC-ash43 were 7.25 times, 10 times and 4.5 times higher than the k_{obs} of the BC-ash0 (Figure 3.2a and Figure S3.10). BC-ash16, which possessed the highest EDC value, showed the best performance for DEET removal with a k_{obs} of (4.0 ± 0.1) × 10^{-4} s^{-1} (Figure S3.10). This k_{obs} value was 1.4 times higher compared to the BC450/Fe(III)/PDS system (Figure 3.1a and Figure S3.8). The amendment of ash during pyrolysis thus seems to be a useful strategy to produce biochars with a high EDC, which can be used for improved DEET transformation in the presence of Fe(III) and PDS.

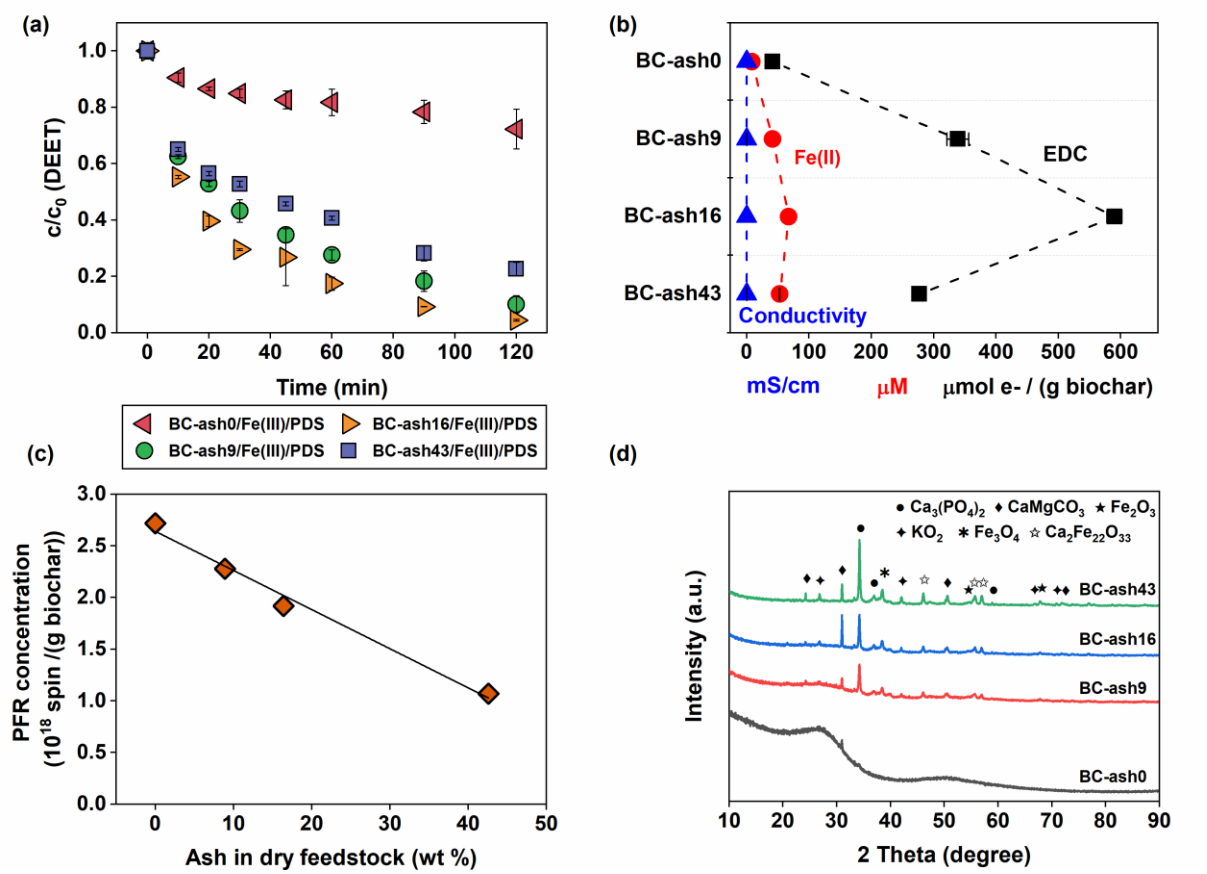

Figure 3.2. (a) DEET removal in the biochar/Fe(III)/PDS system with ash-amended biochars (BC-ash9, BC-ash16, and BC-ash43) and a non-ash amended control biochar (BC-ash0). [Biochar] = 1 g L^{-1}, [Fe(III)] = 0.2 mM, [PDS] = 8 mM, $[DEET]_0 = c_0$ ~ 40 μM after sorption equilibrium, c = measured DEET concentration over time, pH 2.5. Error bars indicate the standard deviation of triplicate experiments. (b) Electron donating capacity (EDC, E_h (MEO) = 0.61 V, black) and electrical conductivity (EC, pressure 5 tons, blue) of BC-ash0, BC-ash9, BC-ash16, and BC-ash43, and corresponding Fe(II) formation (red) in biochar suspensions spiked with Fe(III). [Biochar] = 1 g L^{-1}, [Fe(III)] = 0.2 mM, pH 2.5. Error bars indicate the standard deviation of triplicate experiments. (c) Linear correlation of persistent free radical (PFR) concentrations and weight percent of amended ash to dry feedstock during biochar pyrolysis (R^2 = 0.99). (d) X-ray diffraction (XRD) spectra of BC-ash0, BC-ash9, BC-ash16, and BC-ash43 with indicated formation of β-tricalcium phosphate ($Ca_3(PO_4)_2$, dot), dolomite ($CaMgCO_3$, rhombus),Hematite (Fe_2O_3, solid five-pointed star), potassium superoxide (KO_2, four-pointed star), magnetite (Fe_3O_4, asterisk), calcium ferrites ($Ca_2Fe_{22}O_{33}$, hollow five-pointed star).

Linking redox-active properties of biochars with their performance

We further characterized the ash-amended biochars to gain a better understanding of which properties govern their performance in the biochar/Fe(III)/PDS system. The non-ash amended as well as the ash-amended softwood sawdust biochars contained PFR concentrations in the range of 10^{18} spins (g bichar)$^{-1}$ (Figure 3.2c and Table S3.3). The PFR concentration decreased linearly (R^2 = 0.99) but only slightly with increasing ash amendment (Figure 3.2c). The BC-ash0 mainly contained carbon-centered PFRs as indicated by a g-value of 2.0029[191]. This finding is consistent with beech wood biochars, which had a similar final ash content (2.1 – 3.5%, Table S3.2) than the BC-ash0 (2.3 % ash) and g-values of 2.0028 – 2.0029 (Table S3.3). For the ash-amended biochars, the g-values were in the range of 2.0030-2.0031 (Table S3.3) indicating carbon-centered radicals with an adjacent oxygen atom[191]. These results hint at a potential transition of redox-active PFRs from aryl radicals (carbon-centered) to semiquinoid radicals (intermediate of the phenolic C-OH and quinoid C=O groups)[188]. The potential formation of semiquinoid radicals in ash-amended biochars may be beneficial for Fe(III) reduction and PDS activation.

Despite the similar PFR concentrations and types of the ash-amended biochars, we observed differences in DEET removal performance (Figure 3.2a). These differences may arise from differences in their redox-active moieties including oxygen functional groups or metals. FTIR measurements showed that electron donating oxygen functional groups, mainly C=O and –COOH goups, decreased with increasing ash amendment, and almost no peaks were observed for BC-ash43 (Figure S3.3). The ash, which was added during biochar pyrolysis, contained metals that can form redox-active crystalline minerals in the biochars during pyrolysis[128,196]. Indeed, the Fe and Mn contents of the biochars increased with increasing ash amendment (Table S3.1). The BC-ash43 had the highest Fe and Mn content of 178 µmol (g biochar)$^{-1}$ and 22 µmol (g biochar)$^{-1}$, respectively. These values are 28 times and 1.8 times higher than the Fe and Mn content of BC-ash0 (Table S3.1). When calculating the contribution of the metal species to the EDCs in molar ratio, 64% of the EDC of the BC-ash43 could

be attributed to Fe, while for BC-ash16, BC-ash-9, and BC-ash0 the contribution of Fe was in a similar range of 16% (Table S3.1). Metals in biochars usually exist as metal-based minerals[197]. XRD analysis showed pronounced differences in mineralogy of the biochars with and without ash amendment (Figure 3.2d). BC-ash0 showed an amorphous profile with almost no peaks. In contrast, the ash-amended biochars showed distinct peaks, indicating the formation of ash-derived crystalline minerals. Hematite (Fe_2O_3) and magnetite (Fe_3O_4), two common redox-active iron minerals were observed in all ash-amended biochars (Figure 3.2d). These results hint at that the formation of redox-active Fe crystalline minerals in the ash-amended biochars, which likely contributed to the higher EDCs and enhanced Fe(III) reduction and PDS activation compared to the non-ash amended control biochar. Although the highest amount of Fe crystalline minerals was formed in BC-ash43, their beneficial effect might be reduced by the combined lack of redox-active C=O and –COOH functional groups (Figure S3.3) and lower PFR concentration (Figure 3.2c). These results indicate a complex interplay and potentially more pronounced role of redox-active oxygen functional groups and FPRs in ash-amended biochars.

All softwood sawdust biochars showed low ECs as they were produced at relatively low pyrolysis temperature (500°C) where conductive conjugated aromatic structures were hardly formed, which is consistent with a relatively high H/C of the biochars (Table S3.3). Altogether, the characterization of the softwood sawdust biochars with and without ash amendment demonstrated the contribution of oxygen functional groups and PFRs to their redox-active properties, which was consistent with the conclusion for beech wood biochars. Particularly, ash amendment led to the formation of redox-active Fe crystalline minerals and semiquinoid persistent free radicals that promoted Fe(III) reduction and PDS activation in biochar/Fe(III)/PDS system.

3.4 Environmental implications

Biochar can facilitate electron transfer by surface redox-active moieties and/or inner carbon matrices[76,106], which is greatly dependent on the biochar pyrolysis temperature. We showed that biochar derived at low pyrolysis temperature (< 500°C) is generally enriched with oxygen functional groups and PFRs that can reversibly accept and donate electrons. Low temperature biochars exhibited the best performance for DEET transformation in the presence of Fe(III) and persulfate, due to efficient Fe(III) reduction to Fe(II), which can activate persulfate. In contrast, high temperature biochars possessed a high content of conjugated aromatic structures and did not lead to DEET removal. Low temperature biochars containing high amounts of oxygen functional groups and PFRs thus seem to be best suited for applications in the biochar/Fe(III)/PDS system. We showed that the amendment of ash during pyrolysis enhanced the redox-active properties of biochars, where biochars with high EDCs are produced that can efficiently be employed for DEET removal in the biochar/Fe(III)/PDS system. Ash amendments of 16 wt% produced the best-performing biochar with high content of redox-active functional groups and PFRs. Since the characteristics and performance of the biochars have been shown to depend on the amount of ash added, future research is needed to systematically identify the optimal conditions for biochar pyrolysis.

Our study can inform the production of engineered biochars with optimal redox-active properties tailored for different applications such as persulfate activation in the presence of Fe(III) for target contaminant removal from water. The production of biochars with high amounts of oxygen functional groups, PFRs, and redox-active minerals seems promising for enhancing the removal of organic contaminants in heterogeneous persulfate-based oxidation processes. Future research is needed to gain a better understanding of e.g., the impact of feedstock or post-pyrolysis treatments on the redox properties of biochars and their performance also on longer time scales. To use these highly complex materials for specific applications such as

water treatment, we also need more standardized biochar production procedures as well as performance monitoring strategies to ensure consistent biochar production as well as consistent performance.

Acknowledgement

This work was funded by the China Scholarship Council (CSC, File No. 201904910454). We thank Claudia Schmalsch for support in the laboratory, Marvin Sens and Christiane Herzog for analyzing the metal contents of the biochar samples.

Supporting Information to

Chapter 3

S3.1 Chemicals

All chemicals in this study were used as received. Sodium persulfate (PDS, $Na_2S_2O_8$, ≥99% for analysis EMSURE®), methanol (MeOH, HPLC grade ≥99.9%), 2,2'-azino-bis(3-ethylbenzothiazoline-6-sulfonic acid) diammonium salt (ABTS, ≥98.0%) were purchased from Sigma-Aldrich. Sulfuric acid (H_2SO_4, 95-97% for analysis EMSURE®), sodium hydroxide solution (NaOH, 1 M, TitriPUR®), potassium chloride (KCl, for analysis EMSURE®), monopotassium phosphate (KH_2PO_4, for analysis EMSURE®) were purchased from Merck. 3-(2-pyridyl)-5,6-diphenyl-1,2,4-triazine-p,p'-disulfonic acid, disodium salt hydrate (ferrozine, 97+%, ACROS Organics™), and ammonium acetate (98+%, ACROS Organics™) were purchased from Fisher Scientific. Formic acid, Iron(III) sulfate hydrate ($Fe_2(SO4)_3 \cdot H_2O$, 21-23% Fe basis puriss. p.a.) was purchased from Fluka. *N,N*-diethyl-*m*-toluamide (DEET, ≥98%) was purchased from Tokyo Chemical Industry (TCI) GmbH. Mn^{2+} in ZnS (100% manganese isotope ^{55}Mn with the nuclear spin of I = 5/2) was from Magnettech GmbH, Berlin. Suwannee River standard fulvic acid was from the International Humic Substances Society, IHSS, St. Paul, MN, USA. *N,N*-bis(3-sulfonatopropyl)-4-4'-bipyridinium (zwitterionic viologen, ZiV) was synthesized in the lab and characterized by Fourier-Transform Infrared Spectroscopy (FTIR), for details see Schlögl et al. 2022[176]. Aqueous solutions were prepared with deionized water (18.1 MΩ x cm, Arium® Pro Water Purification System).

S3.2 Characterization of biochars

S3.2.1 Specific surface area

The specific surface area of the beech wood biochars was determined using 5-point Brunauer–Emmett–Teller (BET) measurements (TU Freiberg, Germany). The samples were prepared in a gas adsorption sample preparation device Smart VacPrep (Micromeritics, Germany) and measured in a surface area system ASAP 2460 (Micromeritics, Germany). For the determination of ash biochars see Grafmüller et al., 2022 [129].

S3.2.2 Size distribution

The biochar size distribution was determined by a Mastersizer 2000 (Malvern Inc., UK) coupled with a sample dispersion unit (Hydro 2000S, Malvern Inc., UK) using the wet sample mode. 10 g biochar L^{-1} suspensions were prepared and kept on the table shaker overnight to obtain a fully dispersed suspension before measurement. The samples were continuously stirred directly until measurement. A 15% obscuration bar was applied to ensure identical sample amounts between biochar samples added. Data quality was optimized by adjusting the stir speed to a residual of weight below 1%.

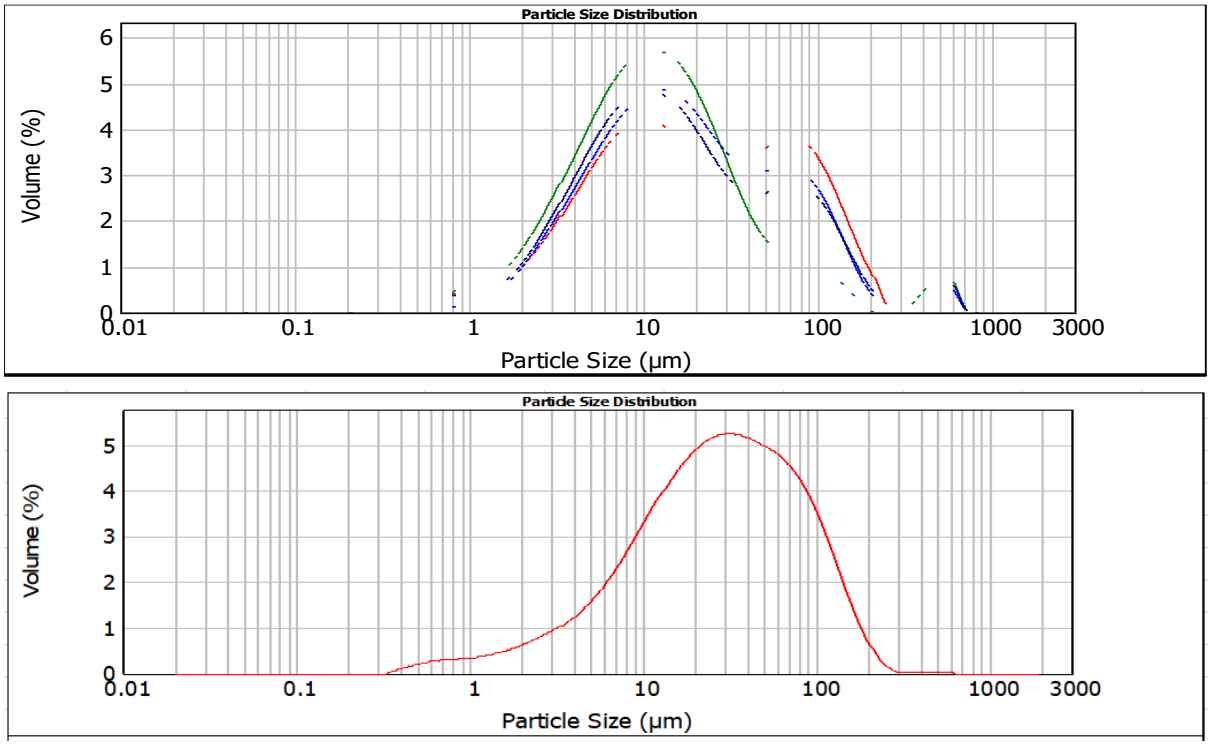

Figure S3.1. Particle size distribution of wood biochars (upper panel, BC450 (red line), BC450HF (black line), BC600 (green line) and BC750 (blue line)), and BC-ash 43 measured as representative for ash-amended biochars (bottom panel).

S3.2.3 Electron exchange capacity (EEC)

The electron exchange capacity (EEC) was determined using a mediated electrochemical reduction (MER) and mediated electrochemical oxidation (MEO) method adopted from Klüpfel et al., 2014[58]. All analyses were conducted in a glovebox under anoxic conditions. The biochars were placed under vacuum in the antechamber overnight to remove adsorbed O_2 and then transferred into the glovebox to prepare a 10 g L^{-1} biochar suspension in anoxic deionized water. The biochar suspensions were stirred at least 24 hours to ensure complete dispersion before analysis. For the electrochemical setup, eight 9 mL glassy carbon cells (Sigradur G, HTW, Germany) with copper wires attached (four for MER and four for MEO) served as both working electrodes and the reaction vessels. The counter electrodes were coiled platinum wires (0.5 mm, 99.9%, Sigma-Aldrich Co., USA) connected to platinum gauzes (52 mesh, 99.9%, Sigma Aldrich Co., USA) in glass tubes with porous glass frits filled with phosphate buffer (0.1 M KCl, 0.1 M KH_2PO_4, pH 7). The reference electrodes were Ag/AgCl electrodes (Bioanalytical Systems Inc., USA) but redox potentials are reported with reference to the standard hydrogen electrode. The reaction vessels were filled with 7 mL phosphate buffer (0.1 M KCl, 0.1 M KH_2PO_4, pH 7) and equilibrated to desired redox potentials (E_h = -0.38 V for MER and + 0.61 V for MEO) using an eight-channel potentiostat CHI1000 (CH Instruments, USA). To start the measurement, 100 µL of a 10 mM mediator stock solution, either zwitterionic viologen (ZiV) for reduction or 2,2'-azino-bis(3-ethylbenzothiazoline-6-sulfonic acid) (ABTS) for oxidation, was spiked into the continuously stirred reaction vessels resulting in reductive or oxidative current peaks. Then, different amounts of biochar samples were added consecutively into the vessels and caused sharp and clear current peaks.

For the data analysis, the current peaks were integrated by Matlab R2020Ra over an analysis time of 4000 s. The electron accepting capacity (EAC) and electron donating capacity (EDC) were calculated in µmol e^- (g biochar)$^{-1}$ according to Klüpfel et al., 2014[58]. Furthermore, the obtained EAC and EDC values were normalized to the carbon mass of the biochar in µmol e^- (g carbon)$^{-1}$ according to the carbon content.

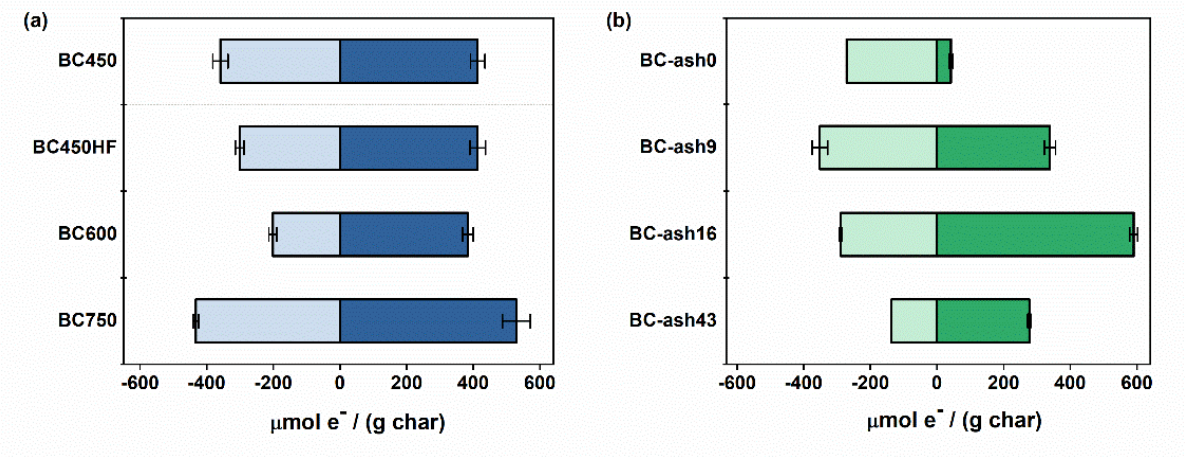

Figure S3.2. Electron accepting capacity (EAC, light color) and electron donating capacity (EDC, dark color) of (a) BC450, BC450HF, BC600 and BC750, and (b) BC-ash0, BC-ash9, BC-ash16, and BC-ash43. The electron exchange capacity (EEC) corresponds to the whole bar (EEC = EAC + EDC). E_h (MER) = -0.38 V and E_h (MEO) = 0.61 V.

S3.2.4 Fourier-transform infrared spectroscopy (FTIR)

The spectra were collected with a Nicolet 670 FT-IR spectrometer (Thermo Fisher Scientific GmbH) equipped with an EverGlo source, a KBr beam splitter, and a deuterated L-alanine doped Triglycine sulphate (DLaTGS) detector. The measurements were performed in attenuated total reflection (ATR) mode in a “Golden Gate” sample holder. The sample holder was cleaned with ethanol and acetone between measurements. Four measurements were conducted with different portions of the biochar sample over the range of 4000 – 600 cm^{-1} at 4 cm^{-1} and 32 co-added scans. All spectra were captured in absorbance units and ATR correction was applied in atmospheric conditions. Data were processed with standard normal variate (SNV) scatter-correction, followed with an asymmetric least squares baseline correction and a smoothing procedure with a Savitzky–Golay algorithm function (polynomial = 2 and points = 27).

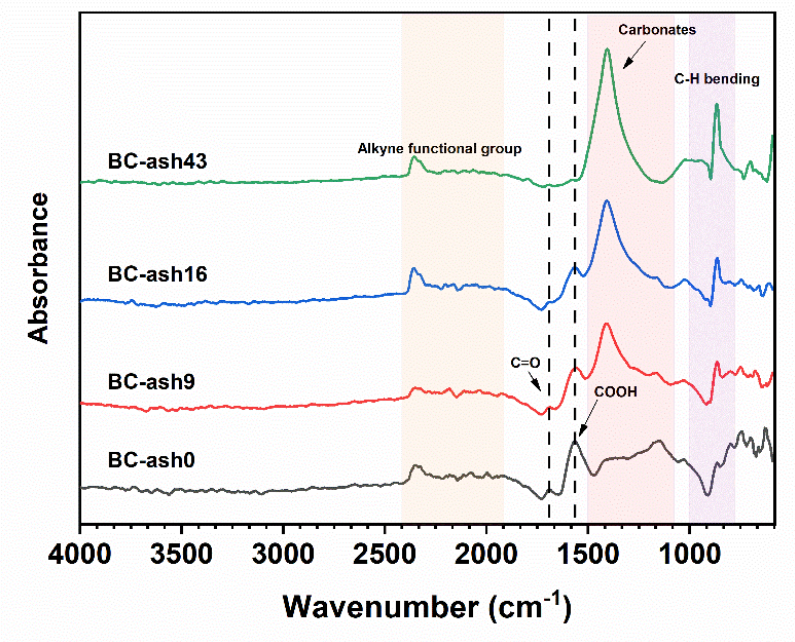

Figure S3.3. ATR-FTIR spectra of ash-amended biochars (BC-ash0, BC-ash9, BC-ash16, and BC-ash43).

S3.2.5 X-ray diffraction analysis (XRD)

In situ XRD measurements were performed on a Bruker D2 PHASER X-ray diffractometer coupled with a SSD160-2 detector. The spectra were collected with Co Kα (λ = 1.79026 Å) source emitting radiation over the angular range 10° ≤ 2θ ≤ 90° with 0.015° step size and 0.6 s time steps. The tube was operated at 30 kV and 10 mA. DIFFRAC.EVA software was used for data evaluation and a crystallography open database was employed for phase identification.

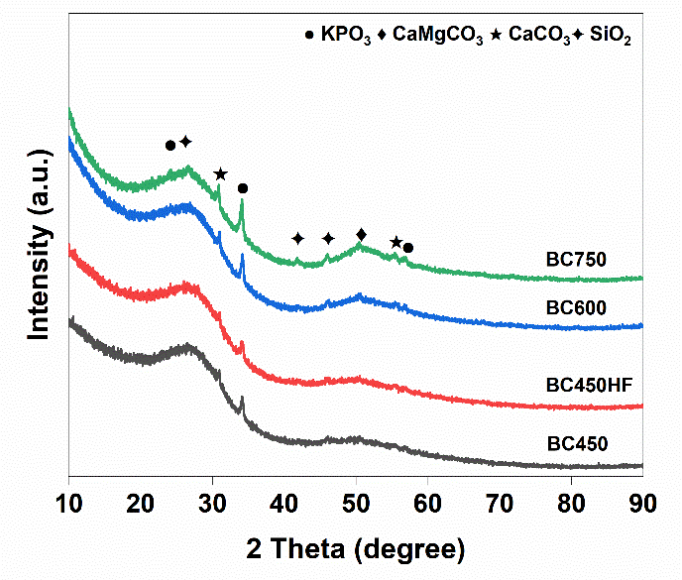

Figure S3.4. X-ray diffraction (XRD) spectra of wood biochars (BC450, BC450HF, BC600 and BC750).

S3.2.6 Electrical conductivity (EC) of the beech wood biochars

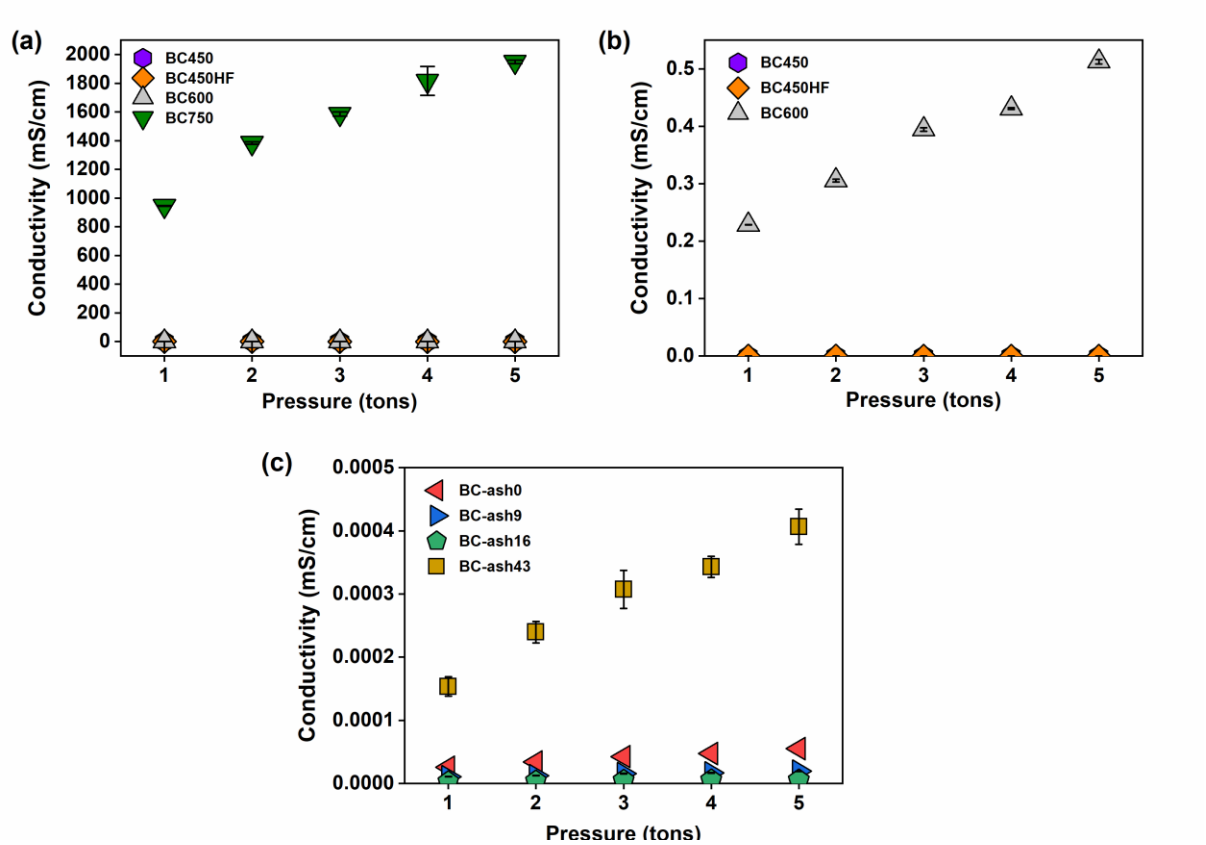

Figure S3.5. (a) Electrical conductivities of beech wood biochars (BC450, BC450HF, BC600, and BC750) measured at different pressures; (b) The magnification plot of BC450, BC450HF, and BC600 in Figure a. (c) Electrical conductivities of ash-amended biochars (BC-ash9, BC-ash16, and BC-ash43) and a non-ash amended control biochar (BC-ash0) measured at different pressures.

S3.2.7 Metal content

The metal content of the biochars was determined by inductively coupled plasma-optical emission spectroscopy (ICP-OES, ICP iCAP7000 Series, Thermo Fisher Scientific Inc.) after microwave acid digestion. 50 mg sample was digested in a mixture of 6 mL nitric acid and 2 mL hydrochloric acid. The digested solution was filled up to 50 mL for ICP-OES analysis.

Table S3.1. Concentrations of iron (Fe) and manganese (Mn) in the beech wood biochars and ash-amended biochars expressed in absolute numbers in µmol (g biochar)$^{-1}$ and as ratio of the metal content to the electron accepting capacity (EAC), electron donation capacity (EDC) and electron exchange capacity (EEC) of the biochars.

	Metal content		Metal content /EAC		Metal content /EDC		Metal content /EEC	
	µmol (g biochar)$^{-1}$		µmol metal/µmol e-					
	Fe	Mn	Fe	Mn	Fe	Mn	Fe	Mn
BC450	5.36	6.77	0.015	0.019	0.013	0.016	0.007	0.009
BC450HF	5.31	7.70	0.018	0.021	0.013	0.015	0.007	0.009
BC600	7.03	9.46	0.035	0.039	0.020	0.020	0.012	0.013
BC750	10.61	9.56	0.024	0.022	0.018	0.018	0.011	0.010
BC-ash0	6.44	12.09	0.047	0.088	0.155	0.291	0.036	0.068
BC-ash9	59.11	14.53	0.204	0.050	0.174	0.043	0.094	0.023
BC-ash16	98.28	17.27	0.279	0.049	0.167	0.029	0.104	0.018
BC-ash43	178.2	21.60	0.658	0.080	0.643	0.078	0.325	0.039

S3.2.8 Elemental composition

The elemental composition as well as the ash and water contents of the beech wood biochars were analyzed by Eurofins Ost GmbH (Freiberg, Germany) according to the European Biochar Certificate (EBC, 2023) (www.european-biochar.org). The values are shown in Table S2. For the determination of ash biochars see Grafmüller et al., 2022[129].

S3.2.9 Average carbon oxidation state (C_{ox}), double bond equivalent (DBE) and aromaticity index (AI)

The average carbon oxidation state (C_{ox}), double bond equivalent (DBE), and aromaticity index (AI) of the four biochars were calculated from the elemental composition (Table S3.1), where C_{ox} was derived from equations reported by Masiello et al., 2008[178], and DBE and AI were obtained from the molecular formulas according to Koch and Dittmar, 2006[179]. The average carbon oxidation state C_{ox} was calculated using Equation S3.1.

$$C_{ox} = \frac{2[O] - [H] - k[N] - m[S]}{[C]} \quad \text{(S3.1)}$$

where [O], [H], [N], [S] and [C] is the content of the element O, H, N, S and C, respectively, and k and m are factors that describe the oxidation state of N and S, respectively. k can vary between -3 (for ammonia) and +5 (for nitrate) and m between -2 (for sulfide) and +6 (for sulfate)[178]. Because of the small sulfur content (Table S3.1), the contribution of sulfur is negligible and m = 0 was used for the calculations. Varying k between the extreme values of -3 and +5 for fully reduced and oxidized N did not change the overall trend of the four biochars, and the values reported in Table S2 were calculated from k = +5 [58].

The double bond equivalent normalized to the total number of carbons DBE/C was calculated following equation S2. As DBE/C = 0.67 for benzene, a threshold of DBE/C ≥ 0.67 can be set for the presence of condensed aromatic ring structures[179].

$$\mathrm{DBE/C} = \frac{1 + 0.5\,(2\mathrm{C} - \mathrm{H} + \mathrm{N})}{\mathrm{C}} \qquad \text{(S2)}$$

The aromaticity index (AI) was calculated following equation S3 and takes into account heteroatoms that contribute to aromatic structures. A threshold of AI ≥ 0.67 was set for the presence of condensed aromatic ring structures [179].

$$\mathrm{AI} = \frac{\mathrm{DBE_{AI}}}{\mathrm{C_{AI}}} = \frac{1 + \mathrm{O} - \mathrm{C} - \mathrm{S} - 0.5\,(\mathrm{H} + \mathrm{N})}{\mathrm{C} - \mathrm{O} - \mathrm{S} - \mathrm{N}} \qquad \text{(S3)}$$

where DBE_{AI} is the minimum number of C-C double bonds plus rings in a common molecular structure containing heteroatoms[179] and C_{AI} is the number of C atoms reduced by the number of potential double bonds contributed by heteroatoms[179].

Table S3.2. BET surface areas, persistent free radical (PFR) concentrations, electrical conductivity (EC), electron accepting and donating capacity (EAC, EDC), elemental composition, as well as water and ash contents of BC450, BC450HF, BC600, and BC750. Values in % are given on a dry basis in mmol element (g char)$^{-1}$.

Characteristic	BC450	BC450HF	BC600	BC750
BET surface area (m^2 g^{-1})	120 ± 7	131 ± 5	354 ± 0.6	435 ± 0.3
PFRs (10^{17} spins g^{-1})	350 ± 40	370 ± 40	61 ± 5	1.9 ± 0.1
g-value	2.0028	2.0028	2.0029	2.0029
EC[a] (mS cm^{-1})	(7.6 ± 0.3) × 10^{-5}	(1.2 ± 0.1) × 10^{-4}	0.5 ± 0.0	1949 ± 12
EAC (µmol e^- (g biochar)$^{-1}$)	359 ± 23	302 ± 13	202 ± 12	433 ± 8
EAC (µmol e^- (g carbon)$^{-1}$)	549 ± 35	460 ± 20	257 ± 15	502 ± 9
EDC (µmol e^- (g biochar)$^{-1}$)	413 ± 22	413 ± 23	384 ± 16	529 ± 42
EDC (µmol e^- (g carbon)$^{-1}$)	632 ± 33	631 ± 36	488 ± 20	625 ± 15
EEC (µmol e^- (g biochar)$^{-1}$)	772 ± 45	715 ± 36	586 ± 28	962 ± 50
EEC (µmol e^- (g carbon)$^{-1}$)	1181 ± 56	1091 ± 38	745 ± 15	1127 ± 13
C (%)	83.7	84.4	90.7	91.1
H (%)	3.0	3.1	2.0	1.0
O (%)	10.6	9.0	3.1	2.5
N (%)	0.60	0.59	0.67	0.72
S (%)	0.07	0.06	0.07	0.06
H/C (mol H (mol C)$^{-1}$)	0.43	0.44	0.26	0.13
O/C (mol O (mol C)$^{-1}$)	0.095	0.080	0.026	0.021
DBE/C[b] (mol DBE (mol C)$^{-1}$)	0.80	0.80	0.89	0.95
AI[c] (mol DBE_{AI} (mol C_{AI})$^{-1}$)	0.78	0.78	0.88	0.95
C_{ox}[d]	-0.27	-0.31	-0.24	-0.12
Water (%)	3.3	2.9	2.2	2.7
Ash (%)	2.1	2.9	3.5	3.5

[a] Electrical conductivity measured at a pressure of 5 tons

[b] Double-bond equivalent normalized by total number of carbons

[c] Aromaticity index

[d] Average carbon oxidation state

Table S3.3. BET surface areas, persistent free radical (PFR) concentrations, electrical conductivity (EC), electron accepting and donating capacity (EAC, EDC), elemental composition, as well as water and ash contents of BC-ash0, BC-ash9, BC-ash16, and BC-ash43. Values in % are given on a dry basis in mmol element (g char)$^{-1}$.

Characteristic	BC-ash0	BC-ash9	BC-ash16	BC-ash43
BET surface area[a] (m^2 g^{-1})	420[b]	316[b]	237[b]	121[b]
PFRs (10^{18} spins g^{-1})	2.7 ± 0.1	2.3 ± 0.1	1.9 ± 0.1	1.1 ± 0.1
g-value	2.0029	2.0030	2.0031	2.0031
EC[c] (mS cm^{-1})	(4.1 ± 0.3) × 10^{-4}	6.0 × 10^{-6} [b]	(1.9 ± 0.1) × 10^{-5}	5.5 × 10^{-5} [b]
EAC (µmol e^- (g biochar)$^{-1}$)	137 ± 0.5	290 ± 5	352 ± 23	271[b]
EAC (µmol e^- (g carbon)$^{-1}$)	157 ± 0.5	407 ± 7	715 ± 47	1088[b]
EDC (µmol e^- (g biochar)$^{-1}$)	42 ± 6	335 ± 17	590 ± 12	227 ± 5
EDC (µmol e^- (g carbon)$^{-1}$)	48 ± 7	477 ± 24	1200 ± 24	1112 ± 18
EEC (µmol e^- (g biochar)$^{-1}$)	179 ± 7	625 ± 22	942 ± 35	498 ± 5
EEC (µmol e^- (g carbon)$^{-1}$)	205 ± 8	884 ± 32	1915 ± 71	2200 ± 18
C[a] (%)	86.8	71.1	49.2	24.9
H[a] (%)	3.4	1.5	1.9	0.9
N[a] (%)	0.2	0.2	0.1	0.1
S[a] (%)	<0.1	0.1	<0.1	<0.1
H/C (mol H (mol C)$^{-1}$)	0.47	0.25	0.46	0.43
DBE/C[b] (mol DBE (mol C)$^{-1}$)	0.99	1.00	1.00	1.02
Ash[a] (%)	2.3	24.4	41.1	69.0

[a] values from Grafmüller et al., 2022[129]

[b] vaues only measured once due to the limited sample quantity

Electrical conductiivity measured at a pressure of 5 tons

[b] Double-bond equivalent normalized by total number of carbons

S3.3 Sorption capacity of the beech wood and ash-amended biochars

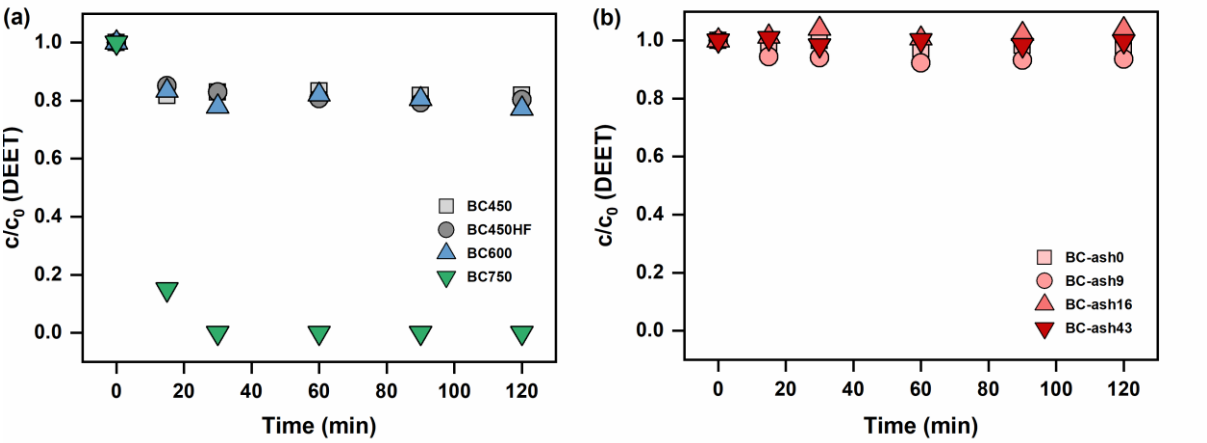

Figure S3.6. (a) Adsorption of DEET onto BC450, BC450HF, BC600, and BC750. [Biochar] = 1 g L^{-1}, c_0 = 50 µM, c = measured DEET concentration over time, pH 6 - 8 (no pH adjustment). (b) Adsorption of DEET onto BC-ash0, BC-ash9, BC-ash16, and BC-ash43. [Biochar] = 1 g L^{-1}, c_0 = 50 µM, pH 6 - 9 (no pH adjustment).

S3.4 DEET removal in the BC450/Fe(III)/PDS system and control experiments

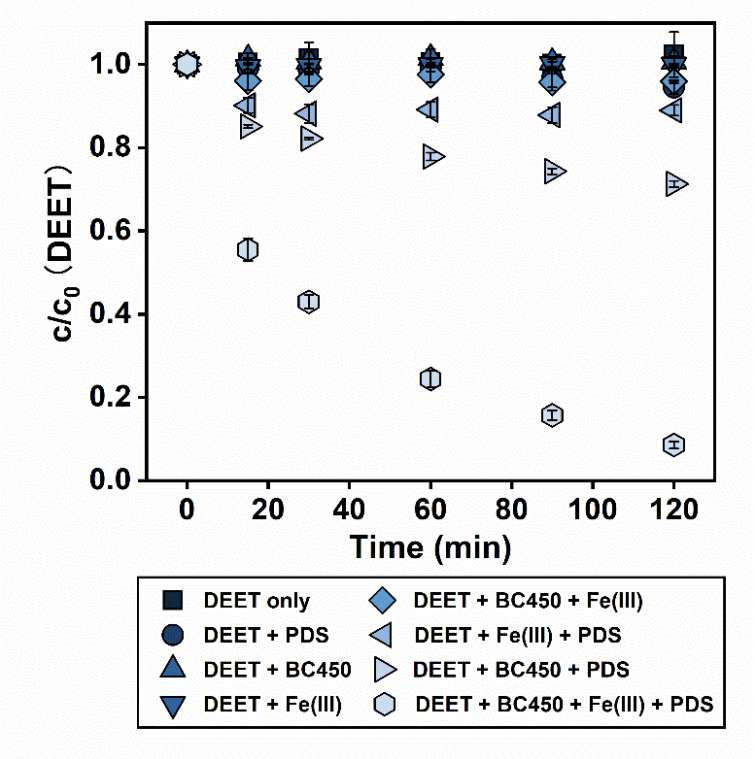

Figure S3.7. DEET removal in the BC450/Fe(III)/PDS system and corresponding control experiments with DEET only, DEET and PDS, DEET and BC450, DEET and Fe(III), and combinations thereof. [BC450] = 1 g L^{-1}, [Fe(III)] = 0.2 mM, [PDS] = 8 mM, $[DEET]_0 = c_0$ ~ 40 µM after sorption equilibrium, c = measured DEET concentration over time, pH 2.5.

S3.5 DEET removal and degradation kinetics in the biochar/Fe(III)/PDS system with beech wood biochars

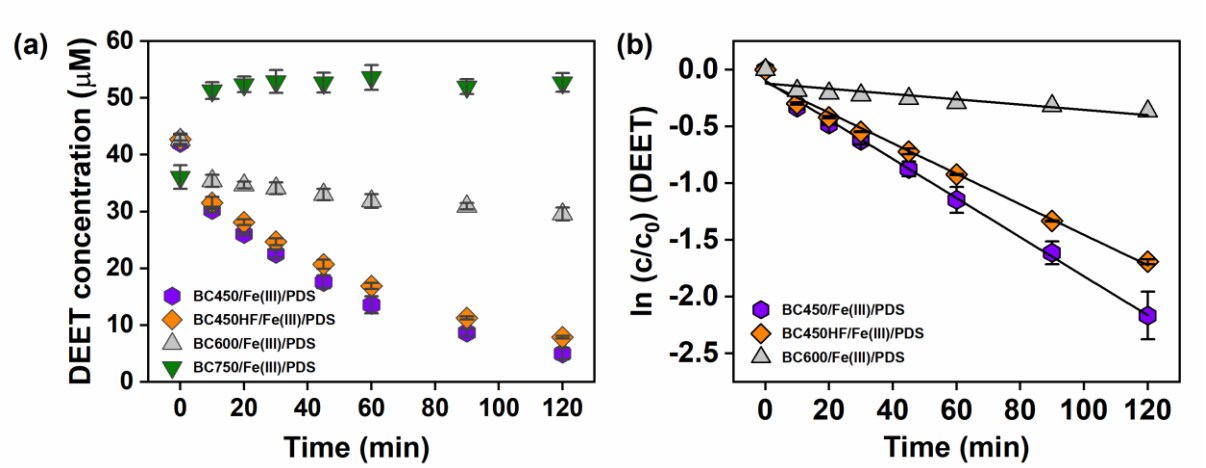

Figure S3.8. (a) DEET removal in the biochar/Fe(III)/PDS system with BC450, BC450HF, BC600, and BC750. (b) DEET degradation in the biochar/Fe(III)/PDS system followed (pseudo) first-order reaction kinetics. BC450: k_{obs} = (2.9 ± 0.1) × 10^{-4} s^{-1}, BC450HF: k_{obs} = (2.2 ± 0.1) × 10^{-4} s^{-1}, BC600: k_{obs} = (0.4 ± 0.1) × 10^{-4} s^{-1}. [Biochar] = 1 g L^{-1}, [Fe(III)] = 0.2 mM, [PDS] = 8 mM, $[DEET]_0$ = c_0 ~ 40 μM, pH 2.5. Error bars represent standard deviations of triplicate experiments.

S3.6 Fe(II) formation from Fe(III) in beech wood biochar suspensions

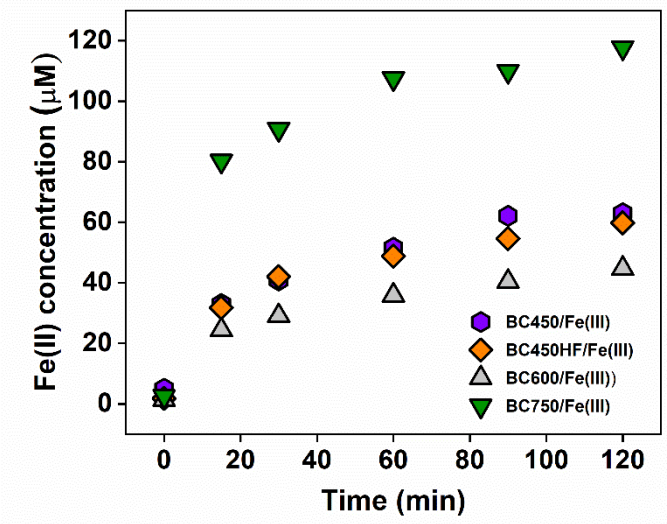

Figure S3.9. Fe(II) formation in beech wood biochar suspensions (BC450, BC450HF, BC600, and BC750) spiked with Fe(III). [Biochar] = 1 g L^{-1}, [Fe(III)] = 0.2 mM, pH 2.5.

S3.7 DEET removal and degradation kinetics in the biochar/Fe(III)/PDS system with ash-amended biochars

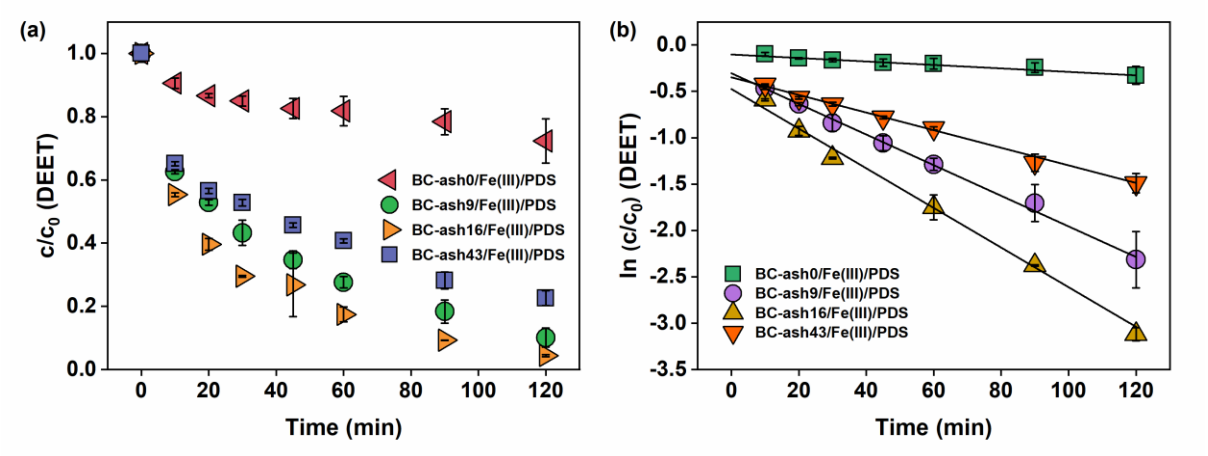

Figure S3.10. (a) DEET removal in the biochar/Fe(III)/PDS system with the four ash-amended biochars (BC-ash0, BC-ash9, BC-ash16, and BC-ash43). (b) DEET degradation in the biochar/Fe(III)/PDS system followed (pseudo) first-order reaction kinetics. BC-ash0: k_{obs} = (0.4 ± 0.1) × 10^{-4} s^{-1}, BC-ash9: k_{obs} = (2.9 ± 0.4) × 10^{-4} s^{-1}, BC-ash16: k_{obs} = (4.0 ± 0.1) × 10^{-4} s^{-1}, BC-ash43: (1.8 ± 0.2) × 10^{-4} s^{-1}. [Biochar] = 1 g L^{-1}, [Fe(III)] = 0.2 mM, [PDS] = 8 mM, $[DEET]_0$ = c_0 ~ 40 µM, pH 2.5. Error bars represent standard deviations of triplicate experiments.

S3.8 Fe(II) formation from Fe(III) in ash-amended biochar suspensions

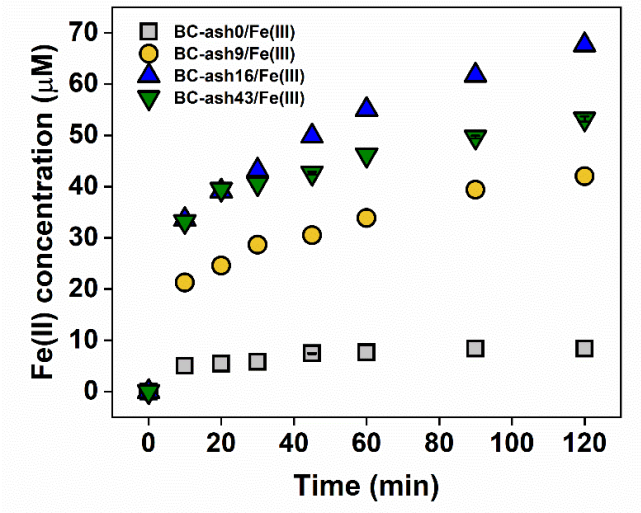

Figure S3.11. Fe(II) formation in ash amended biochar suspensions (BC-ash0, BC-ash9, BC-ash16 and BC-ash43) spiked with Fe(III). [Biochar] = 1 g L^{-1}, [Fe(III)] = 0.2 mM, pH 2.5.

Chapter 4

Persulfate activation by biochar for trace organic contaminant removal from urban stormwater

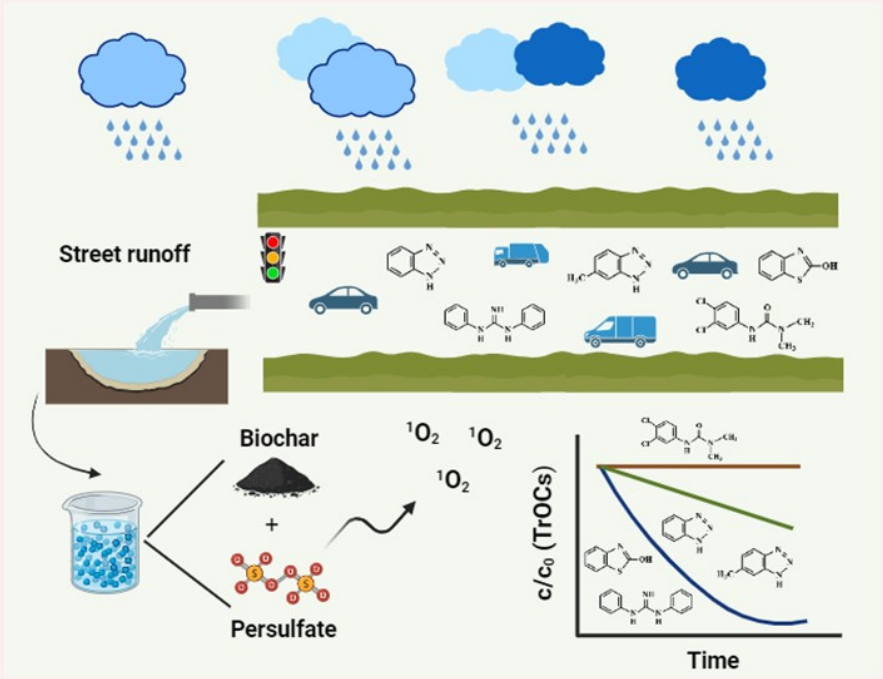

Yiling Zhuang, Stefan B. Haderlein, Holger V. Lutze, Chen Sun, Friedrich Fink, Andrea Paul, Stephanie Spahr. In preparation for submission to *Environmental Science and Technology.*

Y. Zhuang: designed and conducted all experiments, analyzed data, produced all figures, wrote and revised the manuscript; S. B. Haderlein: supervised the project, contributed to the discussion of the results, revised the manuscript; H. V. Lutze: contributed to the experimental design and the discussion of results, revised the manuscript; C. Sun: produced the biochar sample; F. Fink: performed Fourier-transform infrared spectroscopy (FTIR) spectroscopy and the corresponding data analysis, wrote the experimental section on FTIR; A. Paul: performed the continuous X-band electron spin resonance (ESR) measurements and corresponding data analysis; S. Spahr: supervised the project, contributed to the experimental design and discussion of the results, revised the manuscript.

Abstract

Numerous trace organic contaminants in urban stormwater are persistent and mobile and difficult to eliminate by conventional sedimentation- or sorption-based stormwater treatment, posing a risk to aquatic ecosystems and drinking water resources. We demonstrate that the chemical oxidant persulfate can be activated by biochar at pH 7 to form reactive species that react with the widely detected stormwater contaminants 1,3-diphenylguanidine, 2-hydroxybenzothiazole, 1*H*-benzotriazole, and 5-methyl-benzotriazole. Laboratory batch experiments conducted in actual street runoff and a synthetic water matrix showed that the water matrix, particularly dissolved organic carbon and chloride, had a minor effect on the formation of reactive species and contaminant removal. Using a set of scavengers and probe compounds, we provide evidence for singlet oxygen ($^1O_2$) as dominant reactive species in the biochar/persulfate system. Quantitative structure–activity relationship considerations supported the experimentally observed selectivity of $^1O_2$ towards anilines, aromatic amines, and phenols *via* an electrophilic substitution reaction, but not alkoxy benzenes. The results of our study inform new strategies for stormwater treatment using oxidation processes.

4.1 Introduction

In the face of global water scarcity, urban stormwater is increasingly being recognized as an untapped freshwater resource[198–200], particularly in water-stressed urban areas[201]. However, the capture and use of stormwater for water supply bears risks because urban stormwater can be contaminated with potentially harmful organic chemicals[9,11,199]. Numerous trace organic contaminants (TrOCs) have been detected in urban stormwater including herbicides (e.g., diuron, mecoprop)[202–205], corrosion inhibitors (e.g., benzotriazoles)[206–209], tire wear chemicals (e.g., 1,3-diphenylguanidine, benzothiazoles)[207,210–212], plasticizers (e.g., *N*-butylbenzenesulfonamide)[203,208], and flame retardants (e.g., tris(2-chloroethyl)phosphate)[202,208,209,213]. Many of these compounds are persistent and mobile and, thus, difficult to remove from water through conventional stormwater treatment, which is often based on sedimentation (e.g., in stormwater ponds), sorption (e.g., in biofilters), or biodegradation (e.g., in constructed wetlands)[136–138,214]. While hydrophobic, particle-associated contaminants can be easily removed in urban blue-green infrastructure[214], dissolved and mobile organic contaminants are poorly eliminated[138,215,216], putting receiving streams, groundwater or stormwater harvesting strategies at risk.

Recently, there have been increasing efforts to remove mobile TrOCs from urban stormwater through the amendment of biofilters with carbonaceous adsorbents such as biochar[49–51,140,217]. Biochar is considered a cost-effective and sustainable material produced from biomass pryrolysis[218,219]. Due to its high surface area, biochar can adsorb a variety of organic contaminants and enhance their removal from urban stormwater[49,51]. However, carbonaceous adsorbents alone cannot fully remove poorly adsorbing and persistent TrOCs from stormwater.

Oxidation processes have been successfully used to abate organic contaminants in wastewater[30,220,221], drinking water[222–224], and groundwater[31,225,226]. However, only a few attempts have been made to employ oxidation processes for the treatment of stormwater[227–230]. Peroxydisulfate (PDS, here called persulfate), a chemical oxidant commonly used for in situ chemical oxidation in the field[31,231], bears great potential for

stormwater purification, especially in decentralized treatment systems. Persulfate can be activated by redox-active biochar forming highly reactive radical or non-radical species that react with organic contaminants[69,88,97,232]. Biochar can thus serve as an adsorbent for TrOCs and as an electron donor for persulfate activation. The combination of biochar and persulfate has, however, not yet been assessed for the purification of urban stormwater.

In our study, we investigated the removal of selected TrOCs from urban stormwater by biochar and persulfate. We studied (i) the treatment efficiency of the biochar/persulfate system for the removal of TrOCs, (ii) the effects of the water matrix on the treatment performance, (iii) the formation of reactive species from persulfate, and (iv) the selectivity of the biochar/persulfate system with regard to different TrOCs. To this end, laboratory batch experiments were conducted using a shrimp shell biochar pyrolyzed at 750°C to activate peroxydisulfate for the removal 11 TrOCs from pure water, a synthetic water matrix, and street runoff. Different radical scavengers and probe compounds were employed to determine the major reactive species formed. Quantitative structure–activity relationship (QSAR) analyses investigated the relationship between the structures of aromatic TrOCs and their reactivity towards reactive species. This work evaluates the potential of biochar-assisted persulfate-based oxidation for urban stormwater purification and forms the basis for further investigations of factors relevant to field-scale applications.

4.2 Materials and methods

A list of all chemicals including suppliers and purities is provided in Section S4.1 of the Supporting Information.

4.2.1 Biochar preparation

Shrimp shells were used as feedstock for biochar production and pyrolyzed in a tube furnace at 750°C. The temperature gradient for pyrolysis was 10°C min^{-1} under N_2 atmosphere, with a N_2 flow rate of 10 L min^{-1} and a residence time of 2 hours. The biochar was washed with 1 M HNO_3 to remove ash and dried at 105°C. The sample was stored in a desiccator until further use. For details on the biochar characterization see Section S4.3.

4.2.2 TrOC degradation with biochar and PDS in different water matrices

The degradation of 11 TrOCs (1,3-diphenylguanidine (DPG), 2-hydroxybenzothiazole (OHBT), 1*H*-benzotriazole (BTA), 5-methyl-benzotriazole (MBTA), benzothiazole-2-sulfonic acid (BTSA), diuron, 2,4-dichlorophenoxyacetic acid (2,4-D), 2-methyl-4-chlorophenoxyacetic acid (MCPA), mecoprop, *N*-butylbenzenesulfonamide (NBBS), and tris(2-chloroethyl)phosphate (TCEP), physicochemical properties see Table S4.1) was investigated in batch reactors containing 15 mg of biochar in 15 mL of deionized water corresponding to a 1 g L^{-1} biochar suspension. The latter was stirred at 300 rpm and the pH was adjusted to 7.0 with 1 M H_2SO_4. Subsequently, 1 mL of an aqueous stock solution containing the 11 TrOCs (preparation see Section S4.2 in the Supporting Information) was spiked to achieve an initial nominal concentration of ~ 6 µM of each compound. After 30 min contact time, the measured TrOC concentration was taken as initial aqueous concentration (c_0). Subsequently, 30 µL of PDS was added from a 0.5 M aqueous stock solution to initiate the reaction and obtain an initial nominal PDS concentration of 1 mM, which is a typical concentration used for in situ

chemical oxidation in the field. The pH was controlled at 7.0 ± 0.1 by continuous titration with 0.25 M H_2SO_4 or 0.25 M NaOH throughout the reaction (titration procedure see Section S4.4). No any buffer was used to avoid reaction with potential radicals formed. At predefined time points, 1 mL sample was withdrawn and mixed with 100 µL of pure methanol (2 M in the sample, ≈ 9% v/v) to quench the reaction. Samples were filtered through 0.22 µm PES syringe filters (BGB Analytik, Germany; recovery of TrOCs see Table S4.2) into 1.5 mL amber glass vials and stored in the dark at 4°C until analysis. Two types of control experiments were set up identically to assess the sorption of TrOCs onto biochar in the absence of PDS and the reaction of TrOCs with PDS in the absence of biochar.

Four TrOCs, with the highest degradation rate (DPG, OHBT, BTA, MBTA) were selected to study the effects of the water matrix, particularly dissolved organic carbon (DOC) and chloride (Cl^-), on contaminant degradation in the biochar/PDS system. Degradation experiments were conducted as described above in a synthetic water matrix containing 6.4 mg L^{-1} DOC from Suwannee River humic acid in the presence and absence of 1 mM or 100 mM Cl^-. DPG, OHBT, BTA, and MBTA were added as a mixture to the 1 g L^{-1} biochar suspension at low concentrations of 3 µM, 6 µM, 3 µM, and 5 µM, respectively. The TrOCs were equilibrated overnight with the biochar to reach an apparent sorption equilibrium and a similar initial concentration prior to PDS addition. This low concentration ensured that the contribution of TrOCs to the scavenging of $SO_4^{\bullet-}$ and $^{\bullet}OH$ was below 10% compared to the water matrix compounds, simulating the typical situation in oxidative treatment process. Identical degradation experiments were also conducted in real street runoff water collected from a main street in Berlin, Germany in October 2023. The water sample was analyzed for pH, DOC, total dissolved nitrogen, major ions as well as metals (see Section S4.6 and Table S4.5).

4.2.3 Identification of reactive species

To investigate the major reactive species in the biochar/PDS system, SMX was selected as a model compound with known reaction rate constants with $SO_4^{\bullet-}$ and $^{\bullet}OH$ (k (SMX + $SO_4^{\bullet-}$) = 1.25 × 10^{10} M^{-1} s^{-1} [233], k (SMX + $^{\bullet}OH$) = 5.5 × 10^{9} M^{-1} s^{-1} [234]). Different scavengers were added to a 1 g L^{-1} biochar suspension containing 10 µM SMX and 1 mM PDS: 1 M methanol was added to scavenge > 99% of both $SO_4^{\bullet-}$ (k ($SO_4^{\bullet-}$) = 1.1 × 10^{7} M^{-1} s^{-1} [159]) and $^{\bullet}OH$ (k ($^{\bullet}OH$) = 9.7 × 10^{8} M^{-1} s^{-1} [119]). 5 mM *tert*-butanol (TBA) was employed to scavenge a large fraction (98%) of $^{\bullet}OH$ (k ($^{\bullet}OH$)= 6.0 × 10^{8} M^{-1} s^{-1} [119]) but only 3% of $SO_4^{\bullet-}$ (k ($SO_4^{\bullet-}$) = 8.0 × 10^{5} M^{-1} s^{-1} [159]). Surface-bound $SO_4^{\bullet-}$ and $^{\bullet}OH$ were completely scavenged by 10 mM dimethyl sulfoxide (DMSO) through coating on the biochar surface (k (DMSO + $SO_4^{\bullet-}$) = 2.7 × 10^{9} M^{-1} s^{-1} [235], k (DMSO + $^{\bullet}OH$) = 7.0 × 10^{9} M^{-1} s^{-1} [119]). For calculations of the fractions by which scavengers react with an oxidant see Section S4.11. Carbonate (CO_3^{2-}), an efficient superoxide radical ($O_2^{\bullet-}$) scavenger (5.0 × 10^{8} M^{-1} s^{-1})[236], was added in different concentrations of 1 – 50 mM with absence of $SO_4^{\bullet-}$ and $^{\bullet}OH$.

To further identify the reactive species formed, different probe compounds were employed according to a protocol of Lutze et al.[143]. 3 µM of 4-nitrobenzoic acid (*p*NBA) and 4-chlorobenzoic acid (*p*CBA) were added to a 1 g L^{-1} biochar suspension containing 1 mM PDS to study the formation of radical species. *p*NBA reacts very slow with $SO_4^{\bullet-}$ but rapidly with $^{\bullet}OH$ (k (*p*NBA + $SO_4^{\bullet-}$) ≤ 10^{6} M^{-1} s^{-1} [120], k (*p*NBA + $^{\bullet}OH$) = 2.6 × 10^{9} M^{-1} s^{-1} [119]). *p*CBA demonstrates high reactivity towards both $SO_4^{\bullet-}$ and $^{\bullet}OH$ (k (*p*CBA + $SO_4^{\bullet-}$) = 3.6 × 10^{8} M^{-1} s^{-1} [120], k (*p*CBA + $^{\bullet}OH$) = 5 × 10^{9} M^{-1} s^{-1} [119]). The ratio of the second order rate constants corresponds to the slope in a double logarithmic plot of ln(c/c_0) (*p*NBA) vs. ln(c/c_0) (*p*CBA)[160] with a slope of 0.52 for $^{\bullet}OH$ based processes and close to 0 for $SO_4^{\bullet-}$ [143]. Analogously, two probe compounds, 3-methoxyphenol (MOP) and 2,4,6-trichlorophenol (TCP) were chosen as indicators for singlet oxygen ($^1O_2$) in both pure water and actual street runoff. In case of a $^1O_2$-based process, leads to a theoretical slope of 0.76 in plot of ln(c/c_0) (TCP) vs. ln(c/c_0) (MOP) (k (TCP + $^1O_2$) = 1.7 × 10^{7} M^{-1} s^{-1}, k (MOP + $^1O_2$) = 1.3 × 10^{7} M^{-1} s^{-1} [237]). All probe

compounds were added at low concentration (3 µM for *p*NBA and *p*CBA, 5 µM for TCP and MOP) resulting in < 10% scavenging of the reactive species. Two different types of control experiments were conducted: (i) a sorption control containing only probe compounds (*p*NBA + *p*CBA or TCP + MOP) and biochar, and (ii) a control containing only the probe compounds and PDS.

To validate the formation of $^1O_2$, a reference experiment was performed using the reaction of H_2O_2 and NaClO to degrade TCP and MOP. H_2O_2/NaClO reaction is the benchmark process for the production of $^1O_2$ due to its well-established confirmation of producing sole $^1O_2$[238,239] and with no discernible intermediacy involving radicals[240,241]. Experimental details are described in Section S4.14.

Persulfate decomposition experiments were carried out in a 1 g L^{-1} biochar suspension containing 1 mM PDS in the presence and absence of SMX. Samples were withdrawn over time and filtered through 0.22 µm PES syringe filters (101 ± 1.3% recovery) for persulfate analyses. To investigate the involvement of dissolved oxygen in the reaction, SMX degradation and persulfate decomposition experiments were also conducted under anoxic conditions by purging the 1 g L^{-1} biochar suspension with N_2 and conducting the experiment in a glovebox under N_2 atmosphere.

4.2.4 Analytical methods

Biochar characterization

The electron exchange capacity (EEC), i.e., the sum of electron accepting capacity (EAC) and the electron donating capacity (EDC), was determined using a mediated electrochemical method modified from Klüpfel et al.[58]. Continuous wave X-band electron spin resonance (ESR) spectroscopy was performed (MiniScope MS 300, Magnettech GmbH, Germany) to determine persistent free radicals. The zeta potential of the biochar was measured by a nanoparticle size analyzer (Zetasizer Nano ZSP, Malvern Inc., UK). Attenuated total reflectance Fourier transform infrared (ATR-FTIR) spectroscopy was recorded using a Nicolet 670 FT-IR spectrometer (Thermo Fisher Scientific GmbH) equipped with an EverGlo source, a KBr beam splitter, and a

deuterated L-alanine-doped triglycene sulphate (DLaTGS) detector to characterize the functional groups on the biochar surface. In situ X-ray diffraction analysis (XRD) measurements were performed on a Bruker D2 PHASER X-ray diffractometer for biochar surface structure properties study. The metal content of the biochar was determined by inductively coupled plasma-optical emission spectrometry (ICP-OES, ICP iCAP7000series, Thermo Fisher Scientific Inc.) after microwave acid digestion. For detailed information of the biochar characterization see Section S4.3.

TrOC analysis

The concentrations of the TrOCs were quantified by liquid chromatography coupled with tandem mass spectrometry (LC–MS/MS) in positive and negative electrospray ionization mode (for details see Section S4.5). SMX and probe compounds *p*NBA, *p*CBA, TCP, and MOP were quantified using high-performance liquid chromatography equipped with a diode array detector (HPLC UV-vis, see Section S4.5).

Persulfate measurements

Persulfate decomposition was quantified using a modified KI colorimetric method[242]. Briefly, 0.1 mL sample was added into a solution containing 4.9 mL of 0.55 M KI and 0.76 mM $NaHCO_3$. The samples were incubated for 25 minutes in the dark and analyzed spectrophotometrically at 352 nm.

QSAR analysis

A quantitative structure-activity relationship (QSAR) model was employed to investigate the relationship between the structures of aromatic TrOCs and their reactivity towards singlet oxygen. Hammett σ+ constants were calculated to represent the electron-donating or electron-withdrawing properties of substituents on aromatic compounds[243–245] (details shown in Section S4.18). For structurally complex substituents which no descriptor variables were available in literature, a structural approximation was used.

4.3 Results and discussion

4.3.1 Biochar and persulfate to degrade dissolved TrOCs

A preliminary batch screening experiment was conducted in which the degradation of 11 TrOCs was investigated in pure water containing 1 g L^{-1} biochar and 1 mM PDS at pH 7 (Figure 4.1a and Figure S4.4). Within one hour, none of the TrOCs reacted directly with PDS. Only one compound (diuron) was adsorbed to a significant extent (45%) on biochar, while all other compounds showed minor sorption (< 20%). In the presence of biochar and persulfate, DPG and OHBT showed more than 95% degradation (Figure 4.1a). BTSA, BTA, and MBTA exhibited moderate degradation (21 – 34%). DPG exhibited the highest degradation rate following pseudo-first order kinetics with a k_{obs} value of (10.4 ± 0.5) × 10^{-4} s^{-1}. BTSA showed the slowest degradation with a k_{obs} of (0.6 ± 0.01) × 10^{-4} s^{-1}. No degradation was observed for TCEP, NBBS, 2,4-D, MPCA, and mecoprop. In actual street runoff, 1 g L^{-1} biochar and 1 mM PDS also led to the degradation of DPG, OHBT, BTA, and MBTA at pH 7 (Figure 4.1b). DPG and OHBT was almost completely removed (> 90%) within one hour. BTA and MBTA both were removed by around 30%. These results show that the biochar/PDS system can be applied to actual street runoff to remove certain persistent and mobile organic compounds, which cannot be removed through adsorption onto biochar alone.

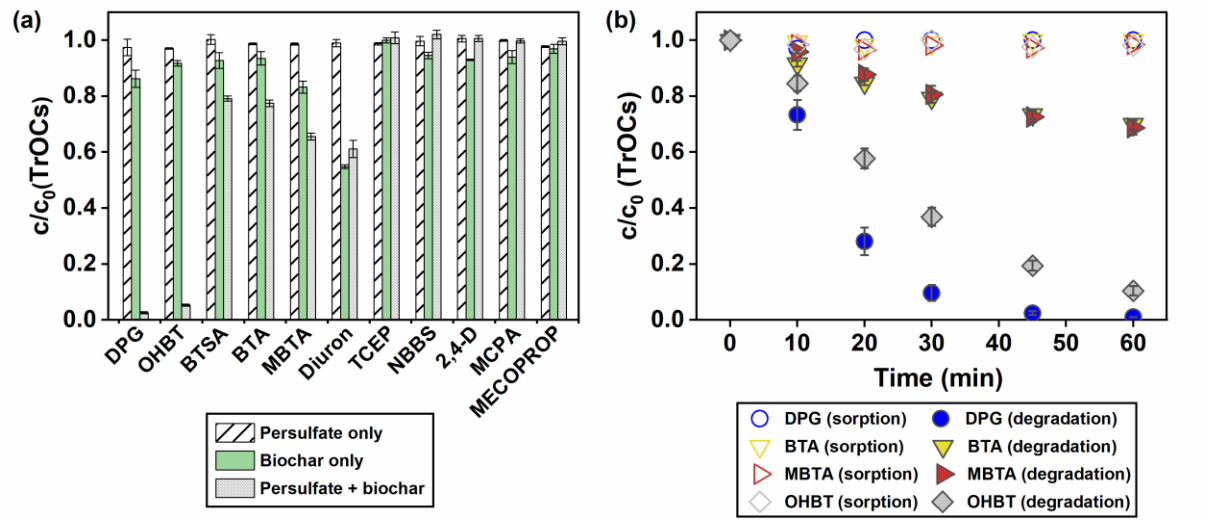

Figure 4.1. (a) Removal of TrOCs (in mixture) in batch experiments containing (i) persulfate only (striped bars), (ii) biochar only (solid bars), and (iii) persulfate and biochar (dotted bars). [Biochar] = 1 g L^{-1}, [persulfate] = 1 mM, $[TrOCs]_{spiked}$ ~ 6 µM, c_0 = concentration after 30 min sorption, c = measured TrOCs concentration after 1 h reaction, pH 7 (titrated with H_2SO_4 and NaOH), in pure water without buffer. Error bars indicate the standard deviation of triplicates. (b) Removal of DPG, BTA, MBTA, and OHBT (in mixture) in batch experiments with street runoff containing (i) biochar only as sorption control, and (ii) persulfate and biochar over time. [Biochar] = 1 g L^{-1}, [PDS] = 1 mM, $[DPG]_0 = c_0$ = 0.98 µM (206 µg L^{-1}), $[OHBT]_0 = c_0$ = 1.26 µM (190 µg L^{-1}), $[BTA]_0 = c_0$ = 1.46 µM (172 µg L^{-1}), $[MBTA]_0 = c_0$ = 1.33 µM (177 µg L^{-1}), c = measured TrOCs concentration over time, pH 7(titrated with H_2SO4 and NaOH), without buffer. Error bars indicate the standard deviation of triplicates.

4.3.2 Effect of the water matrix on TrOCs degradation by biochar and PDS

The street runoff collected contained 7.5 mg L^{-1} DOC and a low concentration of Cl^- (0.1 mM, Table S4.5). As the quality of runoff can vary significantly depending on the land use and season[10,246,247], knowledge about the effects of the water matrix on TrOC degradation is crucial for the potential application of the biochar/PDS system for stormwater treatment. In particular, the Cl^- concentrations in runoff can vary strongly due to de-icing activities in winter that can lead to very high concentrations of Cl^- up to hundreds of mM[248,249]. We investigated the degradation of DPG, OHBT, BTA, and MBTA in a synthetic water matrix containing 6.4 mg L^{-1} DOC and two concentrations of Cl^- (1 mM and 100 mM Cl^-, Figure 4.2 and Figure S4.7). Both Cl^- concentrations did not affect the degradation of the BTA and MBTA (Figure 4.2 and Figure S4.7). The removal of DPG and OHBT was not impacted by Cl^- (>95% removal). For OHBT, the addition of 1mM Cl^- led to a decrease in degradation rate from $(10.0 \pm 0.2) \times 10^{-4}$ s^{-1} to $(8.5 \pm 0.0) \times 10^{-4}$ s^{-1}. Increasing the concentration of Cl^- to 100 mM, did not lead to a further decrease in reaction rate. That TrOCs could be degraded in the biochar /PDS system in the presence of 100 mM Cl^- indicates its applicability also in winter during deicing events of rods using salt. Also, dissolved organic carbon (DOC as Suwannee River humic acid) did not impact the removal of the TrOCs in the biochar/PDS system compared to pure water (Figure 4.2 and Figure S4.6). The absence of water matrix effects on the reaction kinetics of the contaminants could be an indication of the formation of reactive species that do not react strongly with water matrix components.

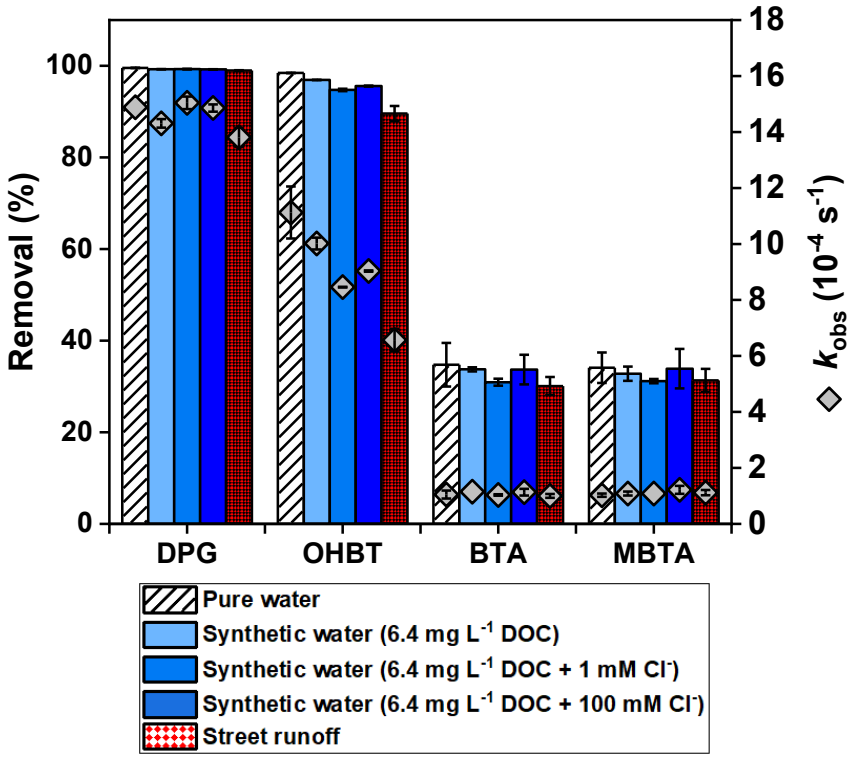

Figure 4.2. Removal of DPG, OHBT, BTA, and MBTA (in mixture) in different water matrices and corresponding pseudo-first order rate constants (k_{obs}) (i) in pure water (striped bars), (ii) in synthetic water (containing DOC and Cl^-) (solid bars), and (iii) in street runoff (checkered bars). [Biochar] = 1 g L^{-1}, [PDS] = 1 mM, $[DPG]_{spiked}$ = 3 µM (634 µg L^{-1}), $[OHBT]_{spiked}$ = 6 µM (907 µg L^{-1}), $[BTA]_{spiked}$ = 3 µM (357 µg L^{-1}), $[MBTA]_{spiked}$ = 5 µM (666 µg L^{-1}), c = measured TrOC concentration after 1h reaction, pH 7 (titrated with H_2SO4 and NaOH), without buffer.

4.3.3 Identification of reactive species in the biochar/persulfate system

To elucidate which reactive species were formed in the biochar/PDS system, we selected SMX as a model compound with known reaction rate constants with many radical and non-radical species and investigated SMX transformation kinetics in the presence of different scavengers. Methanol served as a scavenger for both $SO_4^{\bullet-}$ and $^{\bullet}OH$, while TBA only scavenges $^{\bullet}OH$. Neither methanol nor TBA affected SMX degradation kinetics (Figure 4.3a), indicating that neither $SO_4^{\bullet-}$ nor $^{\bullet}OH$ were involved to a significant extent in the biochar/PDS system. This conclusion was further verified by employing *p*CBA and *p*NBA as probe compounds (see method section), where hardly any *p*CBA and *p*NBA was degraded (Figure S4.8). DMSO, which served as a scavenger for surface-bound radicals, did not cause changes in SMX degradation neither (Figure 4.3a). These results point to the involvement of non-radical species in the biochar/PDS system.

Competition kinetics experiments were conducted using MOP and TCP as probe compounds to study the generation of singlet oxygen ($^1O_2$). The probe compounds neither adsorbed to biochar, nor reacted with 1 mM persulfate during the course of our experiments (Figure S4.9). A plot of $\ln(c/c_0)$ (TCP) vs. $\ln(c/c_0)$ (MOP) (Figure 4.3b) yielded a slope of 0.776 ± 0.015 in pure water, in good agreement with the ratio of the second order rate constant of $^1O_2$ with MOP and TCP (k (TCP + $^1O_2$) /k (MOP + $^1O_2$) = 0.76)[237]. The same slope (0.766 ± 0.030) was obtained in street runoff water (Figure 4.3b) demonstrating that $^1O_2$ is likely the major reactive species in both pure water and street runoff. The water matrix did not seem to affect (i) the type of reactive species formed and (ii) the $^1O_2$ exposure as can also be seen by the high contaminant degradation kinetics in the street runoff (Figure 2). A direct electron transfer pathway between biochar, persulfate and SMX was considered unlikely as discussed in Section S4.15.

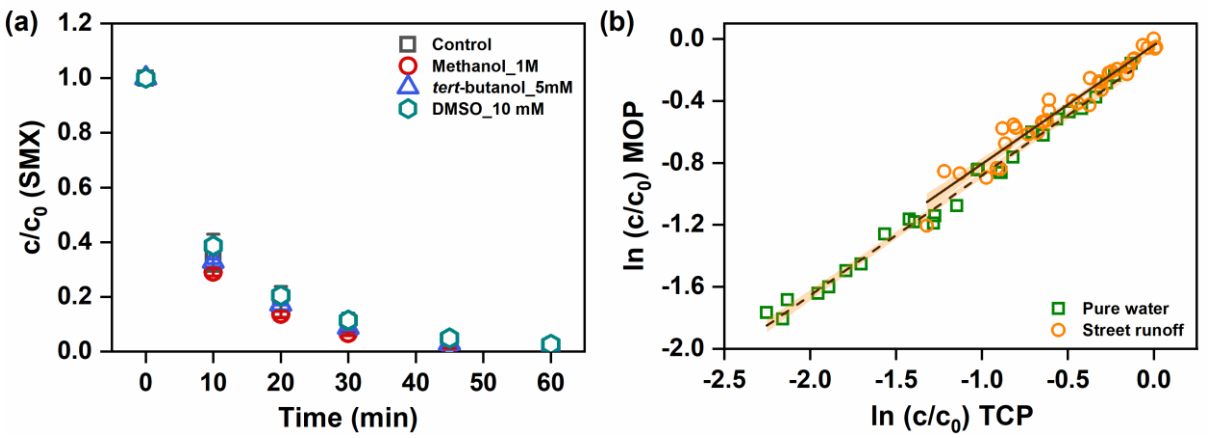

Figure 3. (a) SMX degradation over time in the biochar/PDS system in the absence (control) and presence of 1 M methanol, 5 mM tert-butanol (TBA), or 10 mM DMSO. [Biochar] = 1 g L^{-1}, [PDS] = 1 mM, $[SMX]_0 = c_0 \sim 7.5$ µM, c is the measured SMX concentration over time, pH 7 (titrated with H_2SO4 and NaOH), in pure water without buffer. Error bars indicate the standard deviation of triplicates. (b) Competition plot $\ln(c/c_0)$ of TCP vs. MOP in pure water (dashed line and squares, slope 0.776 ± 0.015; intercept 0.104 ± 0.020) and in street runoff (7.5 mg L^{-1} DOC and 2.9 mg L^{-1} Cl^-, other water constituents see Table S5) (full line and circles, slope 0.766 ± 0.030; intercept 0.01 ± 0.019). [Biochar] = 0.5 g L^{-1}, [PDS] = 1 mM, $[MOP]_{spiked}$ = $[TCP]_{spiked}$ = 5 µM, pure water: $[MOP]_{0,\ after\ 30min\ sorption}$ = 3.29 µM; $[TCP]_{0,\ after\ 30min\ sorption}$ = 2.59 µM, street runoff: $[MOP]_{0,\ after\ 30min\ sorption}$ = 3.54 µM; $[TCP]_{0,\ after\ 30min\ sorption}$ = 2.17 µM, c is the measured MOP and TCP concentration over time, pH 7 (titrated with H_2SO4 and NaOH), in pure water without buffer. Orange areas show the 95% confidence intervals of the linear fit.

A known pathway to form $^1O_2$ is the reaction of persulfate and ketonic groups of carbonaceous materials[99]. ATR-FTIR spectra indicated the presence of C = O bonds (C = O stretching vibrations with ketones, Figure S4.2), which might be crucial functional groups for the generation of $^1O_2$ from persulfate. A mechanism for the generation of $^1O_2$ is proposed in Scheme 1, according to the activation of persulfate by carbon nanotubes[99]. First, one molecule of $S_2O_8^{2-}$ attacks the carbonyl groups on the biochar to form a peroxide adduct (reaction 1). The peroxide adduct decomposes to a dioxirane intermediate via intramolecular nucleophilic displacement of alkoxide oxygen at the O–O bond and forms one molecule of SO_4^{2-} (reaction 2 and 3).

Subsequently, another molecule of $S_2O_8^{2-}$ reacts with the dioxirane adduct and generates one molecule of $^1O_2$ (reaction 4). Overall, two molecules of $S_2O_8^{2-}$ form four molecules of SO_4^{2-} and one molecule of $^1O_2$. A stoichiometric ratio of SO_4^{2-} produced per $S_2O_8^{2-}$ lost in SMX degradation experiment was calculated to be approximately 2 (Figure S4.11), which was consistent with the proposed reactions.

Superoxide radicals ($O_2^{\bullet-}$) are usually recognized as an intermediate product involved in the generation of $^1O_2$ by direct oxidation from dissolved oxygen[147] or recombination of two $O_2^{\bullet-}$[250]. To assess the possible involvement of $O_2^{\bullet-}$, different concentrations of carbonate (1 – 50 mM CO_3^{2-}, $k_2 = 5 \times 10^8$ M^{-1} s^{-1})[236] were added as selective scavenger of $O_2^{\bullet-}$. No significant difference was observed in SMX degradation even at high carbonate concentrations of 50 mM (Figure S4.12). Dissolved oxygen as the source of $^1O_2$ was ruled out in an experiment under anoxic conditions, in which no differences in SMX degradation and persulfate decomposition could be observed compared to the experiment under oxic conditions (Figure S4.13). These results demonstrated the nonparticipation of dissolved oxygen and $O_2^{\bullet-}$ in $^1O_2$ generation.

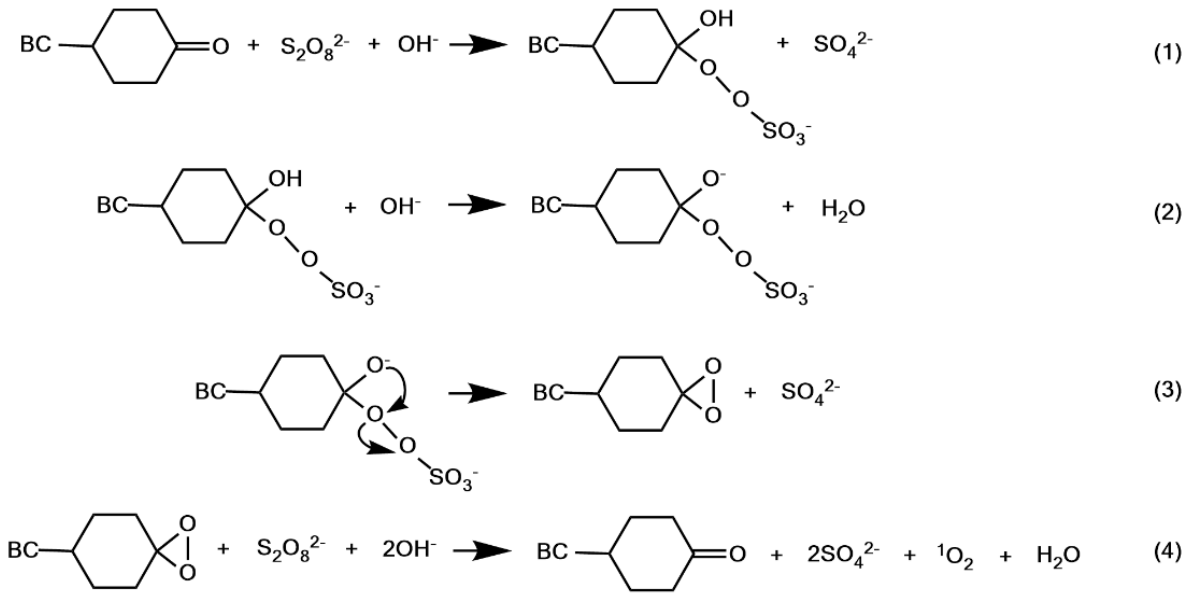

Scheme 4.1. Proposed mechanism for the generation of $^1O_2$ from PDS activation by biochar (Based on Chen et al., 2017)[99].

4.3.4 Reactivity and selectivity of TrOCs for future application

Singlet oxygen is known to selectively react with electron-rich organic compounds[251,252]. In fact, in our experiments only DPG, BTA, MBTA, OHBT, and BTSA were degraded but not diuron, 2,4-D, MCPA, mecropop, NBBS, and TCEP (Figure 4.1a). Understanding the reactivity between TrOCs and singlet oxygen in the biochar/PDS system is essential for a good process design and future applications. The 11 investigated TrOCs were grouped into anilines (DPG, diuron), aromatic amines (BTA, MBTA, OHBT, BTSA,), alkoxy benzenes (2,4-D, MCPA, mecropop) and other compounds (NBBS, TCEP). No degradation was observed for 2,4-D, MCPA, and mecoprop, indicating that singlet oxygen shows low reactivity towards alkoxy benzenes (Figure 4.4a and Figure S4.4). Anilines were well degraded in the biochar/PDS system, except for diuron where degradation could not be distinguished from adsorption onto biochar (Figure 4.4a and Figure S4.4). Aromatic amines including benzotriazoles and benzothiazoles showed high reactivity with singlet oxygen. The degradation rate constants (k_{obs}) of TrOCs obtained in the competition experiments described above were used to quantitatively describe the effect of substitution (Figure S4.5). The Hammett constants σ^+ as the TrOCs substituent descriptors were estimated[243–245] (Section S4.18 and Table S4.6). A quantitative structure–activity relationship (QSAR) was developed for the reaction activity of the TrOCs that reacted with singlet oxygen and the Hammett σ^+ constants, where a good correlation with linear regression was obtained ($R^2 = 0.94$) (Figure 4.4b). The decrease in the oxidation rates of TrOCs with the increase of σ^+ suggests a typical electrophilic substitution reaction between singlet oxygen and the TrOCs. All highly reactived TrOCs have negative σ^+ values with electron-donating properties, consistent with the fact that singlet oxygen favors to react with electron-rich moieties[253]. A linear relationship between the reaction of singlet oxygen and 14 substituted phenols and Hammett σ^+ constants was also proposed by Jawad et al., 2020 where k_{obs} decreased with the increased σ^+[251]. Consistent results were obtained in our study where a faster degradation was observed for TCP ($k_{obs} = (26.4 \pm 0.5) \times 10^{-4}$ s^{-1}) with a larger σ^+

(0.2552) than MOP (k_{obs} = (21.1 ± 0.4) × 10^{-4} s^{-1}, σ^+ = 0.05). QSAR analyses could serve as a useful tool to evaluate the degradation of certain substituted compounds in the reaction with singlet oxygen.

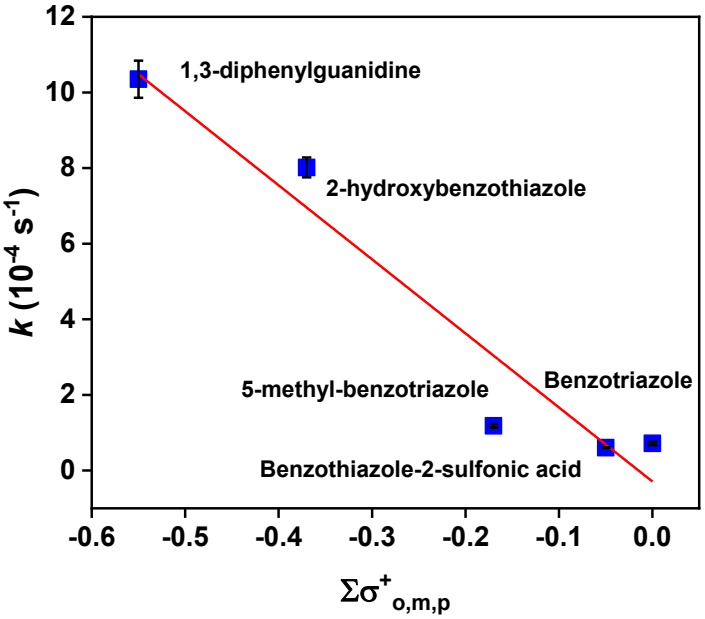

Figure 4.4. Correlation between the pseudo-first order rate constant (k_{obs}) for the reactions of singlet oxygen with aniline TrOCs vs. $\sum\sigma^{+}_{o,m,p}$.

4.4 Implications for stormwater treatment

In light of increasing global efforts to capture and use stormwater for water supply, it is critical to remove persistent, mobile, and potentially toxic chemicals from stormwater[9,11,199]. Our study demonstrates that biochar can activate peroxydisulfate to eliminate organic contaminants from urban stormwater. The oxidation process with biochar and PDS can, thus, be a complementary approach to conventional stormwater treatment systems. Moreover, the degradation of organic contaminants in the biochar/persulfate system through a non-radical singlet oxygen pathway has practical benefits as the water matrix did not strongly impact contaminant removal.

The biochar/persulfate system is selective towards oxidizing trace organic contaminants in urban stormwater, especially electrophilic compounds like anilines, aromatic amines, and phenols. For the TrOCs that are not reactive in the

biochar/persulfate system, alternative treatments need to be considered to broaden the spectrum of mobile organic contaminants that can be removed.

Our laboratory-scale tests form the basis for further investigations of factors relevant to field-scale applications of oxidation processes for stormwater treatment. Further research is needed to assess the feasibility and applicability of the biochar/PDS-based oxidation process for stormwater treatment in the field. For example, laboratory-scale column studies need to be conducted to simulate the application of biochar and persulfate in biofilter systems. Moreover, operational parameters have to be tested to ensure a constant persulfate supply, control the large amount of sulfate ion emit from the decomposition of persulfate, and assess potential effects of variable flow rates and accumulation of high DOC through filter systems on the treatment efficacy of organic contaminants. Lastly, pilot-scale field studies are needed to test the actual implementation and performance of this biochar-assisted persulfate-based oxidation for urban stormwater treatment.

Acknowledgement

This work was funded by the China Scholarship Council (CSC, File No. 201904910454). We thank Claudia Schmalsch for support in the laboratory, Tobias Goldhammer, Marvin Sens, and Thomas Rossoll for providing and analyzing the street runoff sample. The TOC art was generated with BioRender (https://biorender.com/).

Supporting Information to

Chapter 4

S4.1 Chemicals

All chemicals in this study were used as received. Benzotriazole (BTA, 99%), 5-methyl-benzotriazole (MBTA, 98%), 2-hydroxybenzothiazole (OHBT, 98%), 2-methyl-4-chlorophenoxyacetic acid (MCPA, analytical standard), mecoprop (analytical standard), diuron (≥ 99.0%), tris(2-chloroethyl)phosphate (TCEP, 97%), 2,4-dichlorophenoxyacetic acid (2,4-D, analytical standard), sulfamethoxazole (SMX, analytical standard), sodium peroxydisulfate (PDS, $Na_2S_2O_8$, ≥ 99% for analysis EMSURE®), methanol (MeOH, HPLC grade ≥ 99.9%), *tert*-butanol (TBA, ≥ 99.0%), 2,2'-azino-bis(3-ethylbenzothiazoline-6-sulfonic acid) diammonium salt (ABTS, ≥ 98.0%), formic acid (LC/MS, Fluka®), potassium iodide (KI, 99%, ReagentPlus®), 4-nitrobenzoic acid (*p*NBA, ≥ 98.0% for HPLC), 4-chlorobenzoic acid (*p*CBA, 99% for HPLC), 3-methoxyphenol (MOP, 96%), 2,4,6- trichlorophenol (TCP, 98%) and ascorbic acid (for analysis EMSURE®) were purchased from Sigma-Aldrich. 1,3-diphenylguanidine (DPG, 99.2%), and *N*-butylbenzenesulfonamide (NBBS, 99.94%) were purchased from HPC standards GmbH. Benzothiazole-2-sulfonic acid (BTSA, 99.99%) was from BLD Pharma Ltd. Sulfuric acid (H_2SO_4, 95-97%), sodium hydroxide solution (NaOH, 1 M, TitriPUR®), acetic acid (100%), potassium chloride (KCl), monopotassium phosphate (KH_2PO_4), sodium chloride (NaCl), sodium hydrogen carbonate ($NaHCO_3$), and sodium carbonate (Na_2CO_3) were purchased from Merck and were with for analysis EMSURE® purity except mentioned otherwise. Dimethyl sulfoxide (DMSO, >99.5%) was purchased from Fisher Scientific. Sodium hypochlorite (12% Cl, technical grade) was purchased from Carl Roth. Suwannee River humic acid and Suwannee River standard fulvic acid were from the International Humic Substances Society (IHSS), St. Paul, MN, USA. *N,N*-bis(3-sulfonatopropyl)-4-4'-bipyridinium (zwitterionic viologen, ZiV) was synthesized in the lab and characterized by Fourier-transform infrared spectroscopy (FTIR), for details see Schlögl et al., 2022[176]. Aqueous solutions were prepared with deionized water (18.1 MΩ x cm, Arium® Pro Water Purification System).

Table S4.1. The molecular structure, molecular weight (MW), *pK*a, log *D*ow, solubility in water, and use class of the 11 studied TrOCs.

No.	Name	Molecular structure	MW (g mol^{-1})	*pK*a	log *D*ow (pH 7.4)[a]	Solubility in water (g L^{-1})	Use class	Source in stormwater
1	1,3-Diphenylguanidine (DPG)	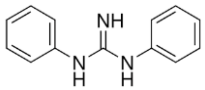	211.26	10.12	2.46	1	Vulcanization accelerator	210–212
2	Benzotriazole (BTA)	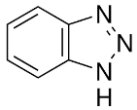	119.13	8.2	1.50	20	Corrosion inhibitor	206,208,209
3	5-Methyl-benzotriazole (MBTA)	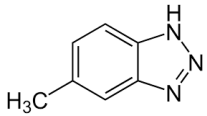	133.15	8.74	1.69	6	Corrosion inhibitor	202,208
4	2-Hydroxybenzothiazole (OHBT)	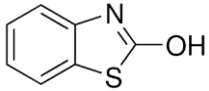	151.19	8.9	-1.33	1.7	Vulcanization accelerator	207,254,255
5	Benzothiazole-2-sulfonic acid (BTSA)	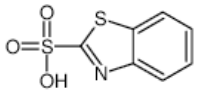	215.3	2.4-1..0	-3.01	0.7	Corrosion inhibitor	207,256,257

6	2.4-D	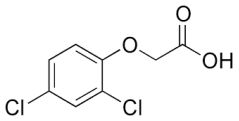	221.04	2.64	-0.83	0.9	Herbicide	202,204,205
7	MCPA	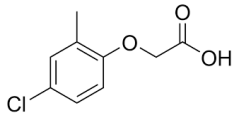	200.62	3.1	-1.09	0.825	Herbicide	205
8	Mecoprop	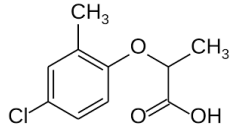	214.64	3.78	-0.65	0.7	Herbicide	206,209
9	Diuron	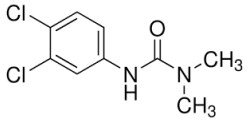	233.09	13.2	0.13	0.04	Herbicide	202–205
10	N-Butylbenzenesulfonamide (NBBS)	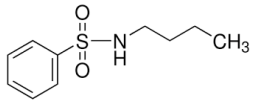	213.3	11.62	1.85	0.46	Plasticizer	208
11	Tris(2-chloroethyl)phosphate (TCEP)	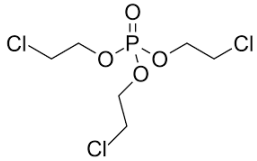	285.5	9.75	1.42	7.8	Organophosphate flame retardant	202,208,209,213

[a] log *D*ow at pH 7.4 predicted by ACD labs

S4.2 TrOC stock solution preparation

Solid or liquid raw chemicals were dissolved in deionized water to prepare a stock solution containing the 12 TrOCs investigated as a mixture (100 µM, each). The prepared stock solution was analyzed by LC-MS/MS to obtain the actual concentrations of the TrOCs in the aqueous stock solution.

Table S4.2. Concentrations of TrOCs in the stock solution and recoveries of TrOCs after filtration with PES syringe filters.

No.	Name	Concentration in stock (µM)	0.2 µm PES filter recovery (%)
1	Sulfamethoxazole (SMX)	--[1]	87 ± 0.3
2	1,3-diphenylguanidine	73	82 ± 0.8
3	Benzotriazole	83	97 ± 1.0
4	5-methyl-benzotriazole	81	93 ± 0.1
5	2-hydroxybenzothiazole	85	88 ± 0.7
6	Benzothiazole-2-sulfonic acid	165	99 ± 0.4
7	2.4-D	81	97 ± 0.9
8	MCPA	83	99 ± 1.6
9	Mecoprop	78	95 ± 1.6
10	Diuron	85	38 ± 0.8[2]
11	N-Butylbenzenesulfonamide	75	60 ± 1.4[2]
12	Tris(2-chloroethyl)phosphate	76	87 ± 1.5

[1] not detected as SMX was not included in TrOC stock solution.

[2] for compounds with recovery below 80%, the recovery was taken into account for concentration and removal calculations

S4.3 Biochar characterization

S4.3.1 Electron exchange capacity (EEC)

The electron exchange capacity (EEC), which is the sum of the electron accepting capacity (EAC) and electron donating capacity (EDC), was determined by mediated electrochemical reduction (MER) and mediated electrochemical oxidation (MEO) modified from the method reported by Klüpfel et al., 2014[58]. All analyses were conducted under anoxic conditions in a glovebox. A 10 g biochar L^{-1} suspension was prepared and stirred for at least 24 h before analysis. For the electrochemical setup, the working electrodes as well as the reaction vessels were eight glassy carbon cells (each 9 mL, Sigradur G, HTW, Germany) with copper wires attached (four for MER and four for MEO). The counter electrodes were coiled platinum wires (0.5 mm, 99.9%, Sigma-Aldrich Co., USA) connected to platinum gauzes (52 mesh, 99.9%, Sigma Aldrich Co., USA) in glass tubes with porous glass frits filled with phosphate buffer (0.1 M KCl, 0.1 M KH_2PO_4, pH 7). The reference electrodes were Ag/AgCl electrodes (Bioanalytical Systems Inc., USA) but redox potentials are reported with reference to the standard hydrogen electrode. To start the measurement, 7 mL phosphate buffer solution was added into the continuously stirred reaction vessels, and redox potentials (E_h = -0.38 V for MER and +0.61 V for MEO) were applied using an eight-channel potentiostat CHI1000 (CH Instruments, USA). Subsequently, 100 µL of a 10 mM mediator stock solution, either zwitterionic viologen (ZiV) for reduction or 2,2'-azino-bis(3-ethylbenzothiazoline-6-sulfonic acid) (ABTS) for oxidation, was spiked to be completely oxidized or reduced. Then, 10 µL of the biochar sample was added consecutively into the vessels and sharp and clear current peaks were recorded. For the data analysis, the current peaks were integrated over an analysis time of 4000 s using Matlab R2020Ra. The electron accepting capacity (EAC) and electron donating capacity (EDC) were calculated in µmol e^- (g biochar)$^{-1}$ according to Klüpfel et al., 201[58].

S4.3.2 Zeta potential

The zeta potential of the biochar was measured by a nanoparticle size analyzer (Zetasizer Nano ZSP, Malvern Inc., UK). 40 mg biochar was suspended in 80 mL of 10 mM NaCl solution to prepare a 0.5 g L^{-1} biochar suspension, which was measured in the pH range of 6 – 12 by adjusting with HCl or NaOH. The measurements were performed in triplicate.

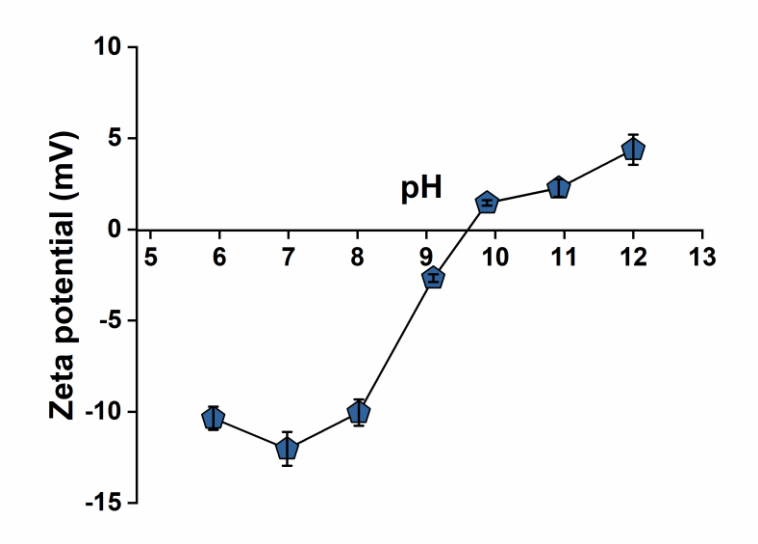

Figure S4.1. Zeta potential of the biochar at different pH values. Error bars indicate the standard deviation of triplicates.

S4.3.3 Persistent free radicals (PFRs)

Continuous X-band electron spin resonance (ESR) spectra were recorded with an ESR spectrometer (MiniScope MS 300, Magnettech GmbH, Berlin, Germany) for the determination of persistent free radicals. For the estimation of spin concentrations, the spectra were accumulated 3-fold over 90 s at a microwave power of 0.1 mW (sweep width 15 mT). Suwannee River standard fulvic acid (1S101F, IHSS) was used as a reference for the calculation of spin concentrations with a free radical content of 0.54 x 10^{17} spins g^{-1}. The g-values were determined in separate scans by measuring a certified internal manganese standard (Mn^{2+} in ZnS) simultaneously with the sample.

S4.3.4 Fourier-transform infrared spectroscopy (FTIR)

The spectra were collected with a Nicolet 670 FT-IR spectrometer (Thermo Fisher Scientific GmbH) equipped with an EverGlo source, a KBr beam splitter, and a deuterated L-alanine doped triglycene sulphate (DLaTGS) detector. The measurements were performed in attenuated total reflection (ATR) mode in a "Golden Gate" sample holder. The sample holder was cleaned with ethanol and acetone between measurements. Four measurements were conducted with different portions of the biochar sample over the range of 4000 – 600 cm^{-1} at 4 cm^{-1} and 32 co-added scans. All spectra were captured in absorbance units and ATR correction was applied in atmospheric conditions. Data were processed with standard normal variate (SNV) scatter-correction, followed with an asymmetric least squares baseline correction and a smoothing procedure with a Savitzky–Golay algorithm function (polynomial = 2 and points = 27).

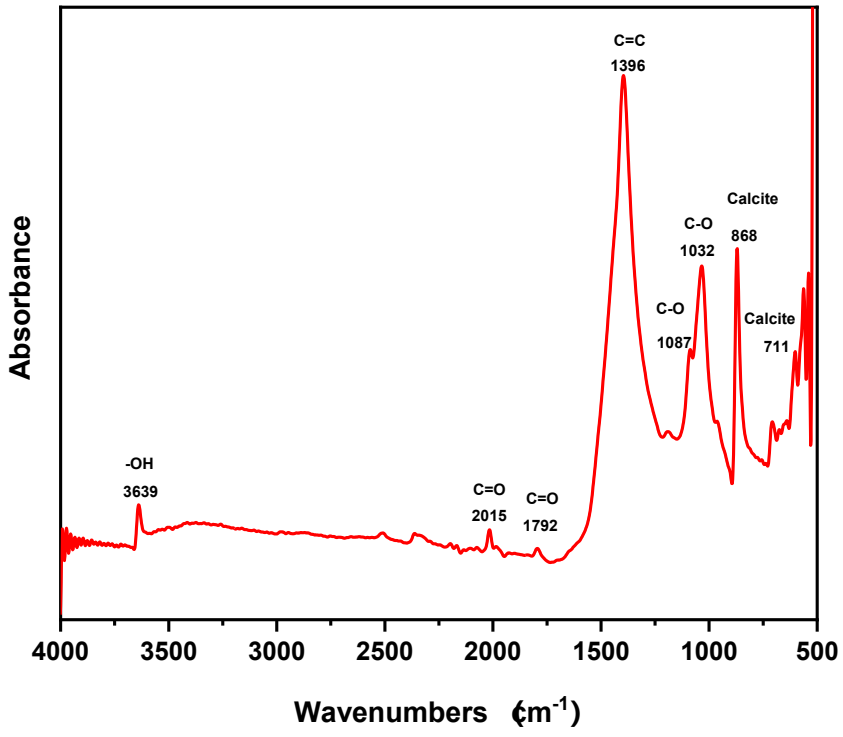

Figure S4.2. Fourier-transform infrared spectroscopy (FTIR) spectra of the biochar sample. Data are presented in quadruplicate measurements.

S4.3.5 X-ray diffraction analysis (XRD)

In situ XRD measurements were performed on a Bruker D2 PHASER X-ray diffractometer coupled with a SSD160-2 detector. The spectra were collected with Co Kα (λ = 1.79026 Å) source emitting radiation over the angular range 10° ≤ 2θ ≤ 90° with 0.015° step size and 0.6 s time steps. The tube was operated at 30 kV and 10 mA. DIFFRAC.EVA software was used for data evaluation and a crystallography open database was employed for phase identification.

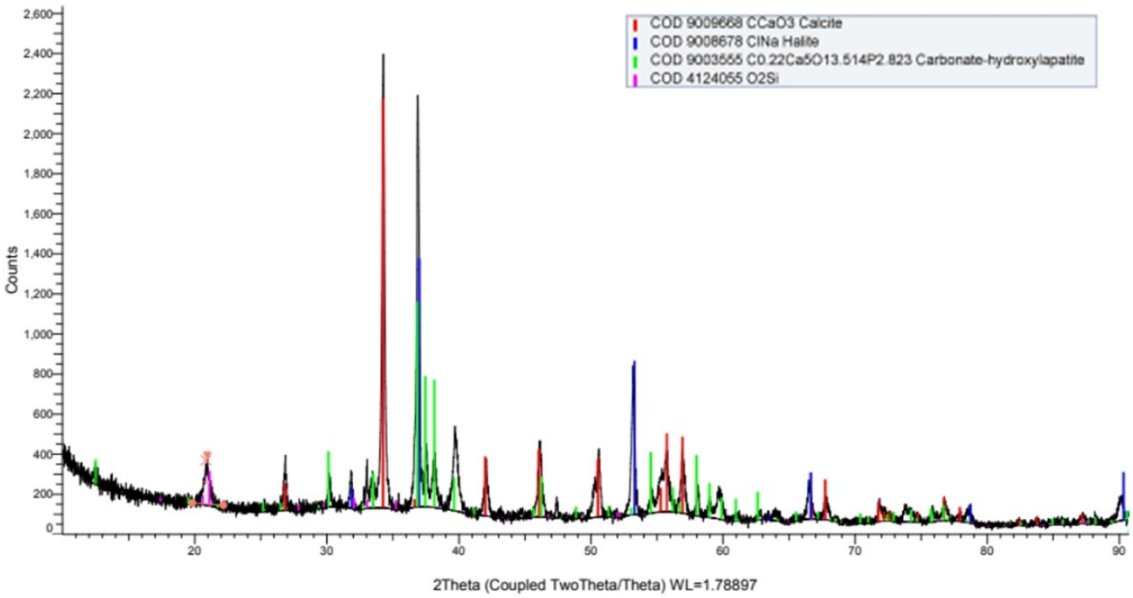

Figure S4.3. X-ray diffraction (XRD) pattern of biochar sample.

S4.3.6 Metal content

The metal content of the biochar was determined by inductively coupled plasma-optical emission spectroscopy (ICP-OES, ICP iCAP7000 Series, Thermo Fisher Scientific Inc.) after microwave acid digestion. 50 mg sample was digested in 6 mL nitric acid and 2 mL hydrochloric acid mixture. The digested solution was make up to 50 mL for ICP-OES analysis.

Table S4.3. Electron accepting and donating capacity (EAC, EDC), persistent free radical (PFR) concentration, and metal content of the biochar.

Characteristic	Value	Characteristic	Value
EAC (μmol e^- (g biochar)$^{-1}$)	244 ± 8	PFRs (10^{16} spins g^{-1})	5.07 ± 0.30
EDC (μmol e^- (g biochar)$^{-1}$)	244 ± 37	Cu (mg kg^{-1})	206
K (mg kg^{-1})	16100	Al (mg kg^{-1})	1090
Ca (mg kg^{-1})	268500	Ti (mg kg^{-1})	72
Mg (mg kg^{-1})	19500	Zn (mg kg^{-1})	106
Mn (mg kg^{-1})	54	Cd (mg kg^{-1})	<10
P (mg kg^{-1})	31500	Co (mg kg^{-1})	<10
S (mg kg^{-1})	5910	Cr (mg kg^{-1})	<10
Fe (mg kg^{-1})	1000	Ni (mg kg^{-1})	<10
Na (mg kg^{-1})	65460	Pb (mg kg^{-1})	<10

S4.4 Titration procedure in batch experiments

Before adding the PDS, the pH of the biochar suspension was adjusted to 7 and it stayed in constant during sorption time. One sample was withdrawn and the measured TrOC concentration was taken as initial aqueous concentration. After adding the PDS to initial the reaction, the solution slowly acidify because protons could be released due to the reaction of reactive species and the compounds. Therefore, during the reaction, 4 µL of 0.25 M NaOH was added every 10 minutes to the solution to keep the pH stay at 7 ± 0.1. In total 24 µL of NaOH in a reaction time of 1 hour was added at the end and no significant effect on compound determined concentration was caused by the titration.

S4.5 Analyses of TrOCs and probe compounds

S4.5.1 LC-MS/MS method

TrOCs were quantified using an Agilent 1290 InfinityII Ultra-High-Performance Liquid chromatography (UPLC) coupled to an Agilent 6470 triple-quadrupole mass spectrometer with an Agilent Jet Stream source in electrospray ionization (ESI) mode (Agilent, USA). 1,3-diphenylguanidine (DPG), 2-hydroxybenzothiazole (OHBT), 1*H*-benzotriazole (BTA), 5-methyl-benzotriazole (MBTA), benzothiazole-2-sulfonic acid (BTSA), *N*-butylbenzenesulfonamide (NBBS), tris(2-chloroethyl)phosphate (TCEP), and diuron were quantified in positive ionization mode and 2,4-dichlorophenoxyacetic acid (2,4-D), 2-methyl-4-chlorophenoxyacetic acid (MCPA), and mecoprop in negative ionization mode (Table S4.4). Aqueous samples were analyzed using a XBridge BEH C18 column (5 cm × 2.1 mm, 3.5 µm, Waters) equipped with a XBridge BEH C18 VanGuard cartridge (5 mm × 2.1 mm, 3.5 µm, Waters). The mobile phase consisted of LC-MS grade water (solvent A, LiChrosolv®, Sigma) and LC MS grade methanol (solvent B, ROTISOLV®, > 99.95%, Roth) each acidified with 0.1 vol% formic acid (Fluka). The eluent gradient increased linearly from 10% B to 95% B in 15 min and was kept constant at 95% B for 1 min at a flow rate of 200 µL min^{-1}. Quantification of analytes was carried out using external calibration standards ranging from 1 µg L^{-1} to 100 µg L^{-1}. The limit of quantification was defined as the lowest concentration standard with a signal to noise ratio ≥10. Data analyses were performed with MassHunter Workstation Software (Version Build9.0.647.0).

Table S4.4. Substance-specific MS/MS settings for quantification of trace organic contaminants

	m/z Precursor mass	m/z Product mass	ESI mode	Fragmentor voltage (V)	Collision energy (V)
DPG	212.1	119	+	105	24
	212.1	77	+	105	40
BTA	120.0	92	+	75	16
	120.0	65	+	75	24
MBTA	134.0	79	+	90	20
	134.0	77	+	90	28
OHBT	152.0	80	+	110	32
	152.0	65	+	110	36
BTSA	215.9	134	+	110	24
	215.9	89.9	+	110	40
2.4-D	221.0	177	-	55	0
	221.0	163	-	65	12
MCPA	199.0	155	-	60	4
	199.0	141	-	60	12
Mecoprop	213.0	141	-	70	8
	213.0	71	-	70	8
Diuron	235.0	72	+	85	24
	233.0	72	+	75	20
NBBS	214.1	158	+	84	8
	214.1	141	+	84	12
	214.1	77	+	84	28
TCEP	284.9	223	+	75	12
	284.9	99	+	75	24
	284.9	62.9	+	75	28

S4.5.2 HPLC UV-vis method

The concentrations of SMX, *p*CBA, *p*NBA, MOP, and TCP were quantified by HPLC (1200 Series, Agilent) equipped with a UV-vis detector. Aqueous samples were analyzed using an Agilent ZORBAX Eclipse XDB-C18 column (4.6 mm x 150 mm, 5 µm) and a ZORBAX Eclipse XDB-C18 guard cartridge. For SMX analysis, 20 µL of sample was injected and the eluent mixture consisted of 35% methanol and 65% water (pH 3, 1 mM H_2SO_4) at a flow rate of 0.5 mL min^{-1}. The wavelength was set to 270 nm. The concentration of SMX was quantified by external calibration from 0.25 µM to 20 µM. Analysis of *p*CBA and *p*NBA was carried out by injecting 50 µL of sample with an eluent mixture of 70% methanol and 30% water (pH 3, 1 mM H_2SO_4) at a flow rate of 0.5 mL min^{-1}. *p*CBA and *p*NBA were analyzed at 234 nm and 262 nm, respectively, and concentrations were quantified by external calibration from 0.025 µM to 5 µM. For MOP and TCP analysis, 50 µL of sample was injected and the mobile phase consisted of 60% methanol and 40% water with 1% acetic acid, and 80% methanol and 20% water with 1% acetic acid , respectively with a flow rate of 0.5 mL min^{-1}. The wavelength was 210 nm for MOP and 280 nm for TCP. Concentrations of MOP and TCP were quantified by external calibration from 0.5 µM to 10 µM.

S4.6 Characterization of street runoff

The pH of the collected street runoff was measured using a multi-parameter probe (Multi 340i, WTW, Germany). The dissolved organic carbon (DOC) and total dissolved nitrogen (TDN) concentration were analyzed by a TOC analyzer (TOC/TN, Shimadzu, Japan). The soluble reactive phosphorus (SRP) concentration was determined by a modified ammonium molybdate spectrophotometric method[184]. The concentration of major ions (Cl^-, SO_4^{2-}, NH_4^+, NO_2^-, NO_3^-) was determined by ion chromatography (930 Compact IC Flex, Metrohm, Germany). Metals were quantified by ICP-OES (iCAP 7000 Series, Thermo Fisher Scientific).

Table S4.5. Characteristics and composition of street runoff collected in Berlin.

Parameter	Value	Parameter	Value
pH	6.55	Ca (mg L^{-1})	5.23
DOC (mg L^{-1})	7.5	Cu (mg L^{-1})	0.01
TDN (mg L^{-1})	1	Fe (mg L^{-1})	0.05
SRP (mg L^{-1})	186	K (mg L^{-1})	2.99
NH_4^+ - N (mg L^{-1})	0.36	Mg (mg L^{-1})	0.54
NO_2^- - N (mg L^{-1})	<0.005	Mn (mg L^{-1})	<0.01
NO_3^- - N (mg L^{-1})	0.29	Na (mg L^{-1})	1.52
Cl^- (mg L^{-1})	2.9	P (mg L^{-1})	0.21
SO_4^{2-} (mg L^{-1})	0.6	S (mg L^{-1})	<1.0
Al (mg L^{-1})	0.03	Si (mg L^{-1})	0.36
B (mg L^{-1})	0.02	Zn (mg L^{-1})	0.03

.

S4.7 Degradation of TrOCs by biochar and PDS in pure water

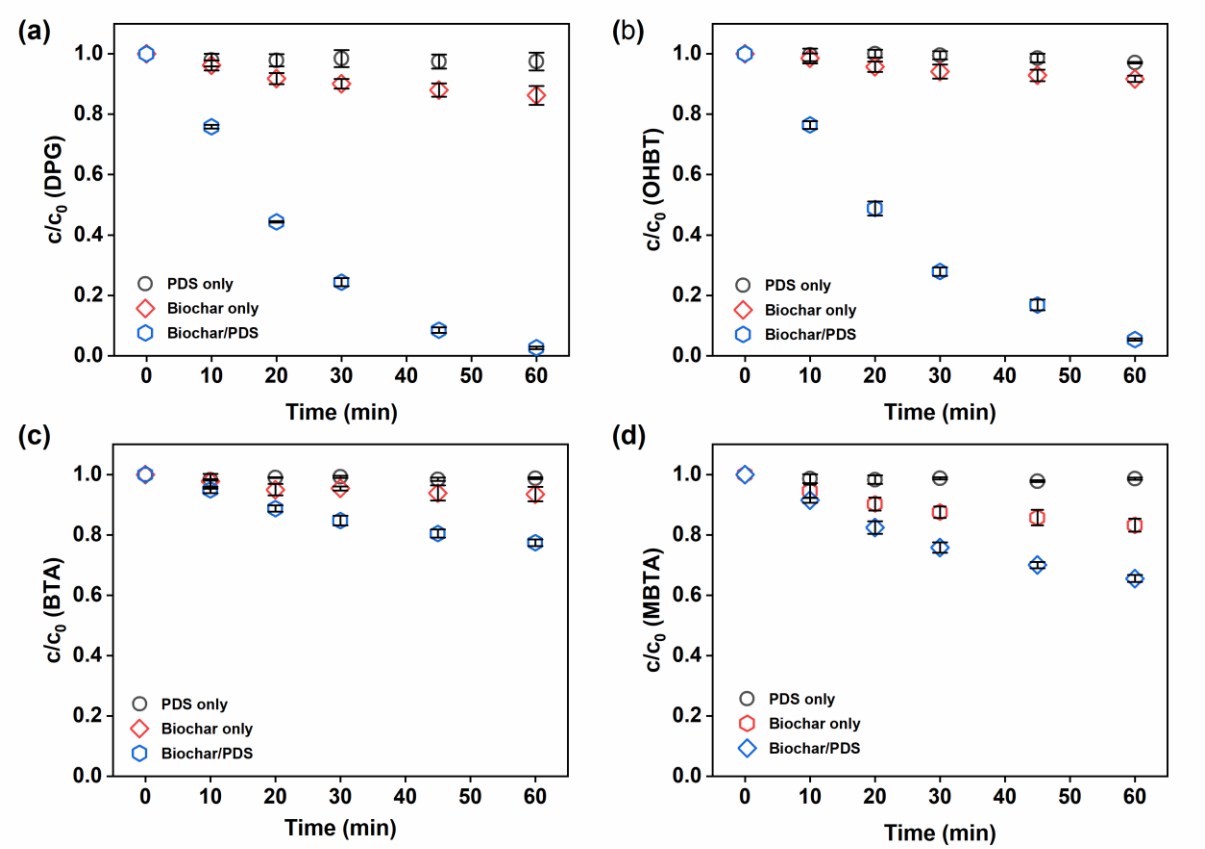

Figure S4.4-1. Removal of (a) 1,3-diphenylguanidine (DPG), (b) 2-hydroxybenzothiazole (OHBT), (c) benzotriazole (BTA), and (d) 5-methyl-benzotriazole (MBTA) (in mixture) over time in batch experiments containing (i) persulfate only, (ii) biochar only, and (iii) persulfate and biochar. [Biochar] = 1 g L^{-1}, [persulfate] = 1 mM, $[TrOCs]_{spiked}$ ~ 6 µM, c_0 = concentration after 30 min sorption, c = measured TrOCs concentration overtime, pH 7 (titrated with H_2SO4 and NaOH), in pure water without buffer. Error bars indicate the standard deviation of duplicates.

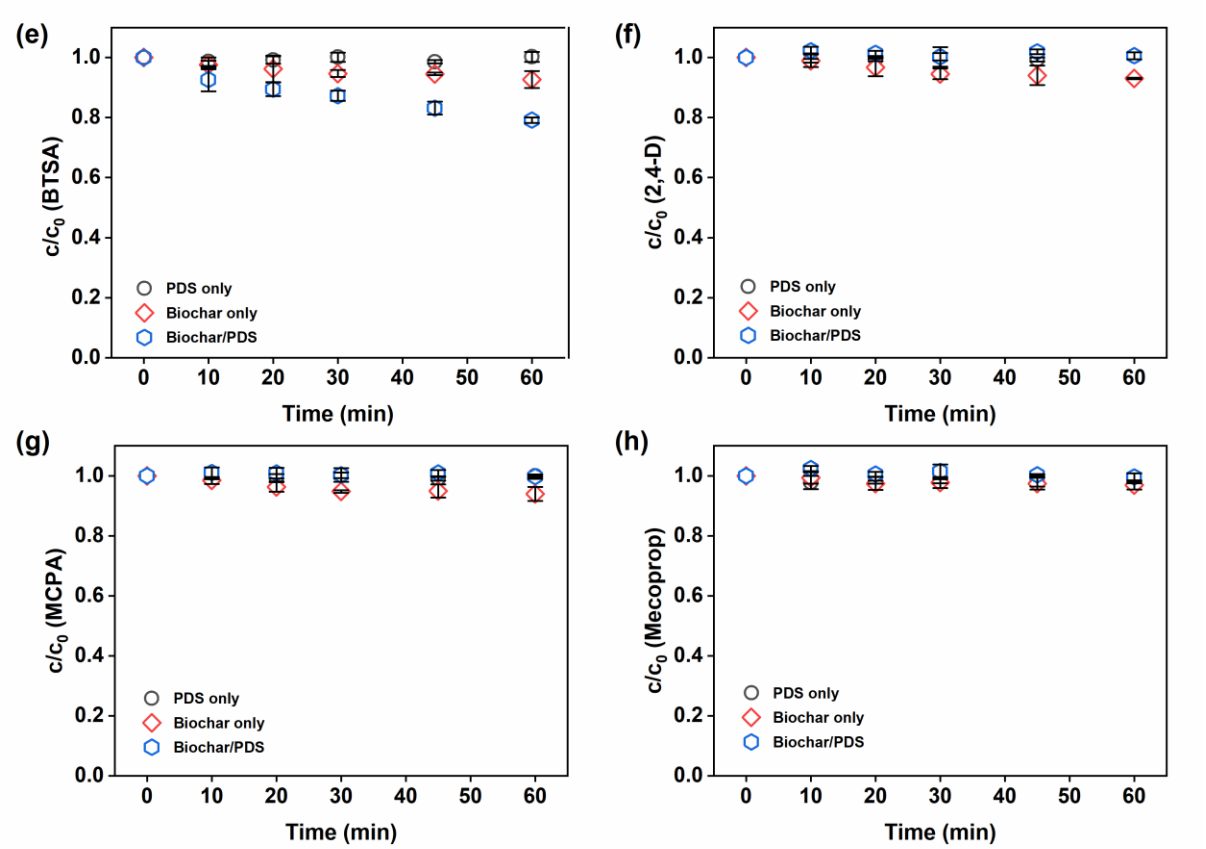

Figure S4.4-2. Removal of (e) benzothiazole-2-sulfonic acid (BTSA), (f) 2,4-dichlorophenoxyacetic acid (2,4-D), (g) 2-methyl-4-chlorophenoxyacetic acid (MCPA), and (h) mecoprop (in mixture) over time in batch experiments containing (i) persulfate only, (ii) biochar only, and (iii) persulfate and biochar. [Biochar] = 1 g L^{-1}, [persulfate] = 1 mM, $[TrOCs]_{spiked}$ ~ 6 µM, c_0 = concentration after 30 min sorption, c = measured TrOCs concentration overtime, pH 7 (titrated with H_2SO4 and NaOH), in pure water without buffer. Error bars indicate the standard deviation of duplicates.

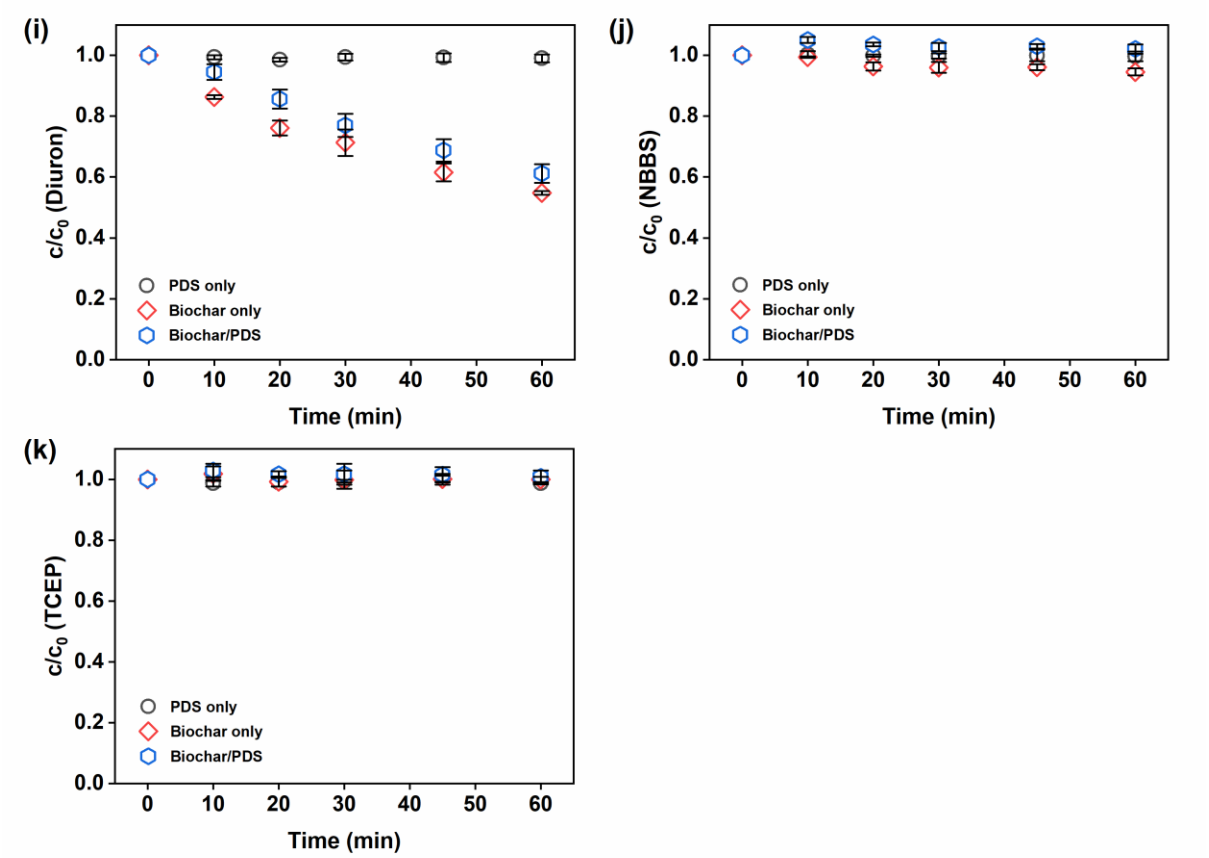

Figure S4.4-3. Removal of (i) diuron (j) *N*-Butylbenzenesulfonamide (NBBS) (k) tris(2-chloroethyl)phosphate (TCEP) (in mixture) over time in batch experiments containing (i) persulfate only, (ii) biochar only, and (iii) persulfate and biochar. [Biochar] = 1 g L^{-1}, [persulfate] = 1 mM, $[TrOCs]_{spiked}$ ~ 6 µM, c_0 = concentration after 30 min sorption, c = measured TrOCs concentration overtime, pH 7 (titrated with H_2SO4 and NaOH), in pure water without buffer. Error bars indicate the standard deviation of duplicates.

S4.8 Degradation kinetics of degraded TrOCs by biochar and PDS in pure water

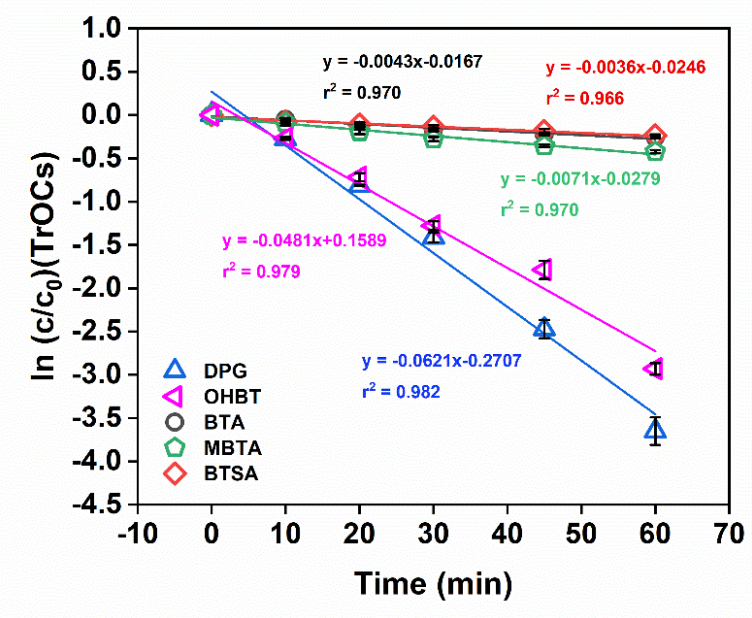

Figure S4.5. Degradation kinetics of 1,3-diphenylguanidine (DPG), 2-hydroxybenzothiazole (OHBT), benzotriazole (BTA), 5-methyl-benzotriazole (MBTA), and benzothiazole-2-sulfonic acid (BTSA) in the biochar/PDS system. [Biochar] = 1 g L^{-1}, [persulfate] = 1 mM, $[TrOCs]_{spiked}$ ~ 6 µM, c_0 = concentration after 30 min sorption, c = measured TrOCs concentration overtime, pH 7 (titrated with H_2SO4 and NaOH), in pure water without buffer. Error bars indicate the standard deviation of duplicates.

S4.9 Effect of humic acid on TrOCs degradation by biochar and PDS

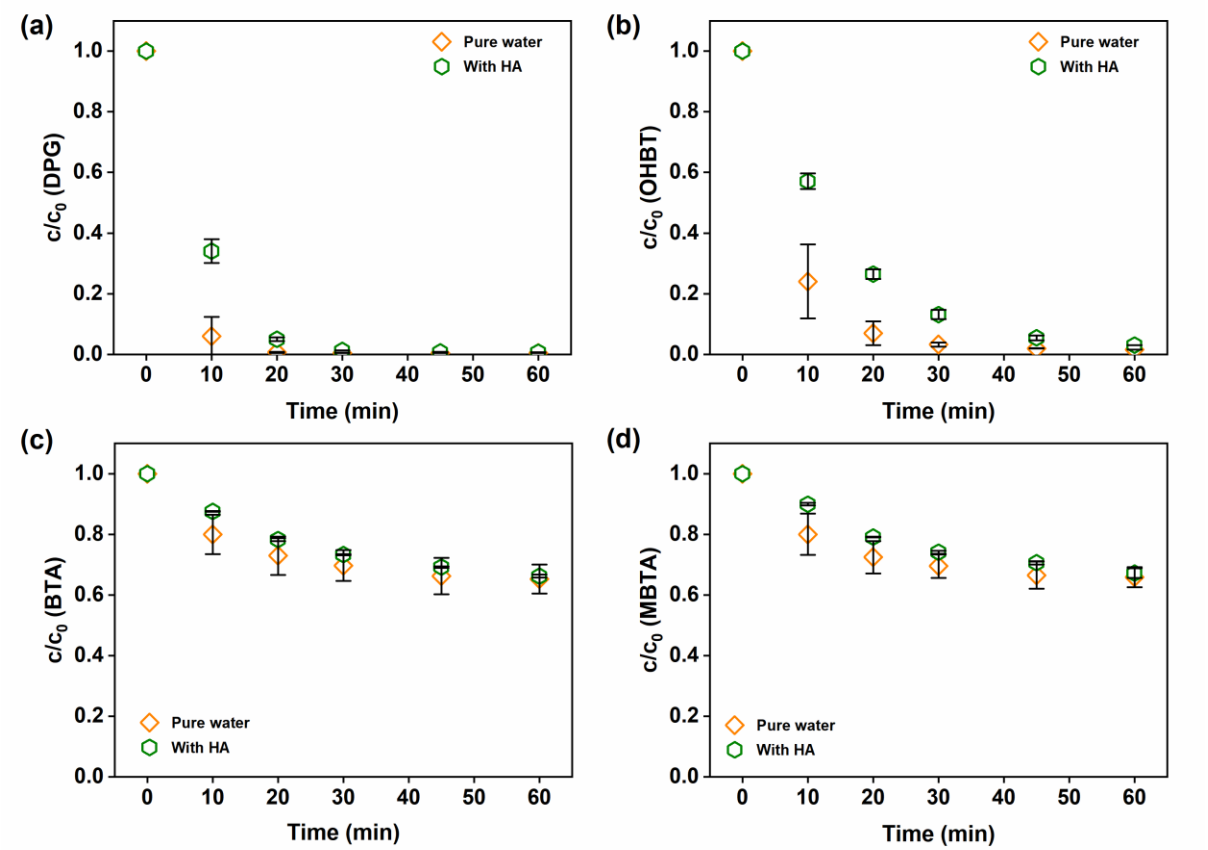

Figure S4.6. Removal of (a) 1,3-diphenylguanidine (DPG), (b) 2-hydroxybenzothiazole (OHBT), (c) benzotriazole (BTA), and (d) 5-methyl-benzotriazole (MBTA) (in mixture) over time in pure water and in the presence of Suwannee River humic acid. [Biochar] = 1 g L^{-1}, [PDS] = 1 mM, [DOC] = 6.4 mg L^{-1}, $[DPG]_{0,\text{ after overnight sorption}} = c_0$ = 0.8 µM,, $[OHBT]_{0,\text{ after overnight sorption}} = c_0$ = 0.8 µM, $[BTA]_{0,\text{ after overnight sorption}} = c_0$ = 1.2 µM, $[MBTA]_{0,\text{ after overnight sorption}} = c_0$ = 0.95 µM, c = measured TrOCs concentration over time, pH 7 (titrated with H_2SO4 and NaOH), in synthetic water without buffer. Error bars indicate the standard deviation of duplicates.

S4.10 Effect of chloride on TrOCs degradation by biochar and PDS

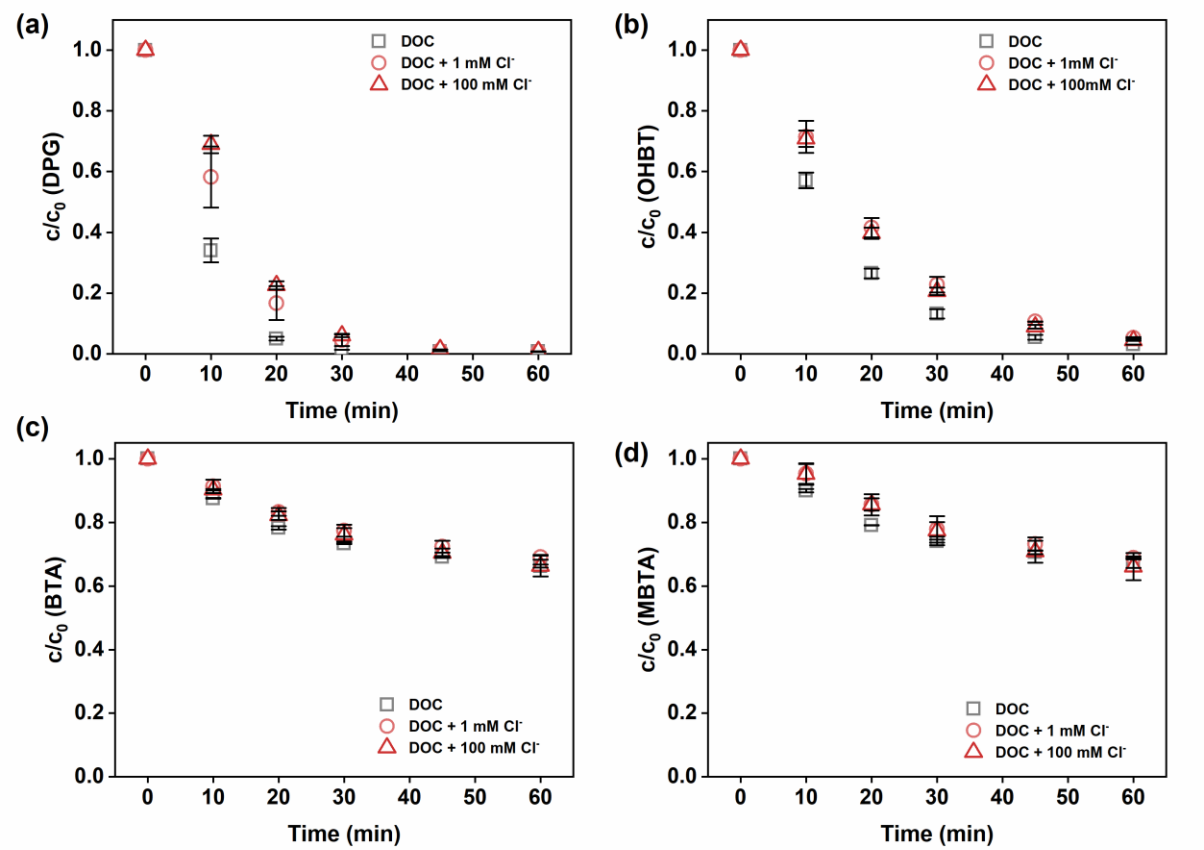

Figure S4.7. Removal of (a) 1,3-diphenylguanidine (DPG), (b) 2-hydroxybenzothiazole (OHBT), (c) benzotriazole (BTA), and (d) 5-methyl-benzotriazole (MBTA) (in mixture) in synthetic water containing 6.4 mg/L DOC (Suwannee River humic acid) in absence and presence of different concentrations of chloride over time. [Biochar] = 1 g L^{-1}, [PDS] = 1 mM, [DOC] = 6.4 mg L^{-1}, $[DPG]_{0,\text{ after overnight sorption}} = c_0 = 0.7$ µM, $[OHBT]_{0,\text{ after overnight sorption}} = c_0 = 0.96$ µM, $[BTA]_{0,\text{ after overnight sorption}} = c_0 = 1.3$ µM, $[MBTA]_{0,\text{ after overnight sorption}} = c_0 = 1.0$ µM, c = measured TrOCs concentration over time, pH 7(titrated with H_2SO4 and NaOH), in synthetic water without buffer. Error bars indicate the standard deviation of duplicates

S4.11 Competition kinetics calculations

The fraction of a reactive species, f, reacting with a certain compound in competition with other substrates can be calculated with the corresponding known concentrations and reaction rate constants[143]. The fraction corresponds to the concentration ($c_{compound}$) times the reaction rate constant ($k_{compound}$) of the compound at study, divided by the sum of the concentrations (c_1, c_2 to c_n) times the reaction rate constants (k_1, k_2 *to* k_n) of all substrates that can react with the reactive species according to Equation S4.1:

$$f = \frac{c_{compound} \cdot k_{compound}}{c_{compound} \cdot k_{compound} + c_1 \cdot k_1 + c_2 \cdot k_2 + \cdots + c_n \cdot k_n} \quad \text{(S4.1)}$$

Reaction rate constants for different scavengers and SMX with •OH and $SO_4^{\bullet-}$:

MeOH: k (•OH) = 9.7 × 10^8 M^{-1} s^{-1}; k ($SO_4^{\bullet-}$) = 1.1 × 10^7 M^{-1} s^{-1}

TBA: k (•OH) = 6.0 × 10^8 M^{-1} s^{-1}; k ($SO_4^{\bullet-}$) = 8.0 × 10^5 M^{-1} s^{-1}

DMSO: k (•OH) = 7.0 × 10^9 M^{-1} s^{-1}; k ($SO_4^{\bullet-}$) = 2.7× 10^9 M^{-1} s^{-1}

SMX: k (•OH) = 5.5 × 10^9 M^{-1} s^{-1}; k ($SO_4^{\bullet-}$) = 1.25 × 10^{10} M^{-1} s^{-1}

Experiment 1: 1 g L^{-1} biochar, 1 mM PDS, 10 µM SMX, 1 M MeOH

The fraction of •OH reacting with MeOH:

$$f\,(\mathrm{MeOH}) = \frac{[\mathrm{MeOH}] \times k_{\bullet\mathrm{OH},\ \mathrm{MeOH}}}{[\mathrm{MeOH}] \times k_{\bullet\mathrm{OH,MeOH}} + [\mathrm{SMX}] \times k_{\bullet\mathrm{OH,SMX}}} = 100\%$$

The fraction of $SO_4^{\bullet-}$ reacting with MeOH:

$$f\,(\mathrm{MeOH}) = \frac{[\mathrm{MeOH}] \times k_{SO_4^{\bullet-},\ \mathrm{MeOH}}}{[\mathrm{MeOH}] \times k_{SO_4^{\bullet-},\mathrm{MeOH}} + [\mathrm{SMX}] \times k_{SO_4^{\bullet-},\mathrm{SMX}}} = 99\%$$

Experiment 2: 1 g L^{-1} biochar, 1 mM PDS, 10 μM SMX, 5 mM TBA

The fraction of •OH reacting with TBA:

$$f\,(\mathrm{TBA}) = \frac{[\mathrm{TBA}]\ \times k_{\bullet\mathrm{OH},\ \mathrm{TBA}}}{[\mathrm{TBA}]\ \times k_{\bullet\mathrm{OH,TBA}} + [\mathrm{SMX}] \times k_{\bullet\mathrm{OH,SMX}}} = 98\%$$

The fraction of $SO_4^{\bullet-}$ reacting with TBA:

$$f\,(\mathrm{TBA}) = \frac{[\mathrm{TBA}]\ \times k_{\mathrm{SO}_4^{\bullet-},\ \mathrm{TBA}}}{[\mathrm{TBA}]\ \times k_{\mathrm{SO}_4^{\bullet-},\mathrm{TBA}} + [\mathrm{SMX}] \times k_{\mathrm{SO}_4^{\bullet-},\mathrm{SMX}}} = 3\%$$

Experiment 3: 1 g L^{-1} biochar, 1 mM PDS, 10 μM SMX, 10 mM DMSO

The fraction of •OH reacting with DMSO:

$$f\,(\mathrm{DMSO}) = \frac{[\mathrm{DMSO}]\ \times k_{\bullet\mathrm{OH},\ \mathrm{DMSO}}}{[\mathrm{DMSO}]\ \times k_{\bullet\mathrm{OH,DMSO}} + [\mathrm{SMX}] \times k_{\bullet\mathrm{OH,SMX}}} = 100\%$$

The fraction of $SO_4^{\bullet-}$ reacting with DMSO:

$$f\,(\mathrm{DMSO}) = \frac{[\mathrm{DMSO}]\ \times k_{\mathrm{SO}_4^{\bullet-},\ \mathrm{DMSO}}}{[\mathrm{DMSO}]\ \times k_{\mathrm{SO}_4^{\bullet-},\mathrm{DMSO}} + [\mathrm{SMX}] \times k_{\mathrm{SO}_4^{\bullet-},\mathrm{SMX}}} = 3\%$$

S4.12 Removal of *p*CBA and *p*NBA by biochar and PDS

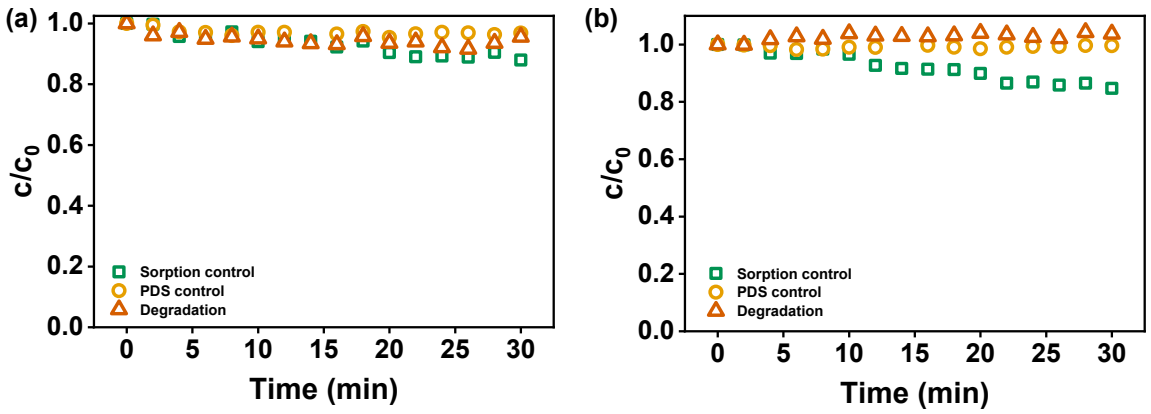

Figure S4.8. *p*CBA and *p*NBA removal over time in batch experiments containing (i) only biochar (sorption control), (ii) only PDS (PDS control), and (iii) biochar and PDS (degradation). [Biochar] = 1 g L^{-1}, [PDS] = 1 mM, $[pCBA]_{spiked} = [pNBA]_{spiked}$ = 3 µM, $[pCBA]_{0,\ after\ 30min\ sorption}$ = 2.2 µM; $[pNBA]_{0,\ after\ 30min\ sorption}$ = 1.8 µM, c is the measured *p*CBA and *p*NBA concentration over time, pH 7 (titrated with H_2SO4 and NaOH), in pure water without buffer.

S4.13 Stability of MOP and TCP in control systems containing only biochar or PDS

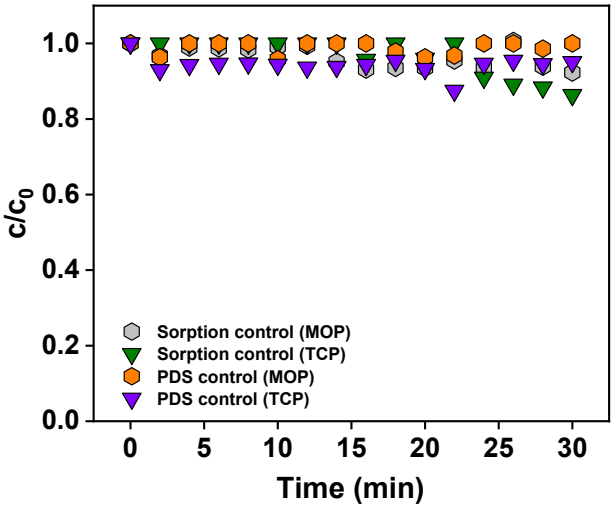

Figure S4.9. Stability of MOP and TCP in batch experiments containing (i) only biochar (sorption control) and (ii) only persulfate (PDS control) over time. [Biochar] = 0.5 g L^{-1}, [PDS] = 1 mM, $[MOP]_{spiked} = [TCP]_{spiked}$ = 5 µM, c is the measured *p*CBA and *p*NBA concentration over time, pH 7 (titrated with H_2SO4 and NaOH), in pure water without buffer.

S4.14 Degradation of MOP and TCP in the H_2O_2/NaClO reference system

The reaction of hydrogen peroxide (H_2O_2) with hypochlorite (ClO^-) is known to exclusively produce $^1O_2$ according to Equation S4.2 [238–240].

$$H_2O_2 + ClO^- \rightarrow {}^1O_2 + H_2O + Cl^- \qquad k = 3.4 \times 10^3\ M^{-1}\ s^{-1} \qquad (S4.2)$$

Therefore, the H_2O_2/ClO^- system was employed as a $^1O_2$ reference system to study the degradation of the probe compounds MOP and TCP in competition kinetics experiments. As the H_2O_2/ClO^- reaction happens in microseconds, samples could not be collected over time. Therefore, the competition kinetics experiments followed the reaction rate constants determination method with the measurement of only a single endpoint[160]. Experiments were conducted by adding a fixed dosage of H_2O_2 (10 mM from an aqueous stock solution of 0.5 M) to twenty well-mixed solutions containing 5 µM MOP and 5 µM TCP. Subsequently, the reaction was immediately initiated by adding different amounts of NaClO solution to obtain a ClO^- concentration of 1 – 20 mM. The pH of the reaction solutions was 10 ± 1, which is reported to produce the highest $^1O_2$ yield[258]. No buffer was used in the experiments to avoid any effects of the buffer on the reaction kinetics. 1 mL sample was withdrawn after 30s reaction and immediately mixed with 100 µL of 0.1 M ascorbic acid to scavenge any residual reactive species or oxidant. Samples were analyzed immediately on the same day to determine the final concentration, c, of MOP and TCP. Initial concentrations, c_0, of MOP and TCP were determined in a simultaneously conducted control experiment containing MOP, TCP, and 10 mM H_2O_2 only.

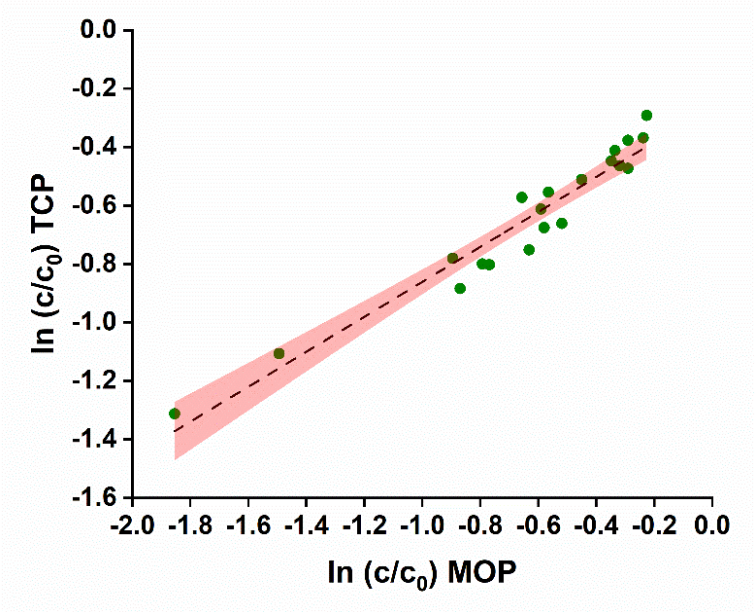

Figure S4.10. Competition plot ln(c/c$_0$) of MOP vs. TCP in the H_2O_2/NaClO system (slope 0.60 ± 0.04; intercept -0.26 ± 0.03). [H_2O_2] = 10 mM, [ClO^-] = 1 - 20 mM, $[MOP]_{spiked}$ = $[TCP]_{spiked}$ = 5 µM; c_0 is the measured MOP and TCP concentration of a control containing only 10 mM H_2O_2, c is the measured MOP and TCP concentration after 30s reaction, pH 10 ± 1 without buffer. Red areas show the 95% confidence intervals of the linear fit.

As shown in Figure S4.10, the competition plot of ln(c/c$_0$) (MOP) vs. ln(c/c$_0$) (TCP) yielded a slope of 0.60 ± 0.04, which is the same as the ratio of the second order rate constant of $^1O_2$ with MOP and TCP (k (TCP + $^1O_2$) /k (MOP + $^1O_2$) = 0.59) calculated by the rate constants reported by Tratnyek and Hoigne, 1991[237]. The rate constants used here in the H_2O_2/NaClO system refer to the reaction of $^1O_2$ with MOP and TCP in their phenolate forms (k (MOP + $^1O_2$) = 2.85 × 10^8 M^{-1} s^{-1} and k (TCP + $^1O_2$) = 1.67 × 10^8 M^{-1} s^{-1} [237] because the reaction pH was above the pKa of MOP (pKa = 9.65) and TCP (pKa = 6.23). The rate constants of MOP and TCP in its phenol forms determined in the same study[237] were used for the biochar/PDS system at pH 7. MOP and TCP can serve as sensitive indicators for singlet oxygen.

S4.15 Electron transfer process

Direct electron transfer pathway might involve in the biochar/PDS system, where biochar acts as catalyst and mediator between organic contaminants (electron donor) and PDS (electron acceptor)[105]. In a case of electron transfer process, an enhancement of persulfate decomposition should be observed with the addition of organics[105,259] . The decrease of PDS decomposition after SMX addition (Figure S4.11) ruled out the contribution of direct electron transfer pathway in the biochar/PDS system. Moreover, the biochar has relatively low electron donating capacity (EDC, 244 ± 8 (μmol e^- (g biochar)$^{-1}$)) and low concentration of persistent free radicals (waiting for the data from Andrea) (Table S4.3). Additionally, the biochar shows negative charge at pH 7 (Figure S4.1). $S_2O_8^{2-}$ ion is hard to adsorb onto biochar surface to form biochar-persulfate complex, which is necessary for an electron transfer process[105].

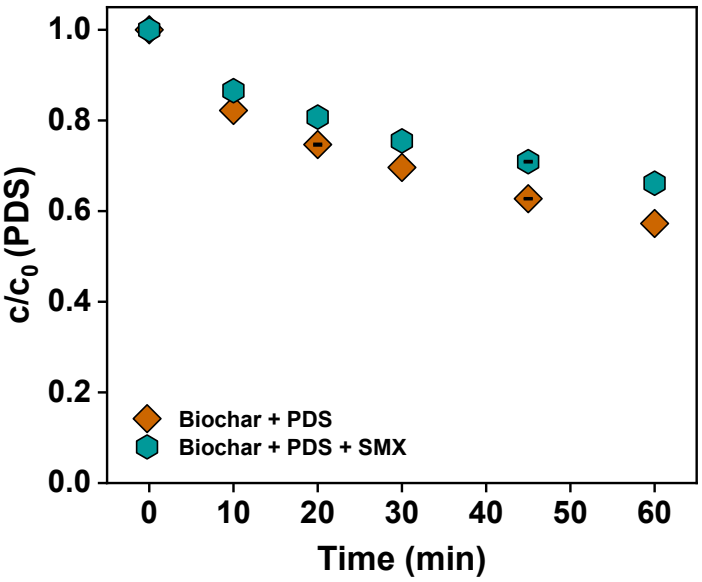

Figure S4.11. (a) Persulfate decomposition over time in batch experiments containing biochar and PDS without and with SMX. [Biochar] = 1 g L^{-1}, [PDS] = 1 mM, $[SMX]_{spiked}$= 10 μM, c_0 (PDS) = 1 mM, c is the measured persulfate concentration over time, pH 7 (titrated with H_2SO4 and NaOH), in pure water without buffer. Error bars indicate the standard deviation of triplicates.

Note: The loss of PDS in presence of SMX was 0.33 mM and sulfate ion formed was measured to be 0.70 mM.

S4.16 SMX degradation by biochar and PDS in the presence of carbonate

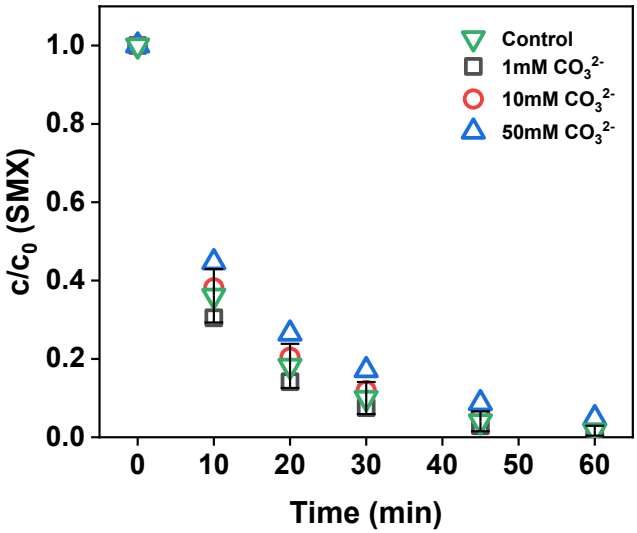

Figure S4.12. SMX degradation over time in the biochar/PDS system in the absence (control) and presence of different concentrations of carbonate (CO_3^{2-}) employed as superoxide radical scavenger. [Biochar] = 1 g L^{-1}, [PDS] = 1 mM, $[SMX]_0 = c_0 \sim$ 7.5 µM, c is the measured SMX concentration over time, pH 7 (titrated by H_2SO_4 and NaOH), in pure water without buffer. Error bars indicate the standard deviation of triplicates.

S4.17 SMX degradation by biochar and PDS in the presence and absence of dissolved oxygen

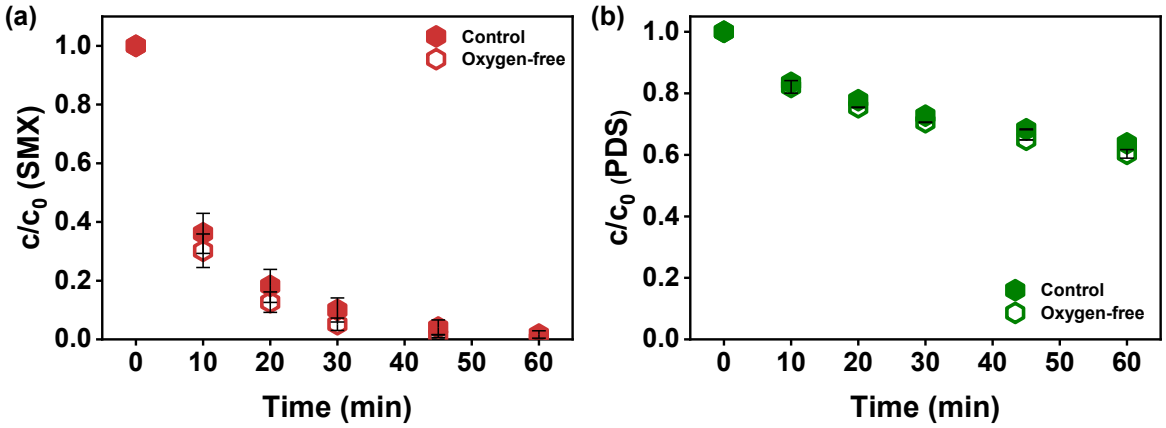

Figure S13. (a) SMX degradation and (b) $S_2O_8^{2-}$ decomposition over time in the biochar/PDS system in the absence (control) and presence (oxygen free) of dissolved oxygen. [Biochar] = 1 g L^{-1}, [PDS] = 1 mM, (a): $[SMX]_0 = c_0 \sim$ 7.5 μM, c is the measured SMX concentration over time; (b) : c_0 = 1mM, c is the measured $S_2O_8^{2-}$ concentration over time, pH 7 (titrated by H_2SO_4 and NaOH), in pure water without buffer. Error bars indicate the standard deviation of triplicates.

S4.18 Calculations of Hammett σ^+ constants

Hammett (σ, σ^+,σ^-) constants are the most common substituent descriptors in physical organic chemistry and are relatively easily accessible and applicable[243–245]. Hammett constants in σ^+ scale was used in the study as the σ scale fails to characterize reactions where resonance effects are expected to have a major impact. Moreover, it gives a better correlation when dealing with electron-donating substituents (e.g., –OH, $–OCH_3$, and $–NH_2$ groups) compared to σ^- scale. Hammett σ^+ constants quantitatively express the electron-donating (large negative value) or electron-withdrawing (large positive value) properties of substituents on aromatic compounds, including the inductive and resonance effects of substituents. Hammett σ^+ constants have corresponding σ_p^+, σ_m^+ and σ_o^+ values representing the substituents in the *ortho*-, *meta*-, and *para*-positions, respectively in the parent structure. For a compound with many substituents, the summed $\Sigma\sigma_{o,\,m,\,p}^+$ was used to account for the effects of all substituents on the aromatic ring[243]. The σ_p^+ values of a compound were obtained from literature[243–245], while the *ortho*-, *meta*-effects (σ_o^+, and σ_m^+) were calculated from relationships of $\sigma_o^+ = 0.66\sigma_p^+$, and $\sigma_m^+ = \sigma_p^+$. Also, a structural approximation was used to simplify the complex structures of the organic compounds at study, in which only one or two neighboring atoms from an aromatic ring determined the inductive/resonance effects of whole substituents[243].

Table S4.6. Structural approximation, descriptors and their corresponding ∑σ+ values of the studied aromatic organic contaminants.

No.	Name	Original structure	Approximated structure	descriptors	∑σ+
1	1,3-Diphenylguanidine (DPG)	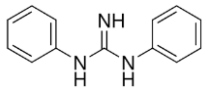	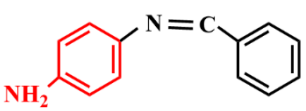	-N=CHC$_6$H$_5$ σ_p^+ = -0.55	-0.55
2	Benzotriazole (BTA)	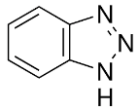	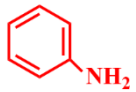	--	0
3	5-Methyl-benzotriazole (MBTA)	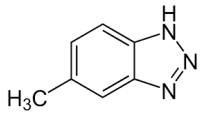	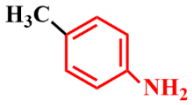	-CH$_3$ σ_p^+ = -0.17	-0.17
4	2-Hydroxybenzothiazole (OHBT)	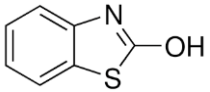	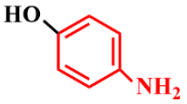	-OH σ_p^+ = -0.37	-0.37
5	Benzothiazole-2-sulfonic acid (BTSA)	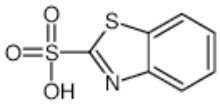	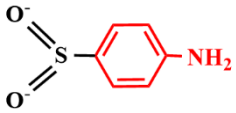	-SO^{2-} σ_p^+ = -0.05	-0.05
6	Diuron	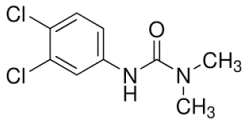	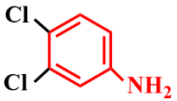	-Cl σ_p^+ = 0.11, σ_m^+ = 0.4	0.51

7	2.4-D	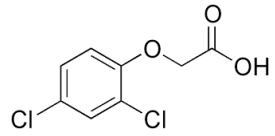	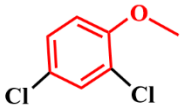	-Cl $\sigma_p^+ = 0.11$, $\sigma_o^+ = 0.0726$	0.1826
8	MCPA	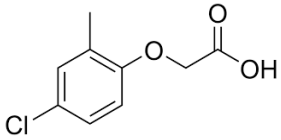	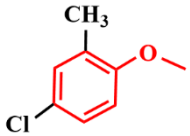	-Cl $\sigma_p^+ = 0.11$ $-CH_3$ $\sigma_o^+ = -0.2046$	-0.0924
9	Mecoprop	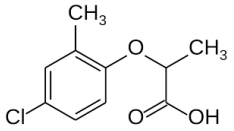	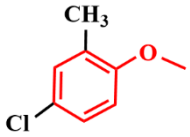	-Cl $\sigma_p^+ = 0.11$ $-CH_3$ $\sigma_o^+ = -0.2046$	-0.0924
10	N-Butylbenzenesulfonamide (NBBS)	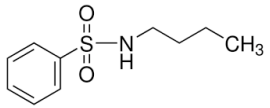		$-SO_2NH_2$ $\sigma_o^+ = 0.57$	0.57
11	3-methoxyphenol (MOP)	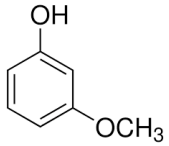	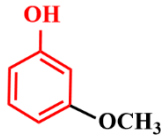	$-OCH_3$ $\sigma_m^+ = 0.05$	0.05
12	2,4,6-trichlorophenol (TCP)	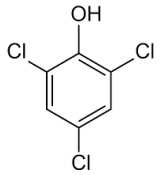	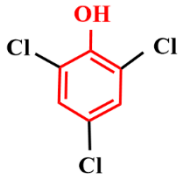	-Cl $\sigma_p^+ = 0.11$, $\sigma_o^+ = 0.0726$	0.2552

Chapter 5

Conclusion and outlook

5.1 Identification of major reactive species in persulfate-based oxidation processes

The formation of reactive species such as $SO_4^{\bullet-}$, $^{\bullet}OH$, and $^1O_2$ in persulfate-based as well as other oxidation processes is of great interest in both natural and engineered water treatment systems because reactive species can oxidize a wide range of contaminants[148,260,261]. An accurate and easy-to-achieve identification of the major reactive species is crucial for the assessment of established oxidation processes as well as for the development of new oxidation processes to identify suitable applications in terms of target contaminants and water matrix[121]. The qualitative and quantitative analysis of reactive species utilizing probe compounds is widely employed to unravel the underlying mechanisms in oxidation processes[173–175].

However, inappropriate usage of probe compounds can result in misleading mechanistic interpretations, for instance, overlooking or overestimating the contribution of reactive species in oxidation processes. This dissertation showcases the importance of a careful selection of probe compounds to study reactive species, particularly in persulfate-based oxidation processes. As discussed in Chapter 2, the use of PMSO as a probe compound to diagnose the presence of ferryl ion (Fe(IV)) species in persulfate-based oxidation processes needs careful re-evaluation as evidence was provided that $SO_4^{\bullet-}$ also play a role in the transformation of sulfoxides to sulfones.

The selection of suitable probe compounds should be based on the following criteria[121,122]: 1) probe compounds should not physically interact with the system under investigation, e.g., the compounds should not adsorb onto solid material, which is of particular importance for heterogeneous advanced oxidation processes, 2) probe compounds should react rapidly with the reactive species of interest with known second order reaction rate constants, and 3) probe compounds should selectively react with the reactive species of interest in a well-defined reaction, preferably with a clear defined reaction mechanism[121,122]. However, it is difficult to always find suitable probe compounds for the system of interest, especially in complex heterogeneous

oxidation systems, such as the biochar/persulfate system, because selected probe compounds might react with components involved in the oxidation system or might directly consume persulfate[30,122,123]. Therefore, it is of crucial importance to conduct control experiments to check for the suitability of probe compounds and avoid misinterpretation of results.

While in this thesis, the focus was on the use of probe compounds for the identification of reactive species in the biochar/Fe(III)/persulfate system, it may be useful to search for and identify transformation products of selected model compounds (in this dissertation: DEET). The search for suspected or unknown transformation products using high-resolution mass spectrometry may provide additional evidence for the suggested presence or absence of reactive species and, in addition, can help to reveal transformation mechanisms of specific contaminants of interest.

When focusing more on the transformation mechanism of selected organic contaminants, compound-specific isotope analysis (CSIA) using gas or liquid chromatography coupled to isotope ratio mass spectrometry (GC/IRMS or LC/IRMS) can be a powerful tool to elucidate reaction mechanisms of organic compounds involving reactive species[262,263]. In addition to the presented data in this dissertation, a CSIA method was developed for stable carbon isotope analysis of DEET (Figure 5.1). This method can be expanded to nitrogen isotope analysis of DEET and then employed in future studies to further elucidate the transformation pathways of DEET in biochar-assisted persulfate-based oxidation processes. To this end, laboratory experiments should be conducted to determine kinetic isotope effects associated with the reaction of DEET upon radical and non-radical pathways induced by different reactive species.

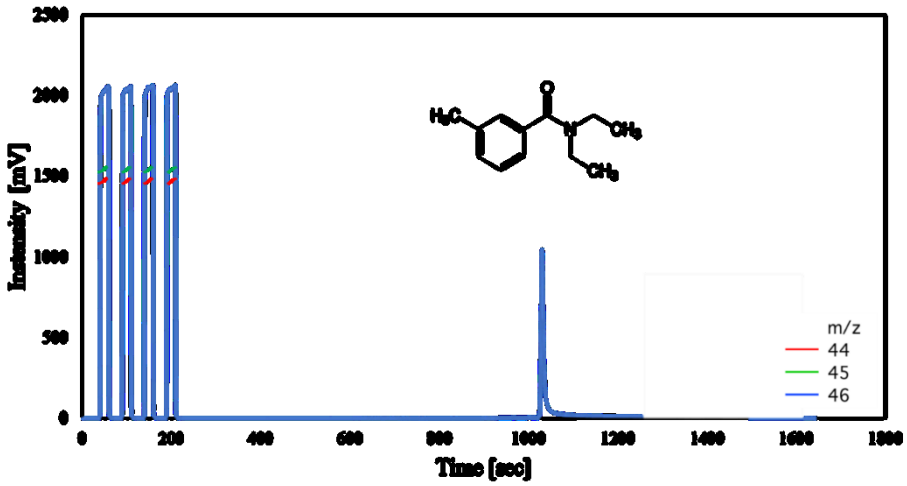

Figure 5.1. Chromatogram of C isotope analysis of 1 mM DEET using GC/IRMS.

The data presented in Chapter 2 also demonstrate that the water matrix, specifically natural organic matter and chloride, can shift reactive species from sulfate radicals to hydroxyl radicals and reactive chlorine species in both synthetic and actual water matrices. Such shifts in reactive species might be easily overlooked when conducting laboratory or pilot-scale experiments in only one water matrix. The effects of the water matrix on the formation of reactive species should be studied and well understood for the intended specific applications as the composition of water can vary considerably among different raw and treated waters. Future studies should combine the evaluation of the degradation efficiency of the actual target pollutants with studies of the major reactive species, which may also help to assess the reactivity of organic contaminants and the formation of by-products or transformation intermediates[121].

5.2 Production of redox-active biochars for persulfate activation and water treatment

Biochar engineering is attracting increasing interest as it allows to harness and optimize favorable features of biochar and to enhance its efficiency through tailoring specific biochar properties for target applications[69,188,264,265]. As highlighted in Chapter 3, the redox-active properties of biochars, governed by surface oxygen functional

groups and persistent free radicals (PFRs), are particularly important for biochar-mediated persulfate activation in the presence of Fe(III) at low pH. Biochars produced at low pyrolysis temperature were most suitable for Fe(III) reduction and persulfate activation in the biochar/Fe(III)/PDS system due to high amounts of surface oxygen functional groups and PFRs. Chapter 3 also shows that ash amendments during the pyrolysis of feedstock material can increase the electron donating capacity of the biochars, resulting in improved performance of the biochar/Fe(III)/persulfate system. Future systematic research is needed to determine the optimal amount of ash that should be added to different feedstocks under specific pyrolysis conditions to produce biochars with optimized performance for the targeted applications.

Apart from ash amendments, there are also other opportunities for improving and tailoring the redox properties of biochars. For instance, to manipulate the persistent free radicals in biochar, Fang et al., 2015 reported that loading biomass with metals (Fe^{3+}, Cu^{2+}, Ni^{2+}, or Zn^{2+}) and phenolic compounds (hydroquinone, catechol, and phenol) not only increased the concentrations of PFRs in biochar, but also changed the types of PFRs formed in biochar, which improved the persulfate activation for the elimination of pollutants[69]. Many in-situ and ex-situ oxidation treatments (e.g. air oxidation, plasma oxidation) in the pyrolysis and post pyrolysis procedure have also been applied successfully to tune biochar oxygen functional groups[266–270]. However, there is a lack of standard procedures for the production of engineered biochars, particularly for application in oxidative water treatment. Additional research is needed to comprehensively understand the critical parameters in biochar production, which will facilitate the refinement and implementation of standardized procedures.

Future studies should also focus on the interrelation of the biochar properties and the formation of reactive species in persulfate-based oxidation processes. Chapter 2 provides an in-depth discussion on the formation of reactive species in the biochar/Fe(III)/persulfate system by using one biochar produced from beech wood at 450°C. Chapter 3 investigates the impact of biochar pyrolysis temperature as well as ash amendments during pyrolysis on the biochar performance in terms of DEET removal in the biochar/Fe(III)/persulfate system. Future experiments are needed to

assess the impact of biochar pyrolysis conditions and the resulting biochar properties on the formation of reactive species in biochar-mediated persulfate-based oxidation processes.

The majority of the biochars used in this dissertation (i.e., all beech wood biochars and all softwood sawdust biochars) were only able to activate persulfate in the presence of Fe(III), which limits the applicability of the oxidation process to low pH values (Chapter 2 and 3). In contrast, one biochar produced from shrimp shells could directly activate persulfate without Fe(III) at circumneutral pH (Chapter 4). While radical species were the major reactive species when employing beech wood in the biochar/Fe(III)/persulfate system at pH 2.5, non-radical species (likely singlet oxygen) were formed from persulfate in the presence of the shrimp shell biochar. The controlling factors that determine whether or not a particular biochar can activate persulfate in the absence or presence of Fe(III) remain to be studied together with the impact of the biochar characteristics on reactive species formation. Once these controlling factors are identified and understood, certain biochar characteristics may serve as indicator to explain and potentially predict the performance of biochars for persulfate activation and organic contaminant removal from water.

5.3 Roadmap for field application of the biochar/persulfate system for organic contaminant removal from water

Biochars that can activate persulfate in the presence of iron under acidic conditions may be applied to improve the performance of so called persulfate-based Fenton-like oxidation processes. Persulfate-based Fenton-like processes have attracted much attention for the treatment of industrial wastewaters containing a mixture of pollutants in a wide range of concentrations[107–109]. However, the reduction of Fe(III) to Fe(II) is the limiting step for persulfate activation. In this case, Fe(III) has to be dissolved, which results in the operation of the biochar/Fe(III)/persulfate system being limited to low pH values (Chapter 2 and 3). Efforts have been made to use chelated Fe(III) as a possible solution for operation at neutral pH values, by using chelating agents such as

ethylenediaminetetraacetic acid (EDTA)[271], nitrilotriacetic acid[272], or citrate[273]. However, especially the addition of EDTA or nitrilotriacetic acid is undesirable in water treatment operations because it might induce secondary pollution causing risks to the water resouces[274].

For in situ chemical oxidation, it was found that persulfate can also be activated by subsurface minerals at environmentally relevant pH values[275–277]. However, the rate of persulfate decomposition by naturally occurring minerals such as iron or manganese oxides is slow[275–277]. Here, redox-active biochar might be a suitable addition to promote the reduction of Fe(III) or Mn minerals to their reduced form of Fe(II) or Mn(II) minerals[63], which can efficiently activate persulfate for contaminant degradation[278,279]. Future research should test different minerals, especially Fe(III)-containing minerals such as ferrihydrite or hematite, for the activation of persulfate in the presence of biochar.

For biochars that can directly activate persulfate such as the shrimp shell biochar used in Chapter 4, this dissertation demonstrates that the combination of biochar and persulfate can enhance the removal of dissolved organic contaminants from urban stormwater. However, the oxidation process was selective towards electrophilic compounds like anilines, aromatic amines, and phenols, which is likely due to the formation of singlet oxygen as major reactive species. Yet, the combination of biochar and persulfate bears promise to enhance the removal of a variety of persistent and mobile organic contaminants from water through adsorption and oxidation. The use of biochar and persulfate seems particularly suited for upgrading conventional, decentralized stormwater treatment systems such as biofilters, which can otherwise not remove many dissolved organic contaminants from urban stormwater[9,10]. Future studies should investigate the transformation of a broader range of organic contaminants during water treatment with biochar and persulfate under different treatment conditions using e.g., column experiments to mimic biochar and persulfate-amended biofilters with different flow rates. For organic compounds that are not reactive in the biochar/persulfate system, alternative adsorbent/oxidant systems should be investigated using e.g., hydrogen peroxide, which can also be activated by

biochars, whereby non-selective •OH may lead to a wider spectrum of compounds being removed[280–283].

While this dissertation is based on laboratory bench-scale experiments to gain insights into fundamentals such as formation of reactive species and effects of water matrix in the biochar/persulfate system with and without iron, future research is needed to assess the feasibility and applicability of these oxidation processes at full-scale and in the field. One factor relevant to field-scale applications of persulfate-based oxidation processes is the formation of large amounts of sulfate (SO_4^{2-}), which may cause changes in water composition and pH of the treated water[30]. Such effects of the oxidation process on the overall water quality should be monitored and controlled. In the biochar/Fe(III)/persulfate system, one mole SO_4^{2-} is formed with one mole of decomposed $S_2O_8^{2-}$ (Equation 5.1, chapter 2 and 3), while in the biochar/persulfate system, one mole of $S_2O_8^{2-}$ forms two moles of SO_4^{2-} (Equation 5.2, chapter 4). The concentrations of $S_2O_8^{2-}$ applied in the batch experiments in this dissertation were in the millimolar range, which, depending on the targeted application, might be rather high. Future experiments should focus on optimizing the persulfate concentrations employed to achieve optimal treatment performance, while at the same time controlling and minimizing SO_4^{2-} concentrations released.

$$Fe(II) + S_2O_8^{2-} \rightarrow SO_4^{\bullet-} + Fe(III) + SO_4^{2-} \quad (5.1)$$

$$2\ S_2O_8^{2-} + 4\ OH^- \rightarrow {}^1O_2 + 4\ SO_4^{2-} + 2\ H_2O \text{ (mediated by biochar)} \quad (5.2)$$

Furthermore, it is crucial to investigate the effects of real water matrices on the formation of reactive species, given that different types of reactive species react differently with water constituents and target contaminants. Certain water matrix components in water may induce a transformation and shift of reactive species (for example chloride as described in Chapter 3), while others may hamper the treatment efficiency by reacting with and consuming reactive species (such as natural organic matter)[30,31]. Building on such detailed process understanding, oxidation processes combining biochar and persulfate could be employed to treat a wide range of water types.

Bibliography

1. Medema, G. J. et al. Safe drinking water: an ongoing challenge. Assessing Microbial Safety of Drinking Water 11 (2003).
2. Pal, A., He, Y., Jekel, M., Reinhard, M. & Gin, K. Y.-H. Emerging contaminants of public health significance as water quality indicator compounds in the urban water cycle. Environment International 71, 46–62 (2014).
3. McGrane, S. J. Impacts of urbanisation on hydrological and water quality dynamics, and urban water management: a review. Hydrological Sciences Journal 61, 2295–2311 (2016).
4. Wang, Z., Walker, G. W., Muir, D. C. & Nagatani-Yoshida, K. Toward a global understanding of chemical pollution: a first comprehensive analysis of national and regional chemical inventories. Environmental Science & Technology 54, 2575–2584 (2020).
5. Tran, N. H., Reinhard, M. & Gin, K. Y.-H. Occurrence and fate of emerging contaminants in municipal wastewater treatment plants from different geographical regions-a review. Water Research 133, 182–207 (2018).
6. Tijani, J. O., Fatoba, O. O. & Petrik, L. F. A review of pharmaceuticals and endocrine-disrupting compounds: sources, effects, removal, and detections. Water, Air, & Soil Pollution 224, 1–29 (2013).
7. Morin-Crini, N. et al. Emerging contaminants: analysis, aquatic compartments and water pollution. Emerging Contaminants Vol. 1: Occurrence and Impact 1–111 (2021).
8. Chaturvedi, M. et al. Emerging contaminants in wastewater: sources of contamination, toxicity, and removal approaches. Emerging Treatment Technologies for Waste Management 103–132 (2021).
9. Mutzner, L., Zhang, K., Luthy, R. G., Arp, H. P. H. & Spahr, S. Urban stormwater capture for water supply: look out for persistent, mobile and toxic substances. Environmental Science: Water Research & Technology 9, 3094–3102 (2023).
10. Spahr, S., Teixidó, M., Sedlak, D. L. & Luthy, R. G. Hydrophilic trace organic contaminants in urban stormwater: occurrence, toxicological relevance, and the need to enhance green stormwater infrastructure. Environmental Science: Water Research & Technology 6, 15–44 (2020).
11. LeFevre, G. H. et al. Review of dissolved pollutants in urban storm water and their removal and fate in bioretention cells. Journal of Environmental Engineering 141, 04014050 (2015).

12. Geyer, H. J. et al. Bioaccumulation and occurrence of endocrine-disrupting chemicals (EDCs), persistent organic pollutants (POPs), and other organic compounds in fish and other organisms including humans. Bioaccumulation – New Aspects and Developments 1–166 (2000).
13. Bernardes, M. F. F., Pazin, M., Pereira, L. C. & Dorta, D. J. Impact of pesticides on environmental and human health. Toxicology Studies-cells, Drugs and Environment 195–233 (2015).
14. Mezzelani, M., Gorbi, S. & Regoli, F. Pharmaceuticals in the aquatic environments: evidence of emerged threat and future challenges for marine organisms. Marine Environmental Research 140, 41–60 (2018).
15. Vystavna, Y. et al. Multi-tracing of recharge seasonality and contamination in groundwater: A tool for urban water resource management. Water Research 161, 413–422 (2019).
16. Cosgrove, W. J. & Loucks, D. P. Water management: Current and future challenges and research directions. Water Resources Research 51, 4823–4839 (2015).
17. Horne, A. C. et al. Research priorities to improve future environmental water outcomes. Frontiers in Environmental Science 5, 89 (2017).
18. Michael-Kordatou, I. et al. Dissolved effluent organic matter: characteristics and potential implications in wastewater treatment and reuse applications. Water Research 77, 213–248 (2015).
19. Shahid, M. K., Kashif, A., Fuwad, A. & Choi, Y. Current advances in treatment technologies for removal of emerging contaminants from water – A critical review. Coordination Chemistry Reviews 442, 213993 (2021).
20. Khanzada, N. K. et al. Removal of organic micropollutants using advanced membrane-based water and wastewater treatment: A review. Journal of Membrane Science 598, 117672 (2020).
21. Chen, G. Electrochemical technologies in wastewater treatment. Separation and Purification Technology 38, 11–41 (2004).
22. Margot, J. et al. Treatment of micropollutants in municipal wastewater: ozone or powdered activated carbon? Science of the Total Environment 461, 480–498 (2013).
23. Stalter, D., Magdeburg, A., Wagner, M. & Oehlmann, J. Ozonation and activated carbon treatment of sewage effluents: Removal of endocrine activity and cytotoxicity. Water Research 45, 1015–1024 (2011).
24. Cheng, N. et al. Adsorption of emerging contaminants from water and wastewater by modified biochar: A review. Environmental Pollution 273, 116448 (2021).
25. Jagadeesh, N. & Sundaram, B. Adsorption of pollutants from wastewater by biochar: a review. Journal of Hazardous Materials Advances 9, 100226 (2023).

26. Ambaye, T., Vaccari, M., van Hullebusch, E. D., Amrane, A. & Rtimi, S. Mechanisms and adsorption capacities of biochar for the removal of organic and inorganic pollutants from industrial wastewater. International Journal of Environmental Science and Technology 1–22 (2021).
27. Deng, Y. & Zhao, R. Advanced oxidation processes (AOPs) in wastewater treatment. Current Pollution Reports 1, 167–176 (2015).
28. Parsons, S. Advanced Oxidation Processes for Water and Wastewater Treatment. (IWA publishing, 2004).
29. O'Shea, K. E. & Dionysiou, D. D. Advanced oxidation processes for water treatment. The Journal of Physical Chemistry Letters 3, 2112–2113 (2012).
30. Lee, J., Von Gunten, U. & Kim, J.-H. Persulfate-based advanced oxidation: critical assessment of opportunities and roadblocks. Environmental Science & Technology 54, 3064–3081 (2020).
31. McGachy, L. & Sedlak, D. L. From Theory to Practice: Leveraging Chemical Principles To Improve the Performance of Peroxydisulfate-Based In Situ Chemical Oxidation of Organic Contaminants. Environmental Science & Technology (2023).
32. Giannakis, S., Lin, K.-Y. A. & Ghanbari, F. A review of the recent advances on the treatment of industrial wastewaters by Sulfate Radical-based Advanced Oxidation Processes (SR-AOPs). Chemical Engineering Journal 406, 127083 (2021).
33. Guerra-Rodríguez, S., Rodríguez, E., Singh, D. N. & Rodríguez-Chueca, J. Assessment of sulfate radical-based advanced oxidation processes for water and wastewater treatment: a review. Water 10, 1828 (2018).
34. Li, N. et al. Thermal activation of persulfates for organic wastewater purification: Heating modes, mechanism and influencing factors. Chemical Engineering Journal 450, 137976 (2022).
35. Wu, Z., Gong, S., Liu, J., Shi, J. & Deng, H. Progress and problems of water treatment based on UV/persulfate oxidation process for degradation of emerging contaminants: A review. Journal of Water Process Engineering 58, 104870 (2024).
36. Guo, J. et al. Insight into sludge dewatering by advanced oxidation using persulfate as oxidant and Fe^{2+} as activator: performance, mechanism and extracellular polymers and heavy metals behaviors. Journal of Environmental Management 288, 112476 (2021).
37. Ma, Y. et al. Comparative study of Fe^{2+}/H_2O_2 and Fe^{2+}/persulfate systems on the pre-treatment process of real pharmaceutical wastewater. Water Science & Technology 89, 811–822 (2024).
38. Rehman, F. et al. The Catalytic Degradation of the Inflammatory Drug Diclofenac Sodium in Water by Fe^{2+}/Persulfate, Fe^{2+}/Peroxymonosulfate and Fe^{2+}/H_2O_2 Processes: A Comparative Analysis. Water 15, 885 (2023).

39. Cha, J. S. et al. Production and utilization of biochar: A review. Journal of Industrial and Engineering Chemistry 40, 1–15 (2016).
40. Weber, K. & Quicker, P. Properties of biochar. Fuel 217, 240–261 (2018).
41. Brown, R. Biochar production technology. Biochar for Environmental Management 159–178 (2012).
42. Kwapinski, W. et al. Biochar from biomass and waste. Waste and Biomass Valorization 1, 177–189 (2010).
43. Sohi, S., Lopez-Capel, E., Krull, E. & Bol, R. Biochar, climate change and soil: A review to guide future research. CSIRO land and water science report 5, 17–31 (2009).
44. Enaime, G. & Lübken, M. Agricultural waste-based biochar for agronomic applications. Applied Sciences 11, 8914 (2021).
45. Wani, I., Ramola, S., Garg, A. & Kushvaha, V. Critical review of biochar applications in geoengineering infrastructure: moving beyond agricultural and environmental perspectives. Biomass Conversion and Biorefinery 1–29 (2021).
46. Yang, G.-X. & Jiang, H. Amino modification of biochar for enhanced adsorption of copper ions from synthetic wastewater. Water Research 48, 396–405 (2014).
47. Shimabuku, K. K. et al. Biochar sorbents for sulfamethoxazole removal from surface water, stormwater, and wastewater effluent. Water Research 96, 236–245 (2016).
48. Chen, H., Xie, A. & You, S. A review: advances on absorption of heavy metals in the waste water by biochar. Materials Science and Engineering in vol. 301 012160 (IOP Publishing, 2018).
49. Ashoori, N. et al. Evaluation of pilot-scale biochar-amended woodchip bioreactors to remove nitrate, metals, and trace organic contaminants from urban stormwater runoff. Water Research 154, 1–11 (2019).
50. Lu, L. & Chen, B. Enhanced bisphenol A removal from stormwater in biochar-amended biofilters: Combined with batch sorption and fixed-bed column studies. Environmental Pollution 243, 1539–1549 (2018).
51. Ulrich, B. A., Im, E. A., Werner, D. & Higgins, C. P. Biochar and activated carbon for enhanced trace organic contaminant retention in stormwater infiltration systems. Environmental Science & Technology 49, 6222–6230 (2015).
52. He, M. et al. Waste-derived biochar for water pollution control and sustainable development. Nature Reviews Earth & Environment 3, 444–460 (2022).
53. Hagemann, N. et al. Wood-based activated biochar to eliminate organic micropollutants from biologically treated wastewater. Science of the Total Environment 730, 138417 (2020).

54. Jha, S., Gaur, R., Shahabuddin, S. & Tyagi, I. Biochar as sustainable alternative and green adsorbent for the remediation of noxious pollutants: a comprehensive review. Toxics 11, 117 (2023).
55. Yang, Y. et al. Nonmetal function groups of biochar for pollutants removal: a review. Journal of Hazardous Materials Advances 100171 (2022).
56. Keiluweit, M., Nico, P. S., Johnson, M. G. & Kleber, M. Dynamic molecular structure of plant biomass-derived black carbon (biochar). Environmental Science & Technology 44, 1247–1253 (2010).
57. Prévoteau, A., Ronsse, F., Cid, I., Boeckx, P. & Rabaey, K. The electron donating capacity of biochar is dramatically underestimated. Scientific Reports 6, 32870 (2016).
58. Klüpfel, L., Keiluweit, M., Kleber, M. & Sander, M. Redox properties of plant biomass-derived black carbon (biochar). Environmental Science & Technology 48, 5601–5611 (2014).
59. Oh, S.-Y., Son, J.-G., Lim, O.-T. & Chiu, P. C. The role of black carbon as a catalyst for environmental redox transformation. Environmental Geochemistry and Health 34, 105–113 (2012).
60. Yuan, Y. et al. Applications of biochar in redox-mediated reactions. Bioresource Technology 246, 271–281 (2017).
61. Harter, J. et al. Linking N_2O emissions from biochar-amended soil to the structure and function of the N-cycling microbial community. The ISME Journal 8, 660–674 (2014).
62. Xu, S. et al. Biochar-facilitated microbial reduction of hematite. Environmental Science & Technology 50, 2389–2395 (2016).
63. Kappler, A. et al. Biochar as an electron shuttle between bacteria and Fe (III) minerals. Environmental Science & Technology Letters 1, 339–344 (2014).
64. Zhou, L. et al. Stimulation of pyrolytic carbon materials as electron shuttles on the anaerobic transformation of recalcitrant organic pollutants: A review. Science of the Total Environment 801, 149696 (2021).
65. Dorner, M., Lokesh, S., Yang, Y. & Behrens, S. Biochar-mediated abiotic and biotic degradation of halogenated organic contaminants–A review. Science of the Total Environment 852, 158381 (2022).
66. Oh, S., Son, J. & Chiu, P. C. Biochar‐mediated reductive transformation of nitro herbicides and explosives. Environmental Toxicology and Chemistry 32, 501‐508 (2013).
67. Ruan, X. et al. Formation, characteristics, and applications of environmentally persistent free radicals in biochars: a review. Bioresource technology 281, 457–468 (2019).

68. Luo, K. et al. A critical review on the application of biochar in environmental pollution remediation: Role of persistent free radicals (PFRs). Journal of Environmental Sciences 108, 201–216 (2021).
69. Fang, G., Liu, C., Gao, J., Dionysiou, D. D. & Zhou, D. Manipulation of persistent free radicals in biochar to activate persulfate for contaminant degradation. Environmental Science & Technology 49, 5645–5653 (2015).
70. Deng, R., Luo, H., Huang, D. & Zhang, C. Biochar-mediated Fenton-like reaction for the degradation of sulfamethazine: Role of environmentally persistent free radicals. Chemosphere 255, 126975 (2020).
71. Tomczyk, A., Sokołowska, Z. & Boguta, P. Biochar physicochemical properties: pyrolysis temperature and feedstock kind effects. Reviews in Environmental Science and Bio/Technology 19, 191–215 (2020).
72. Jayakumar, M. et al. Comprehensive review on lignocellulosic biomass derived biochar production, characterization, utilization and applications. Chemosphere 140515 (2023).
73. Venkatachalam, C. D., Sekar, S., Sengottian, M., Ravichandran, S. R. & Bhuvaneshwaran, P. A critical review of the production, activation, and morphological characteristic study on functionalized biochar. Journal of Energy Storage 67, 107525 (2023).
74. Schlederer, F., Martín-Hernández, E. & Vaneeckhaute, C. Micropollutants in biochar produced from sewage sludge: A systematic review on the impact of pyrolysis operating conditions. Waste Management 174, 618–629 (2024).
75. Xu, Z., Xu, X., Zhang, Y., Yu, Y. & Cao, X. Pyrolysis-temperature depended electron donating and mediating mechanisms of biochar for Cr (VI) reduction. Journal of Hazardous Materials 388, 121794 (2020).
76. Shen, Y. et al. Role of redox-active biochar with distinctive electrochemical properties to promote methane production in anaerobic digestion of waste activated sludge. Journal of Cleaner Production 278, 123212 (2021).
77. Wacławek, S. et al. Chemistry of persulfates in water and wastewater treatment: A review. Chemical Engineering Journal 330, 44–62 (2017).
78. Wang, J. & Wang, S. Activation of persulfate (PS) and peroxymonosulfate (PMS) and application for the degradation of emerging contaminants. Chemical Engineering Journal 334, 1502–1517 (2018).
79. Oh, W.-D., Dong, Z. & Lim, T.-T. Generation of sulfate radical through heterogeneous catalysis for organic contaminants removal: current development, challenges and prospects. Applied Catalysis B: Environmental 194, 169–201 (2016).

80. Khan, Z. U. H. et al. Removal of organic pollutants through hydroxyl radical-based advanced oxidation processes. Ecotoxicology and Environmental Safety 267, 115564 (2023).
81. Scaria, J. & Nidheesh, P. V. Comparison of hydroxyl-radical-based advanced oxidation processes with sulfate radical-based advanced oxidation processes. Current Opinion in Chemical Engineering 36, 100830 (2022).
82. Zhang, B.-T., Zhang, Y., Teng, Y. & Fan, M. Sulfate radical and its application in decontamination technologies. Critical Reviews in Environmental Science and Technology 45, 1756–1800 (2015).
83. Gao, Y., Gao, N., Deng, Y., Yang, Y. & Ma, Y. Ultraviolet (UV) light-activated persulfate oxidation of sulfamethazine in water. Chemical Engineering Journal 195, 248–253 (2012).
84. Pirsaheb, M., Hossaini, H. & Janjani, H. An overview on ultraviolet persulfate based advances oxidation process for removal of antibiotics from aqueous solutions: A systematic review. Water Treat 165, 382–395 (2019).
85. Arvaniti, O. S., Ioannidi, A. A., Mantzavinos, D. & Frontistis, Z. Heat-activated persulfate for the degradation of micropollutants in water: A comprehensive review and future perspectives. Journal of Environmental Management 318, 115568 (2022).
86. Anipsitakis, G. P. & Dionysiou, D. D. Radical generation by the interaction of transition metals with common oxidants. Environmental Science & Technology 38, 3705–3712 (2004).
87. Ling, S. K., Wang, S. & Peng, Y. Oxidative degradation of dyes in water using Co^{2+}/H_2O_2 and Co^{2+}/peroxymonosulfate. Journal of Hazardous Materials 178, 385–389 (2010).
88. Wang, C., Huang, R., Sun, R., Yang, J. & Sillanpää, M. A review on persulfates activation by functional biochar for organic contaminants removal: Synthesis, characterizations, radical determination, and mechanism. Journal of Environmental Chemical Engineering 9, 106267 (2021).
89. Li, F., Duan, F., Ji, W. & Gui, X. Biochar-activated persulfate for organic contaminants removal: Efficiency, mechanisms and influencing factors. Ecotoxicology and Environmental Safety 198, 110653 (2020).
90. Wang, J. & Wang, S. Reactive species in advanced oxidation processes: Formation, identification and reaction mechanism. Chemical Engineering Journal 401, 126158 (2020).
91. Hayat, W., Zhang, Y., Hussain, I., Huang, S. & Du, X. Comparison of radical and non-radical activated persulfate systems for the degradation of imidacloprid in water. Ecotoxicology and Environmental Safety 188, 109891 (2020).

92. Peng, W. et al. Non-radical reactions in persulfate-based homogeneous degradation processes: A review. Chemical Engineering Journal 421, 127818 (2021).
93. Xiao, R. et al. Activation of peroxymonosulfate/persulfate by nanomaterials for sulfate radical-based advanced oxidation technologies. Current Opinion in Chemical Engineering 19, 51–58 (2018).
94. Fang, G., Gao, J., Dionysiou, D. D., Liu, C. & Zhou, D. Activation of persulfate by quinones: free radical reactions and implication for the degradation of PCBs. Environmental Science & Technology 47, 4605–4611 (2013).
95. Criquet, J. & Leitner, N. K. V. Degradation of acetic acid with sulfate radical generated by persulfate ions photolysis. Chemosphere 77, 194–200 (2009).
96. Yao, C., Zhang, Y., Du, M., Du, X. & Huang, S. Insights into the mechanism of non-radical activation of persulfate via activated carbon for the degradation of p-chloroaniline. Chemical Engineering Journal 362, 262–268 (2019).
97. Cui, Q., Zhang, W., Chai, S., Zuo, Q. & Kim, K.-H. The potential of green biochar generated from biogas residue as a heterogeneous persulfate activator and its non-radical degradation pathways: Adsorption and degradation of tetracycline. Environmental Research 204, 112335 (2022).
98. Liu, Z. et al. Singlet oxygen in biochar-based catalysts-activated persulfate process: From generation to detection and selectivity removing emerging contaminants. Chemical Engineering Journal 149724 (2024).
99. Cheng, X., Guo, H., Zhang, Y., Wu, X. & Liu, Y. Non-photochemical production of singlet oxygen via activation of persulfate by carbon nanotubes. Water Research 113, 80–88 (2017).
100. Zhu, S., Jin, C., Duan, X., Wang, S. & Ho, S.-H. Nonradical oxidation in persulfate activation by graphene-like nanosheets (GNS): Differentiating the contributions of singlet oxygen ($^1O_2$) and sorption-dependent electron transfer. Chemical Engineering Journal 393, 124725 (2020).
101. Zhao, Y. et al. Selective degradation of electron-rich organic pollutants induced by CuO@ Biochar: the key role of outer-sphere interaction and singlet oxygen. Environmental Science & Technology 56, 10710–10720 (2022).
102. Wang, Z. et al. Is sulfate radical really generated from peroxydisulfate activated by iron (II) for environmental decontamination? Environmental Science & Technology 52, 11276–11284 (2018).
103. Li, H., Shan, C. & Pan, B. Fe (III)-doped g-C_3N_4 mediated peroxymonosulfate activation for selective degradation of phenolic compounds via high-valent iron-oxo species. Environmental Science & Technology 52, 2197–2205 (2018).

104. Li, H., Shan, C., Li, W. & Pan, B. Peroxymonosulfate activation by iron (III)-tetraamidomacrocyclic ligand for degradation of organic pollutants via high-valent iron-oxo complex. Water Research 147, 233–241 (2018).
105. Ren, W. et al. Origins of electron-transfer regime in persulfate-based nonradical oxidation processes. Environmental Science & Technology 56, 78–97 (2021).
106. Sun, T. et al. Rapid electron transfer by the carbon matrix in natural pyrogenic carbon. Nature Communications 8, 14873 (2017).
107. Bautista, P., Mohedano, A., Casas, J., Zazo, J. & Rodriguez, J. An overview of the application of Fenton oxidation to industrial wastewaters treatment. Journal of Chemical Technology & Biotechnology: International Research in Process, Environmental & Clean Technology 83, 1323–1338 (2008).
108. Matavos-Aramyan, S. & Moussavi, M. Advances in Fenton and Fenton based oxidation processes for industrial effluent contaminants control-a review. International Journal of Environmental Sciences & Natural Resources 2, 1–18 (2017).
109. Gamarra-Güere, C. D., Dionisio, D., Santos, G. O. S., Lanza, M. R. V. & de Jesus Motheo, A. Application of Fenton, photo-Fenton and electro-Fenton processes for the methylparaben degradation: A comparative study. Journal of Environmental Chemical Engineering 10, 106992 (2022).
110. Zhao, L., Hou, H., Fujii, A., Hosomi, M. & Li, F. Degradation of 1, 4-dioxane in water with heat-and Fe^{2+}-activated persulfate oxidation. Environmental Science and Pollution Research 21, 7457–7465 (2014).
111. Wang, S. et al. Removal of acetaminophen in the Fe^{2+}/persulfate system: kinetic model and degradation pathways. Chemical Engineering Journal 358, 1091–1100 (2019).
112. Luo, H., Zeng, Y., He, D. & Pan, X. Application of iron-based materials in heterogeneous advanced oxidation processes for wastewater treatment: A review. Chemical Engineering Journal 407, 127191 (2021).
113. Liang, J. et al. Biomass-derived pyrolytic carbons accelerated Fe(III)/Fe(II) redox cycle for persulfate activation: Pyrolysis temperature-depended performance and mechanisms. Applied Catalysis B: Environmental 297, 120446 (2021).
114. Tang, Y., Dou, J., Lu, Z., Xu, J. & He, Y. Accelerating Fe^{2+}/Fe^{3+} cycle via biochar to improve catalytic degradation efficiency of the Fe^{3+}/persulfate oxidation. Environmental Pollution 316, 120669 (2023).
115. Wang, H. et al. Biochar-induced Fe(III) reduction for persulfate activation in sulfamethoxazole degradation: Insight into the electron transfer, radical oxidation and degradation pathways. Chemical Engineering Journal 362, 561–569 (2019).

116. Zeng, L. et al. Dual roles of biochar redox property in mediating 2, 4-dichlorophenol degradation in the presence of Fe^{3+} and persulfate. Chemosphere 279, 130456 (2021).
117. Li, S. et al. State-of-the-Art on the Sulfate Radical-Advanced Oxidation Coupled with Nanomaterials: Biological and Environmental Applications. Journal of Functional Biomaterials 13, 227 (2022).
118. Davies, M. J. Detection and characterisation of radicals using electron paramagnetic resonance (EPR) spin trapping and related methods. Methods 109, 21–30 (2016).
119. Buxton, G. V., Greenstock, C. L., Helman, W. P. & Ross, A. B. Critical review of rate constants for reactions of hydrated electrons, hydrogen atoms and hydroxyl radicals (•OH/•O−) in aqueous solution. Journal of Physical and Chemical Reference Data 17, 513–886 (1988).
120. Neta, P., Madhavan, V., Zemel, H. & Fessenden, R. W. Rate constants and mechanism of reaction of sulfate radical anion with aromatic compounds. Journal of the American Chemical Society 99, 163–164 (1977).
121. Hübner, U.; Spahr, S.; Lutze, H.; Wieland, A.; Rüting, S.; Gernjak, W.; Wenk, J. Emerging Advanced Oxidation Processes for Water and Wastewater Treatment–Guidance for Systematic Future Research. Preprint on Earth ArXiv, 2022. DOI: https://doi.org/10.31223/X5MH05.
122. Lei, Y. et al. Assessing the Use of Probes and Quenchers for Understanding the Reactive Species in Advanced Oxidation Processes. Environmental Science & Technology 57, 5433–5444 (2023).
123. Chen, Y., Miller, C. J., Xie, J. & Waite, T. D. Challenges Relating to the Quantification of Ferryl (IV) Ion and Hydroxyl Radical Generation Rates Using Methyl Phenyl Sulfoxide (PMSO), Phthalhydrazide, and Benzoic Acid as Probe Compounds in the Homogeneous Fenton Reaction. Environmental Science & Technology (2023).
124. Kemmou, L., Frontistis, Z., Vakros, J., Manariotis, I. D. & Mantzavinos, D. Degradation of antibiotic sulfamethoxazole by biochar-activated persulfate: factors affecting the activation and degradation processes. Catalysis Today 313, 128–133 (2018).
125. Zhang, Y., Xu, X., Cao, L., Ok, Y. S. & Cao, X. Characterization and quantification of electron donating capacity and its structure dependence in biochar derived from three waste biomasses. Chemosphere 211, 1073–1081 (2018).
126. Pitman, R. M. Wood ash use in forestry – a review of the environmental impacts. Forestry 79, 563–588 (2006).

127. Cairns, S. et al. Wood ash amended biochar for the removal of lead, copper, zinc and cadmium from aqueous solution. Environmental Technology & Innovation 24, 101961 (2021).
128. Wu, W. et al. Combustion ash addition promotes the production of K-enriched biochar and K release characteristics. Journal of Cleaner Production 311, 127557 (2021).
129. Grafmüller, J. et al. Wood Ash as an Additive in Biomass Pyrolysis: Effects on Biochar Yield, Properties, and Agricultural Performance. ACS Sustainable Chemistry & Engineering 10, 2720–2729 (2022).
130. Zhao, C. et al. Activation of peroxymonosulfate by biochar-based catalysts and applications in the degradation of organic contaminants: A review. Chemical Engineering Journal 416, 128829 (2021).
131. Liu, T. et al. Applications and influencing factors of the biochar-persulfate based advanced oxidation processes for the remediation of groundwater and soil contaminated with organic compounds. Science of the Total Environment 836, 155421 (2022).
132. Pan, X., Gu, Z., Chen, W. & Li, Q. Preparation of biochar and biochar composites and their application in a Fenton-like process for wastewater decontamination: A review. Science of the Total Environment 754, 142104 (2021).
133. Tian, K. et al. Recent advances in persulfate-based advanced oxidation processes for organic wastewater treatment. Chinese Chemical Letters 33, 4461–4477 (2022).
134. Kang, Z. et al. A Review on Application of Biochar in the Removal of Pharmaceutical Pollutants through Adsorption and Persulfate-Based AOPs. Sustainability 14, (2022).
135. Rauert, C. et al. Concentrations of tire additive chemicals and tire road wear particles in an Australian urban tributary. Environmental Science & Technology 56, 2421–2431 (2022).
136. McFarland, A. R., Larsen, L., Yeshitela, K., Engida, A. N. & Love, N. G. Guide for using green infrastructure in urban environments for stormwater management. Environmental science: Water Research & Technology 5, 643–659 (2019).
137. Blecken, G.-T., Zinger, Y., Deletić, A., Fletcher, T. D. & Viklander, M. Influence of intermittent wetting and drying conditions on heavy metal removal by stormwater biofilters. Water Research 43, 4590–4598 (2009).
138. Jasper, J. T. et al. Unit process wetlands for removal of trace organic contaminants and pathogens from municipal wastewater effluents. Environmental Engineering Science 30, 421–436 (2013).

139. Stiegler, A. N., Cecchetti, A. R., Scholes, R. C. & Sedlak, D. L. Persistent Trace Organic Contaminants Are Transformed Rapidly under Sulfate-and Fe (III)-Reducing Conditions in a Nature-Based Subsurface Water Treatment System. Environmental Science & Technology 57, 16616–16627 (2023).
140. Boehm, A. B. et al. Biochar-augmented biofilters to improve pollutant removal from stormwater–can they improve receiving water quality? Environmental Science: Water Research & Technology 6, 1520–1537 (2020).
141. Matzek, L. W. & Carter, K. E. Activated persulfate for organic chemical degradation: a review. Chemosphere 151, 178–188 (2016).
142. Zhou, Z. et al. Persulfate-based advanced oxidation processes (AOPs) for organic-contaminated soil remediation: A review. Chemical Engineering Journal 372, 836–851 (2019).
143. Lutze, H. V., Kerlin, N. & Schmidt, T. C. Sulfate radical-based water treatment in presence of chloride: Formation of chlorate, inter-conversion of sulfate radicals into hydroxyl radicals and influence of bicarbonate. Water Research 72, 349–360 (2015).
144. Fang, G.-D., Dionysiou, D. D., Wang, Y., Al-Abed, S. R. & Zhou, D.-M. Sulfate radical-based degradation of polychlorinated biphenyls: Effects of chloride ion and reaction kinetics. Journal of Hazardous Materials 227–228, 394–401 (2012).
145. Nie, M. et al. Degradation of chloramphenicol by persulfate activated by Fe^{2+} and zerovalent iron. Chemical Engineering Journal 279, 507–515 (2015).
146. Lu, J., Lu, Q., Di, L., Zhou, Y. & Zhou, Y. Iron-based biochar as efficient persulfate activation catalyst for emerging pollutants removal: A review. Chinese Chemical Letters 108357 (2023).
147. Nosaka, Y. & Nosaka, A. Y. Generation and detection of reactive oxygen species in photocatalysis. Chemical Reviews 117, 11302–11336 (2017).
148. Burns, J. M. et al. Methods for reactive oxygen species (ROS) detection in aqueous environments. Aquatic Sciences 74, 683–734 (2012).
149. Zhou, L., Sleiman, M., Ferronato, C., Chovelon, J.-M. & Richard, C. Reactivity of sulfate radicals with natural organic matters. Environmental Chemistry Letters 15, 733–737 (2017).
150. Rosario-Ortiz, F. L. & Canonica, S. Probe compounds to assess the photochemical activity of dissolved organic matter. Environmental Science & Technology 50, 12532–12547 (2016).
151. Yao, J. et al. Methyl phenyl sulfoxide (PMSO) as a quenching agent for high-valent metal-oxo species in peroxymonosulfate based processes should be reconsidered. Chemical Engineering Journal Advances 12, 100378 (2022).
152. Bennedsen, L. R., Muff, J. & Søgaard, E. G. Influence of chloride and carbonates on the reactivity of activated persulfate. Chemosphere 86, 1092–1097 (2012).

153. Qian, Y. et al. Perfluorooctanoic Acid Degradation Using UV–Persulfate Process: Modeling of the Degradation and Chlorate Formation. Environmental Science & Technology 50, 772–781 (2016).
154. Lutze, H. V. et al. Degradation of chlorotriazine pesticides by sulfate radicals and the influence of organic matter. Environmental Science & Technology 49, 1673–1680 (2015).
155. Stackelberg, P. E. et al. Efficiency of conventional drinking-water-treatment processes in removal of pharmaceuticals and other organic compounds. Science of the Total Environment 377, 255–272 (2007).
156. Costanzo, S., Watkinson, A., Murby, E., Kolpin, D. W. & Sandstrom, M. W. Is there a risk associated with the insect repellent DEET (N, N-diethyl-m-toluamide) commonly found in aquatic environments? Science of the Total Environment 384, 214–220 (2007).
157. Dickenson, E. R. V., Drewes, J. E., Sedlak, D. L., Wert, E. C. & Snyder, S. A. Applying Surrogates and Indicators to Assess Removal Efficiency of Trace Organic Chemicals during Chemical Oxidation of Wastewaters. Environmental Science & Technology 43, 6242–6247 (2009).
158. Pestovsky, O. & Bakac, A. Aqueous ferryl (IV) ion: Kinetics of oxygen atom transfer to substrates and oxo exchange with solvent water. Inorganic chemistry 45, 814–820 (2006).
159. Neta, P., Huie, R. E. & Ross, A. B. Rate constants for reactions of inorganic radicals in aqueous solution. Journal of Physical and Chemical Reference Data 17, 1027–1284 (1988).
160. Dodd, M. C., Buffle, M.-O. & von Gunten, U. Oxidation of Antibacterial Molecules by Aqueous Ozone: Moiety-Specific Reaction Kinetics and Application to Ozone-Based Wastewater Treatment. Environmental Science & Technology 40, 1969–1977 (2006).
161. Yang, B., Liu, H. & Zhang, J. High-valent metals in advanced oxidation processes: A critical review of their identification methods, formation mechanisms, and reactivity performance. Chemical Engineering Journal 460, 141796 (2023).
162. Hou, K. et al. A critical review on the mechanisms of persulfate activation by iron-based materials: Clarifying some ambiguity and controversies. Chemical Engineering Journal 407, 127078 (2021).
163. Yuan, J., Wen, Y., Dionysiou, D. D., Sharma, V. K. & Ma, X. Biochar as a novel carbon-negative electron source and mediator: electron exchange capacity (EEC) and environmentally persistent free radicals (EPFRs): a review. Chemical Engineering Journal 429, 132313 (2022).

164. Pang, S.-Y., Jiang, J. & Ma, J. Oxidation of sulfoxides and arsenic (III) in corrosion of nanoscale zero valent iron by oxygen: evidence against ferryl ions (Fe (IV)) as active intermediates in Fenton reaction. Environmental Science & Technology 45, 307–312 (2011).
165. Von Gunten, U. Ozonation of drinking water: Part II. Disinfection and by-product formation in presence of bromide, iodide or chlorine. Water Research 37, 1469–1487 (2003).
166. Ershov, B. G. Kinetics, mechanism and intermediates of some radiation-induced reactions in aqueous solutions. Russian Chemical Reviews 73, 101–113 (2004).
167. McElroy, W. J. A laser photolysis study of the reaction of SO_4^- with Cl^- and the subsequent decay of chlorine in aqueous solution. Journal of Physical Chemistry 94, 2435–2441 (1990).
168. Lai, X. et al. Formation and transformation of reactive species in the Fe^{2+}/peroxydisulfate/Cl^- system. Journal of Environmental Management 316, 115219 (2022).
169. Willach, S. et al. Degradation of sulfamethoxazole using ozone and chlorine dioxide-Compound-specific stable isotope analysis, transformation product analysis and mechanistic aspects. Water Research 122, 280–289 (2017).
170. Jayson, G., Parsons, B. & Swallow, A. J. Some simple, highly reactive, inorganic chlorine derivatives in aqueous solution. Their formation using pulses of radiation and their role in the mechanism of the Fricke dosimeter. Journal of the Chemical Society, Faraday Transactions 1: Physical Chemistry in Condensed Phases 69, 1597–1607 (1973).
171. Sichel, C., Garcia, C. & Andre, K. Feasibility studies: UV/chlorine advanced oxidation treatment for the removal of emerging contaminants. Water Research 45, 6371–6380 (2011).
172. Nagarajan, V. & Fessenden, R. W. Flash photolysis of transient radicals. 1. X_2^- with X= Cl, Br, I, and SCN. The Journal of Physical Chemistry 89, 2330–2335 (1985).
173. Fang, J., Fu, Y. & Shang, C. The roles of reactive species in micropollutant degradation in the UV/free chlorine system. Environmental Science & Technology 48, 1859–1868 (2014).
174. Li, L. et al. Insights into reactive species generation and organics selective degradation in Fe-based heterogeneous Fenton-like systems: A critical review. Chemical Engineering Journal 454, 140126 (2023).
175. Lian, L. et al. Kinetic study of hydroxyl and sulfate radical-mediated oxidation of pharmaceuticals in wastewater effluents. Environmental Science & Technology 51, 2954–2962 (2017).

176. Schlögl, J. et al. Heavy rainfall following a summer drought stimulates soil redox dynamics and facilitates rapid and deep translocation of glyphosate in floodplain soils. Environmental Science: Processes & Impacts 24, 825–838 (2022).
177. Eurofins Umwelt-Ost. (2023). Conductivity meter Black Gauss I - technical documentation. Zenodo. https://doi.org/10.5281/zenodo.8197758
178. Masiello, C., Gallagher, M., Randerson, J., Deco, R. & Chadwick, O. Evaluating two experimental approaches for measuring ecosystem carbon oxidation state and oxidative ratio. Journal of Geophysical Research: Biogeosciences 113, (2008).
179. Koch, B. P. & Dittmar, T. From mass to structure: An aromaticity index for high‐resolution mass data of natural organic matter. Rapid Communications in Mass Spectrometry 20, 926‐932 (2006).
180. Stookey, L. L. Ferrozine – a new spectrophotometric reagent for iron. Analytical Chemistry 42, 779–781 (1970).
181. Amstaetter, K., Borch, T. & Kappler, A. Influence of humic acid imposed changes of ferrihydrite aggregation on microbial Fe (III) reduction. Geochimica et Cosmochimica Acta 85, 326–341 (2012).
182. Tay, K., Rahman, N. & Bin Abas, M. Chemical oxidation of *N, N*-diethyl-*m*-toluamide by sulfate radical-based oxidation: kinetics and mechanism of degradation. International Journal of Environmental Science and Technology 10, 103–112 (2013).
183. Song, W. et al. Free-radical-induced oxidative and reductive degradation of *N, N*-diethyl-*m*-toluamide (DEET): Kinetic studies and degradation pathway. Water Research 43, 635‐642 (2009).
184. Murphy, J. & Riley, J. P. A modified single solution method for the determination of phosphate in natural waters. Analytica chimica acta 27, 31–36 (1962).
185. Harvey Jr, A. E., Smart, J. A. & Amis, E. S. Simultaneous spectrophotometric determination of iron (II) and total iron with 1, 10-phenanthroline. Analytical Chemistry 27, 26–29 (1955).
186. Huang, D. et al. Nonnegligible role of biomass types and its compositions on the formation of persistent free radicals in biochar: insight into the influences on Fenton-like process. Chemical Engineering Journal 361, 353–363 (2019).
187. Chacón, F. J., Cayuela, M. L., Roig, A. & Sánchez-Monedero, M. A. Understanding, measuring and tuning the electrochemical properties of biochar for environmental applications. Reviews in Environmental Science and Bio/Technology 16, 695–715 (2017).
188. Chacon, F. J., Sanchez-Monedero, M. A., Lezama, L. & Cayuela, M. L. Enhancing biochar redox properties through feedstock selection, metal preloading and post-pyrolysis treatments. Chemical Engineering Journal 395, 125100 (2020).

189. Joseph, S. et al. The electrochemical properties of biochars and how they affect soil redox properties and processes. Agronomy 5, 322–340 (2015).
190. Luo, L., Xu, C., Chen, Z. & Zhang, S. Properties of biomass-derived biochars: Combined effects of operating conditions and biomass types. Bioresource Technology 192, 83–89 (2015).
191. Von Bardeleben, H. et al. Spins and microstructure of hydrogenated amorphous carbon: A multiple frequency electron paramagnetic resonance study. Applied Physics Letters 78, 2843–2845 (2001).
192. Qin, J., Chen, Q., Sun, M., Sun, P. & Shen, G. Pyrolysis temperature-induced changes in the catalytic characteristics of rice husk-derived biochar during 1, 3-dichloropropene degradation. Chemical Engineering Journal 330, 804–812 (2017).
193. Xu, W., Pignatello, J. J. & Mitch, W. A. Role of black carbon electrical conductivity in mediating hexahydro-1, 3, 5-trinitro-1, 3, 5-triazine (RDX) transformation on carbon surfaces by sulfides. Environmental Science & Technology 47, 7129–7136 (2013).
194. Ren, W. et al. The intrinsic nature of persulfate activation and N-doping in carbocatalysis. Environmental Science & Technology 54, 6438–6447 (2020).
195. Dou, J. et al. Neglected but Efficient Electron Utilization Driven by Biochar-Coactivated Phenols and Peroxydisulfate: Polyphenol Accumulation Rather than Mineralization. Environmental Science & Technology 57, 5703–5713 (2023).
196. Buss, W., Jansson, S. & Mašek, O. Unexplored potential of novel biochar-ash composites for use as organo-mineral fertilizers. Journal of Cleaner Production 208, 960–967 (2019).
197. Joseph, S. et al. Shifting paradigms: development of high-efficiency biochar fertilizers based on nano-structures and soluble components. Carbon Management 4, 323–343 (2013).
198. Bradshaw, J. L., Osorio, M., Schmitt, T. G. & Luthy, R. G. System modeling, optimization, and analysis of recycled water and dynamic storm water deliveries to spreading basins for urban groundwater recharge. Water Resources Research 55, 2446–2463 (2019).
199. Luthy, R. G., Sharvelle, S. & Dillon, P. Urban stormwater to enhance water supply. Environmental Science & Technology 53, 5534–5542 (2019)
200. Luthy, R. G. & Sedlak, D. L. Urban water-supply reinvention. Daedalus 144, 72–82 (2015).
201. Liu, J. et al. Water scarcity assessments in the past, present, and future. Earth's Future 5, 545–559 (2017).

202. Fairbairn, D. J. et al. Contaminants of emerging concern in urban stormwater: Spatiotemporal patterns and removal by iron-enhanced sand filters (IESFs). Water Research 145, 332–345 (2018).
203. Gasperi, J. et al. Micropollutants in urban stormwater: occurrence, concentrations, and atmospheric contributions for a wide range of contaminants in three French catchments. Environmental Science and Pollution Research 21, 5267–5281 (2014).
204. Ensminger, M. P., Budd, R., Kelley, K. C. & Goh, K. S. Pesticide occurrence and aquatic benchmark exceedances in urban surface waters and sediments in three urban areas of California, USA, 2008–2011. Environmental Monitoring and Assessment 185, 3697–3710 (2013).
205. Rippy, M. A. et al. Pesticide occurrence and spatio-temporal variability in urban run-off across Australia. Water Research 115, 245–255 (2017).
206. Beckers, L.-M., Busch, W., Krauss, M., Schulze, T. & Brack, W. Characterization and risk assessment of seasonal and weather dynamics in organic pollutant mixtures from discharge of a separate sewer system. Water Research 135, 122–133 (2018).
207. Kloepfer, A., Jekel, M. & Reemtsma, T. Occurrence, sources, and fate of benzothiazoles in municipal wastewater treatment plants. Environmental Science & Technology 39, 3792–3798 (2005).
208. Launay, M. A., Dittmer, U. & Steinmetz, H. Organic micropollutants discharged by combined sewer overflows–characterisation of pollutant sources and stormwater-related processes. Water Research 104, 82–92 (2016).
209. Burant, A., Selbig, W., Furlong, E. T. & Higgins, C. P. Trace organic contaminants in urban runoff: Associations with urban land-use. Environmental Pollution 242, 2068–2077 (2018).
210. Johannessen, C., Helm, P., Lashuk, B., Yargeau, V. & Metcalfe, C. D. The tire wear compounds 6PPD-quinone and 1, 3-diphenylguanidine in an urban watershed. Archives of Environmental Contamination and Toxicology 1–9 (2022).
211. Hou, F. et al. Quantification of organic contaminants in urban stormwater by isotope dilution and liquid chromatography-tandem mass spectrometry. Analytical and Bioanalytical Chemistry 411, 7791–7806 (2019).
212. Zhang, H.-Y. et al. Occurrence and risks of 23 tire additives and their transformation products in an urban water system. Environment International 171, 107715 (2023).
213. Regnery, J. & Püttmann, W. Seasonal fluctuations of organophosphate concentrations in precipitation and storm water runoff. Chemosphere 78, 958–964 (2010).

214. Wiest, L. et al. Priority substances in accumulated sediments in a stormwater detention basin from an industrial area. Environmental Pollution 243, 1669–1678 (2018).
215. Becouze-Lareure, C., Dembélé, A., Coquery, M., Cren-Olivé, C. & Bertrand-Krajewski, J.-L. Assessment of 34 dissolved and particulate organic and metallic micropollutants discharged at the outlet of two contrasted urban catchments. Science of the Total Environment 651, 1810–1818 (2019).
216. Sébastian, C., Barraud, S., Gonzalez-Merchan, C., Perrodin, Y. & Visiedo, R. Stormwater retention basin efficiency regarding micropollutant loads and ecotoxicity. Water Science & Technology 69, 974–981 (2014).
217. Premarathna, K. et al. Biofilters and bioretention systems: the role of biochar in the blue-green city concept for stormwater management. Environmental Science: Water Research & Technology 9, 3103–3119 (2023).
218. Gwenzi, W., Chaukura, N., Noubactep, C. & Mukome, F. N. Biochar-based water treatment systems as a potential low-cost and sustainable technology for clean water provision. Journal of Environmental Management 197, 732–749 (2017).
219. Qambrani, N. A., Rahman, M. M., Won, S., Shim, S. & Ra, C. Biochar properties and eco-friendly applications for climate change mitigation, waste management, and wastewater treatment: A review. Renewable and Sustainable Energy Reviews 79, 255–273 (2017).
220. Miklos, D. B. et al. Evaluation of advanced oxidation processes for water and wastewater treatment–A critical review. Water Research 139, 118–131 (2018).
221. Oturan, M. A. & Aaron, J.-J. Advanced oxidation processes in water/wastewater treatment: principles and applications. A review. Critical Reviews in Environmental Science &Technology 44, 2577–2641 (2014).
222. Sillanpää, M., Ncibi, M. C. & Matilainen, A. Advanced oxidation processes for the removal of natural organic matter from drinking water sources: A comprehensive review. Journal of Environmental Management 208, 56–76 (2018).
223. Mosteo, R., Miguel, N., Martin-Muniesa, S., Ormad, M. P. & Ovelleiro, J. L. Evaluation of trihalomethane formation potential in function of oxidation processes used during the drinking water production process. Journal of Hazardous Materials 172, 661–666 (2009).
224. Qi, C. et al. Activation of persulfate by modified drinking water treatment residuals for sulfamethoxazole degradation. Chemical Engineering Journal 353, 490–498 (2018).
225. Liu, T. et al. Applications and influencing factors of the biochar-persulfate based advanced oxidation processes for the remediation of groundwater and soil contaminated with organic compounds. Science of The Total Environment 836, 155421 (2022).

226. Zappi, M. et al. Treatment of groundwater contaminated with high levels of explosives using advanced oxidation processes. International Journal of Environmental Science & Technology 13, 2767–2778 (2016).
227. Duan, Y. & Sedlak, D. L. An electrochemical advanced oxidation process for the treatment of urban stormwater. Water Research X 13, 100127 (2021).
228. Zheng, Z. et al. Stormwater herbicides removal with a solar-driven advanced oxidation process: A feasibility investigation. Water Research 190, 116783 (2021).
229. Zheng, Z., Zhang, K., Toe, C. Y., Amal, R. & Deletic, A. Photo-electrochemical oxidation flow system for stormwater herbicides removal: Operational conditions and energy consumption analysis. Science of the Total Environment 898, 166375 (2023).
230. Feng, W., McCarthy, D. T., Wang, Z., Zhang, X. & Deletic, A. Stormwater disinfection using electrochemical oxidation: A feasibility investigation. Water Research 140, 301–310 (2018).
231. Tsitonaki, A. et al. In situ chemical oxidation of contaminated soil and groundwater using persulfate: a review. Critical Reviews in Environmental Science &Technology 40, 55–91 (2010).
232. Yin, R. et al. Singlet oxygen-dominated peroxydisulfate activation by sludge-derived biochar for sulfamethoxazole degradation through a nonradical oxidation pathway: Performance and mechanism. Chemical Engineering Journal 357, 589–599 (2019).
233. Ahmed, M. M., Barbati, S., Doumenq, P. & Chiron, S. Sulfate radical anion oxidation of diclofenac and sulfamethoxazole for water decontamination. Chemical Engineering Journal 197, 440–447 (2012).
234. Mandal, S. Reaction rate constants of hydroxyl radicals with micropollutants and their significance in advanced oxidation processes. Journal of Advanced Oxidation Technologies 21, 178–195 (2018).
235. Kishore, K. & Asmus, K.-D. Radical cations from one-electron oxidation of aliphatic sulphoxides in aqueous solution. A radiation chemical study. Journal of the Chemical Society, Perkin Transactions 2 2079–2084 (1989).
236. Lin, J.-M., Arakawa, H. & Yamada, M. Flow injection chemiluminescent determination of trace amounts of hydrogen peroxide in snow-water using KIO4–K_2CO_3 system. Analytica Chimica Acta 371, 171–176 (1998).
237. Tratnyek, P. G. & Hoigne, J. Oxidation of substituted phenols in the environment: a QSAR analysis of rate constants for reaction with singlet oxygen. Environmental Science & Technology 25, 1596–1604 (1991).
238. Connick, R. E. The interaction of hydrogen peroxide and hypochlorous acid in acidic solutions containing chloride ion. Journal of the American Chemical Society 69, 1509–1514 (1947).

239. Foote, C. S., Wexler, S., Ando, W. & Higgins, R. Chemistry of singlet oxygen. IV. Oxygenations with hypochlorite-hydrogen peroxide. Journal of the American Chemical Society 90, 975–981 (1968).
240. Uemi, M. et al. Cholesterol hydroperoxides generate singlet molecular oxygen [O_2 ($^1\Delta_g$)]: Near-IR emission, ^{18}O-labeled hydroperoxides, and mass spectrometry. Chemical Research in Toxicology 24, 887–895 (2011).
241. Held, A., Halko, D. & Hurst, J. Mechanisms of chlorine oxidation of hydrogen peroxide. Journal of the American Chemical Society 100, 5732–5740 (1978).
242. Kim, T.-K. & Sedlak, D. L. Mineralization of a Fully Halogenated Organic Compound by Persulfate under Conditions Relevant to in Situ Reduction and Oxidation: Reduction of Hexachloroethane by Ethanol Addition Followed by Oxidation. Environmental Science & Technology 57, 13691–13698 (2023).
243. Lee, Y. & Von Gunten, U. Quantitative structure–activity relationships (QSARs) for the transformation of organic micropollutants during oxidative water treatment. Water Research 46, 6177–6195 (2012).
244. Hansch, C., Leo, A. & Taft, R. A survey of Hammett substituent constants and resonance and field parameters. Chemical Reviews 91, 165–195 (1991).
245. Hansch, C., Leo, A. & Hoekman, D. Exploring QSAR: Hydrophobic, Electronic, and Steric Constants. vol. 2 (American Chemical Society Washington, DC, 1995).
246. Fiener, P., Auerswald, K. & Van Oost, K. Spatio-temporal patterns in land use and management affecting surface runoff response of agricultural catchments—A review. Earth-Science Reviews 106, 92–104 (2011).
247. Helmreich, B., Hilliges, R., Schriewer, A. & Horn, H. Runoff pollutants of a highly trafficked urban road–Correlation analysis and seasonal influences. Chemosphere 80, 991–997 (2010).
248. Rommel, S. H. & Helmreich, B. Influence of temperature and de-icing salt on the sedimentation of particulate matter in traffic area runoff. Water 10, 1738 (2018).
249. Huber, M. et al. Heavy metal removal mechanisms of sorptive filter materials for road runoff treatment and remobilization under de-icing salt applications. Water Research 102, 453–463 (2016).
250. Hayyan, M., Hashim, M. A. & AlNashef, I. M. Superoxide ion: generation and chemical implications. Chemical Reviews 116, 3029–3085 (2016).
251. Jawad, A. et al. Tuning of persulfate activation from a free radical to a nonradical pathway through the incorporation of non-redox magnesium oxide. Environmental Science & Technology 54, 2476–2488 (2020).
252. Zong, Y. et al. Do We Appropriately Detect and Understand Singlet Oxygen Possibly Generated in Advanced Oxidation Processes by Electron Paramagnetic Resonance Spectroscopy? Environmental Science & Technology (2023).

253. Clennan, E. L. & Pace, A. Advances in singlet oxygen chemistry. Tetrahedron 61, 6665–6691 (2005).
254. Gasperi, J. et al. Micropollutants in urban runoff from traffic areas: target and non-target screening on four contrasted sites. Water 14, 394 (2022).
255. Klöckner, P. et al. Characterization of tire and road wear particles from road runoff indicates highly dynamic particle properties. Water Research 185, 116262 (2020).
256. Sandré, F. et al. Road Runoff Characterization: Ecotoxicological Assessment Combined with (Non-) Target Screenings of Micropollutants for the Identification of Relevant Toxicants in the Dissolved Phase. Water 14, 511 (2022).
257. Tian, Z., Wark, D. A., Bogue, K. & James, C. A. Suspect and non-target screening of contaminants of emerging concern in streams in agricultural watersheds. Science of the Total Environment 795, 148826 (2021).
258. Lim, S., McArdell, C. S. & von Gunten, U. Reactions of aliphatic amines with ozone: Kinetics and mechanisms. Water Research 157, 514–528 (2019).
259. Yun, E.-T., Lee, J. H., Kim, J., Park, H.-D. & Lee, J. Identifying the nonradical mechanism in the peroxymonosulfate activation process: singlet oxygenation versus mediated electron transfer. Environmental Science & Technology 52, 7032–7042 (2018).
260. Dong, C., Fang, W., Yi, Q. & Zhang, J. A comprehensive review on reactive oxygen species (ROS) in advanced oxidation processes (AOPs). Chemosphere 136205 (2022).
261. Fernández‐Castro, P., Vallejo, M., San Román, M. F. & Ortiz, I. Insight on the fundamentals of advanced oxidation processes. Role and review of the determination methods of reactive oxygen species. Journal of Chemical Technology & Biotechnology 90, 796–820 (2015).
262. Spahr, S. et al. Compound-Specific Carbon, Nitrogen, and Hydrogen Isotope Analysis of N-Nitrosodimethylamine in Aqueous Solutions. Analytical Chemistry 87, 2916–2924 (2015).
263. Hofstetter, T. B. et al. Perspectives of compound-specific isotope analysis of organic contaminants for assessing environmental fate and managing chemical pollution. Nature Water 1–17 (2024).
264. Rajapaksha, A. U. et al. Engineered/designer biochar for contaminant removal/immobilization from soil and water: potential and implication of biochar modification. Chemosphere 148, 276–291 (2016).
265. Wang, B., Gao, B. & Fang, J. Recent advances in engineered biochar productions and applications. Critical Reviews in Environmental Science & Technology 47, 2158–2207 (2017).
266. Dai, L. et al. Tuning oxygenated functional groups on biochar for water pollution control: A critical review. Journal of Hazardous Materials 420, 126547 (2021).

267. Qin, Q. et al. Optimization of multiscale structure and electrochemical properties of bamboo-based porous activated biochar by coordinated regulation of activation and air oxidation. Chemical Engineering Journal 477, 146763 (2023).
268. Xiao, F. et al. Production of granular activated carbon by thermal air oxidation of biomass charcoal/biochar for water treatment in rural communities: A mechanistic investigation. Chemical Engineering Journal Advances 4, 100035 (2020).
269. Zhang, H. et al. Derivation of oxygen-containing functional groups on biochar under non-oxygen plasma for mercury removal. Fuel 275, 117879 (2020).
270. Guo, X. et al. Influence of thermal air oxidation on the chemical composition and uranium binding property of intrinsic dissolved organic matter from biochar. Chemosphere 317, 137896 (2023).
271. Liang, C., Liang, C.-P. & Chen, C.-C. pH dependence of persulfate activation by EDTA/Fe (III) for degradation of trichloroethylene. Journal of Contaminant Hydrology 106, 173–182 (2009).
272. De Luca, A., Dantas, R. F. & Esplugas, S. Study of Fe (III)-NTA chelates stability for applicability in photo-Fenton at neutral pH. Applied Catalysis B: Environmental 179, 372–379 (2015).
273. Wang, L. et al. Rapid removal of dyes under visible irradiation over activated carbon fibers supported Fe (III)–citrate at neutral pH. Separation and Purification Technology 122, 449–455 (2014).
274. World Health Organization. Guidelines for Drinking-Water Quality. vol. 1 (World Health Organization, 2004).
275. Ahmad, M., Teel, A. L. & Watts, R. J. Persulfate activation by subsurface minerals. Journal of Contaminant Hydrology 115, 34–45 (2010).
276. Liu, H., Bruton, T. A., Doyle, F. M. & Sedlak, D. L. In situ chemical oxidation of contaminated groundwater by persulfate: decomposition by Fe (III)-and Mn (IV)-containing oxides and aquifer materials. Environmental Science & Technology 48, 10330–10336 (2014).
277. Teel, A. L., Ahmad, M. & Watts, R. J. Persulfate activation by naturally occurring trace minerals. Journal of Hazardous Materials 196, 153–159 (2011).
278. Liang, J. et al. Critical Functions of Soil Components for In Situ Persulfate Oxidation of Sulfamethoxazole: Inherent Fe (II) Minerals-Coordinated Nonradical Pathway. Environmental Science & Technology 58, 915–924 (2023).
279. Zhao, J. et al. Insight into in-situ chemical oxidation by Fe (II)-containing minerals: The role of inherent Fe (II)-OH in Fe (II)-Al LDHs. Chemical Engineering Journal 433, 133835 (2022).

280. Zhang, Y., Zhao, L., Yang, Y. & Sun, P. Fenton-like oxidation of antibiotic ornidazole using biochar-supported nanoscale zero-valent iron as heterogeneous hydrogen peroxide activator. International Journal of Environmental Research and Public Health 17, 1324 (2020).
281. Sun, P. et al. Insights into the mechanism of hydrogen peroxide activation with biochar produced from anaerobically digested residues at different pyrolysis temperatures for the degradation of BTEXS. Science of the Total Environment 788, 147718 (2021).
282. Fang, G. et al. Key role of persistent free radicals in hydrogen peroxide activation by biochar: implications to organic contaminant degradation. Environmental Science & Technology 48, 1902–1910 (2014).
283. Yan, J., Han, L., Gao, W., Xue, S. & Chen, M. Biochar supported nanoscale zerovalent iron composite used as persulfate activator for removing trichloroethylene. Bioresource Technology 175, 269–274 (2015).